Characterisation of the expression profile and endothelial function of Rho GTPase RhoJ

---

by

Sukhbir Kaur

A thesis submitted to
The University of Birmingham
for the degree of
DOCTOR OF PHILOSOPHY

Molecular Angiogenesis Group
Department of Immunity and Infection
College of Medical and Dental Sciences
The University of Birmingham
March 2011

Abstract

Rho GTPases are molecular switches that regulate many aspects of cell physiology. A number of Rho GTPases are essential for the formation of new vessels from pre-existing ones, a process known as angiogenesis. RhoJ/TCL belongs to the Cdc42 subfamily of Rho GTPases. Previous bioinformatic and primary cell line analyses identified RhoJ as being highly expressed in endothelial cells. The aim of this project was to investigate the expression pattern and endothelial function of RhoJ, particularly in the processes necessary for angiogenesis. Silencing RhoJ with siRNA impaired tube formation and migration. On the cellular level, RhoJ knockdown increased focal adhesions, actin stress fibres and collagen gel contraction, suggesting increased actomyosin contractility. Pharmacological inhibition of ROCK and myosin II, two regulators of actomyosin contractility, restored motility and tube formation after RhoJ knockdown. RhoJ localised to blood vessels of developing mice and in various human normal and pathological tissues. In zebrafish embryos RhoJ was not expressed in endothelial cells, instead RhoJ was expressed in the musculature where it was involved in regulating somite formation. This study is the first to describe a role for RhoJ as a negative regulator of focal adhesion numbers and actomyosin contractility and to demonstrate a critical role of this Rho GTPase in endothelial cell migration and tube formation, thus identifying a potential new player in angiogenesis.

Vaheguru Jee, tera lakh lakh shukar hai

Kabeer, mera mujh mehi kich nehee, jo kich hai so tera
Dhan Dhan Sri Guru Granth Sahib Jee Maharaj.

Acknowledgements

I thank Victoria Heath for being an inspiration, and for her close supervision, dedication, guidance and patience. I am grateful to Roy Bicknell for his support and advice. I express my gratitude to Katarzyna Leszczynska for being a good friend and sharing the entire RhoJ adventure with me. I also express my thanks to the British Heart Foundation and Cancer Research UK for their funding, and the University of Birmingham for providing me with 6 years of stimulation and great memories.

My deepest heartfelt thanks go to my wonderful husband for his endless support, friendship and constant encouragement. He has shared with me the many highs and lows, and without him, it would have taken much longer to complete. I am equally indebted to my lovely parents, especially both mums, for being immensely patient and understanding during the more demanding and challenging times.

Table of contents

List of illustrations

Chapter 1

Chapter 3

Chapter 4

Chapter 5

List of tables

Chapter 1

Chapter 6

List of abbreviations

ANOVA	One-way analysis of variance
ADP	Adenosine diphosphate
ATPase	Adenosine triphosphatase
ATP	Adenosine triphosphate
bp	Base pair
BSA	Bovine serum albumin
CA	Caudal artery
CAAX	C-cysteine, A-aliphatic amino acid, X-any amino acid
cDNA	Complementary DNA
CRIB	Cdc42/Rac1 interacting binding motif
CV	Caudal vein
D1	RhoJ specific siRNA duplex 1
D2	RhoJ specific siRNA duplex 2
DA	Dorsa aorta
da	Dominant active
DLAV	Dorsal longitudinal anastomotic vessel
DNA	Deoxyribonucleic acid
EC	Endothelial cell
ECs	Endothelial cells
ECM	Extracellular matrix
EF1α	Elongation factor 1 alpha
F-actin	Filamentous actin
FACS	Fluorescent activated cell scanner/sorter
FAK	Focal adhesion kinase
FCS	Fetal calf serum
FGF	Fibroblast growth factor
Fli1	Friend leukemia virus integration 1
FITC	Fluorescein isothiocyanate
GAP	GTPase-activating protein
GAPDH	Glyceraldehyde 3-phosphate dehydrogenase
GDI	Guanine nucleotide dissociation inhibitor
GDP	Guanosine diphosphate
GEF	Guanine nucleotide exchange factor
GFP	Green fluorescent protein
GIT	G protein-coupled receptor kinase-interacting protein
GM130	Cis-Golgi matrix protein
GTPase	Guanosine triphosphatase
GTP	Guanosine triphosphate
H_2O	Water
HASMC	Human aortic smooth muscle cells
HDMEC	Human dermal microvascular endothelial cells
HMEC-1	Human microvascular endothelial cell line-1
hPC-PL	Human pericytes derived from placenta
hpf	Hours post fertilisation
HPRT	Hypoxanthine phosphoribosyl transferase
HUVEC	Human umbilical vein endothelial cells
ICAM-1	Intercellular adhesion molecule 1/CD54

ISA	Intersegmental arteries
ISG20	Interferon-stimulated gene of 20 kDa
kb	Kilobase
kDa	Kilodalton
MLC	Myosin light chain
MLCK	Myosin light chain kinase
MMP	Matrix metalloproteinase
MO	Morpholino
mRNA	Messenger RNA
MTOC	Microtubule organising centre
MyoD	Myogenic differentiation 1
NADPH	Nicotinamide adenine dinucleotide phosphate-oxidase
NCD	Negative control siRNA duplex
NTC	No template control
OAS1	2', 5’-oligoadenylate synthetase 1
P-value	Probability value
PA	Plasminogen activator
PAK	P21 activated kinase
PBS	Phosphate buffered saline
PBST	Phosphate buffered saline with tween-20
PCR	Polymerase chain reaction
PCV	Posterior cardinal vein
Phospho-	Phosphorylated
Pi	Inorganic phosphate
PIX	PAK interacting exchange factor
RISC	RNA-induced silencing complex
RNA	Ribonucleic acid
RNAi	RNA interference
ROCK	Rho-kinase
RT	Reverse transcription
SDS-PAGE	SDS-polyacrylamide gel electrophoresis
shRNA	Short hairpin RNA
siRNA	Small interfering RNA
TNF-α	Tumour necrosis factor-alpha
TRITC	Tetramethylrhodamine isothiocyanate
UEAI	*Ulex europeaus* agglutinin I
VE-Cadherin	Vascular endothelial cadherin
VEGF	Vascular endothelial growth factor
VEGFR	Vascular endothelial growth factor receptor
wt	Wild type

Chapter one

Introduction

1.1 The endothelium

1.1.1 Overview

The endothelium is a single layer of simple squamous endothelial cells (ECs) that line the interior surface of all blood and lymphatic vessels. Depending on their location, vascular ECs have unique structural and functional properties. The vascular endothelium acts as a physical barrier that separates the blood from underlying tissue but also plays an important part in many physiological functions. ECs control transcellular and paracellular transport of proteins, solutes, gases and cells across the blood vessel wall (1, 2). ECs also regulate blood coagulation and haemostasis, vasomotor tone and inflammatory responses (3). In addition, the *de novo* or angiogenic development of blood vessels, is orchestrated by ECs (4). Thus, the endothelium is a heterogeneous and dynamic organ that has vital secretory, metabolic and immunological functions (5, 6).

1.1.2 Morphology of the vascular endothelium

The endothelium of the entire adult vascular system weighs approximately 1 kg and contains around 1-6 x 10^{13} ECs, which are each between 10-15 μm in diameter and 2-5 μm thick (5). ECs overlap along their perimeter and are attached to one another at these sites through cell-cell contacts known as adherens junctions and tight junctions (7). These junctions also mediate contact inhibition signalling to prevent EC growth and motility (7, 8).

In all blood vessels, the endothelial layer is surrounded by a basement membrane; these two together are known as the *tunica intima*. In arteries and veins, but not capillaries, the *tunica intima* is surrounded by a single or multiple layers of vascular smooth muscle cells (*tunica media*) and an additional layer of collagenous connective tissue, synthesised by fibroblasts (*tunica adventitia*) (9). Capillaries only consist of the *tunica intima* layer and are partially

covered by pericytes (10). Vascular smooth muscle cells and pericytes, also known as mural cells, provide structural support to blood vessels but evidence also shows that endothelial-mural cell signalling is vital for the switch between endothelial quiescence and activity (11-13).

ECs have been shown to display great morphological heterogeneity across the vascular system (14). Phenotypic differences in the appearance of capillary endothelium among and within tissue vascular beds have been reported. For example, capillaries in the brain and retina are lined continuously with endothelium to maintain the blood brain barrier and low permeability (5). In contrast, the capillary endothelium in the sinusoids of the liver, lymph nodes, bone marrow and spleen is discontinuous, enabling cells to pass through the gaps between ECs (5, 15, 16). Moreover, intestinal villi, endocrine glands and kidney glomeruli have fenestrated capillary ECs to facilitate selective permeability needed for efficient absorption, secretion and filtration (17, 18). The shape of ECs also varies across the vascular tree. In response to high shear stress and hydrostatic pressure, arterial ECs align in the direction of flow and are long and narrow whereas venous and capillary ECs are cuboidal, plump and show a cobblestone morphology (17, 19). Furthermore, the expression and organisation of tight junctions across the vascular system also differs. For example, arterial vessels and brain capillaries are rich in tight junctions to maintain vessel integrity but postcapillary venules display disorganised and loose cell-cell junctions to facilitate the inflammation-induced movement of leukocytes into tissues (19, 20).

ECs from different sites of the vascular tree also show diverse gene expression profiles (21). There is endothelial gene expression heterogeneity between macro and microvessels, arteries and veins and different organs. Morphological and genotypic differences in the endothelium across the vascular tree reflect specialised functions of ECs depending on their location. An

example of molecular endothelial heterogeneity is the exclusive expression of lung specific EC adhesion molecule (LuECAM-1), a homing receptor involved in cell trafficking, by pulmonary microvessels and some splenic venules (22). In addition, brain endothelium is found to express a large number of unique cell surface transporters, several of which have been shown to be important for blood brain barrier function (23).

1.1.3 Endothelial cell functions

The endothelium was initially thought of as an inert physical barrier that simply separated the blood from surrounding tissue. However, over the last three decades much work has shown that ECs are highly metabolically active with many regulatory functions.

ECs play an important role in the control of vasomotor tone and blood pressure by secreting vasodilators (nitric oxide, prostacyclin) or vasoconstrictors (platelet-activating factor, endothelin) in response to mechanical stimuli (5). Since ECs have direct contact with the blood, the endothelium is also vital to coagulation and haemostasis. In the physiological setting, the luminal side of the endothelium acts as an antithrombotic surface, preventing clot formation. However, in response to vascular damage, the endothelial layer transforms into a procoagulant surface and thus triggers clotting and then fibrinolysis (5). Moreover, ECs act as ‘gate-keepers’ to regulate vessel permeability and the transport of molecules and cells through the vascular wall. Transport through the endothelium is achieved in two ways; using specialised vesicle transport systems (transcellular) or through EC retraction and disruption of cell-cell junctions (paracellular) (7). In addition, ECs play an important role during inflammation whereby they express adhesion molecules (selectins and ICAM-1) on their surface to allow leukocytes to roll along and tether to vessel walls and transmigrate into

tissues (24). And finally, in response to positive growth factors, ECs undergo a cascade of signalling events that are vital to the development of new blood vessels (25).

1.2 Development of the vasculature

1.2.1 Overview

Angiogenesis is the formation of new vessels from pre-existing vasculature and is essential for fetal development. Angiogenesis rarely occurs in normal adults and is only physiologically observed during wound healing and in the female reproductive organs (4, 26). Angiogenic vascular development requires a fine balance between stimulatory and inhibitory signals. A tilt in this equilibrium can give rise to excessive or insufficient angiogenesis, which can substantially contribute to a number of pathologies such as diabetic retinopathy, heart ischaemia, rheumatoid arthritis and cancer metastasis (4). Anti-VEGF therapy is currently being used to treat angiogenesis dependent diseases, but the complex reactions to these drugs highlights the importance for further development of future therapeutic strategies.

1.2.2 Vasculogenesis

Vasculogenesis is the *de novo* formation of primary blood vessels during early embryogenesis. This process involves the differentiation of mesodermal germ cells into angioblasts. Following that, these stem cells further differentiate into ECs (27). ECs then aggregate and assemble to form blood islands, which subsequently fuse together to form the primitive vascular plexus (4, 26). This primary structure is then further expanded and developed through angiogenesis, which is the process of microvessel formation from pre-existing vessels (4).

1.2.3 Angiogenesis

The cellular mechanism of sprouting angiogenesis is a multistep process (summarised in figure 1.1). The process is initiated by angiogenic growth factors activating ECs (tip cells) on parental blood vessels to secrete proteolytic enzymes, such as matrix metalloproteinases (MMP) and plasminogen activators (PAs), to breakdown the surrounding basement membrane (28, 29). Once ECs lose their contact with surrounding mural cells, tip cells begin to invade and migrate into the degraded matrix area and are followed by proliferating ECs (30). ECs then differentiate and assemble to form capillary-like sprouts, which extend and elongate further into the interstitial space. Following that, lumen formation occurs and to stabilise the newly formed vessels, new basement membranes are synthesised and pericytes are recruited to the abluminal surface. New angiogenic sprouts fuse with one another or existing vessels to form loops and blood flow is established. (31, 32).

1.2.3.1 Pro-angiogenic factors

Numerous factors that promote the events underlying blood vessel growth have been identified, however, here only the major molecules involved in stimulating angiogenesis will be briefly discussed.

Soluble growth factors are secreted from surrounding macrophages, astrocytes, fibroblasts, mural cells or ECs and are sometimes sequestered in the extracellular matrix (ECM) and basement membrane. Upon degradation of the matrix, they are released to activate ECs (33). One of the most well-characterised soluble factor that potently stimulates vasculogenesis and angiogenesis is vascular endothelial growth factor-A (VEGF-A) (34). VEGF-A binds to transmembrane tyrosine kinase receptors (VEGFR-1, VEGFR-2) and non-tyrosine kinase neuropilin co-receptors on ECs and stimulates all the major steps in the angiogenesis cascade

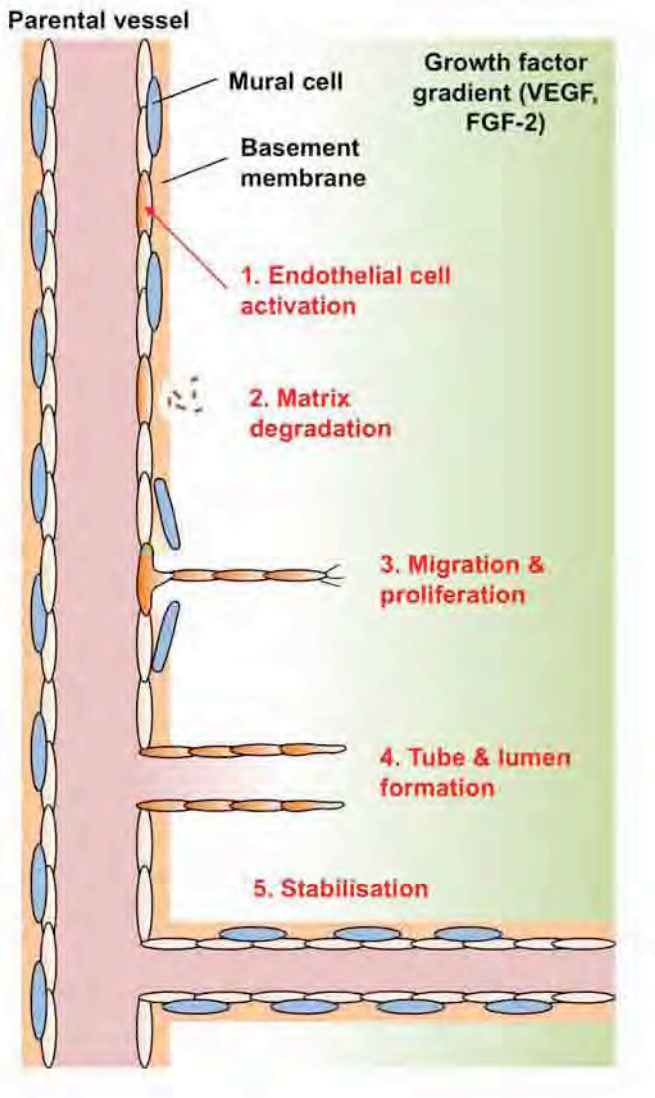

Figure 1.1 The cellular mechanism of sprouting angiogenesis. (1) Endothelial cells on existing vessels are activated in response to growth factor stimulation. (2) Activated endothelial tip cells secrete proteolytic enzymes to breakdown the basement membrane. (3) Endothelial cells lose contact with surrounding mural cells and migrate into the degraded matrix area. Behind the leading tip cell, endothelial cells are stimulated to proliferate. (4) Endothelial cells differentiate into a lumen-containing tubule. (5) The new microvessel is stabilised by the recruitment of a new basement membrane and pericyte cells.

such as EC migration, proliferation, survival, and tube formation/sprouting in response to hypoxia (35-37). Much evidence has shown that activation of angiogenesis is mediated mainly downstream of VEGF-A/VEGFR-2 signalling (38-40). Loss of VEFG-A results in embryonic lethality (41, 42) thus it is vital for normal angiogenesis in the developing embryo. Another member of the VEGF family, placenta-derived growth factor (PlGF) stimulates vessel formation by binding to VEGFR-1 and VEGFR-2.

Fibroblast growth factor-2 (FGF-2) also plays a pivotal role in activating angiogenesis and was one of the first pro-angiogenic growth factors to be identified. FGF-2 signals through FGF transmembrane tyrosine kinase receptors on ECs and stimulates their migration, invasion, proliferation and differentiation, and also has been shown to induce the release of proteases such as collagenase, MMPs and PAs (43-45).

The binding of angiopoietin (Ang) ligands to the endothelial Tie-2 tyrosine kinase receptor also modulates angiogenesis. Ang1 and Ang2 both bind with similar affinity to Tie-2 receptor but have opposing effects. Ang2 is a naturally occurring antagonist of Ang1. In response to hypoxia, Ang2 blocks Ang1 induced Tie-2 phosphorylation, by competitively binding to Tie-2 (46, 47). In the presence of VEGF, the binding of Ang2 to Tie-2 enables ECs to dissociate from one another to allow cells to migrate and undertake mitosis (30, 32, 48). In addition, Ang1/Tie-2 signalling stimulates the interactions between ECs and pericytes, to stabilise newly formed capillaries (27, 40).

The binding of Ang1 to Tie-2 on ECs leads to the endothelial secretion of platelet-derived growth factor-BB homodimer (PDGF-BB). The tyrosine kinase receptor for PDGF-BB ligand, PDGFRβ, is found on the surface of pericytes and vascular smooth muscle cells (48, 49). Thus the release of PDGF-BB generates a gradient to stimulate the movement of

pericytes to the region of new vessel formation for stabilisation (10, 44). PDGF-BB has also been found to stimulate EC tube formation and sprouting (32).

In addition to soluble factors, many integrins (cell surface heterodimeric matrix adhesion molecules) such as vitronectin receptors (αvβ3 and αvβ5) have been shown to stimulate angiogenesis by mediating EC migration and tube formation (32, 47, 50, 51). Chemokines derived from immune cells are also important in modulating angiogenesis. For example, in pathological angiogenesis the binding of interleukin-8 (IL-8) to its receptors on ECs leads to increased EC proliferation and also increases the activity of MMPs (32, 46).

1.2.3.2 Endogenous inhibitors of angiogenesis

Fragments of the degraded basement membrane and ECM can act as endogenous inhibitors of angiogenesis (52). For example, arresten is derived from type IV collagen and inhibits MMP activation, VEGF-dependent EC migration and FGF-2-dependent EC proliferation (53, 54). Similarly, other fragments of type IV collagen such as canstatin and tumstatin have also been shown to inhibit EC proliferation, migration and tube formation by stimulating apoptosis and binding to integrins necessary for angiogenesis (52, 54-56). A fragment of collagen XVIII, known as endostatin has also been found to directly inhibit EC proliferation and migration by inducing EC apoptosis and G1 arrest. Endostatin also indirectly suppresses MMP activity and blocks the binding of VEGF-A to VEGFR-2 (52, 57). Thrombospondins (TSPs) are glycoproteins stored in the ECM and are potent inhibitors of angiogenesis. TSP-1 induces the recruitment of mural cells to the site of angiogenesis, thus blocking EC migration and TSP-2 mainly inhibits EC migration by increasing EC apoptosis (52, 58).

Cytokines and growth factors derived from cells and blood plasma have also been recognized for their anti-angiogenic effects. The type 1 interferon, IFN-α is an anti-angiogenic cytokine released from leukocytes, fibroblasts and macrophages and was one of the first molecules found to have inhibitory activity on ECs. The effects of IFN-α include inhibition of FGF-2 production, downregulation of IL-8, VEGF-A gene expression and direct impairment of EC proliferation and migration (52, 59). Surrounding leukocytes and mast cells can also release IL molecules to suppress angiogenic growth, for example, IL-4, IL-12 and IL-18 all show anti-angiogenic activity. IL-4 acts to block FGF-2-induced angiogenesis whereas IL-12 and IL-18 induce the expression of other inhibitory cytokines (52, 59).

Moreover, fragments of blood coagulation factors also inhibit angiogenesis. For example, angiostatin, a fragment of plasminogen, inhibits the growth of ECs by binding directly to ATP synthase on their surface, and triggering apoptosis (52, 60). In addition, cleavage of antithrombin III and prothrombin also produces anti-angiogenic molecules, which act to inhibit EC proliferation. Furthermore, platelet factor-4 is a protein released by platelet α-granules during blood clotting and directly binds to FGF-2 thus inhibiting its role in stimulating EC growth (52, 60). Also, fragments of the central E-domain of fibrinogen (alphastatin, β43-63) have been shown to have anti-angiogenic activity by blocking EC migration and differentiation (61-64). Tissue inhibitors of matrix metalloproteinases (TIMPs) inhibit the breakdown of the basement membrane by binding to the active sites of MMP enzymes. TIMPs are also known to inhibit EC growth, differentiation and induce apoptosis, independent of MMP inhibition (60). There are many other matrix, cell and blood derived endogenous inhibitors of angiogenesis but since this is not an exhaustive review, they have not all been discussed here. The various positive and negative regulators of angiogenesis that have been mentioned are summarised in table 1.1.

Stage of angiogenesis	Stimulators	Inhibitors
Matrix degradation	MMPs, PAs, Collagenase, FGF-2 (FGFR), IL-8	TIMPs, Arresten, Endostatin
Migration	VEGF-A (VEGFR-2), FGF-2 (FGFR), Ang2 (Tie-2), Integrins	Arresten/Canstatin/Tumstatin, Endostatin, TSP-1/TSP-2, IFN-α, Fibrinogen-E, Ang1 (Tie-2)
Proliferation	VEGF-A (VEGFR-2), FGF-2 (FGFR), Ang2 (Tie-2), IL-8	Arresten/Canstatin/Tumstatin, Endostatin, IFN-α, IL-4, Angiostatin, Platelet factor-4, Antithrombin III/Prothrombin fragments, Ang1 (Tie-2)
Tube formation & sprouting	VEGF-A (VEGFR-2), FGF-2 (FGFR), PDGF-BB (PDGFRβ), Ang2 (Tie-2), Integrins PlGF (VEGFR-1/2)	Canstatin/Tumstatin, TSP-2, IL-4, Fibrinogen-E, Ang1 (Tie-2)
Vessel stabilisation	PDGF-BB (PDGFRβ), Ang1 (Tie-2)	Ang2 (Tie-2)

Table 1.1 Summary of the stimulatory and inhibitory factors of the angiogenesis cascade. Brackets indicate receptors.

1.2.3.3 Physiological and pathological angiogenesis

In physiological conditions, angiogenesis occurs in the embryo where it establishes the primary vasculature, but in adults, capillary growth is an infrequent event and the ECs of most tissues are quiescent with a low mitotic rate (65). However, angiogenic growth and regression is known to occur in regular cycles in female reproductive organs such as the ovaries and the endometrium (65, 66). The development and growth of the follicles and corpus luteum of the ovary leading up to ovulation requires an adequate blood supply, which is delivered through angiogenesis (66). During each menstrual cycle, the regeneration of the uterine endometrial tissue (in preparation for implantation) is also supported by angiogenesis (67). Moreover,

angiogenesis is also vital for wound healing and tissue repair. In response to inflammation and growth factors, released by immune cells, ECs are activated to undertake angiogenesis to re-establish the supply of oxygen and nutrients to wounded tissues by replacing damaged capillaries (68).

In normal conditions, angiogenesis is a tightly controlled and highly ordered process, which is only switched ‘on’ for brief periods then completely inhibited under the balanced regulation of angiogenic activators and inhibitors (69). When the balance between stimulatory and inhibitory signals is lost, aberrant angiogenesis occurs and this leads to numerous pathologies.

Folkman and colleagues (1971) were the first to show that tumour growth and survival beyond a few millimetres is dependent on a rich blood supply (70-72). In tumour angiogenesis, growth factors (such as VEGF-A) are produced at high levels from tumour cells and tumour stromal cells and are released in response to hypoxia to induce ECs to invade, migrate and proliferate into the developing tumour to form new vessels (27, 70, 71, 73, 74). Correlations have been found between the level of VEGF-A expression (and other pro-angiogenic factors), disease progression and survival of several cancers (75). It is thought that the pro-angiogenic factors involved in activating angiogenesis are similar for both physiological and pathological angiogenesis. However, in contrast to physiological angiogenesis, the blood vessels formed from tumour angiogenesis are disorganised and tortuous. They frequently display fenestrated endothelium, have physical contact with tumour cells and do not generate well-ordered, hierarchically branched vascular networks. Also they fail to undergo full maturation (pericytes are often absent) and so are highly leaky and unstable (51, 76-79).

Destabilisation of atherosclerotic lesions is also an angiogenesis-dependent process. Similar to the tumour microenvironment, atherosclerotic plaques become hypoxic as they increase in size. Thus the angiogenic development of new vessels leads to the progression of atherosclerotic plaques and their subsequent rupture, which can lead to thrombosis (80). Retinal neovascularisation in ocular disease, which is the main cause of blindness in diabetes mellitus sufferers is another example of uncontrolled VEGF-induced angiogenesis (81, 82). Furthermore, angiogenesis is also an inducer of the pathogenesis of certain inflammatory diseases such as psoriasis and rheumatoid arthritis (83, 84). Moreover, pathologies of the female reproductive system have been found that are associated with disturbances of the angiogenic process such as dysfunctional uterine bleeding, endometriosis, failed implantation and polycystic ovary syndrome (67, 85). Conversely, insufficient or inadequate angiogenesis, where poor capillary growth leads to poor perfusion of tissues and in some cases tissue death, underlies several pathologies such as coronary and brain ischaemia, non-healing fractures, delayed wound healing and chronic ulcers (86).

1.2.3.4 Anti-angiogenic agents in cancer therapy

Given that VEGF has a central role in promoting tumour growth and metastasis, the VEGF signalling pathway became an attractive target for anti-cancer therapeutic intervention. Two strategies have been employed to inhibit the VEGF signalling pathway, one of which includes the use of monoclonal antibodies. Bevacizumab (avastin) is a humanised anti-VEGF-A monoclonal antibody. By binding to circulating VEGF-A, it limits the binding of the soluble factor to cell surface receptors and reduces angiogenesis. It was the first commercially available angiogenesis inhibitor and is currently used to treat colorectal, lung, breast and renal cancers in combination with standard chemotherapy (77, 87). The other approach used to inhibit the VEGF signalling pathway is to target VEGFRs. Tyrosine kinase inhibitors,

sorafenib (nexavar) and sunitinib (stutent) are also currently being used clinically to treat cancers. These work by inhibiting VEGFR phosphorylation and the subsequent activation of the angiogenesis cascade (88).

The use of anti-angiogenic drugs in cancer therapy has been effective in improving overall survival of cancer patients however in many cases there is a lack of response or disease reoccurrence (25, 77, 79). This occurs due to tumours acquiring resistance against the anti-VEGF treatment (89). It is has been hypothesised that resistance to VEGF pathway inhibition may be mediated through tumour cells increasing the expression levels of VEGF/VEGFRs or by tumour cells upregulating alternative pro-angiogenic pathways leading to more aggressive and wide-spread disease (79). It has been proposed that a combination of different pro-angiogenic pathways need to be inhibited in order for anti-angiogenic drugs in tumours to be effective. Therefore, to maximise efficiency of angiogenesis inhibition, other anti-angiogenic agents are currently being tested in preclinical and clinical trials to use alongside anti-VEGF drugs. These include cilengitide (αvβ3/αvβ5 inhibitor), abergin (αvβ3 antagonist), S247 (αvβ3/αvβ5 antagonist), ABT-510 (inhibitor derived from TSP-1), YH-16 (recombinant endostatin), angiostatin, PEG IFN-α (a modified form of IFN-α with longer half life) (79, 86, 90). The difficulty in completely eradicating solid tumour growth with anti-VEGF treatment alone reflects our incomplete understanding of angiogenesis signalling and highlights the need for new future targets to be developed.

1.2.3.5 Models of angiogenesis

In vitro angiogenesis assays are important for furthering our understanding of the molecular mechanisms involved in angiogenesis and useful in identifying new regulators of the angiogenesis cascade (91). The most commonly used *in vitro* assays involve looking at

isolated ECs in systems that aim to mimic each step of the angiogenesis cascade (migration, proliferation and tube formation). EC migration can be assessed by creating a 'wound' in a confluent monolayer of ECs and monitoring the rate and extent of wound closure. Moreover, chemotaxis can be examined using Boyden chemotaxis chambers, which involves the three-dimensional movement of cells toward a gradient of chemotactic stimuli. The easiest method of analysing proliferation is to perform direct cell-counting assays, whereby cells are seeded and counted after a set period of time. Furthermore, plating ECs onto or into gelled matrices can stimulate EC tube formation and sprouting, thus creating a framework in which the differentiation stage of angiogenesis can be examined. Another form of tubule assay known as the organotypic assay involves co-culturing ECs with fibroblasts. The fibroblasts naturally produce extracellular matrix components such as collagen to act as scaffolding for the 3-dimensional tube formation. Evidence shows that tubes that form in this assay contain lumens and that tube formation is dependent on VEGF (secreted by the fibroblasts) making it a more physiological representation of *in vivo* angiogenesis (92). Organ culture experiments such as aortic ring assays, where segments of the aorta are cultured *in vitro* in a 3-dimensional matrix, are the most representative of the *in vivo* situation since they encompass all the aspects of the angiogenic process such as proliferation, migration and tubular outgrowth. However, these assays are difficult to quantitate and determination of successful gene expression modulation is troublesome. Although these overly simplistic *in vitro* assays have many limitations and do not completely simulate the *in vivo* situation, they provide valuable information and are the essential first steps towards validating a potential new therapeutic target (93-95).

In order to validate findings observed *in vitro*, animal models of angiogenesis are needed. Zebrafish, *danio rerio*, are small tropical freshwater fish that are increasingly being used for studying *in vivo* angiogenesis (91, 96). This model has many advantages over other models, for example, embryogenesis occurs outside the mother's body, embryos are transparent and

vascular development is very rapid. Thus real-time physiological blood vessel formation can be directly observed over a relatively short period of time (97). In addition, zebrafish gene expression can be modified with great ease making them model organisms for *in vivo* knockdown/overexpression studies (98). Other commonly used *in vivo* models of angiogenesis include the mouse Matrigel plug or sponge assay, corneal angiogenesis assay and chick chorioallantoic membrane assay (91, 93-95).

1.3 Cell migration

1.3.1 Overview

Cell migration is essential to all multi-cellular organisms and is a highly orchestrated process that involves cell polarisation, protrusion, adhesion and retraction. To begin with, cells reorientate toward the direction of movement and establish front-rear polarity. Subsequent actin polymerisation at the front of the cell drives the extension of lamellipodia and filopodia. New focal adhesions are formed at the leading edge underneath these protrusions to enable the intracellular actin cytoskeleton to anchor to the ECM. In order to move forward, contraction of the actin cytoskeleton (mediated through the activation of myosin II in stress fibres) exerts force on focal adhesion sites. Focal adhesions then disassemble at the rear to allow the cell to retract the trailing edge (99-101).

1.3.2 Cell polarisation

In order for a cell to migrate, it firstly needs to asymmetrically remodel its molecular mechanisms in the direction of movement (figure 1.2A). In response to migration-promoting stimuli, cells redirect their intracellular vesicle trafficking to the cell front to augment cell-surface receptors at the leading edge, thus aiding cells to chemically sense their direction

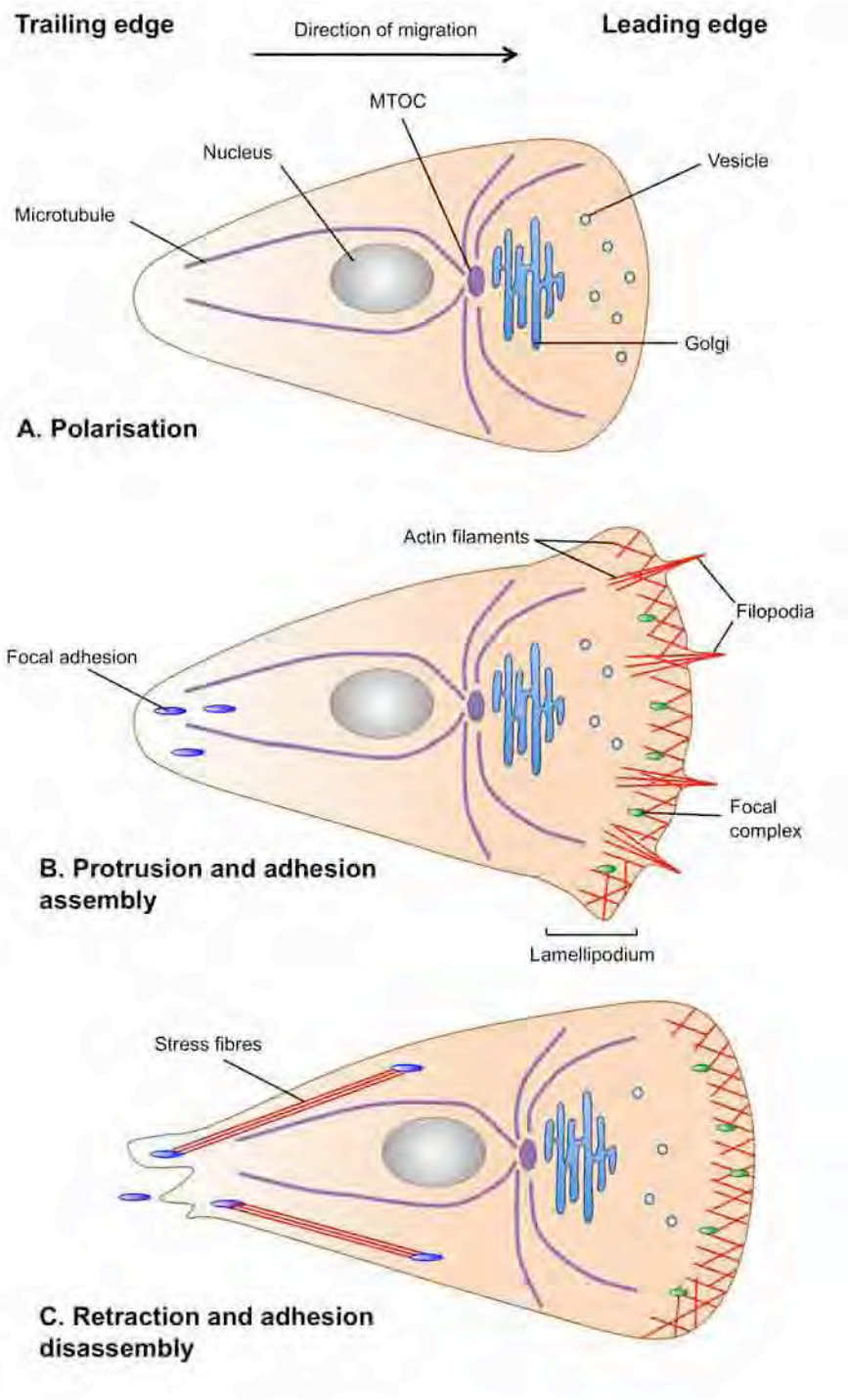

Figure 1.2 The major steps of cell migration. (A) During polarisation, the cell reorientates its cell shape in preparation for movement. During this process, the Golgi and microtubule organising centre (MTOC) are translocated to the front of the cell. (B) The cell then extends protrusions, driven by actin polymerisation, in the direction of migration such as lamellipodia (which initiate the formation of focal complexes at the front of the cell) and filopodia (which sense direction and probe the local environment). (C) Stress fibres that terminate at focal adhesion sites contract, enabling the cell to retract its trailing edge in order to propel forward.

(101). The polarisation of vesicular traffic has also been shown to be important for the delivery of adhesion and cytoskeletal proteins to the front of the cell, which are later needed for cell protrusion (102). To ensure that cells have a direct line of supply to the front of the cell, the Golgi apparatus translocates to the anterior side of the nucleus (103, 104). In this way, Golgi-derived vesicles can be rapidly transported to the leading edge. The microtubule organising centre (MTOC) also reorientates to face the cell front to provide structural stability to the asymmetrical cell shape and to promote cellular protrusion (103, 104).

1.3.3 Actin dynamics

Actin treadmilling is essential to many cellular processes, especially cell migration. Monomeric adenosine triphosphate (ATP)-bound globular actin subunits polymerise to form helical actin filaments (105). Filamentous actin (f-actin) is a polar structure; it has a fast growing end (the plus end) where actin monomers quickly bind and elongate filaments and a slow growing end (the minus end) where actin depolymerises (105). Upon binding to the fast growing end, ATP-bound globular actin subunits are converted to adenosine diphosphate (ADP)-bound monomers by slow hydrolysis and the release of inorganic phosphate (P_i) prompts depolymerisation at the slow growing end (100). Several types of proteins that bind to actin have been identified such as actin nucleators and cross-linkers, as well as components of adhesion complexes. Actin filaments can undergo constant rearrangement and adopt different functions depending on their structure and the type of actin-binding proteins that they are associated with (100, 101).

In cell migration, once cells have acquired polarised morphology, they spread out cellular protrusions in the direction of migration (figure 1.2B). This process is driven by the dynamic growth of actin filaments, whereby actin filaments are arranged with their plus ends facing the

cell edge and polymerisation of these filaments drives the outward extension of the plasma membrane (105). Lamellipodia are flat, sheet-like protrusions, which are built of mesh-like networks of branched actin filaments. Lamellipodia formation induces integrin receptor clustering and the formation of nascent focal complexes (to anchor and stabilise protrusions to the ECM) (106, 107). Filopodia are finger-like structures that extend beyond the cell front and are filled with long, parallel bundles of actin filaments. Filopodia sense chemoattractant stimuli and explore the local environment for appropriate sites of adhesion. Although, actin filaments in lamellipodia and filopodia are nucleated through distinct mechanisms (Arp2/3 complexes and formins, respectively), they co-exist at the leading cell edge (101, 107).

1.3.4 Focal adhesions

Focal adhesions are mechanosensory sites of cell adhesion to the underlying ECM. They structurally link the intracellular actin cytoskeleton to the ECM and serve as traction sites for migration as the cell moves forward over them. These links are mediated via ECM receptors known as integrins. Integrins are transmembrane heterodimers of α and β chains with large ligand-binding extracellular domains and short cytoplasmic domains. Pairing of different α and β subunit isoforms generates distinct receptors for specific ECM ligands (108). So far around 18 α and 8 β subunits have been identified in humans, which can combine to make 24 different integrin receptors (109). Integrin activation typically occurs from the inside out but integrins can also serve as outside-in mechanosensors whereby information about the physical state of the ECM is transmitted into cells to alter actin cytoskeletal dynamics (101, 110). In outside-in signalling, the binding of ECM ligands to integrin receptors induces a conformational change. This unveils their cytoplasmic tails and stimulates the recruitment of adaptor molecules, scaffold and signalling proteins and actin filaments to the cytoplasmic domain (110, 111).

Focal adhesions are dynamic in their size, location and composition. In migrating cells, nascent ‘dot-like’ focal complexes appear at the cell’s leading edge and are linked to the actin filaments of lamellipodia and filopodia (figure 1.2B) (112). Focal complexes are short-lived and have a high rate of turnover since the dynamic flow of actin in cellular protrusions triggers their disassembly and assembly (113). However, some of these do not disassemble and go on to mature into larger complexes known as focal adhesions (figure 1.3). These are mainly found centrally and at the rear of motile cells. Focal adhesions are linked to the ends of stress fibres, so upon contraction of these fibres, they act as sites for force transmission (114-116). As traction forces move the migrating cell forwards, the trailing edge is retracted and focal adhesions at the back of the cell disassemble. These are then partly recycled (turned-over) to the front of the cell to form new focal complexes (see figures 1.2C and 1.3).

It has been reported that focal adhesions are made up of over 100 different proteins and are structurally heterogeneous depending on their age and location (117). However, focal adhesions are composed of several fundamental components that are always present, some of which will be described below. A key event in activating integrins inside-out is the binding of talin to the cytoplasmic region of integrin receptors. Talin is a cytoskeletal adaptor molecule that physically couples integrins to actin filaments. Its N-terminus binds to the cytoplasmic tail of integrin β-chains (which increases their affinity for ECM ligands) and its C-terminal end contains binding sites for f-actin and vinculin, another cytoskeletal adaptor protein (118, 119). Vinculin consists of globular head and tail domains (120). The head domain binds to talin and its tail domain contains binding sites for actin filaments and paxillin (121, 122). By binding to f-actin, vinculin strengthens the talin-mediated link between the actin cytoskeleton and the integrin receptor. Paxillin, a signal transduction adaptor protein, binds to the vinculin tail domain and contains tyrosine phosphorylation sites (121, 122). Non-receptor tyrosine

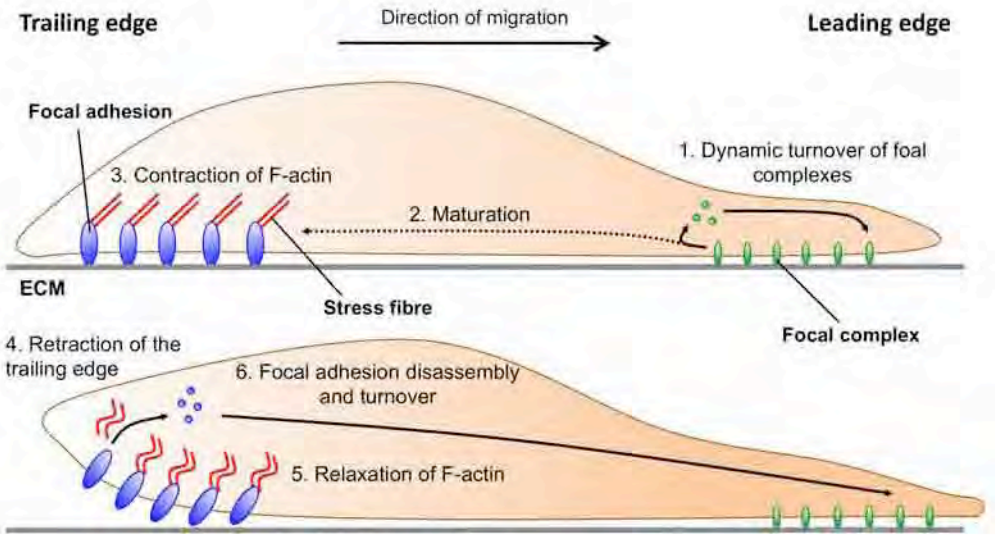

Figure 1.3 Focal adhesion turnover during cell migration. (1) New focal complexes at front of the cell dynamically turnover as the lamellipodium protrudes out. (2) Some of these do not disassemble but mature into focal adhesions, which attach to the ends of stress fibres. (3 & 4) In order to retract the trailing edge, stress fibres contract and cause focal adhesions to disassemble. (5) Stress fibres relax to allow the cell to protrude forward. (6) Some of the focal adhesion proteins are recycled to the front of the cell to make new focal complexes as the cell moves forward.

kinase, focal adhesion kinase (FAK) binds to talin and paxillin through its C-terminal focal adhesion targeting (FAT) domain (123). In response to integrin activation, FAK becomes autophosphorylated at Y397 (124). Activated FAK then phosphorylates several other focal adhesion proteins, including paxillin at Tyr118, which provides docking sites for other signalling molecules (125-127). This prompts the recruitment of other adaptor and signalling proteins to focal adhesions (such as Src kinase, p130CAS-CRK, G protein-coupled receptor kinase-interacting protein (GIT) and β-PIX), leading to their enlargement, maturation and increased strength (116, 124, 127). The basic molecular structure of a focal adhesion is illustrated in figure 1.4.

1.3.5 Stress fibres and actomyosin contractility

In order for a migrating cell to detach from the substrate, cytoskeletal contractility needs to exceed the adhesive strength of focal adhesions (128). This contractile force is generated by stress fibre contraction. Stress fibres are bundles of anti-parallel actin and bipolar non-muscle myosin II, also known as actomyosin (figures 1.2C and 1.5B) (129, 130). Myosin II is a molecular motor protein and is responsible for generating contractility by converting chemical energy (stored in ATP) into mechanical force (127, 131). Myosin II is divided into three structural domains; motor, regulatory and tail (illustrated in figure 1.5A). The motor domain contains the binding sites for ATP and actin and this is the region where ATP is hydrolysed into ADP and P_i for mechanical energy (127). The regulatory domain acts as a ‘lever arm’ for force generation and is associated with two myosin light chains (MLCs); essential and regulatory. The essential light chain helps to structurally support the globular head domain whereas the regulatory light chain is important for regulating myosin head function. The tail domain is a long α-helical coiled-coil region. Several myosins can assemble into bipolar myosin filaments through interactions between their tail domains (see figure 1.5B) (127).

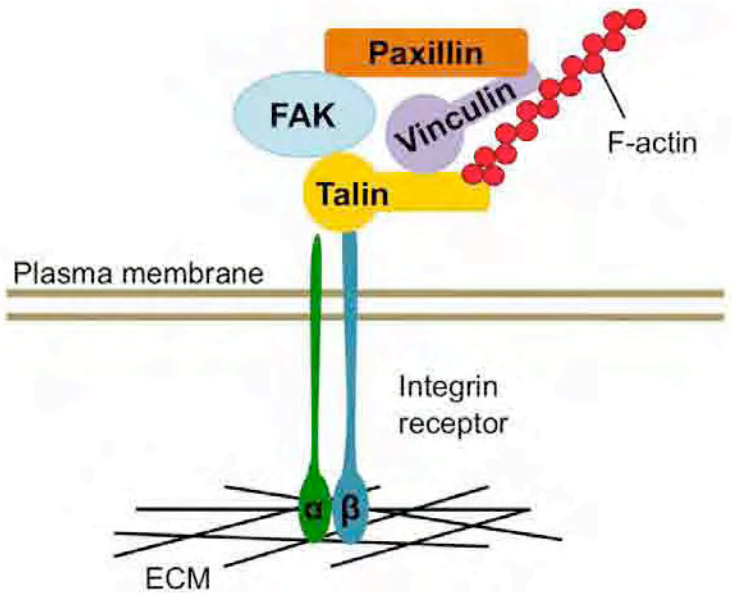

Figure 1.4 Focal adhesion molecular composition. The extracellular domain of transmembrane αβ-integrin receptors bind to extracellular matrix (ECM) proteins. Numerous structural and signalling proteins bind to the intracellular domain of these heterodimers (only talin, vinculin, focal adhesion kinase (FAK) and paxillin are depicted), to form a physical link with intracellular actin filaments (f-actin).

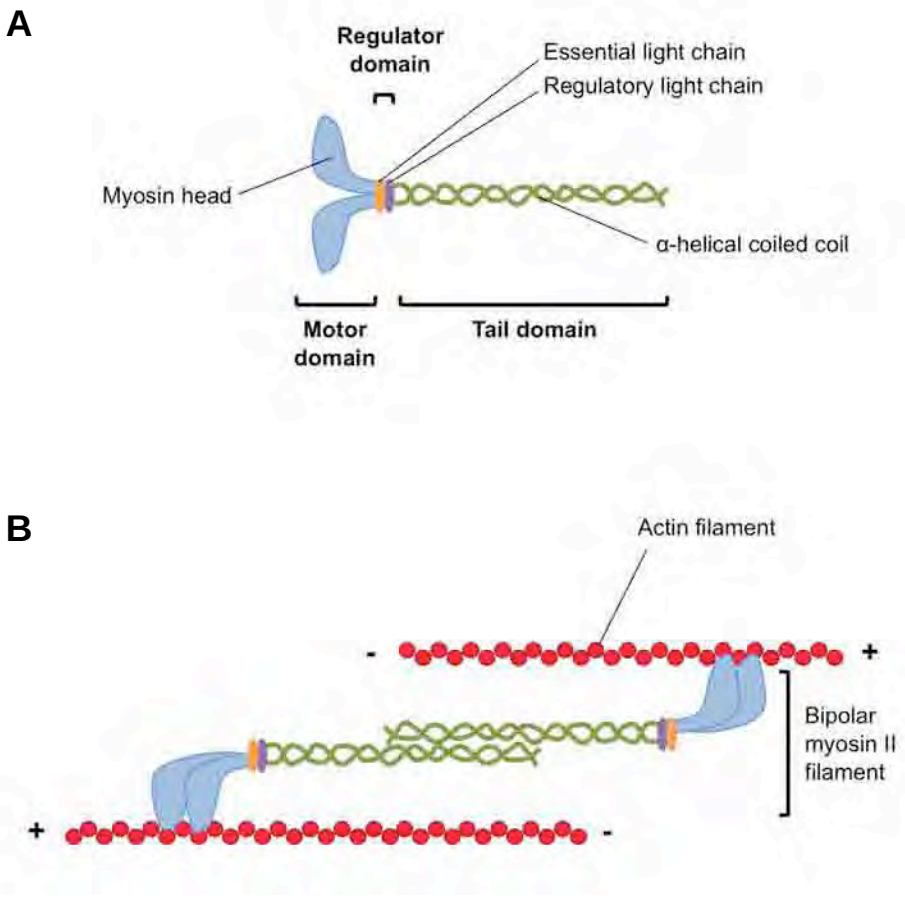

Figure 1.5 The structure of myosin II and actomyosin. (A) Myosin II monomers consist of motor, regulatory and tail domains. The motor domain is made up of two globular myosin heads that contain actin binding sites and ATPase hydrolytic activity. The regulatory domain is comprised of the 'lever arm' and two myosin light chains; essential and regulatory. The tail domain represents the α-helical coiled coil region, which associates with other myosin monomers to form a bipolar structure. (B) Actomyosin bundles contain bipolar myosin filaments, which lie in between antiparallel bundles of actin filaments. Upon activation myosin II interacts with actin through its motor domain. The ATPase activity of the myosin heads induces a conformational change that allows myosin II to slide along the actin filaments towards the plus ends and 'pull' to create actin cytoskeletal tension.

In the activated state, myosin heads that lack a bound nucleotide are locked onto actin filaments, which is often called rigor complex. Upon binding of ATP to the myosin head, a conformational change occurs that reduces the affinity of the myosin head for actin and allows it to move along the actin filaments toward the plus end. ATP is then hydrolysed into ADP and P_i, which results in myosin weakly binding to a new site on the actin filament. P_i release increases the strength of myosin binding to actin and when ADP is dissociated, again the myosin heads tightly lock onto the actin filament. The sliding of myosin II toward the plus end of actin filaments and the upstream tight binding exerts tension on the actin cytoskeleton, also known as actomyosin contractility (132).

Tight control of actomyosin contractility is vital for detachment of the trailing edge during cell migration (116, 133). Myosin II activity is regulated by phosphorylation of the regulatory light chain (referred to as myosin light chain (MLC) hereafter). When MLC is unphosphorylated, the myosin heads of the motor domain exhibit an inactive conformation whereby they interact with one another in a way that blocks ATP hydrolysis and actin binding. Phosphorylation of MLC, at Thr18 and Ser19, disrupts the inhibitory head-head interactions, which unmasks the actin binding site and activates adenosine triphosphatase (ATPase) activity (127). Several kinases have been shown to phosphorylate MLC, these include Rho kinase (ROCK) and myosin light chain kinase (MLCK) (127, 134, 135). However, the activating signals for these kinases differ, for example, Ca^{2+}-calmodulin activates MLCK but ROCK is activated downstream of RhoA, a Rho GTPase protein (127). ROCK can stimulate myosin II ATPase activity in two ways, by directly phosphorylating MLC or by inactivating MLC phosphatase, which dephosphorylates MLC (127). In motile cells, MLC phosphorylation in stress fibres results in increased transmission of tension to sites of adhesion, which is needed for cell body traction and the disassembly of focal adhesions at the cell rear (101). Evidence also shows that contractility is spatiotemporarily regulated

during cell migration, since the formation of cellular protrusions at the cell front needs low cellular tension but the rear requires high contractility (128).

1.4 Rho GTPases

1.4.1 Overview

Rho guanosine triphosphatase (GTPase) proteins are molecular switches found in eukaryotic cells that control a wide array of signal transduction pathways. Among them Rac1, Cdc42 and RhoA are the best characterised. They cycle between inactive GDP-bound and active GTP-bound conformations (136). Upon activation Rho GTPases bind to effector proteins, which control a myriad of cellular processes, such as cell polarity, migration, proliferation, gene transcription, cell adhesion and vesicular trafficking (136-138). Angiogenesis requires many of these diverse cellular events to occur appropriately and evidence shows that Rho GTPases are essential regulators of VEGF-dependant angiogenesis (139, 140).

1.4.2 The small Rho GTPase family

Rho GTPase proteins represent a subfamily within the Ras superfamily of small GTPases, which also include the Ras, Arf, Rab and Ran families (141, 142). To date, more than 150 members of the small GTPase superfamily have been identified in mammals and around 23 of these are Rho GTPases (141). On the basis of amino acid sequence homology, Rho GTPases are classified into six subfamilies; Rho subfamily (RhoA, RhoB and RhoC), Rac subfamily (Rac1, Rac2, Rac3 and RhoG), Cdc42 subfamily (Cdc42, TC10/RhoQ, RhoJ/TCL, Wrch1/RhoU and Wrch2/RhoV), Rnd subfamily (Rnd1, Rnd2, Rnd3/RhoE, RhoD and Rif/RhoF), RhoBTB subfamily (RhoBTB1, RhoBTB2, RhoBTB3 and RhoH/TTF) and the Miro subfamily (Miro1/RhoT1 and Miro2/RhoT2) (143). The phylogenetic relationship between the Rho proteins is illustrated in figure 1.6.

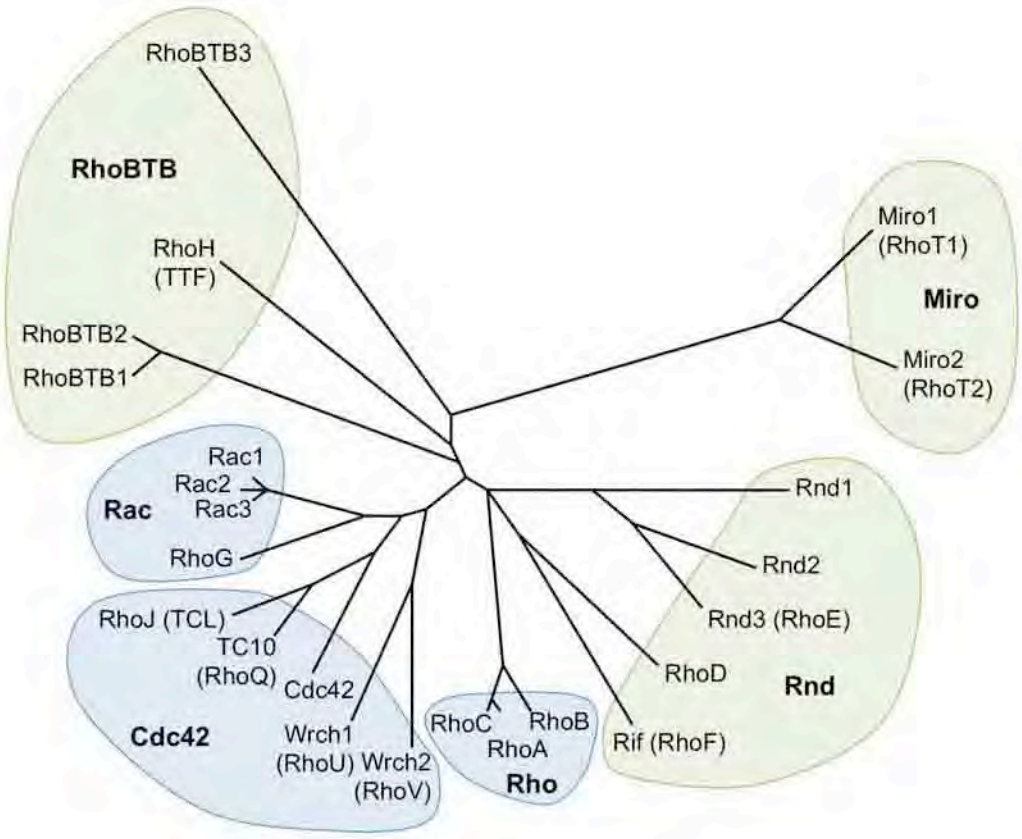

Figure 1.6 Phylogenetic tree of the human small Rho GTPase family. The Rho family of small GTPases are divided into six subfamilies according to amino acid sequence homology. The blue coloured shapes indicate the classical Rho protein subfamily groups (Rho, Rac, Cdc42). The green coloured shapes represent atypical Rho protein subfamilies (Rnd, RhoBTB and Miro) that lack GTPase activity. Dendrogram adapted from Bustelo *et al.* (2007) (143).

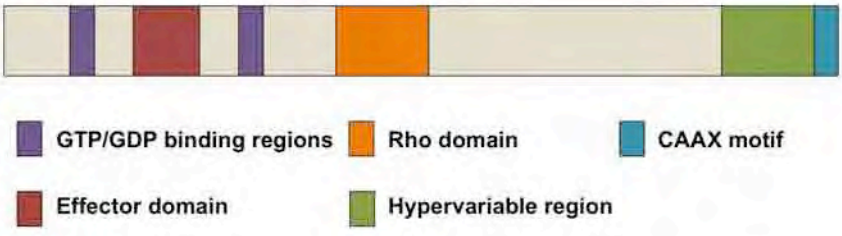

Figure 1.7 Core structural motifs of Rho GTPase proteins. Rho GTPase proteins typically contain a Rho domain, GTP/GDP binding regions, an effector domain, a C-terminal hypervariable region and a CAAX (C-cysteine, A-aliphatic amino acid, X-any amino acid) box motif.

1.4.3 Rho GTPase structure

Small Rho GTPases are highly conserved globular proteins made up of single six-stranded β sheets surrounded by five α-helices, with molecular masses of around 20-25 kDa (144). Rho proteins are defined by the presence of a Rho-type GTPase domain, which is typically sandwiched between short N- and C-terminal ends (142, 145). Rho proteins also contain amino acid residues responsible for guanosine triphosphate (GTP)/guanosine diphosphate (GDP) binding and GTPase activity (142). However, Rnd, RhoBTB and Miro subfamily members lack GTPase activity due to amino acid substitutions in their GTP/GDP binding regions and are considered atypical (figure 1.6) (145). Moreover, Rho GTPase proteins contain effector domains, important for activating downstream effector proteins (144).

Although Rho GTPases share 30-50% homology (146), there is great diversity between them at the C-terminal end, which is known as the hypervariable region (147). In addition, Rho GTPase proteins typically contain a cysteine residue fourth from the C-terminal end, also known as the CAAX (C-cysteine, A-aliphatic amino acid, X-any amino acid) motif (145). Since small GTPases are hydrophilic and do not contain transmembrane domains, the CAAX motif can be isoprenylated by prenyltransferase enzymes to allow them to interact with membranes (145, 147). Although Rho proteins are structurally and biochemically related, variations in their C-terminal ends localises them to specific compartments within the cell, which is vital for their distinct biological functions (144, 147). Even closely related Rho proteins are localised to very different cellular regions, for example, Rac1 is largely located at the plasma membrane but its close relative, Rac2, mainly localises to endomembranes (142). The typical domain structure of a Rho GTPase protein (from Rho, Rac or Cdc42 subfamilies) is depicted in figure 1.7

1.4.4 The GTPase cycle

Rho GTPases behave as ‘molecular switches’ that cycle between inactive GDP-bound and active GTP-bound states. Structural studies reveal that the exchange of GDP for GTP induces a conformational change in loop regions named switch I and switch II, which unmasks the effector domain (144, 146). Thus the conformation of GTP-bound Rho proteins allows them to interact with downstream effector proteins, which trigger various cellular responses, until GTP hydrolysis returns the switch back to the inactive state (137, 148).

1.4.5 Regulation of GTPase activity

The GTPase activation cycle is regulated by three classes of proteins; guanine nucleotide exchange factors (GEFs), GTPase-activating proteins (GAPs) and guanine nucleotide dissociation inhibitors (GDIs) (figure 1.8). GEFs promote the exchange of GDP for GTP and so activate the molecular switch, which leads to effector protein binding and propagation of downstream signalling (149, 150). GAPs inactivate Rho proteins by enhancing GTP hydrolysis, which leaves the molecule in the inactive GDP-bound state. This prevents effector binding and therefore shuts down signalling. GDIs bind to inactive GDP-bound forms of GTPases and prevent the exchange of GDP to GTP thus maintaining the inactive state. Since Rho GTPase activation is accompanied by intracellular translocation to membranes, GDIs also inhibit GTPase activity by masking their prenyl groups, which prevent them from localising to membranes (136). The human genome contains approximately 70 GEFs and around 80 GAPs for the Rho family of small GTPases, which demonstrates the complexity of Rho GTPase regulation in the cell (149). To date, only three GDIs for Rho proteins have been identified; RhoGDI-1, RhoGDI-2 and RhoGDI-3 (149, 151).

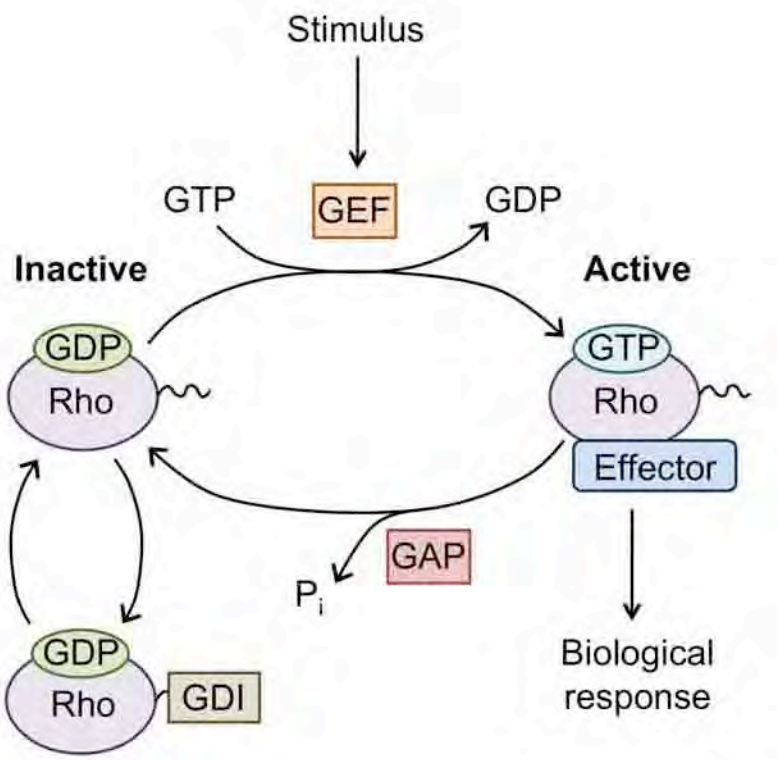

Figure 1.8 The GTPase cycle and its regulatory proteins. Rho GTPase proteins cycle between GDP-bound inactive and GTP-bound active states. In their active form, Rho GTPases can bind to effector molecules, which mediate downstream biological responses. Guanine nucleotide exchange factors (GEF) promote activation by catalysing the exchange of GDP for GTP. GTPase-activating proteins (GAP) inhibit Rho protein activation by enhancing the intrinsic GTPase activity to hydrolyse GTP into GDP, returning it to an inactive state. Guanine nucleotide dissociation inhibitors (GDI) maintain the GDP-bound form of GTPases, making it unable to interact with GEF proteins and cellular membranes.

1.4.6 Upstream activators

Rho proteins are often activated by soluble serum components such as growth factors, hormones and cytokines. These soluble factors signal through cell surface receptors, such as receptor tyrosine kinases, G-protein coupled receptors and cytokine receptors (105). The downstream signalling pathways of these ligand-bound receptors can sequentially act upon GEFs or GAPs to control the activation state of Rho GTPases (152, 153). Rho proteins can also be activated downstream of cell adhesion molecules, integrin receptors and mechanical stresses (tension, compression or shear stress).

1.4.7 Downstream effectors

Once activated, Rho GTPases can interact with a spectrum of intracellular effector proteins to activate a wide variety of signaling pathways and cellular responses. Over 50 target effectors have been identified at present, which include serine/threonine kinases (e.g., ROCK), tyrosine kinases (e.g., Src), lipid kinases (e.g., phosphatidylinositol 4-phosphate (PIP) 5-kinase), lipases (e.g., phospholipase-C), oxidases (e.g., NADPH) and scaffold proteins (e.g., Wiskott-Aldrich syndrome protein (WASP)) (143, 148, 154). Some of these downstream effectors can also sequentially activate further downstream proteins (155). Depending on their cellular context and the mechanism of activation, Rho proteins are capable of activating multiple types of effector proteins. Also distinct Rho proteins can activate identical effector proteins. This reflects the complex and diverse functional properties of Rho GTPases in cell biology.

1.4.8 Functions of Rho GTPases

Rho proteins are involved in regulating a plethora of biological processes such as cell cycle progression, gene transcription, cell polarity and vesicle trafficking (150). However, the major function of Rho GTPases is to regulate the assembly and organisation of the actin

cytoskeleton. Thus Rho proteins are essential mediators of cell processes that require cytoskeletal reorganisation such as cell motility and vascular remodeling. The role that Rho GTPases play in cell migration and in the vasculature will be discussed below.

1.4.8.1 Rho GTPases in cell migration

Cell migration is tightly controlled by the coordinated activity of Rho GTPase proteins (101, 133). Cdc42 is a key regulator of directional sensing and is responsible for the reorientation of the MTOC and Golgi apparatus-derived vesicle trafficking during cell polarisation (156) Moreover, Rac1 and Cdc42 are known to promote actin polymerisation and membrane protrusion formation, both fundamental processes for cell motility (157). Cdc42 promotes filopodia formation at the leading cell edge, whereas Rac1 activation triggers the formation of lamellipodia (158). ROCK, is a downstream effector protein of RhoA and activation of the RhoA-ROCK pathway stimulates the formation of stress fibres (134, 148, 154, 159-162). Actomyosin contractility downstream of RhoA is important for traction of the cell body and detachment of the trailing edge (133, 163, 164). In addition, Rac1 and Cdc42 modulate the formation of focal complexes at the leading cell edge, whereas RhoA regulates the formation and maintenance of focal adhesions at the cell body and trailing edge through the downstream activation of FAK (165).

Rho GTPases coordinate cell migration in a precise spatiotemporal manner. Rac1 and Cdc42 both localise to the leading cell edge, although Cdc42 is also found at the Golgi apparatus. Unlike Cdc42 and Rac1, RhoA localises mostly to the cytosol at the cell body and the trailing cell edge (112, 163). In addition, the Rho proteins activate each other in a hierarchial fashion: active Cdc42 stimulates the activation of Rac1, which both transiently inhibit RhoA activation.

1.4.8.2 Rho GTPases in endothelial cells and angiogenesis

Multiple reports have implicated Rho GTPase proteins as downstream effectors of VEGF-A/VEGFR-2 signalling in ECs (30). VEGF-A stimulation leads to the activation of Rac1, Cdc42 and RhoA within 1-5 minutes of stimulation, indicating that the downstream effectors of Rho proteins function as key mediators of VEGF-dependant processes that drive angiogenesis (140, 166). Reports have suggested that Rho GTPase proteins are essential for every stage of the angiogenesis cascade (table 1.2).

Rho proteins are capable of altering the expression and activity of pro-angiogenic and anti-angiogenic factors. Rho GTPases have been shown to upregulate the expression of VEGF-A and FGF-2 in ECs (167). In addition, Rac1, Cdc42 and RhoA have been shown to induce the transcriptional expression and secretion of MMPs in mural cells. Rac1 and Cdc42 have also been shown to promote the transcription and activity of TIMPs to inhibit basement membrane degradation, which is essential for ECM remodeling in the later stages of angiogenesis (140).

Given their role in regulating the actin cytoskeleton and cell motility, it is not surprising that Rho GTPases modulate EC migration and invasion. VEGF-A is known to induce Cdc42-dependant filopodia, Rac1-induced lamellipodia and RhoA-mediated contractility in ECs (30, 139, 140, 168). Rho proteins also have the ability to influence cell cycle regulation, which is essential for normal angiogenesis. Rac1, Cdc42 and RhoA have been shown to be essential for EC cycle progression from G1 (gap 1) to S (synthesis) phase (140). Furthermore, evidence shows that Rho GTPase activity is essential for EC morphogenesis, tube formation and capillary branching. Active forms of Rac1 and Cdc42 have been shown to increase EC lumen formation, microvessel branching and sprouting (140, 169-171). Studies have also shown a critical and selective role for RhoA activity in regulating angiogenesis. Some reports have suggested that RhoA inhibition impedes angiogenesis (172, 173), whereas some have claimed

Stage of angiogenesis	Rac1	Cdc42	RhoA
Matrix degradation	Increases MMP exp. & secretion, promotes latent increase in TIMP exp. & activity	Increases MMP exp. & secretion, promotes latent increase in TIMP exp. & activity	Increases MMP exp. & secretion
Migration	Membrane protrusion, focal complex turnover	Polarity, membrane protrusion, focal complex turnover	Retraction, focal adhesion turnover
Proliferation	Promotes G1/S transition	Promotes G1/S transition	Promotes G1/S transition
Tube formation	Promotes capillary & lumen formation	Promotes capillary & lumen formation	Promotes capillary formation & branching

Table 1.2 Rho GTPase roles during angiogenesis. (exp.; expression) Adapted from Bryan *et al.* (2007) (140).

that inhibition of RhoA signalling stimulates tube formation (92, 166, 174). Therefore, although it is clear that contractility is essential for EC motility and tubulogenesis, an over-abundance of actomyosin contractility can also disrupt these processes.

In recent years, a growing number of studies have also implicated Rho proteins as essential regulators of endothelial integrity and permeability (175-177). In EC monolayers, active RhoA binds to its effector protein ROCK and promotes an increase in stress fibre formation and actomyosin contractility. This contractile tension evokes the breakdown of cell-cell junctions, which leads to a disruption in the endothelial barrier and an increase in permeability (1, 178). A recent study by Tan *et al.* (2008) shows that specifically deleting the expression of Rac1 in ECs in mice (by using the Cre/Flox conditional knockout approach, under the control of Tie2 expression) causes embryonic lethally and defects in vascular development at around E9.5 (1, 171). Analysis of Rac1 deficient ECs revealed that cells failed

to form lamellipodia, required for proper cell-cell and cell-matrix interactions, resulting in impaired endothelial barrier function and vessel leakiness (171, 179). These findings provide evidence that Rac1 is essential for angiogenic vascular development and endothelium integrity through maintenance of adherens and tight junctions (180). As well as Rac1, Cdc42 also participates in the recovery of endothelial barrier integrity (181-183). After stimulation with thrombin (a protease involved in blood clotting which induces RhoA-mediated permeability), Cdc42 activation is delayed by an hour which coincides with the repair of junctional complexes (182). As already mentioned, Cdc42 plays an essential role in Golgi-derived vesicle trafficking. Thus, in response to breakdown of the endothelial barrier, Cdc42 controls the transport of junctional complex proteins towards the plasma membrane, which help to repair intercellular junctions (175, 184, 185). It has been well documented that Rac1 downregulates RhoA activity, which leads to reversal of the endothelial contractile response (186, 187). A recent study by Ramachandran *et al.* (2008) shows that expression of dominant active Cdc42 in ECs *in vivo* protects endothelial barrier integrity by inhibiting RhoA-dependent permeability (183).

Considering all the functions Rho GTPases regulate in ECs, it is not surprising that aberrant Rho GTPase signalling has been found to be involved in a wide range of vascular diseases such as atherosclerosis, hypertension and coronary/cerebral vasospasm (188, 189). In addition, Rho proteins and GEFs are found to be overexpressed in solid tumours (145, 190-196). Therefore, Rho protein signalling pathways are attractive targets for future anti-cancer therapy.

1.5 RhoJ

1.5.1 Overview

RhoJ, also known as TC10-like (TCL) is a little studied Rho GTPase protein that belongs to the Cdc42 subfamily group and is phylogenetically most closely related to TC10/RhoQ and Cdc42, sharing 85% and 78% amino acid identity, respectively (197). RhoJ is encoded by five exons, which span over 85 kb on human chromosome 14, which is the largest gene encoding a Rho GTPase at present (197). RhoJ has a classical domain structure with conserved GTP/GDP binding regions, GTPase activity and a CAAX box motif (197, 198).

1.5.2 Literature review of RhoJ

Vignal *et al.* identified RhoJ as a new Rho protein that had high sequence homology to TC10 and Cdc42 in 2000, (197). RhoJ was found to have a distinct mRNA expression pattern in mice compared to its closely related proteins; TC10 is found mainly in skeletal muscle, Cdc42 is ubiquitously expressed, and according to Vignal *et al*., RhoJ is highly expressed in heart (197, 199). They also compared the biochemical kinetics of TC10 to RhoJ and found that *in vitro* RhoJ exchanges GDP into GTP 40% more rapidly than TC10, suggesting that RhoJ may be predominantly GTP-bound *in vivo*. (197). Moreover, TC10, Cdc42 and RhoJ share a highly conserved effector domain and are able to bind to identical downstream effector proteins, which contain Cdc42/Rac1 interacting binding motif (CRIB) domains (197). Rac1 can also bind to effector proteins that contain CRIB domains, such as p21 activated kinase (PAK) and WASP. Despite its close relation to TC10 and Cdc42 and the ability to bind identical effector proteins, RhoJ overexpression did not induce filopodia formation like Cdc42 and TC10 (112, 197, 199). Instead, REF-52 fibroblasts that expressed constitutively active RhoJ promoted actin-rich ruffles on the dorsal membrane, large cytoplasmic vesicles, stress fibre reduction and motile cellular morphology (197).

In 2002, Chiang *et al.* demonstrated that the mouse homologue of RhoJ (also called TC10β) was activated by insulin in 3T3-L1 adipocytes (200). More recently, Nishizuka and others (2003 and 2010) showed a vital role for TC10β in the program of adipocyte differentiation in mouse *in vitro* (201, 202). The expression level of mouse RhoJ rose when preadipocyte cells were induced to differentiate into adipocytes and the expression of TC10β in NIH-3T3 fibroblasts, which normally do not differentiate into adipocytes, caused the accumulation of oil droplets and adipogenic markers (201).

In 2003, Toledo *et al.* showed that RhoJ may also be involved in controlling early endocytosis (203). RhoJ was found to co-localise with early/sorting endosomes markers in HeLa cells expressing myc-tagged RhoJ (203). Knockdown of RhoJ expression in HeLa cells perturbed transferrin (Tf) trafficking, whereby Tf release was slowed down. Overexpression of constitutively active RhoJ promoted accumulation of Tf in early/sorting endosomes and the normal release of Tf, suggesting that RhoJ is involved in endocytic vesicle movement (203).

Other studies have shown a role for RhoJ in f-actin reorganisation. Abe *et al.* (2003) reported loss of stress fibres in mouse fibroblasts that expressed dominant active RhoJ (198). In addition, Aspenstrom *et al.* (2004) observed lamellipodia formation and focal adhesion-like assemblies at the cell periphery of porcine aortic ECs that expressed constitutively active RhoJ (204). More recently, Billottet *et al.* (2008), showed that expression of the active form of RhoJ in porcine aortic ECs induced the formation of actin-rich adhesion assemblies known as podosomes (205). Thus like its famous siblings Rac1, Cdc42 and RhoA, RhoJ also plays a role in actin reorganisation in different cell types.

1.5.3 Discovery of RhoJ in endothelial cells

Using a bioinformatics approach, whereby publicly available endothelial cDNA libraries were *in silico* subtracted from non-endothelial libraries, our laboratory previously identified RhoJ as being highly expressed by human ECs (206). This finding was confirmed by looking at the mRNA expression level of RhoJ in various primary cell lines using quantitative PCR (206). High levels of RhoJ mRNA was found in human umbilical ECs (HUVEC) and human dermal microvascular ECs (HDMEC) but not in other cell types such as fibroblasts, epithelial cells, hepatocytes, lymphocytes and keratinocytes (figure 1.9). The bioinformatic analyses also suggested that RhoJ is the most abundantly expressed Rho GTPase protein in human umbilical vein ECs (206).

1.5.3.1 Hypothesis

With increasing evidence showing that Rho proteins are involved in regulating angiogenesis, the hypothesis being tested is that RhoJ signalling is important for aspects of EC biology associated with the angiogenic process.

1.6 Aims

The overall aims of this project were to investigate the function of RhoJ in tubulogenesis and EC motility *in vitro*, to explore the role of RhoJ during zebrafish development and to determine its mammalian expression profile. The methodologies used for each of these aims are outlined below.

1. Investigate the function of RhoJ in tubulogenesis and EC migration

RNA interference (RNAi) was used to silence RhoJ expression in primary ECs and *in vitro* methods were used to test the impact of RhoJ knockdown on endothelial tube formation,

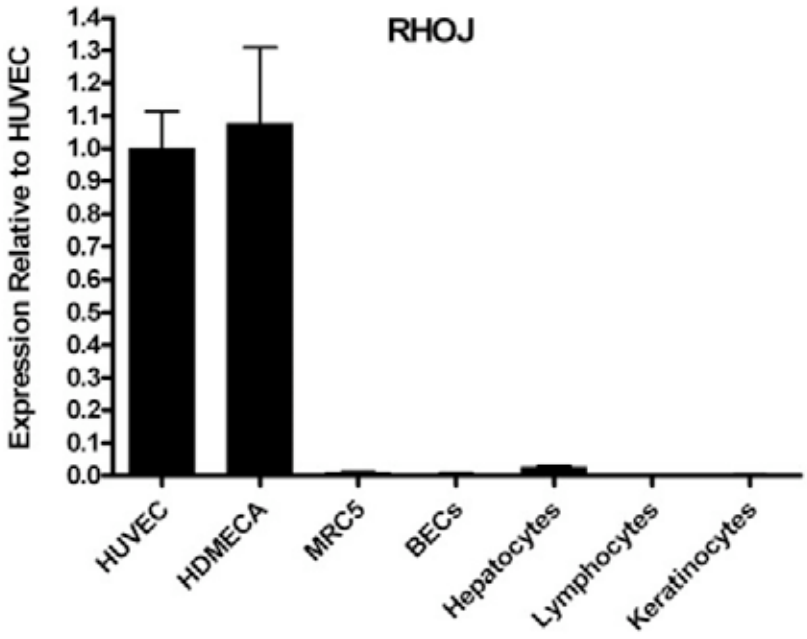

Figure 1.9 RhoJ is highly expressed in human endothelial cells. Quantitative PCR analysis of RhoJ mRNA expression in various normal human primary cell types: HUVEC; human umbilical vein endothelial cells, HDMEC; human dermal microvascular endothelial cells, MRC5; human lung fibroblasts, BECs; human bronchial epithelial cells, hepatocytes, peripheral blood lymphocytes and human adult epidermal keratinocytes**.** Graph taken from Herbert *et al.* (2008) (206).

migration and survival. The molecular mechanism of RhoJ function in EC motility was explored by analysing the effects of RhoJ knockdown/overexpression on aspects of cell migration, such as focal adhesion and stress fibre formation, and cell contractility.

2. Characterise the role of RhoJ during zebrafish embryogenesis

The temporal expression of RhoJ during zebrafish development was investigated using reverse transcription PCR analyses. The localisation of RhoJ expression during physiological embryonic angiogenesis was determined using *in situ* hybridization experiments. The function of RhoJ during zebrafish development was assessed by using morpholino technology to knockdown RhoJ expression *in vivo*.

3. Determine the expression profile of RhoJ in mammals

The localisation of RhoJ in human normal/cancerous tissues and mouse embryos during developmental angiogenesis was determined using *in situ* hybridization experiments. The tissue distribution profile of mammalian RhoJ was also examined using various cell lines and quantitative PCR/Western blotting analyses.

Chapter two

Materials and methods

2.1 Commonly used solutions and media

Buffers	Constituents
1 x Phosphate-buffered saline (PBS)	10 mM Na_2HPO_4, 1.76 mM KH_2PO_4, 2.7 mM KCl and 0.14 M NaCl, pH 7.4
NP40 (lgepal) lysis buffer	1% (v/v) NP40, 10 mM Tris pH 7.5, 150 mM NaCl, 1 mM EDTA pH 8, 0.01% (w/v) sodium azide and 1 x protease inhibitor cocktail
2 x SDS-PAGE sample loading buffer	100 mM Tris-HCl, pH 6.8, 20% (v/v) β-mercaptoethanol, 4% (w/v) SDS, 0.2% (w/v) bromophenol blue, 20% (v/v) glycerol
1 x Stacking gel buffer	125 mM Tris-HCl; pH 6.8, 0.1% SDS
1 x Resolving gel buffer	375 mM Tris-HCl; pH 8.8, 0.1% SDS
1 x SDS-PAGE running buffer	25 mM Tris, 250 mM glycine, 0.1% (w/v) SDS, pH 8.3
1 x Western blotting transfer buffer	6 mM Tris-base, 47.6 mM glycine, 20% (v/v) methanol, pH 8.3
Tris-Buffered Saline Tween-20 (TBST)	20 mM Tris-HCl, pH 7.5, 150 mM NaCl, 0.1% (v/v) tween-20
Western blotting blocking buffer	5% (w/v) dried skimmed milk in TBST
Tris-Borate-EDTA (TBE)	89 mM Tris, 89 mM Boric Acid, 2 mM EDTA
Tris-Acetate-EDTA (TAE)	40 mM Tris, 20 mM Acetic Acid, 1 mM EDTA

2.2 Commonly used reagents

All reagents listed below were purchased from Sigma, UK unless otherwise stated.

Ethylenediaminetetraacetic acid (EDTA)
Protease inhibitor cocktail
Bovine serum albumin (BSA)
Sodium azide
Paraformaldehyde (PFA)
TritonX-100
Ethanol/Methanol
Acetic acid

Deionised formamide
Citric acid
20 x saline-sodium-citrate (SSC)
N,N,N',N'-Tetramethylethylenediamine (TEMED) (Amresco, USA)
Bromophenol blue
Agarose
Igepal (NP40)
Tris-base
Ammonium persulphate (Amresco, USA)
Glycine
Tween-20
Heparin
Proteinase K
Sodium dodecyl sulphate (SDS)
Sodium chloride (NaCl)
β-mercaptoethanol
Glycerol
RNAse A
Isopropanol
Chloroform
CHAPS
Ponceau S
Boric acid

2.3 Antibodies and protein conjugates

Antibody/protein conjugate	Clone no./cat. no.	Immunogen	Isotype	Dilution and application	Source
Alexa Fluor 647 monoclonal mouse anti-human GM130	35/GM130	Rat GM130 aa. 869-982	IgG, κ	1:10 Immunofluorescence	BD Pharmingen, UK
Mouse monoclonal anti-human vinculin	hVIN-1	Human vinculin from uterus	IgG1	20 μg/mL Immunofluorescence	Sigma, UK
Mouse monoclonal anti-human phospho-FAK (pY397)	14/FAK (Y397)	Human FAK (pY397) peptide	IgG1	2.5 μg/mL Immunofluorescence	BD Pharmingen, UK
Rabbit polyclonal anti-human phospho-paxillin (Tyr118)	2541	Human paxillin Tyr118 residues	IgG1	2.8 μg/mL Immunofluorescence	Cell Signalling Technology, UK
Mouse monoclonal anti-human RhoJ	ab57584	Human RhoJ aa. 1-215	IgG1	1 μg/mL Western blotting	Abcam, Taiwan
Mouse monoclonal anti-human tubulin	DM1A	Chicken α-tubulin aa. 426-430	IgG1	100 ng/mL Western blotting	Sigma, UK
Mouse monoclonal anti-human β actin	AC-15	Human β-actin N-terminal peptide	IgG1	100 ng/mL Western blotting	Sigma, UK
Mouse monoclonal anti-human VE-Cadherin	BV9	Mouse VE-Cadherin aa1-486	IgG1	5 μg/mL Immunofluorescence	Dr. Maria Lampugnani, Italy
Goat polyclonal anti-mouse conjugated to HRP	P0447	Mouse IgG	Goat IgG-HRP	1 μg/mL Western blotting	Dako Cytomation, UK
Alexa Fluor 488 polyclonal goat anti-mouse	A11001	Mouse IgG	Goat IgG-FITC	4 μg/mL Immunofluorescence	Invitrogen, UK
Alexa Fluor 488 polyclonal donkey anti-rabbit	A21206	Rabbit IgG	Donkey IgG-FITC	4 μg/mL Immunofluorescence	Invitrogen, UK
Sheep polyclonal anti-digoxigenin conjugated to alkaline phosphatase	1333089	Digoxigenin	Sheep IgG fab fragments-AP	150 mU/mL Whole-mount ISH, 1500 mU/mL Fluorescent ISH	Roche, UK
Sheep polyclonal anti-digoxigenin conjugated to rhodamine	11207750910	Digoxigenin	Sheep IgG fab fragments-rhodamine	1 μg/mL Fluorescent ISH	Roche, UK
Ulex europaeus agglutinin I (UEAI) conjugated to FITC	FL-1061			20 μg/mL Fluorescent ISH	Vector Labs, UK
Phalloidin conjugated to rhodamine	R415			50 μg/mL Immunofluorescence	Sigma, UK
Annexin V conjugated to FITC	556420			1:20 FACS, 1:20 Immunofluorescence	BD Pharmingen, UK

2.4 DNA constructs

Gene	Gene region	PCR amplification of insert	Restriction sites used	Host vector	Source of vector	Application	Enzyme used for linearization	RNA polymerase used for *in vitro* transcription
Zebrafish RhoJ	1-681 of coding region	Amplified from cDNA of zebrafish embryos staged 23-26 hpf. Transformed into bacteria as per the instructions of ZeroBlunt® TOPO® Cloning kit.	5'-BamH1 and 3'-Not1	pCR®-Blunt II-TOPO® (kanamycin resistant)	Invitrogen	Whole-mount ISH probe	Antisense: BamH1 Sense: Not1	Antisense: T7 Sense: SP6
Zebrafish MyoD	18-1397 of NM_131262.2 mRNA	Amplified from cDNA of zebrafish embryos staged 23-26 hpf. Cloned by Dr. Rajeeb Swain following ZeroBlunt® TOPO® Cloning kit instructions.	5'-BamH1 and 3'-Not1	pCR®-Blunt II-TOPO® (kanamycin resistant)	Invitrogen	Whole-mount ISH probe	Antisense: BamH1 Sense: Not1	Antisense: T7 Sense: SP6
Mouse RhoJ	1-645 of coding region	Amplified from sEND cDNA	5'-EcoR1 and 3'HindIII	pGEM-3z (ampicillin resistant)	Promega	Whole-mount ISH probe	Antisense: EcoR1 Sense: HindIII	Antisense: SP6 Sense: T7
Mouse VWF	7838-8387 of NM_011708 mRNA	Amplified from sEND cDNA	5'-BamH1 and 3'-EcoR1	pGEM-3z (ampicillin resistant)	Promega	Whole-mount ISH probe	Antisense: BamH1 Sense: EcoR1	Antisense: T7 Sense: SP6
Human RhoJ	1-645 of coding region	Insert was subcloned from pGEX-2TK (originally cloned by Dr. Victoria Heath)	5'-BamH1 and 3'-EcoR1	pGEM-3z (ampicillin resistant)	Promega	Fluorescent ISH probe	Antisense: BamH1 Sense: EcoR1	Antisense: T7 Sense: SP6

2.5 Oligonucleotides

Gene	Oligonucleotide for quantitative PCR	Exiqon probe (human probe library)
Human β-Actin	Forward 5'-gcacccagcacaatgaaga-3'	63
	Reverse 5'-cgatccacacggagtacttg-3'	
Human RhoJ	Forward 5'-aaaccctgcctcttaccaca-3'	79
	Reverse 5'-catcacggagatcaatctgg-3'	
Human OAS1	Forward 5'-ggtggagttcgatgtgctg-3'	37
	Reverse 5'-aggtttatagccgccagtca-3'	
Human ISG20	Forward 5'-caccctcagcacatggt-3'	17
	Reverse 5'-tggaagtcgtgcttcaggt-3'	
Mouse HPRT	Forward 5'- gaagcggtagcactt-3'	69
	Reverse 5'-gttcatcatcgctaatcacgac-3'	
Mouse GAPDH	Forward 5'-aatgtgtccgtcgtggatct-3'	80
	Reverse 5'-gcttcaccaccttcttgatgt-3'	
Mouse RhoJ	Forward 5'-gatgagctacgccaacgac-3'	6
	Reverse 5'-cggtaactgcgtagtggtca-3'	
Gene	Oligonucleotide for reverse transcription PCR	Annealing temp (°C)
Zebrafish RhoJ (full length)	Forward 5'-ctatcatgcctacactcagctcg-3'	Forward - 58
	Reverse 5'-tcacacgagagcacaacagcac-3'	Reverse - 58
Zebrafish RhoJ (crossing exon boundary 1-2)	Forward 5'-cgcgaatgatgcttttcctg-3'	Forward - 58
	Reverse 5'-ccagcagtatcgtacaatccc-3'	Reverse - 58
Zebrafish RhoJ (crossing exon boundary 2-3)	Forward 5'-gaatgtaacagtatctgggagg-3'	Forward - 58
	Reverse 5'-gcagatgagaaaaacgtctgtg-3'	Reverse - 58
Zebrafish RhoJ (crossing exon boundary 3-5)	Forward 5'-gcctcatgtgccctatatcc-3'	Forward - 58
	Reverse 5'-ccgaacactccagatagcac-3'	Reverse - 58
Zebrafish EF1α	Forward 5'-caccctgggagtgaaaca-3'	Forward - 58
	Reverse 5'-acttgcaggcgatgtgagc-3'	Reverse - 58
Mouse VWF	Forward 5'-tagtagGGATCCgcgtggaggatgcagtgtttg-3'	Forward - 59
	Reverse 5'-tagtagGAATTCggtgcctggaattttcacg-3'	Reverse - 59

Oligonucleotides for quantitative PCR were designed by Roche Applied Science, UK. Quantitative PCR and reverse transcription PCR oligonucleotides were synthesised by Eurogentec, Belgium.

2.6 Cell biology

2.6.1 Cell culture

Primary isolates	Source
Human umbilical vein endothelial cells (HUVEC)	Isolated from umbilical cords obtained from Birmingham Women's Hospital, Birmingham, UK
Human pericytes from placenta (hPC-PL)	Promocell, UK
Human aortic smooth muscle cells (HASMC)	TCS Cell Works, USA
Cell lines	**Source**
Human microvascular endothelial cell line-1 (HMEC-1)	Ades *et al.* (1992) (207)
Mouse subcutaneous endothelial cell line (sEND)	Wagner *et al.* (1988, 1989) (208), (209)
Materials	**Source**
Media 199	Cancer Research UK and Sigma, UK
Dulbecco's modified eagle medium	Sigma, UK
Pericyte Growth Medium	Promocell, UK
Bovine brain extract	Bovine brains were obtained from Pel-Freez, USA. Brains were prepared as described by Maciag *et al.* (1979) (210).
Fetal calf serum	PAA, The Cell Culture Co., UK
L-glutamine	Sigma, UK
Heparin	Sigma, UK
Porcine skin gelatin	Sigma, UK
Trypsin-EDTA	Sigma, UK
FastRead Haemocytometer	Immune Systems, UK
Tryphan Blue	Sigma, UK
Leica DM IL inverted microscope	Leica Microsystems, USA
USB 2.0 2M Xli camera	Leica Microsystems, USA

Human umbilical cords were obtained from Birmingham Women's Health Care NHS Trust at delivery after mothers had given informed consent. Human umbilical vein ECs (HUVECs)

were isolated from umbilical cords by using collagenase type IA by Mr. James Beesley (laboratory manager) according to a standard protocol (211). HUVECs were cultured to around 80-90% confluence in Media 199 containing 4 mM L-glutamine, 90 µg/mL heparin, 10% (v/v) fetal calf serum (FCS) supplemented with bovine brain extract (prepared as described in (210)). Cells were plated in sterile plastic culture dishes that had been coated with 0.1% (w/v) gelatin. HUVEC were split at a ratio of 1:3 once cells were 80-90% confluent and were used between passages 1-6. Human pericytes derived from placenta (hPC-PL) were cultured to 90% confluence in uncoated sterile plastic culture dishes. Cells were grown in medium provided by Promocell, UK and split at a ratio of 1:3 once cells were 90% confluent and used between passages 2-4. Human aortic smooth muscle cells (HASMC) were cultured to 90% confluence in Media 199 supplemented with 4 mM L-glutamine and 10% (v/v) FCS. HASMC were seeded onto sterile plastic culture plates that were coated with 0.1% (w/v) gelatin. Cells were split at a ratio of 1:3 once 90% confluence was reached and used between passages 2-4. Immortalised human microvascular EC line-1 (HMEC-1) was derived from primary human dermal microvascular ECs (HDMEC), which were transfected with simian vacuolating virus 40 T antigen (SV40-T) by Ades *et al.* (1992) (207). HMEC-1 were obtained from Professor Kay Davies (University of Oxford) and were cultured in 0.1% (w/v) gelatin coated sterile plastic culture dishes in Dulbecco's modified eagle medium (DMEM), 4 mM L-glutamine and 10% FCS until 90% confluent. Cells were then split at a 1:3 ratio when 90% confluence was reached. An immortalised EC line derived from murine subcutaneous endothelium (sEND) was cultured in DMEM, 4 mM L-glutamine and 10% (v/v) FCS. This cell line expresses the polyoma virus middle T antigen, has a cobblestone-like morphology, expresses von Willebrand factor and causes hemangiomas *in vivo* (208), (209). Cells were plated in uncoated sterile plastic culture dishes and grown until confluent. sEND were split at a ratio of 1:10 once cells were 100% confluent.

All primary cells and cell lines were maintained in a humidified atmosphere with 5% CO_2 at 37℃. Once cells reached the desired confluence, cells were washed with 1 x phosphate-buffered saline (PBS) and incubated for 5 minutes at 37°C with 1 x trypsin-EDTA solution. Once cells detached from the culture dish they were recovered in complete media, pelleted at 350 RCF for 5 minutes and resuspended in fresh complete media. Cells were then plated out on to new sterile culture dishes for further cultivation.

2.6.2 Transfection of siRNA into mammalian cells

siRNA duplex	Sequence	Targeted nucleotides of coding region	Source
RhoJ duplex 1	5'-ccactgtgtttgaccacta-3'	155-174	Eurogentec, UK
RhoJ duplex 2	5'-agaaacctctcacttacga-3'	455- 474	Eurogentec, UK

Materials	Source
OptiMEM	Invitrogen, UK
Lipofectamine RNAi MAX	Invitrogen, UK
Negative control duplex	Eurogentec, UK

Small interfering RNA (siRNA) duplex 1 (D1) and duplex 2 (D2) were designed according to the criteria determined by Reynolds *et al.* (2004) (212), to the coding region of human RhoJ. A negative control duplex (NCD) was used that has no homology to any known sequence. The siRNA duplexes were made to working stocks of 20 μM in RNase-free water.

For transfecting cells with siRNA in 10 cm culture dishes, 1 x 10^6 cells were seeded on to gelatin-coated dishes one day before transfection. The following day, D1, D2 or NCD was diluted in 680 μL of optiMEM to give a final siRNA concentration of 10 nM because it was the lowest concentration to consistently produce complete knockdown of RhoJ protein (see

appendix 1 for titration of siRNA duplexes). In a separate tube, 10% (v/v) lipofectamine RNAiMAX was prepared in a total volume of 120 µL of optiMEM. After mixing gently, both mixtures were incubated at room temperature for 10 minutes. Then the two mixtures were combined to give a total volume of 800 µL, gently flicked and incubated for a further 10 minutes at room temperature. Meanwhile, the cells were washed twice with PBS before adding 3.2 mL optiMEM to the cells. The final transfection mix was then added to the plate to give a total volume of 4 mL. The plate was then tilted to ensure even distribution of the siRNA across the cell monolayer. Mock cells were transfected using the method above but with no siRNA included. The cells were incubated for 4 hours in 5% CO_2 at 37℃. The siRNA-containing medium was then replaced with fresh media. Cells were assayed 48-72 hours after the transfection. To transfect cells in 6 cm dishes, 6 well plates or 96 well plates the transfection mixes were scaled down according to the surface area of the culture dish being used. The table below shows the culture dish used for transfection and the number of cells transfected for each siRNA-knockdown experiment. Western blotting was performed for every transfection to validate successful knockdown of RhoJ protein.

Assay	Culture dish size	Number of cells
Two-dimensional Matrigel tube formation	10 cm plate	1×10^6
Three-dimensional tube formation	10 cm plate	1×10^6
Wound healing	6-well dish	3×10^5
Boyden chamber chemotaxis	10 cm plate	1×10^6
Dunn chamber chemotaxis	10 cm plate	1×10^6
Proliferation	10 cm plate	1×10^6
Cell cycle	96-well plate	2×10^3
Apoptosis	6 cm plate	3.6×10^5
Cell contraction assay	10 cm plate	1×10^6
Immunofluorescence	6 cm plate	3.6×10^5

2.6.3 *In vitro* functional studies

2.6.3.1 Tube formation

Materials	Source
BD Matrigel, basement membrane matrix	VWR, Canada
Cytodex-3 Beads	Amersham Pharmacia, UK
Aprotinin	Sigma, UK
Fibrinogen Type I	Sigma, UK
Thrombin	Sigma, UK

2.6.3.1.1 Two-dimensional Matrigel tube formation

To assay tube formation in two-dimensions, Matrigel was thawed overnight on ice at 4℃. The wells of a 12 well plate were wetted with PBS prior to adding 70 µL of Matrigel. The basement membrane extract was allowed to solidify at 37℃ for 30 minutes. Cells were harvested and seeded at a density of 1.4 x 10^5 (cell density and Matrigel thickness was optimised by Dr. Victoria Heath) on top of the Matrigel layer in 1 mL of culture medium (see appendix 2 for diagram of set up). Cells were then incubated in 5% CO_2 at 37℃ for a further 24 hours. Tube formation was observed by taking pictures at 10 and 24 hours post seeding using Leica DM IL microscope and USB 2.0 2M Xli camera. Quantitation was to count the number of nodes with either 1, 2, 3 or ≥4 branch points from five random fields of view for each condition at 10 and 24 hour time points. An example of node counting has been provided in appendix 2.

2.6.3.1.2 Three-dimensional tube formation

This method was adapted from that described by Nakatsu *et al.* (2007) (213). Two days after siRNA transfection, cells were harvested and counted to make a cell-bead suspension containing 10^6 HUVEC (a higher cell density was used because this ensured even coverage of

the beads) and 2,500 cytodex-3 micro-carrier beads in a final volume of 1.5 mL in sterile conical tubes. The mix was incubated for 4 hours in 5% CO_2 at 37℃ to allow the cells to adhere to the beads. During this incubation, every 20 minutes the tubes were flicked to ensure even coating of the beads with HUVEC. The coated beads were transferred to a T25 flask in 5 mL of HUVEC media and incubated overnight. The coated beads were transferred to a 15 mL conical tube and allowed to settle for 10 minutes. After aspirating the supernatant, the beads were resuspended in 1 mL of 2.9 mg/mL fibrinogen solution containing 0.15 Units/mL aprotinin. Polymerisation was induced by mixing 0.5 mL of fibrinogen/bead suspension with 6.2 µL of 0.625 Units/mL thrombin in a well of a 12-well plate. After a 10 minute incubation at room temperature, fibrin clots were generated and HUVEC media was added drop wise to the gel. The beads were incubated in 5% CO_2 at 37℃ and three-dimensional sprouting was observed over 7 days. Media was replaced every 2 days. To quantify sprouting, the number of sprouts per bead were counted, and beads were scored as having, <5, 5-10 or >10 sprouts.

2.6.3.2 Cell migration

Materials	Source
Mitomycin C	Sigma, UK
48-well Boyden chemotaxis chamber	Neuro Probe, USA
8µm pore polycarbonate nucleopore filters	Neuro Probe, USA
4',6-diamidino-2-phenylindole (DAPI)	Sigma, UK
Dunn chemotaxis chamber	Hawksley, UK
Zeiss Axiovert 200 inverted high-end microscope	Zeiss, UK
Coolsnap Photometrics camera	Photometrics, USA
Image J software	National Institutes of Health
Slidebook 4.2 software	Intelligent Imaging Innovations, USA

2.6.3.2.1 Scratch wound assay

In 0.1% (w/v) gelatin coated 6 well plates, ECs were seeded at cell density of 3 x 10^5 and incubated overnight. Cells were then transfected with siRNA duplexes and two days later horizontal pen marks were made along the bottom of the wells. Scratches perpendicular to the pen marks were made with 200 µL sterile pipette tips. Cell debris was washed off and fresh media containing 2.5 µg/mL mitomycin C was added (concentration optimised by Dr. Victoria Heath). Mitomycin C is a cell division inhibitor and was added to ensure that cell proliferation did not contribute to wound closure. Cells were incubated in 5% CO_2 at 37℃ for a further 24 hours. Cell migration was observed by taking pictures at 0, 4, 12 and 24 hours using Leica DM IL microscope and USB 2.0 2M Xli camera. To quantify wound closure, the areas of wounds were measured using Image J software. For each condition, the wounds at 0 hour time point were considered to have an area of 100%. The areas of the wounds at the subsequent time points therefore were divided by the area measured at 0 hour time point, and the percentage of the wound closure calculated.

2.6.3.2.2 Boyden chamber chemotaxis

Chemotaxis was assayed using a 48-well modified Boyden chamber (see appendix 3) (214) with 8 µm pore size polycarbonate nucleopore filters. Filters were coated with 0.1% (w/v) gelatin (recommended by Neuro Probe, USA) and placed over a lower chamber containing 30 µL per well of complete HUVEC media, which is supplemented with 10% (v/v) FCS and bovine brain extract (see appendix 3 for optimisation). Cells were rested in serum-free media for 15 minutes before the assay to enhance the response to the chemoattractant. Cells were harvested and 2 x 10^4 cells (cell density recommended by Neuro Probe, USA) were seeded per well of the upper chamber in 50 µL of Media 199 consisting of only 4 mM L-glutamine, 1% (v/v) FCS and no bovine brain extract. After 5 hours incubation in 5% CO_2 at 37℃, the

filters were removed. Cells were fixed in 100% methanol and stained with 100 ng/mL DAPI for 1 minute at room temperature. The filters were then washed with tap water and placed onto a glass slide and non-migrated cells were wiped away with a wet cotton swab. Cells that migrated through the pores towards the chemoattractant were viewed using Axiovert 100M confocal microscope and LSM 510 software. The sum of migrated cells in five random areas for each well was calculated for at least nine replicate wells of each condition. A schematic of the Boyden chamber assay can be found in appendix 3.

2.6.3.2.3 Dunn chamber chemotaxis

Live chemotaxis was analysed using Dunn chambers (215) and time-lapse microscopy (see appendix 4 for a schematic of the Dunn chamber). Alexandra Mazharian from The University of Birmingham, UK optimised this assay. Two days after siRNA transfection, 10^5 HUVEC were plated onto 0.1% (w/v) gelatin coated coverslips (22 mm x 22 mm) and left to adhere for 1 hour in 1% (v/v) FCS media with no bovine brain extract. The coverslips were then inverted onto the Dunn chamber. The chemoattractant (complete HUVEC media with 10% (v/v) FCS and bovine brain extract) was added to the outer well of the Dunn chamber. To set up a chemoattractant gradient, the inner ring was filled with control media (1% (v/v) FCS in Media 199 containing 4 mM L-glutamine and no bovine brain extract). The Dunn chamber was placed in a humidified chamber on a heated stage at 37°C in 5% CO_2 within an inverted microscope setup. Time-lapse images were digitally captured every 60 seconds for 4 hours. The cells that lay on the bridge between the two wells of the chamber were imaged using Axiovert 200 inverted high-end microscope, Coolsnap Photometrics camera and Slidebook 4.2 software. Migration paths of the cells were mapped using Image J to visualise the direction of migration.

2.6.3.3 Cell growth and survival

Materials	Source
Propidium iodide	Sigma, UK
Annexin V-FITC staining kit	BD Pharmingen, UK
10 x Binding Buffer (0.1 M Hepes pH 7.4, 1.4 M NaCl, 25 mM $CaCl_2$)	BD Pharmingen, UK
Tumour necrosis factor-α (TNFα)	Peprotech, UK
FACS-Becton Dickson FACSCalibur	Becton and Dickson, USA
Acumen® eX3 microplate cytometer	TTP Labtech Ltd, UK

2.6.3.3.1 Proliferation

Four hours after siRNA transfection, cells were harvested and 1.5 x 10^4 cells were seeded in 1 mL of media per well of a 24 well plate. Four plates were prepared to count the cells 1-4 days after seeding. For each plate, cells from each condition were plated in triplicate. To determine cell growth, the cells were harvested 1-4 days after seeding and the number of cells obtained from each well was counted using a haemocytometer with tryphan blue and Leica DM IL light microscope.

2.6.3.3.2 Cell cycle

HUVEC were transfected with siRNA in a 96 well plate. Three days later, cells were washed gently with PBS and fixed with ice cold 85% (v/v) ethanol for 10 minutes at room temperature. The cells were washed with PBS once again before being permeabilised with 0.1% (v/v) of triton-X-100 in PBS for 4 minutes at room temperature. Cells were then stained with 1 mg/mL propidium iodide (PI) in PBS containing 10 mg/mL RNAse A for 15 minutes at 37℃ in the dark. Since PI can also bind to double-stranded RNA, it is necessary to treat the cells with RNAse for optimal DNA resolution. The plate was then scanned and the cell cycle

was analysed using an Acumen® eX3 microplate cytometer. This method was optimised by Dr. Zsuzsanna Nagy and colleagues (University of Birmingham).

2.6.3.3.3 Apoptosis

Three days after siRNA transfection, apoptosis was assessed using an annexin V-FITC staining kit according to the manufacturer's instructions. Cells were stained in a volume of 100 µL of 1 x binding buffer that contained 5 µL annexin V-FITC and 50 ng/mL PI. Cells were stained in the dark for 15 minutes before being analysed by FACS-Becton Dickson FACSCalibur to detect apoptosis. An aliquot of 10,000 cells were analysed per condition. Green fluorescence was detected using FL1 channel and red fluorescence was detected using FL3 channel. Cell Quest Software (version 3.1f) displayed the results as a bivariate dot plot of annexin V (FL1) and PI (FL3) fluorescence intensity.

2.6.3.3.4 TNFα-induced apoptosis

Tumour necrosis factor-α (TNFα) is a potent inducer of EC apoptosis (216, 217). TNFα was used as a positive control for detecting endothelial apoptosis. Two days after siRNA transfection, 5 x 10^4 cells were plated on to gelatin-coated 13 mm glass coverslips in a 24-well plate. The following day, cells were washed with PBS and cells were treated with 0, 50, 75 or 100 ng/mL of TNFα in fresh HUVEC media for 4 hours at 5% CO_2 at 37℃. Dosage and incubation period was based on the studies of Petrache *et al.* (2001) (218). Following incubation, cells were fixed and stained with annexin V-FITC using the protocol stated in section 2.7.4. Changes made to the standard immunofluorescence protocol were that the cell permeabilisation step was omitted, 1 x binding buffer was used for annexin V binding and cells were not counterstained with DAPI.

2.6.3.4 Contractility

Materials	Source
Cell contraction assay	Cell Biolabs, Inc., UK
Y27632 (ROCK inhibitor)	Tocris Bioscience, UK
H1152 (ROCK inhibitor)	Tocris Bioscience, UK
Blebbistatin (non muscle myosin II inhibitor)	Tocris Bioscience, UK

2.6.3.4.1 Cell contraction assay

Using cell-populated collagen gels to measure contractility of human fibroblasts was first described by Bell *et al.* (1979) (219). Vernon and Sage (1996) (220) demonstrated that ECs also have the capability to contract collagen type I gels. To assay cell contraction, a collagen type I based cell contraction kit was set up according to the manufacturer's instructions. Twenty-four hours after siRNA transfection, cells were harvested and resuspended in complete HUVEC medium at 3 x 10^6 cells/mL. The collagen gel lattice was prepared by mixing 1 part of cell suspension with 4 parts of ice-cold 3 mg/mL collagen gel solution. A volume of 0.5 mL of the cell-collagen mixture was added to each well of a 24 well plate and incubated for 1 hr at 37°C in 5% CO_2. After collagen polymerisation, 1 mL of HUVEC medium was added drop wise to each collagen gel lattice. After two days, stress had developed in the collagen matrix. Therefore at this point, to initiate cell contraction, the attached collagen gels were gently released from the sides of the culture dishes with a sterile pipette tip. The degree of cell contraction was evaluated by measuring the diameter of the free-floating collagen gels after 5 days.

2.6.3.4.2 Inhibition of Rho-kinase and non-muscle myosin II

Rho-kinase (ROCK) inhibitors Y27632 and H1152 were used at a concentration of 10 µM. An inhibitor of non-muscle myosin II ATPase activity, blebbistatin, was used at a

concentration of 5 μM. The inhibitors were added to the media of *in vitro* functional assays such as two-dimensional Matrigel tube formation, wound healing, Boyden chemotaxis chamber and cell contraction assays. Drug concentrations were based on the work of Abraham *et al.* (2009) (221).

2.7 Protein analyses

2.7.1 Protein extraction

For protein expression analysis, 48-72 hours after siRNA transfection, approximately 2 x 10^5 cells were washed with PBS and lysed in 30 μL of NP40 (Igepal) lysis buffer. The lysates were vortexed for 10 seconds and left on ice for 30 minutes before being centrifuged at 14,000 RCF for 10 minutes at 4℃. An aliquot of the supernatant was used to determine the protein concentration of the cell lysate using DC BioRad protein assay (BioRad Laboratories, UK) according to the manufacturer's instructions. The remaining supernatant was transferred to a new tube containing an equal volume of 2 x SDS-PAGE sample buffer and stored at -20℃.

2.7.2 SDS-polyacrylamide gel electrophoresis

Materials	Source
30% (w/v) Acrylamide/Bisacrylamide (5:1)	National Diagnostics, UK
Precision plus protein standard 250 – 10 kDa	BioRad Laboratories, UK
XCell SureLock™ Mini-Cell electrophoresis apparatus	Invitrogen, UK

To denature the proteins for SDS-polyacrylamide gel electrophoresis (SDS-PAGE), the cell lysate was boiled at 100℃ for 5 minutes. Typically ~10 μg of protein lysate were separated by electrophoresis alongside protein standards (250-10 kDa) in polyacrylamide gels prepared

using 30% (w/v) Acrylamide/Bisacrylamide (5:1), 1 x stacking gel buffer or 1 x resolving gel buffer, 10% (w/v) ammonium persulphate, TEMED in distilled H_2O. Electrophoresis was performed in running buffer at 100 V using XCell SureLock™ Mini-Cell electrophoresis apparatus until the gel front had migrated to the bottom of the gel. The table below lists the volumes used to make a 12% resolving gel (6 mL) and a 5% stacking gel (2 mL).

Resolving gel	Volume (mL)
H_2O	2
30% (w/v) Acrylamide/Bisacrylamide (5:1)	2.4
Resolving gel buffer: 375 mM Tris-HCl; pH 8.8, 0.1% SDS	1.5
10% ammonium persulphate	0.06
TEMED	0.002
Stacking gel	**Volume (mL)**
H_2O	1.4
30% (w/v) Acrylamide/Bisacrylamide (5:1)	0.33
Stacking gel buffer: 125 mM Tris-HCl; pH 6.8, 0.1% SDS	0.25
10% ammonium persulphate	0.02
TEMED	0.002

2.7.3 Western blotting

Materials	Source
Polyvinylidene difluoride membranes	Immobilon-P, Millipore, USA
Chromatography paper (0.8 mm thickness)	Whatman, UK
Enhanced chemi-illuminescent substrate	Amersham Biosciences, UK
Hyperfilm ECL chemiluminescence film	Amersham Biosciences, UK
XCell II™ Blot Module wet transfer apparatus	Invitrogen, UK

Immediately after SDS-PAGE electrophoresis, proteins were transferred to polyvinylidene difluoride membranes. The polyvinylidene difluoride membranes were soaked in 100% methanol for 30 seconds and then soaked in transfer buffer for 5 minutes along with the SDS-

PAGE gels and chromatography paper. Wet transfer was performed with XCell II™ Blot Module wet transfer apparatus at 30 V for 1 hour at 4℃. To check for successful transfer, the membranes were stained with Ponceau S and then blocked for 1 hour at room temperature in blocking buffer. The membrane was then incubated overnight at 4℃ in primary antibody diluted in Tris-Buffered Saline Tween-20 (TBST) containing 3% (w/v) bovine serum albumin (BSA) and 0.01% (w/v) sodium azide. After washing the membrane 6 x 5 minutes with TBST, the appropriate secondary antibody conjugated to horseradish peroxidase (HRP) was diluted in blocking buffer and incubated with the membrane for 1 hour at room temperature. The membrane was then washed 6 x 5 minutes with TBST before being incubated for 1 minute with enhanced chemiluminescent substrate (ECL) at room temperature. The membrane was then exposed to Hyperfilm-ECL high performance chemiluminescence film.

2.7.4 Immunofluorescence

Materials	Source
13 mm glass coverslips, thickness no. 1.5	VWR Canlab, Canada
ProLong Gold Antifade reagent with DAPI®	Invitrogen, UK
Axiovert 100M confocal microscope/LSM 510 software	Carl Zeiss, Germany

Cells were gently washed with PBS and fixed with 4% (w/v) paraformaldehye (PFA) in PBS for 15 minutes. The cells were washed again before being permeabilised with 0.1% (v/v) triton-X-100 in PBS for 4 minutes. The cells were blocked in blocking buffer (3% (w/v) BSA, 10% (v/v) FCS, 0.1% (v/v) tween-20, 0.01% (w/v) sodium azide in PBS) for one hour at room temperature. The cells were then incubated for one hour at room temperature with the primary antibody diluted in blocking buffer. Cells were washed three times with PBS then incubated with the fluorophore conjugated secondary antibody and/or a protein-fluorophore conjugate

for 30 minutes at room temperature in blocking buffer. Cells were washed three times with PBS and once with H_2O. Coverslips were mounted onto microscope slides using ProLong Gold Antifade reagent with DAPI® and left in the dark at room temperature overnight. The following day, the edges of the coverslips were sealed using clear nail-varnish and stored at -20℃. Fluorescent staining was analysed using Axiovert 100M confocal microscope and LSM 510 software (Zeiss).

2.7.4.1 Wound healing

In order to fluorescently stain proteins during wound healing, two days after siRNA transfection, 5 x 10^4 cells were seeded onto 13 mm gelatin-coated glass coverslips in 24-well plates. The following day, the cells were wounded by scraping across the surface with 2 µL sterile pipette tips and washed once with PBS. Fresh media was added and the wounds were allowed to heal for 6 hours in 5% CO_2 at 37℃. The cells were then fixed and stained using the protocol above. Six hours was used as the time point for fixing because these wounds typically healed at 9 hours and six hours represented the 12-hour time point in the larger scale scratch wound assays.

Annexin V-FITC was used to stain cells undergoing apoptosis in wound healing assays. As a positive control for this experiment, apoptosis was induced using TNFα as described in section 2.6.3.3.4.

To visualise f-actin and focal adhesions during wound healing, cells were stained with primary anti-vinculin antibody and Alexa Fluor 488 secondary antibody and protein conjugate, phalloidin-TRITC. For f-actin quantification, LSM 510 confocal software was used to obtain the mean fluorescent intensity of the phalloidin-TRITC staining according to

the following equation: mean intensity = sum of (number of +ve pixels x intensity levels)/number of +ve pixels. Counting the areas of vinculin staining using the cell-counter plugin tool of ImageJ quantitated the numbers of focal adhesions. In both cases, 30 cells were analysed either from the wound edge or monolayer.

The Golgi apparatus was stained using Alexa Fluor 647 anti-GM130 antibody to determine whether cells were polarising in wound healing assays. To quantitate the position of the Golgi apparatus in migrating wound edge cells, cells were divided up into three 120° sectors centering on the nucleus, one of which faced the edge of the wound. Cells in which the Golgi apparatus was within the sector facing the wound were scored positive and counted.

For specific antibody information, refer to section 2.3.

2.7.4.2 Monolayer

Two days after siRNA transfection, 3 x 10^4 cells were plated onto gelatin-coated 13 mm glass coverslips. The cells were incubated in 5% CO_2 at 37℃ and grown to 100% confluence for 7 days. The cells were then fixed and stained using the protocol described in section 2.7.4 with anti-VE-Cadherin primary antibody and Alexa Fluor 488 secondary antibody. All PBS washes and incubations were made with PBS with calcium chloride and magnesium chloride (Sigma, UK) in order for the staining of VE-Cadherin with this antibody to work. For specific antibody information, refer to section 2.3.

2.7.4.3 Subconfluent cells

Two days after siRNA transfection, cells were harvested and seeded at 2 x 10^4 cells per gelatin-coated 13 mm glass coverslips. The cells were incubated in HUVEC medium for 4 hours at 37°C in 5% CO_2 to allow them for cells to adhere to the glass coverslips. The cells

were then fixed and stained according to the protocol described in section 2.7.4. Focal adhesions were stained by using either anti-vinculin, anti-phospho-FAK (pY397) or anti-phospho-paxillin (Tyr118) primary antibodies. For all primary antibodies, the secondary antibody used was Alexa Fluor 488. For focal adhesion quantitation, 30 cells from each condition were picked at random and the staining of the focal adhesion marker was counted using the cell-counter plugin tool of ImageJ. For specific antibody information, refer to section 2.3.

2.8 DNA protocols

2.8.1 Gel electrophoresis

Materials	Source
40% (w/v) Acrylamide/Bisacrylamide (29:1)	BioRad Laboratories
6 x gel-loading buffer	Promega, UK
100 bp/1kb DNA Ladders	Promega, UK
SYBR Safe DNA gel stain	Invitrogen, UK
Gene Genius Bio Imaging System and GeneSnap software	Syngene, UK

2.8.1.1 Neutral polyacrylamide gel electrophoresis

To separate double stranded DNA, non-denaturing polyacrylamide gels were made with 1.66 mL of 40% (w/v) acrylamide/bisacrylamide at a cross linker ratio of 29:1, 6.27 mL of H_2O, 2 mL of 5 x TBE, 70 µL of 10% (w/v) ammonium persulphate and 10 µL of TEMED. Gels were cast at 5% polyacrylamide with a separation range of 80–500 bp. Samples were loaded on to gel with 6 x gel-loading buffer alongside 100 bp/1 kb DNA ladders. The gels were run in 1 x TBE at 100 V using XCell SureLock™ Mini-Cell electrophoresis apparatus. Gels were stained after electrophoresis by immersion into 1 x TAE containing 2% (v/v) SYBR Safe DNA gel stain at room temperature for 1 hour.

2.8.1.2 DNA agarose gel electrophoresis

DNA gel electrophoresis was performed in 1-2% (w/v) agarose gels made up with TAE buffer containing SYBR Safe DNA gel stain diluted at 1:10,000. Samples were loaded using 6 x gel loading dye and DNA ladders of 100 bp and 1 kb were used as size markers. The gels were run in 1 x TAE buffer at 80 V. Gels were visualised and imaged using Gene Genius Bio Imaging System (Syngene, Cambridge, UK).

2.8.2 Cloning

Materials	Source
GeneJET™ Plasmid Miniprep Kit	Fermentas
QIAfilter Plasmid Maxiprep Kit	Qiagen, UK
QIAEX II Agarose Gel Extraction kit	Qiagen, UK
QIAquick PCR Purification Kit	Qiagen, UK
ZeroBlunt® TOPO® Cloning kit	Invitrogen, UK
10 x BSA	New England BioLabs, UK
T4 ligase /10 x T4 ligase buffer	New England BioLabs, UK
HindIII /10 x buffer 2	New England BioLabs, UK
Not1/10 x buffer 3	New England BioLabs, UK
EcoR1/EcoR1 buffer	Fermentas
BamH1/BamH1 buffer	Fermentas

2.8.2.1 Restriction digests and gel purification

Restriction enzyme digestion of purified RT-PCR-amplified DNA or host plasmid vector DNA was performed in a total volume of 50 µL. This consisted of 5 µL of 10 x enzyme buffer, 5 µL of 10 x BSA, 37.5 µL of 5 µg plasmid or PCR product DNA diluted in DEPC treated-H_20 and 2.5 µL of restriction enzyme at 20,000 U/mL. The mixture was then incubated for 2.5 hours at 37°C. The digested DNA fragments were run in broad lanes on a 1% (w/v) agarose gel and purified with QIAEX II agarose gel extraction kit according to

manufacturer's instructions.

2.8.2.2 DNA ligation

DNA inserts were ligated with appropriate plasmids using T4 ligase enzyme at 400,000 U/ml. A reaction volume of 20 µL was set up with 2 µL of enzyme, 2 µL 10 x T4 ligase buffer and 16 µL of insert:vector mix at a ratio of 3:1. Control ligations lacking insert were also prepared. Ligations were incubated at room temperature for 1 hour.

2.8.2.3 Extraction of plasmid DNA

For bacterial colony screening, 10 different colonies after heat-shock transformation of bacteria were incubated overnight at 37°C in 2 mL Luria-Bertani (LB) broth medium containing the required antibiotic. Plasmid DNA from 2 mL overnight cultures was isolated using the GeneJET™ Plasmid Miniprep Kit according to manufacturers instructions. To generate a large amount of plasmid DNA, corresponding bacteria of the miniprep incubation were incubated overnight in 200 mL of LB-broth medium with the same concentration of antibiotics. Plasmid DNA was purified using QIAfilter Plasmid Maxiprep Kit according to the manufacturer's instructions.

2.8.2.4 DNA sequencing

All cloned constructs were verified by sequencing using the plasmid to profile service of the University of Birmingham according to their instructions.

2.9 Microbiology

Materials	Source
Escherichia coli subcloning efficiency™ DH5α™	Invitrogen, UK

α-select competent cells gold efficiency	Bioline, UK
Cellstar incubator	Borolabs Ltd., UK
Orbital shaker	Sanyo Gallenkamp, UK
Ampicillin 100 µg/mL	Sigma, UK
Kanamycin 50 µg/mL	Sigma, UK
Liquid SOC medium	Invitrogen, UK

Buffers	Constituents
LB broth	1% (w/v) bacto-tryptone, 0.5% (w/v) bacto-yeast extract, 1% (w/v) NaCl in H_20
LB agar	1% (w/v) bacto-tryptone, 0.5% (w/v) bacto-yeast extract, 1% (w/v) NaCl, 0.1% (w/v) bacto-agar in H_20

2.9.1 Bacterial culture

Bacteria (Escherichia coli (E.coli) subcloning efficiency DH5α™ or α-select competent cells gold efficiency) were cultured at 37°C either as colonies on LB-agar plates in a Cellstar incubator or in LB-broth medium in an orbital shaker.

2.9.2 Heat-shock transformation of bacteria

Plasmid DNA or 5 µL of a ligation mix were added to 25 µL of chemically competent E.coli subcloning efficiency DH5α™ or α-select gold efficiency bacteria. Cells were incubated for 15 minutes on ice, then at 42°C for 30 seconds and placed on ice again for 2 minutes. After adding 500 µL LB-broth medium, cells were incubated at 37°C shaking for 1 hour and plated on LB-agar plates containing the required antibiotic. The plates were then incubated at 37°C overnight.

2.9.4 Preparation of glycerol stocks

500 µL cultures of E.coli cells transformed with plasmids of interest in LB-broth medium were mixed with the same volume of 30% (v/v) glycerol solution in a cryotube. The tube was placed in a dry ice/isopropanol bath until the bacteria were frozen and then stored at –80°C.

2.10 RNA analyses

2.10.1 RNA extraction

To extract total cellular RNA, approximately 2 x 10^5 cells in a well of a 6 well dish were lysed with 1 mL of TRI reagent (Sigma, UK). Cells were homogenised by pipetting up and down using a 1 mL pipette then incubated for 5 minutes at room temperature. The homogenate was then transferred into a new tube containing 200 µL chloroform (Sigma, UK). Tubes were shaken vigorously for 15 seconds, incubated for 10 minutes at room temperature and centrifuged at 12,000 RCF for 15 minutes at 4℃. Following centrifugation, the mixture separated into a lower red phenol-chloroform phase, interphase and a colorless upper aqueous phase. The upper aqueous phase containing the RNA was removed and mixed with 0.5 mL isopropanol and incubated for 10 minutes at room temperature. To precipitate the RNA, the solution was centrifuged at 12,000 RCF for 10 minutes at 4℃. The supernatant was removed and the pellet was washed with 1 mL of 75% (v/v) ethanol and centrifuged at 12, 000 RCF for 5 minutes at 4℃. The ethanol wash was removed and the RNA pellet was briefly air-dried. RNA was dissolved in water made RNAse-free by diethyl pyrocarbonate (DEPC) treatment. To check RNA quality, total RNA was run on a 1% (w/v) agarose gel and the RNA concentration was measured by using NanoDrop ND-1000 spectrophotometer (Labtech, UK).

2.10.2 Generation of cDNA

Materials	Source
High capacity cDNA Archive Kit	Applied Biosystem, USA
SuperScript III First-Strand Synthesis System	Invitrogen, UK

Total complementary DNA (cDNA) was generated from RNA using High Capacity cDNA Archive kit (RNA obtained from primary cells or cell lines) or SuperScript III First-Strand Synthesis System kit (RNA obtained from whole zebrafish embryos) according to the manufacturer's instructions. Both kits use random hexamer primers to generate cDNA. In each case, 3 µg of isolated RNA was converted to cDNA in a reaction volume of 30 µL. For reverse transcription PCR, each RNA sample was also used to generate a reverse transcription control (reaction without reverse transcriptase enzyme).

2.10.3 Real time quantitative PCR

Materials	Source
Sensimix™	Quantace, UK
Universal ProbeLibrary set, Human	Roche Applied Science, UK
Rotor-Gene RG-3000 qPCR machine	Corbett Research Ltd, Australia
Rotor-Gene 6 software	Corbett Research Ltd, Australia

Real time quantitative PCR (qPCR) was performed using a probe-based system developed by Exiqon and Roche Applied Science. Forward and reverse primers were designed using the Roche web based tool, which if possible would position the PCR product across an exon boundary. cDNA was diluted twenty fold and 10 µL of this was used for every 25 µL of PCR reaction mix (12.5 µL of 2 x qPCR Master mix, 1 µL of 10 µM forward primer, 1 µL of 10 µM reverse primer, 0.25 µL of the corresponding probe and 0.25 µL of deionised water). The PCR was conducted using an initial denaturing interval at 95℃ for 10 minutes followed by 40

cycles of 95℃ for 15 seconds and 60℃ for 45 seconds using Rotor-Gene RG-3000. Expression levels were determined by comparing the results to standard curves generated by Rotor-Gene 6 software from serial dilutions that were made of a known amount of cDNA. To accurately quantify gene expression, the expression level of the gene of interest was divided by the expression level of the housekeeping gene. This method of normalisation permits accurate comparison of expression of the gene of interest between different samples.

2.10.4 Reverse transcription PCR

Materials	Source
Phusion High-Fidelity DNA Polymerase	New England BioLabs , UK
5 x High-Fidelity Buffer	New England BioLabs, UK
100mM Deoxynucleotide triphosphate mix	Bioline, UK
PTC-225 Peltier Thermal Cycler for RT-PCR	MJ Research, UK

To generate inserts for cloning into various vectors, reverse transcription PCR (RT-PCR) was performed in a total volume of 50 µL. 50 µL reaction mixes contained the following: 34 µL of water, 10 µL of 5 x Phusion High Fidelity Buffer, 1 µL of 10 mM dNTP mix, 1 µL of each primer (50 µM) and 1 µL of Phusion High-Fidelity DNA Polymerase. Finally 2 µL of template was added. For the no template control, template was omitted. PCR reactions were performed using Peltier Thermal Cycler set at an initial denaturation step of 98ºC for 30 seconds, then 24 cycles of denaturation at 98℃ for 30 seconds, annealing at 58-60℃ for 30 seconds (this step is primer dependant) and 72℃ for x minutes (where x = the length in kilobases of the region to be amplified). A final extension step of 72ºC for 10 minutes was included. PCR products for cloning were purified using QIAquick PCR Purification Kit according to the manufacturer's instructions. The whole PCR product was loaded on to an agarose gel and gel electrophoresis was performed as mentioned in section 2.8.1.2. The band

of interest was cut out and obtained for cloning using QIAEX II Agarose Gel Extraction kit from Qiagen.

To investigate whether RhoJ was expressed in zebrafish cDNA, reverse transcription PCR (RT-PCR) was performed in a total volume of 20 µL. The reaction mixes contained the following: 8.5 µL of water, 4 µL of 5 x Phusion High Fidelity Buffer, 4 µL of 1 mM dNTP mix, 0.5 µL of each primer (10 µM) and 0.5 µL of Phusion High-Fidelity DNA Polymerase. Finally 2 µL of template was added. For the no template control, template was omitted. PCR reactions were performed using Peltier Thermal Cycler set at an initial denaturation step of 98ºC for 30 seconds, then 30 cycles of denaturation at 98℃ for 10 seconds, annealing at 60℃ for 30 seconds and 72℃ for 30 seconds. A final extension step of 72ºC for 10 minutes was included. PCR products were loaded on to agarose gels and gel electrophoresis was performed as mentioned in section 2.8.1.2. Bands were visualised and imaged using Gene Genius Bio Imaging System (Syngene, Cambridge, UK).

2.10.5 *In situ* hybridization

2.10.5.1 DEPC treatment

Diethyl Pyrocarbonate (DEPC) (Sigma, UK) is a non-specific inhibitor of RNAses. DEPC treatment to water and PBS solutions involved adding 0.1% (v/v) DEPC to water and shaking vigorously for 15 seconds. The solution was then kept at room temperature for up to 16 hours before autoclaving.

2.10.5.2 Riboprobe synthesis

Materials	Source
QIAquick PCR purification kit	Qiagen

10 x DIG RNA Labeling Mix	Roche Applied Science, UK
10 x Transcription Buffer	Roche Applied Science, UK
SP6 RNA polymerase	Roche Applied Science, UK
T7 RNA polymerase	Roche Applied Science, UK
RNAse inhibitor	Roche Applied Science, UK
DNAse I	Fermentas, UK
Mini Quick Spin Columns	Roche Applied Science, UK

Plasmids containing the coding region of the gene of interest were linearised to generate templates for sense and antisense probe generation. The linearised DNA was then purified from the enzymatic reaction with QIAquick PCR purification kit according to the manufacturer's instructions and the concentration of DNA was measured using NanoDrop ND-1000 spectrophotometer. 1 µg of linearised DNA was transcribed and labelled with digoxigenin using 2 µL of 10 x transcription buffer, 2 µL 10 x DIG labelling mix, 1 µL T7/SP6 RNA polymerase, 1 µL RNAse inhibitor and the volume was made up to 20 µL with nuclease-free water. The reaction mix was incubated at 37°C for 2.5 hours. After *in vitro* transcription, 1 µL of DNAse I was added to the reaction mix to digest the linearised DNA. To determine if the reaction was successful, 1 µL of the reaction mix was loaded on a 1% (w/v) agarose gel and then the probe was purified using mini quick spin columns. The concentration of RNA was then measured using NanoDrop ND-1000 spectrophotometer.

2.10.5.3 Whole-mount *in situ* hybridization

Materials	Source
C57BL6 mice	Biomedical Services Unit at The University of Birmingham.
AB wild-type zebrafish	Strain from Max Planck Institute of Developmental Biology, Germany.
Glutaldehyde	Sigma, UK

Boehringer blocking reagent	Roche Applied Science, UK
Torula RNA	Sigma, UK
Heat inactivated goat serum	Sigma, UK
BM Purple substrate	Roche Applied Science, UK
Leica MZ16 stereomicroscope/USB 2.0 2M Xli camera	Leica Microsystems, USA

Buffers	Constituents
Phosphate buffered saline tween-20 (PBST)	0.01 M phosphate buffer, 0.0027 M KCl and 0.137 M NaCl, pH 7.4 with 0.1% tween-20
Hybridization buffer	50% deionised formamide, 1% (w/v) blocking reagent, 5 x SSC, 0.1 mg/mL heparin, 1 mg/mL torula RNA, 0.1% (w/v) CHAPS, adjusted to pH 5.5 with 1 M citric acid
Maleic Acid Buffer– tween 20 (MABT)	0.1 M Maleic acid, 0.15 M NaCl, pH 7.5 using NaOH
Antibody buffer	10% (v/v) heat inactivated serum, 1% (w/v) blocking reagent in MABT
AP1 buffer	0.1 M NaCl, 0.1 M Tris pH 9.5, 50 mM $MgCl_2$
Stop solution	100 mM Tris pH 7.4, 1 mM EDTA

2.10.5.3.1 Zebrafish embryo preparation

Wild-type zebrafish AB strain was obtained from Max Planck Institute of Developmental Biology, Germany. Dr. Rajeeb Swain from University of Birmingham maintained the fish strain using the facilities at the Biomedical Services Unit (BMSU) at the University of Birmingham. The fish were raised at 28°C on a 14 hour light and 10 hour dark cycle. The night before eggs were required, tanks were filled with room temperature water. Male and female fish were added to the tanks but separated from one another by a divider in the tank. The next morning, the dividers were removed and fertilised eggs were collected from the bottom of the tanks 30 minutes–1 hour after mating. These embryos were then grown in Hank's buffer at 28°C to different stages up until 48 hours post fertilisation (hpf). To prevent

pigmentation from forming and thus reducing transparency of the fish, 1 mL of 50 x propylthiouracil (PTU) was added to 10 mL of Hank's buffer containing 24 hpf embryos. Embryos for *in situ* hybridization experiments were dechorionated and fixed in 4% (w/v) PFA at 4°C overnight whilst gently rocking. The embryos were then washed with DEPC-treated PBS before being dehydrated through sequential 5 minute incubations at room temperature in 1 mL 25%, 50%, 75% and then 100% (v/v) methanol in DEPC-treated PBS with 0.1% (v/v) tween-20 (PBST) and stored at -20°C until needed.

2.10.5.3.2 Zebrafish whole-mount in situ hybridization

Zebrafish whole-mount *in situ* hybridization protocol was adapted from the protocol described by Patient *et al.* (2005) (222). Embryos stored in 100% methanol were rehydrated back through sequential 5 minute incubations at room temperature in 1 mL 75%, 50% and then 25% (v/v) methanol in PBST and then 5 minutes in 100% PBST with gentle rocking for all incubations. Embryos at 24 hpf were then digested with 10 µg/mL of proteinase K in PBST for 20 minutes (48 hpf embryos were incubated with 10 µg/mL of proteinase K in PBST for 30 minutes) at room temperature before being re-fixed in 4% (w/v) PFA in PBS for 20 minutes. The embryos were washed 5 x 5 minutes with PBST. The embryos were then equilibrated into hybridization buffer with a 5 minute wash with 50% PBST/50% hybridization buffer followed by 1 hour in 100% hybridization buffer at 65°C. This was replaced with fresh hybridization buffer for another 2 hours before adding 1 mL of fresh hybridization buffer containing 500 ng of riboprobe to the embryos and incubating overnight at 65°C.

The following day, the riboprobe mix was removed and the embryos were washed at 65°C with all saline-sodium citrate (SSC) buffer solutions containing 0.1% (v/v) tween-20 as

follows: 10 minutes incubations at room temperature in 100%, 75%, 50% and 25% hybridization buffer in 2 x SSC. The embryos were then washed once for 10 minutes at 65°C with 2 x SSC and 4 x 15 minutes at 65°C with 0.2 x SSC. The embryos were washed further with 5 minute incubations at room temperature in 25%, 50%, 75% and 100% MABT in 0.2 x SSC. Embryos were then washed in 100% MABT for 5 minutes at room temperature. Embryos were blocked for 1 hour at room temperature with gentle agitation in antibody buffer, which consisted of 2% (w/v) Boehringer blocking reagent (BBR) and 5% (v/v) heat inactivated goat serum in MABT. This was replaced with fresh antibody buffer containing 150 mU/mL anti-digoxigenin antibody conjugated to alkaline phosphatase and embryos were left in this buffer overnight at 4°C with gentle agitation.

The embryos were brought back to room temperature for 1 hour then washed 8 x 15 minutes with MABT. Embryos were washed 2 x 10 minutes in AP1 buffer at room temperature. The AP1 buffer was replaced with 1 mL of BM purple and incubated in the dark until a purple signal developed. The reaction was stopped by washing the embryos 2 x 15 minutes in stop solution at room temperature and dehydrated through a methanol series to 100% methanol as detailed above. Embryos were viewed and imaged using Leica MZ16 stereomicroscope and USB 2.0 2M Xli camera and stored at 4°C indefinitely.

2.10.5.3.3 Zebrafish sections

Twenty-four hours post fertilisation zebrafish embryos used in whole-mount *in situ* hybridization experiments were sent to Cancer Research UK (London central services) where they were paraffin wax embedded, formalin fixed and cut into 1 µm transverse sections.

2.10.5.3.4 Mouse embryo preparation

Mouse embryos were collected from matings of C57Bl6 mice at embryonic day (E) 9.5. Embryos were staged by assigning noon of the day that a vaginal plug is found as E0.5. Biomedical Services Unit (BMSU) at the University of Birmingham set up the matings and culled the pregnant female mice on E9.5. Once culled, the embryos from the pregnant mother were extracted immediately. The embryos were dissected from the mother by removing the uterus and trimming the mesometrium. The decidual swelling was then removed from the uterus and placed in ice cold PBS. The embryos were carefully removed from the deciduas before removing the thin Deichert's membrane from the embryos. The embryos were immediately transferred to freshly prepared 4% (w/v) PFA and incubated at 4°C overnight whilst gently rocking. The embryos were then washed with DEPC-treated PBS before being dehydrated through sequential 5 minute incubations at room temperature in 1 mL 25%, 50%, 75% and then 100% (v/v) methanol in PBST and stored at -20°C.

2.10.5.3.5 Mouse whole-mount in situ hybridization

Mouse whole-mount *in situ* hybridization protocol was adapted from the protocol described by Piette *et al.* (2008) (223). The mouse embryos were rehydrated back through sequential 5 minute incubations at room temperature in 1 mL 75%, 50% and then 25% (v/v) methanol in PBST and then 5 minutes in 100% PBST with gentle rocking for all incubations. The embryos were then digested with 10 µg/mL of proteinase K in PBST for 15 minutes at room temperature and washed once with 2 mg/mL glycine in PBST. Embryos were rinsed once with PBST and washed a further 2 x 5 minutes with PBST before being re-fixed in 4% (w/v) PFA/0.2% (v/v) glutaldehyde in PBS for 20 minutes. The embryos were washed 2 x 5 minutes with PBST and washed once with 50% hybridization buffer/50% PBST for 3 minutes at room temperature. The embryos were washed once in 100% hybridization buffer for 3

minutes at room temperature. This was then replaced with 400 µL of fresh hybridization buffer and the embryos were prehybridized at 65°C for 3 hours. 500 ng of riboprobe was added to 100 µL of hybridization buffer and denatured at 95°C for 5 minutes. This riboprobe-hybridization buffer mix was added to the embryos to bring to a total volume of 500 µL of hybridization buffer and embryos were incubated overnight at 65°C.

The following day, the riboprobe mix was removed and the embryos were washed in 800 µL of hybridization buffer for 5 minutes at 70°C. Added to this solution was 400 µL of 2 x SSC pH 4.5 which was incubated for 5 minutes at 70°C (this step was repeated 3 times leading to a total volume of 2 mL). The mix was removed and the embryos were incubated in 2 x SSC pH 7/0.1% (w/v) CHAPS for 30 minutes at 70°C. The embryos were then washed with MABT in the following order: 2 x 10 minutes with MABT at room temperature, 2 x 30 minutes MABT at 70°C, 2 x 10 minutes PBS at room temperature and finally for 5 minutes in PBST. Embryos were blocked in antibody buffer for at 2 hours at 4°C. This was removed and replaced with antibody buffer containing preblocked 1500 mU/mL anti-digoxigenin conjugated to alkaline phosphatase antibody and incubated overnight at 4°C whilst rocking gently.

Embryos were rinsed and then washed 4 x 45 minutes with 4 mL of PBST/0.1% (w/v) BSA at room temperature. Embryos were then washed 2 x 30 minutes in PBST and then 2 x 10 minutes in AP1 buffer at room temperature. The AP1 buffer was replaced with 1 mL of BM purple and incubated in the dark until a purple signal developed. The reaction was stopped by washing the embryos 2 x 15 minutes in stop solution at room temperature and dehydrated through a methanol series to 100% methanol as detailed above. Embryos were viewed and imaged using Leica MZ16 stereomicroscope and USB 2.0 2M Xli camera and stored at 4°C indefinitely.

2.10.5.4 Fluorescent *in situ* hybridization on human tissue sections

Materials	Source
Paraffin embedded tissue sections	Cancer Research UK histology service, UK or Superbiochips Inc., Korea
Histoclear	National Diagnostics, UK
Sodium phosphate	Sigma, UK
Dextran sulphate	Sigma, UK
Hybriwell hybridization sealing systems	Invitrogen, UK
PCR express thermal cycler	Thermo Hybaid, UK
ProLong Gold Antifade reagent with DAPI®	Invitrogen, UK
Axiovert 100M confocal microscope/LSM 510 software	Carl Zeiss, Germany
Buffers	**Constituents**
Phosphate buffered saline – tween 20 (PBST)	0.01 M phosphate buffer, 0.0027 M KCl and 0.137 M NaCl, pH 7.4 with 0.1% (v/v) Tween-20
Hybridization buffer	50% (v/v) deionised formamide, 2 x SSC, 0.005 M sodium phosphate, 10% (w/v) dextran sulphate, 500 ng digoxigenin labelled riboprobe in nuclease-free H2O
Blocking buffer	1/20 fetal calf serum in PBST

Following removal of paraffin with Histoclear for 3 x 5 minutes, tissues were rehydrated back through sequential 5 minute incubations at room temperature in 100%, 75%, and then 25% (v/v) ethanol in H_2O. Tissues were then washed for 1 minute in H_2O and 10 minutes in PBS at room temperature. Tissues were re-fixed in 4% (w/v) PFA in PBS for 10 minutes at room temperature. Sections were then washed for 30 minutes with PBS at 37°C to ensure the right temperature for digestion. The tissue sections were then digested with 0.2% (v/v) trypsin in PBS for 10 minutes at 37°C. Following digestion, sections were rinsed once with PBS and then dehydrated through sequential 5 minute incubations at room temperature in 25%, 75%

and then 100% (v/v) ethanol in H_2O. Slides were allowed to air dry for 3 minutes before adding 50 µL of hybridization buffer per slide. Sections were completely covered with RNAse-free hybriwell hybridization sealing systems. The probe was then denatured by heating the slide to 80°C for 75 seconds using PCR Express Thermal Cycler before being incubated overnight at 37°C. The following day, the hyrbiwells were removed and sections were gently rinsed in 2 x SSC with 0.1% (v/v) tween-20. Tissues were then washed in 0.1 x SSC for 30 minutes at 68°C. Tissues were treated with 0.1 mg/mL RNAse A for 15 minutes at room temperature then rinsed three times with PBST. Sections were blocked in blocking buffer for 1 hour at room temperature. Tissue sections were then probed with 20 µg/mL of *Ulex europeaus* agglutinin I (UEAI) conjugated to fluorescein and 1 µg/mL anti-digoxigenin conjugated to rhodamine in blocking buffer for 1 hour at room temperature. Sections were rinsed three times with PBST and then once with H_2O. Slides were permanently mounted with Anti-Fade Prolong Gold with DAPI and sections were analysed using Axiovert 100M laser scanning confocal microscope.

2.11 *In vivo* studies

Materials	Source
Fli1-GFP transgenic zebrafish	Strain obtained from Brant M. Weinstein (224)
Phenol red	Sigma, UK
50 x Propylthiouracil (PTU)	Sigma, UK
Hank's buffer	Sigma, UK
Microinjection apparatus	Narishige, Japan
Morpholino	**Sequence**
Zebrafish RhoJ translation blocker	5'-tacttttcgagctgagtgtaggcat-3'
Zebrafish RhoJ splice blocker – targeting Exon2 Intron2 splice junction	5'-ccttaggagaattaactcacttgtc-3'

Fli1-GFP transgenic zebrafish were obtained from Brant M. Weinstein (224) and maintained by Dr. Rajeeb Swain as described in 2.10.5.3.1. For zebrafish *in vivo* gene silencing, a translation blocker morpholino was designed to be complementary to the translational start site and a splice blocker morpholino was designed to be complementary to exon2 intron2 splice junction for zebrafish RhoJ. Morpholinos were designed and synthesised by Gene Tool, USA. Morpholinos were injected with phenol red as an injection indicator into the yolk of one to four cell stage Fli1-GFP transgenic embryos which were then cultured at 28°C in Hank's buffer. Embryos were fixed at 26 hpf with 4% (w/v) PFA after being dechorionated. A Leica DMRE fluorescent microscope was then used to analyse the morpholino injected Fli1-GFP transgenic embryos. The effect of morpholino knockdown on vessel formation was quantitated by scoring the embryos according to whether the vasculature was affected (under-developed intersegmental arteries) or unaffected.

2.12 Statistical analyses

All experiments were repeated at least 3 times with similar results unless otherwise stated. Data are plotted with error bars representing the standard error of the mean. A Shapiro-Wilk normality test was performed on data sets to confirm a normal distribution. In order to test for significant differences in data, P values were determined by using GraphPad Prism 5 software. One-way analysis of variance (ANOVA) was used to test the significance of experiments. If the calculated P value was less than 0.05, then the hypothesis that the means of at least two subgroups differed significantly was accepted. If the ANOVA test was positive ($P<0.05$) then a Tukey's post hoc test for multiple pair-wise comparisons of means were performed and significance levels were determined at 0.05 (95%) confidence intervals. P values <0.05 were considered significant (*), <0.01 highly significant (**) and 0.001 extremely significant (***).

Chapter three

The role of RhoJ in endothelial cell tube formation and migration

3.1 Introduction

Angiogenesis is the process of generating new blood vessels from the existing vasculature. This process is vital to embryogenesis and adult physiology, such as in female menstruation and wound-healing, but also contributes to many pathological diseases including the growth and metastasis of solid tumours (225). The principal cells involved in this process are ECs, which line all blood vessels and capillaries. To achieve the new formation of a blood vessel, ECs of a pre-existing mature vessel degrade the ECM and migrate through the degraded matrix towards angiogenic stimuli. Behind this migrating front, ECs proliferate to provide the necessary number of cells to make a new vessel. This new outgrowth of ECs then reassemble and reorganise into a three-dimensional tubule structure (226). Rho GTPases regulate many essential aspects of cell physiology such as cell growth, adhesion, migration and control of actin dynamics (140). Evidence shows that RhoA, Rac1 and Cdc42 mediate EC processes that are crucial for angiogenesis to occur (139). Expanding our knowledge of the molecular regulatory mechanisms underlying these processes is necessary to further understand the biology of physiological and pathological angiogenesis.

RhoJ, a member of the Cdc42 subfamily group, has previously been shown to be involved in *in vitro* differentiation of 3T3 L1 adipocytes, early endocytosis and filamentous actin rearrangement (197, 198, 201, 203, 204). Using a combination of bioinformatic and expression analyses using reverse transcription and quantitative PCR, our laboratory previously identified RhoJ as being highly expressed by ECs (206). The aim of this study was to further explore the role of RhoJ in ECs, with specific interest in the processes that occur during angiogenesis.

To study RhoJ function, its expression was knocked down in human umbilical vein ECs (HUVEC) or immortalised human microvascular ECs using siRNA technology. To silence RhoJ expression, the regulatory cellular pathway known as RNA interference was exploited by using RhoJ-specific synthetic siRNA (227). Upon entry into cells by lipofection, siRNA are assembled into endoribonuclease-containing complexes, known as RNA-induced silencing complexes (RISC) and unwind to become single stranded. The siRNA strand incorporated into RISC pairs to its complementary mRNA sequence, which results in its cleavage and degradation. This blocks the translation of mRNA into protein thus silencing its expression in the cell.

Key aspects of the angiogenic process were assessed by *in vitro* methods to test the impact of siRNA mediated RhoJ knockdown on endothelial tube formation, migration, growth and cell death. Tube formation was assessed using Matrigel and 3-dimensional sprouting bead assays. Scratch wound and Boyden chamber assays were used to examine EC migration. Cell-counting assays and flow cytometry analyses were used to assess cell proliferation and survival. In summary, this chapter aims to investigate the function of RhoJ in human ECs *in vitro*.

3.2 Results

3.2.1 RNA interference-mediated knockdown of RhoJ *in vitro*

In order to investigate the role of RhoJ in EC biology, RNAi was used to specifically knockdown the expression of RhoJ in human ECs and then their function in various assays was tested. Two RhoJ specific siRNA duplexes, duplex 1 (D1) and duplex 2 (D2) were designed to different nucleotide sequences within the coding region of human RhoJ. A negative control siRNA duplex (NCD) that has no homology to any known human sequence

was used to demonstrate that the effects of RhoJ knockdown were solely due to RhoJ specific siRNA, and not due to effects that are associated with the delivery of double stranded RNA into cells. In addition, cells were mock transfected with transfection reagent only to show that the transfection process did not induce any non-specific effects.

Cells are able to evoke an innate immune interferon response to high concentrations of siRNA duplexes (228), since double stranded RNA can be present in certain virus-infected cells. SiRNA duplexes at high concentrations can also trigger off-target effects such that they can knock down other mRNAs with high silencing efficacy (229). In order to minimise the induction of the interferon response and off-target effects, a low siRNA concentration of 10 nM was chosen to knockdown RhoJ in ECs because it was the lowest concentration to consistently produce complete knockdown of RhoJ protein (see appendix 1 for titration of siRNA duplexes). To check for successful knockdown of RhoJ message in HUVEC transfected with D1 or D2 at 10 nM; RNA was extracted from the cells two days after transfection and reverse-transcribed into cDNA, then real-time quantitative PCR was performed to quantify the expression level of RhoJ relative to housekeeping control, β-actin. Transfection of D1 or D2 at 10 nM successfully reduced RhoJ mRNA expression in HUVEC by approximately 90% compared to NCD and mock-transfected conditions (figure 3.1A).

During an interferon response to double stranded RNA, cells induce the expression of type 1 interferons (IFN), IFN-α and IFN-β. These are a group of cytokines that in turn induce production of 2', 5’-oligoadenylate synthetase 1 (OAS1) and IFN-stimulated gene of 20 kDa (ISG20). OAS1 is an enzyme involved in the OAS pathway that is responsible for degrading viral and cellular RNA, thus inhibiting virus replication and promoting the death of infected cells (230). ISG20 is a 3’-5’ exonuclease protein that can inhibit viral replication by also degrading viral RNA (231). Detecting the up-regulation of OAS1 and ISG20 mRNA can be

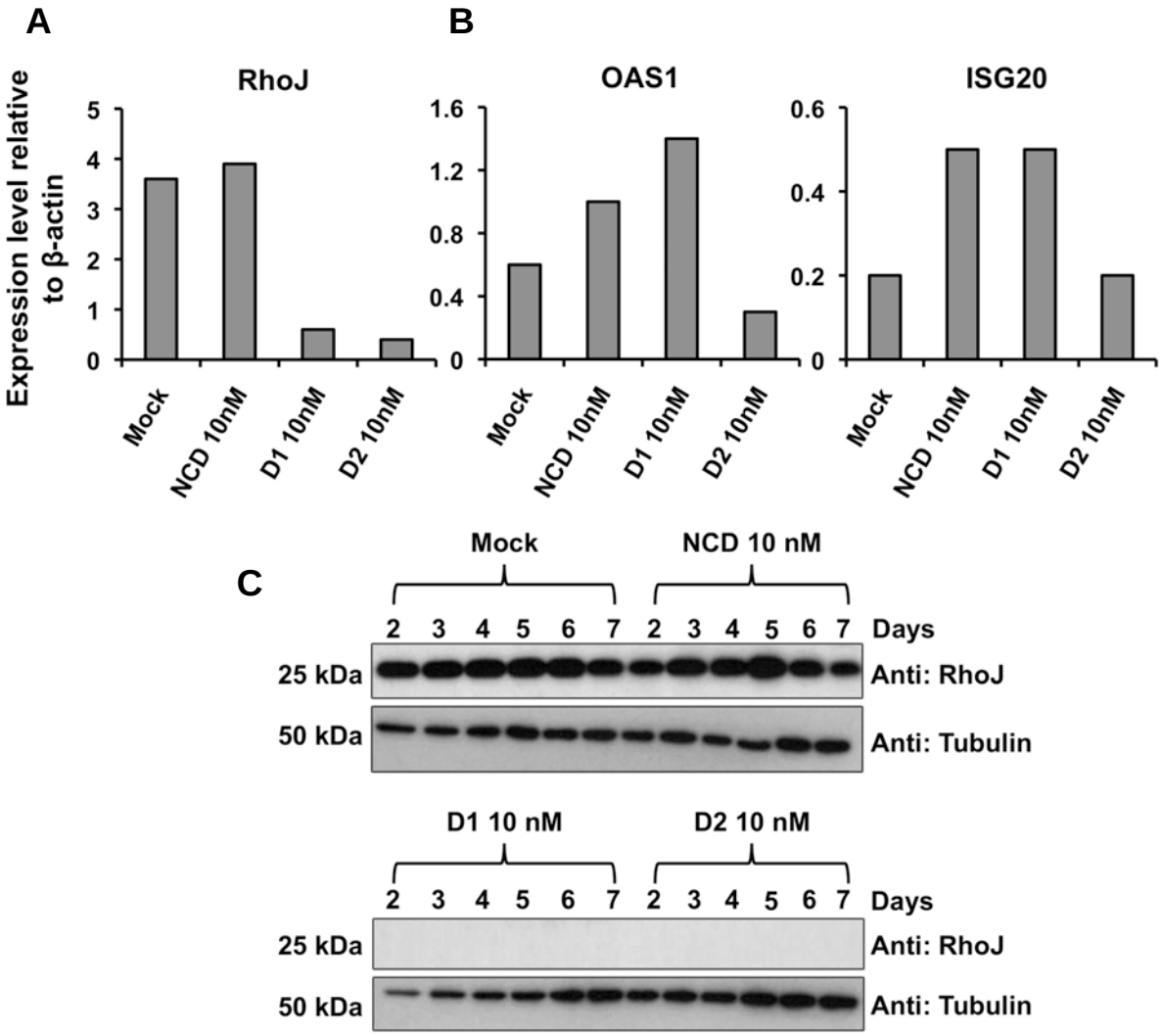

Figure 3.1 Successful RhoJ knockdown at mRNA and protein level and lack of interferon response in RhoJ-specific siRNA transfected cells. Human umbilical vein endothelial cells were either mock transfected or transfected with negative control duplex (NCD), RhoJ duplex 1 (D1) or RhoJ duplex 2 (D2) at 10 nM. (A-B) Two days after transfection, RNA was extracted and converted into cDNA. Expression levels of RhoJ and interferon response-induced genes (OAS1 and ISG20) were determined by quantitative PCR and normalised to β-actin expression levels. (C) Cells were harvested and lysed 2-7 days after transfection and Western blotting was performed using anti-RhoJ and anti-tubulin antibodies to determine the stability of RhoJ knockdown over 7 days using 10 nM siRNA.

used as an indication that the interferon response has been activated. It was important to check whether RhoJ specific duplexes induced an interferon response because activated interferons can trigger undesirable side effects and alter normal cell behaviour and function (232). To determine whether transfection of RhoJ specific duplexes at 10 nM elicited an interferon response, the mRNA expression levels of OAS1 and ISG20 in RhoJ-depleted cells was investigated. Two days after transfection, RNA was extracted and reverse-transcribed into cDNA. Real-time quantitative PCR was performed to quantify the expression level of OAS1 and ISG20 in the transfected cells relative to housekeeping control, β-actin. The expression level of OAS1 and ISG20 when normalised to β-actin was not markedly increased in D1 or D2 transfected cells compared to NCD and mock transfected cells (figure 3.1B). The similar levels of OAS1 and ISG20 expression in all conditions indicated that an interferon response was not activated by transfection of D1 and D2 at 10 nM.

RhoJ was knocked down at the protein level and the duration of RhoJ depletion over 7 days was examined using D1 or D2 at 10 nM. HUVEC were mock transfected or transfected with NCD, D1 or D2. Cells were then lysed 2-7 days after transfection and Western blots were performed. RhoJ protein was successfully knocked down using 10 nM of D1 or D2, with knockdown lasting over the entire 7-day period (figure 3.1C).

These data confirm that these RhoJ-specific duplexes do not induce an interferon response and that RhoJ is successfully depleted at the mRNA and protein level using a low siRNA duplex concentration of 10 nM. This concentration was used in all *in vitro* assays to assess the function of RhoJ in ECs and Western blotting was performed for every experiment to validate knockdown of RhoJ protein.

3.2.2 The effect of RhoJ knockdown on endothelial tube formation

RhoJ was found to be more highly expressed in ECs than in other cell types and since capillary tube formation represents a specialised EC function, the role of RhoJ in endothelial tube formation was explored. Matrigel, a solubilised basement membrane extract derived from mouse Engelbreth–Holm–Swarm sarcoma was used to induce EC differentiation into tube-like structures *in vitro*. Matrigel is rich in extracellular proteins that are present in vascular basement membranes *in vivo* such as collagen IV, laminin, heparan-sulphate proteoglycans and entactin (33). Kubota *et al.* (1988) was the first to reveal that plating ECs onto a reconstituted basement membrane does not induce proliferation but stimulates attachment, migration and differentiation of ECs into interconnecting capillary-like structures in a way that mimics the *in vivo* situation (233, 234). Ultrastructurally it has been shown that the ECs in tube-like structures are attached to one another by tight junctions (235). However there is still dispute over whether these tube-like structures possess lumens, for example, Grant *et al.* (1991) confirmed the presence of lumens in 'tubules' on Matrigel using electron microscopy, however this was not observed by Bikfalvi *et al.* (1991) (170, 236). The *in vitro* Matrigel tube formation assay is considered a model of microvessel development and regarded as representative of the differentiation stage of angiogenesis (95).

To investigate the effect of RhoJ knockdown on tube formation *in vitro*; HUVEC were mock transfected or transfected with NCD, RhoJ specific D1 or D2 and two days later cells were harvested and seeded on to a thin layer of gelled Matrigel. The formation of capillary-like structures were observed at 10 and 24 hours post-seeding. Mock and NCD treated cells differentiated into organised and well-connected capillary-like networks (figure 3.2A). In comparison, cells lacking RhoJ formed networks that showed fewer connections between branches indicating broken connections or connections not being made. They also appeared less stable since more cell retraction was observed at 24 hours. To quantify the effect of RhoJ

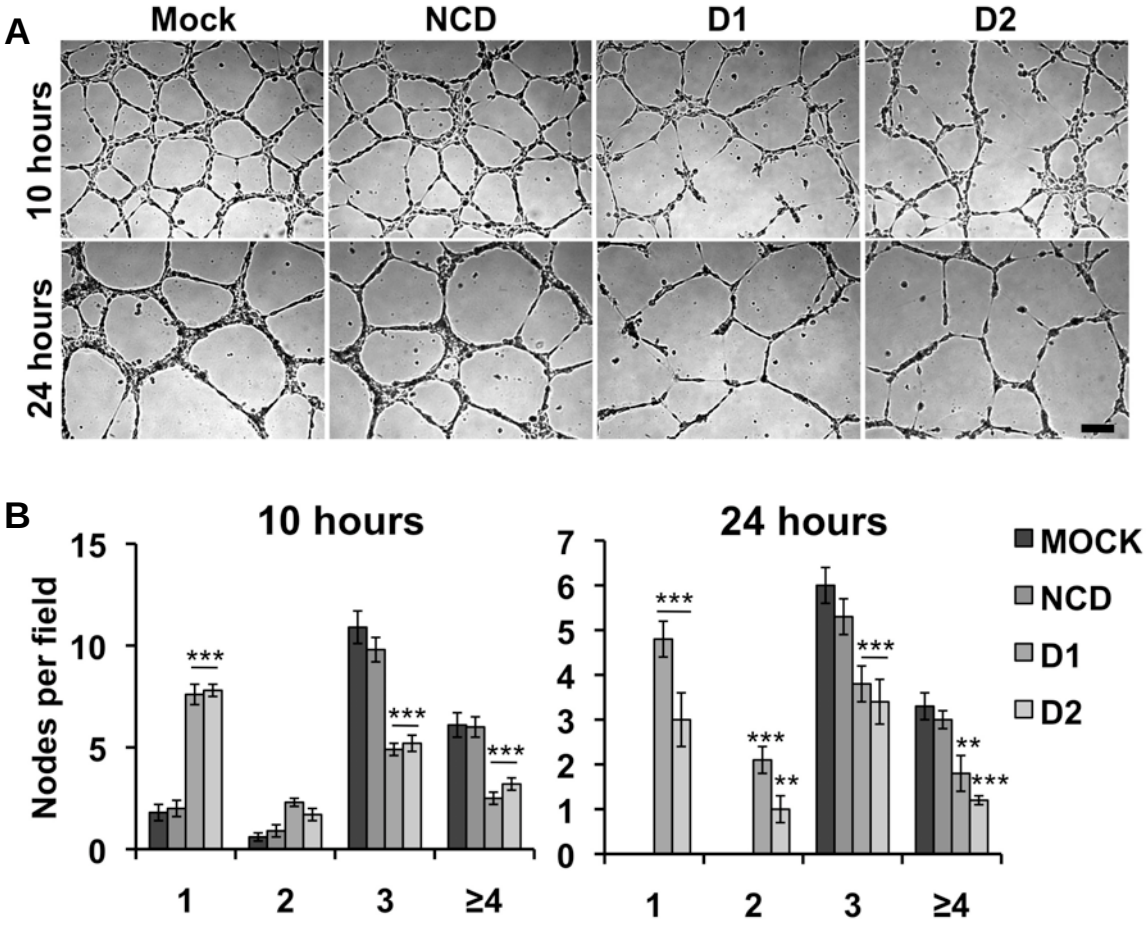

Figure 3.2 Impaired tubule formation with RhoJ knockdown in human umbilical vein endothelial cells. Human umbilical vein endothelial cells were either mock transfected or transfected with negative control duplex (NCD), RhoJ duplex 1 (D1) or RhoJ duplex 2 (D2) at 10 nM. (A) Two days later, cells were plated on to Matrigel and imaged at 10 and 24 hours. Scale bar = 200 μm. (B) Matrigel assays were quantified by counting the number of nodes with 1, 2, 3 or ≥4 branches from five random fields of view. Values represent the means from three independent experiments. Error bars depict the standard error of the mean. One-way ANOVA showed a significant effect of RhoJ knockdown on two-dimensional tubule formation at 10 and 24 hours ($P<0.0001$). Tukey's multiple comparison test was used to compare D1 or D2 with NCD (** = $P<0.01$, *** = $P<0.001$).

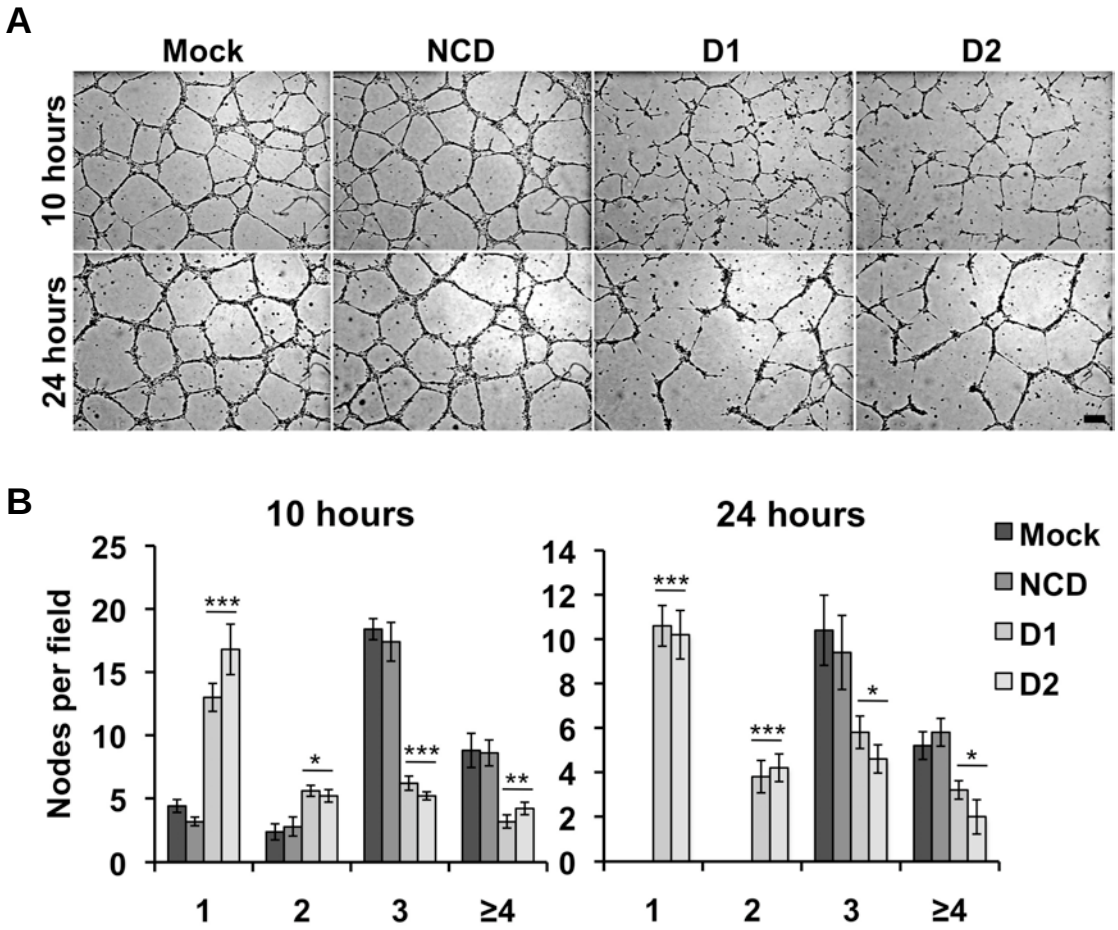

Figure 3.3 Impaired tubule formation with RhoJ knockdown in the microvascular cell line HMEC-1. Human microvascular endothelial cells were either mock transfected or transfected with negative control duplex (NCD), RhoJ duplex 1 (D1) or RhoJ duplex 2 (D2) at 10 nM. (A) Two days after transfection, cells were plated on to Matrigel and incubated for a further 24 hours. Pictures were taken at 10 and 24 hours. Scale bar = 200 μm. (B) Matrigel assays were quantified by counting the number of nodes with 1, 2, 3 or ≥4 branches from five random fields of view. Values represent the means of five fields of view from one experiment. Error bars depict the standard error of the mean. One-way ANOVA showed a significant effect of RhoJ knockdown on two-dimensional tubule formation at 10 and 24 hours ($P<0.0001$ for all nodes). Tukey's multiple comparison test was used to compare D1 or D2 with NCD (* = $P<0.05$, ** = $P<0.01$, *** = $P<0.001$).

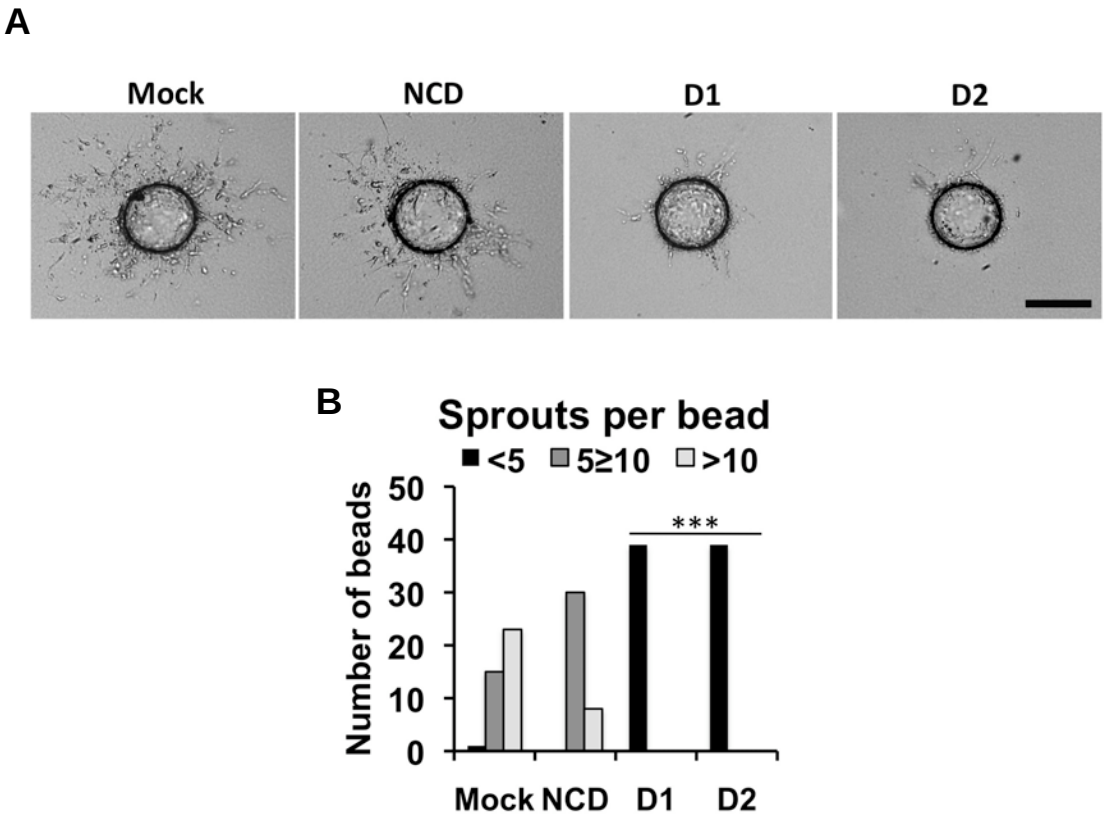

Figure 3.4 Reduced sprouting with RhoJ knockdown in human umbilical vein endothelial cells. Human umbilical vein endothelial cells were either mock transfected or transfected with negative control duplex (NCD), RhoJ duplex 1 (D1) or RhoJ duplex 2 (D2) at 10 nM. (A) Two days after transfection, cells were seeded onto cytodex beads and embedded into fibrin gels for 7 days. Images represent sprouting of tubes from beads at 7 days. Scale bar = 200 μm. (B) The number of sprouts per bead were counted and beads were scored as having, <5, 5≥10 or >10 sprouts. Values represent pooled data from three independent experiments. One-way ANOVA showed a significant reduction of sprouting with RhoJ knockdown ($P<0.0001$). Tukey's multiple comparison test was used to compare D1 or D2 with NCD (*** = $P<0.001$).

knockdown on Matrigel-induced tube formation, the numbers of nodes with 1, 2, 3 or ≥4 tubule branches were counted (nodes with 1 branch indicated an unconnected end). RhoJ knockdown produced a significant increase in unconnected ends and a significant reduction in nodes containing 3 or more branch points at 10 and 24 hours (figure 3.2B).

Since HUVEC are macrovascular ECs, it was important to determine how RhoJ knockdown would affect tube formation in microvascular derived ECs, for this purpose the human microvascular EC cell line-1 (HMEC-1) was used. Knockdown of RhoJ in HMEC-1 cells also impaired tube formation on Matrigel, resulting in more unconnected branches and fewer complex nodes (figure 3.3). *In vivo* angiogenesis occurs in three-dimensions, and so the effect of RhoJ silencing on three-dimensional tube formation was analysed using a sprouting bead assay (213). There has been some dispute over whether lumens are present in the tube-like structures found in two-dimensional Matrigel assays. However, Bayless and colleagues (2000) have confirmed the presence of a lumen in capillary-like structures formed in three-dimensional fibrin matrices (237) thus the sprouting bead assay more closely mimics the *in vivo* situation.

The sprouting bead assay involved siRNA transfection of HUVEC to knockdown RhoJ and two days later cells were harvested and coated onto microcarrier beads. Coated beads were then embedded into a fibrin matrix gel and three-dimensional tube sprouting was monitored over 7 days. By 7 days, mock and NCD transfected cells had migrated into the fibrin gel and differentiated to form tubes (figure 3.4A). In contrast, cells lacking RhoJ formed fewer and shorter tubes. To quantify the effect of RhoJ knockdown on three-dimensional sprouting, the number of sprouts per bead were counted and beads were scored as having, <5, 5≥10 or >10 sprouts. A significant reduction in three-dimensional tube formation was found with RhoJ knockdown (figure 3.4B).

3.2.3 The effect of RhoJ knockdown on endothelial chemokinesis and chemotaxis

Endothelial migration is essential to angiogenesis. Hence, in order to investigate the cause for the impaired tube formation with RhoJ knockdown, scratch wound assays were performed to examine the chemokinetic motility of RhoJ-depleted cells. Scratch wound assays involve gently scraping away cells in a confluent cell monolayer to create a 'wound'. The cells at the edge of the scratch then migrate into the denuded area in order to 'heal the wound' and re-form the monolayer.

HUVEC were mock transfected or transfected with NCD, RhoJ specific D1 or D2. Two days after siRNA transfection a scratch was made and the ability of the cells to close the wound was assessed over 24 hours. The healing of wounds normally depends on a combination of cell migration and proliferation (238). Mitomycin C is an antibiotic that binds to DNA and works by blocking DNA synthesis and inhibiting cell growth (239). Mitomycin C was included in the migration assay to ensure that cell division did not contribute to the closure of the wound. By 24 hours, the denuded area was completely filled with mock and NCD transfected HUVEC (figure 3.5A). However, cells with reduced RhoJ expression did not migrate to close the scratch and at 24 hours a region of the scratch still remained evident. To quantify wound closure, Image J software was used to measure the area of the scratch at different time points. A significant reduction in endothelial chemokinetic migration with RhoJ knockdown was found at 24 hours (figure 3.5B). This experiment was also repeated using immortalised HMEC-1 cells and a similar reduction of random cell motility was found with knockdown of RhoJ (figure 3.6A-B).

In angiogenesis, gradients of secreted signalling proteins such as chemokines, cytokines and growth factors guide growing blood vessels through EC chemotaxis (43). Therefore a chemotaxis assay using a Boyden chamber (214) was used to assess the effect of RhoJ

knockdown on chemotaxis. Boyden chambers consist of upper and lower wells separated by a micro-porous membrane filter. The chemoattractant is placed in the lower wells and cells are added to the top wells. After a period of incubation, the cells that migrated towards the chemoattractant are counted on the lower surface of the membrane.

HUVEC were mock treated or transfected with NCD, RhoJ specific D1 or D2. Two days later, cells were harvested and seeded into upper chamber wells with media containing 1% fetal calf serum (FCS). A 8 μm pore size filter was coated with a gelatin matrix, to more closely mimic the *in vivo* environment and was used to separate the upper chamber from the lower chamber, which was filled with media containing 10% FCS supplemented with bovine brain extract and heparin. Cells were allowed to migrate towards the serum-rich media for 5 hours then non-migrated cells were wiped away. Migrated cells attached to the other side of the filter were fixed and stained with DAPI revealing the migratory response to the chemoattractant. To quantify chemotaxis, the sum of migrated cells in five random areas for each well was calculated for at least nine replicate wells of each condition. A significant reduction in chemotaxis towards serum-rich media was observed with RhoJ knockdown compared to mock and NCD transfected wells (figure 3.5C). RhoJ siRNA treated HMEC-1 cells also displayed reduced migration towards FCS in the Boyden chamber assay (figure 3.6C).

3.2.4 The effect of RhoJ knockdown on endothelial cell proliferation and apoptosis

The formation of new micro-vessels from pre-existing mature vessels is dependent not only on cell migration and tube formation but also on endothelial proliferation. A method used to measure cell proliferation *in vitro* is a direct cell-counting assay. These assays involved equally plating cells from each condition straight after siRNA transfection. Proliferation was

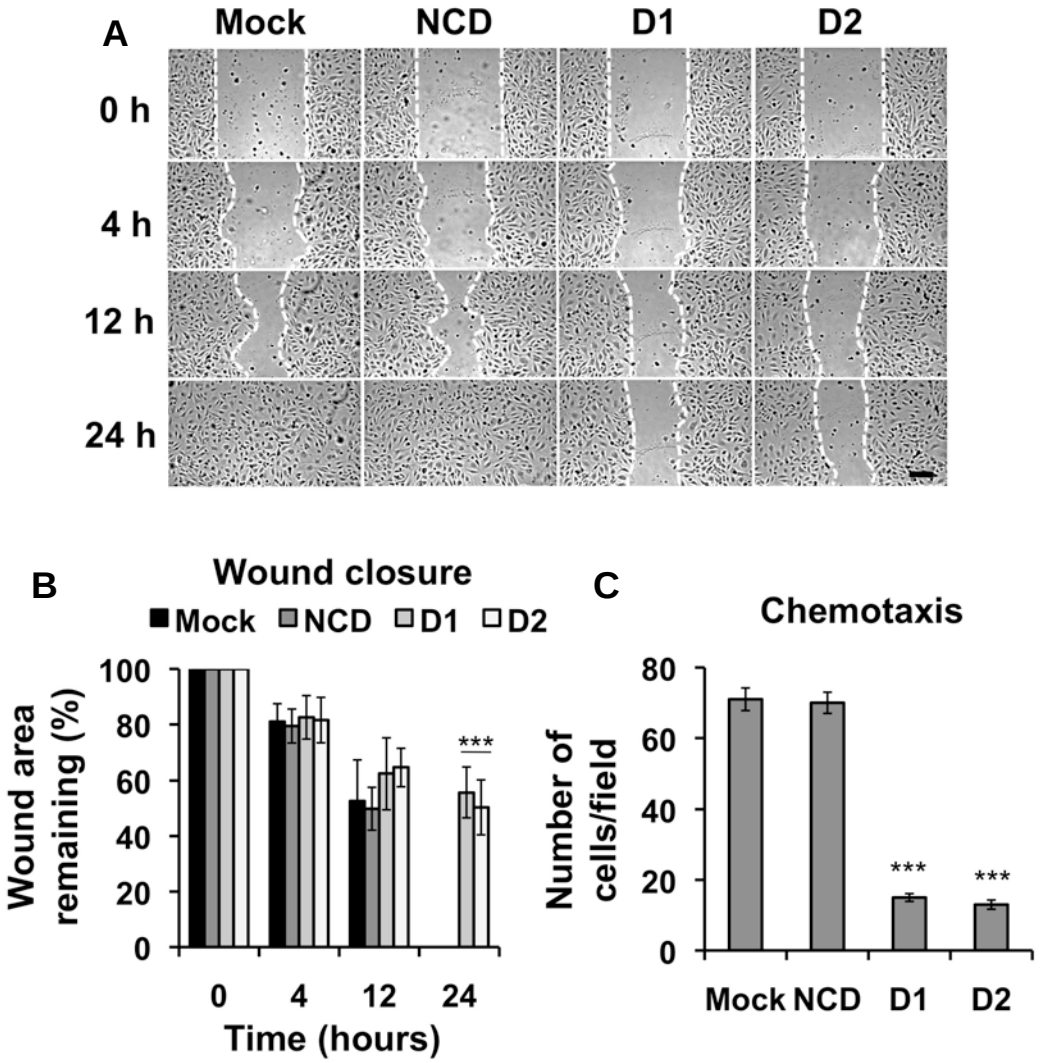

Figure 3.5 Reduced cell motility with RhoJ knockdown in human umbilical vein endothelial cells. Human umbilical vein endothelial cells were either mock transfected or transfected with negative control duplex (NCD), RhoJ duplex 1 (D1) or RhoJ duplex 2 (D2) at 10 nM. (A) Two days after transfection, scratches were made and imaged at 0, 4, 12 and 24 hours. Scale bar = 200 μm. (B) The percentage of wound remaining was measured and plotted. Values represent the means from three independent experiments. Error bars depict the standard error of the mean. One-way ANOVA showed a significant effect of RhoJ knockdown on chemokinesis at 24 hours ($P<0.0001$). Tukey's multiple comparison test was used to compare D1 or D2 with NCD (*** = $P<0.001$). (C) Two days after transfection, a Boyden chamber chemotaxis assay was performed and the number of migrated cells quantified. Values represent the means from three independent experiments with nine or more replicates in each experiment. Error bars depict the standard error of the mean. One-way ANOVA showed a significant reduction of chemotaxis to fetal calf serum in RhoJ-depleted cells ($P<0.0001$). Tukey's multiple comparison test was used to compare D1 or D2 with NCD (*** = $P<0.001$).

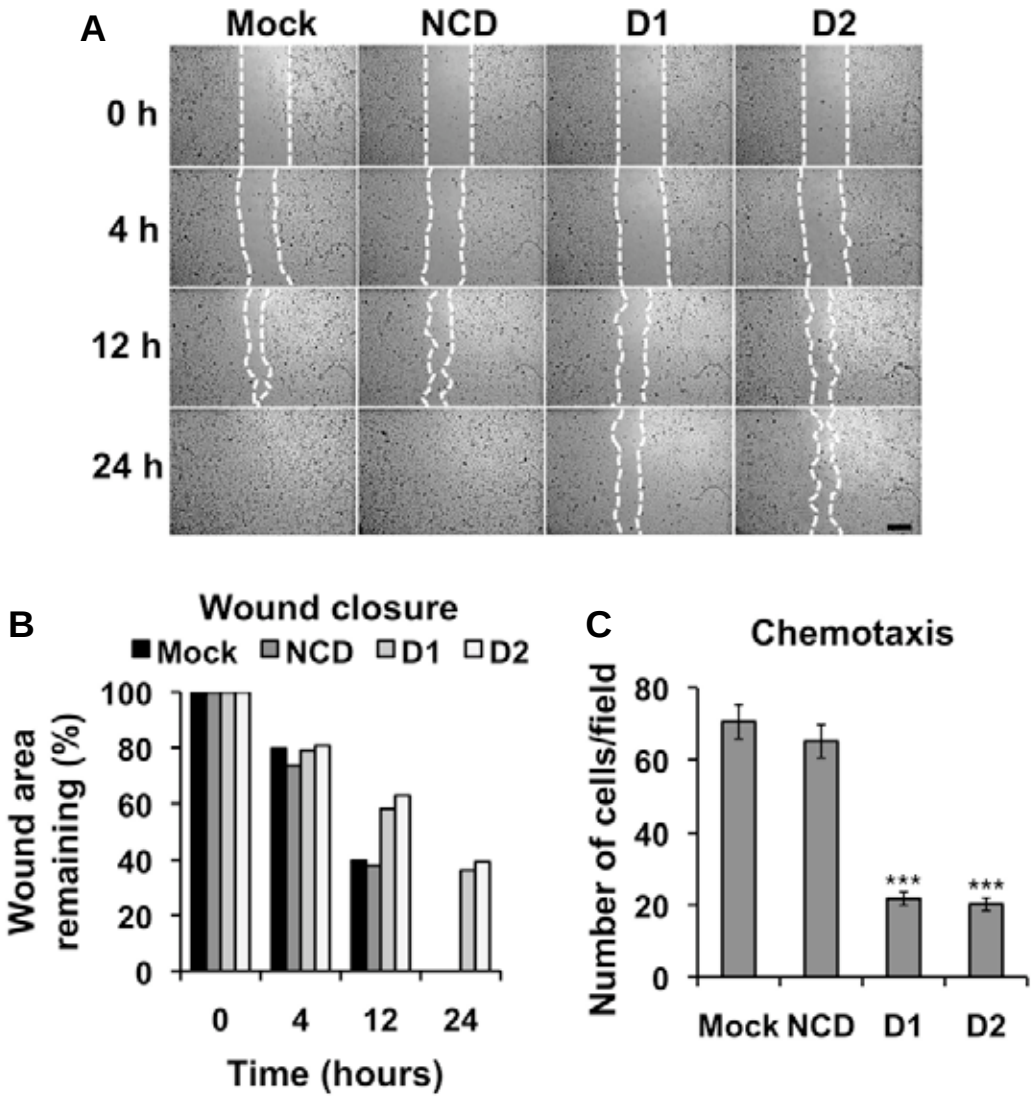

Figure 3.6 Reduced cell motility with RhoJ knockdown in the microvascular cell line HMEC-1. Human microvascular endothelial cells were either mock transfected or transfected with negative control duplex (NCD), RhoJ duplex 1 (D1) or RhoJ duplex 2 (D2) at 10 nM. (A) Two days after transfection, scratches were made and imaged at 0, 4, 12 and 24 hours. Scale bar = 400 μm. (B) The percentage of wound remaining was measured and plotted. Values represent wound closure from one experiment. (C) Two days after transfection, a Boyden chamber chemotaxis assay was performed and the number of migrated cells quantified. Values represent the means of one experiment with nine replicates. Error bars depict the standard error of the mean. One-way ANOVA showed a significant reduction of chemotaxis to fetal calf serum in RhoJ-depleted cells ($P<0.0001$). Tukey's multiple comparison test was used to compare D1 or D2 with NCD (*** = $P<0.001$).

then allowed to occur for a period of time before cells were harvested and counted. Cells were harvested and counted 1-4 days post seeding. A significant reduction in cell growth 2-4 days after seeding was found with RhoJ knockdown (figure 3.7A).

Cell division is regulated by the cell cycle, which consists of interphase gap 1, synthesis and gap 2 and mitosis. RhoA, Rac1 and Cdc42 have been shown to play a critical role in the signalling cascades controlling cell cycle and cell proliferation (240, 241). A reduction in cell proliferation is often due to cell cycle defects or delays. Therefore, in order to explain the cell growth reduction found with RhoJ knockdown, the effect of reduced RhoJ expression on the cell cycle was assessed. HUVEC were transfected with RhoJ specific D1 or D2, NCD, or mock transfected. Three days later the cells were fixed, permeabilised and DNA was stained with propidium iodide (PI). The cells were then scanned and the cell cycle was analysed using an Acumen® eX3 microplate cytometer. PI is used in cell cycle analysis to quantitatively evaluate DNA content in cells. Thus, phases of the cell cycle can be analysed by measuring the fluorescent intensity of PI staining. The cytometer produces a graph that shows the percentage of cells found in G1 (gap 1), S (synthesis) and G2/M (gap 2/mitosis) phases according to their DNA content (PI staining). SiRNA-mediated knockdown of RhoJ did not significantly change the proportion of cells in each phase of the cell cycle when compared to mock and NCD conditions (figure 3.7B). This result suggests that the reduced cell proliferative effects seen with RhoJ knockdown are not likely to be due to deregulation of the cell cycle.

Decreased proliferation may be due to cytotoxic rather than cytostatic effects. Apoptosis related changes in cell morphology can be analysed to discover how many cells in a given population are apoptotic or have already undergone apoptosis. In early apoptosis, a phospholipid, phosphatidylserine, is translocated from the inner to the outer leaflet of the

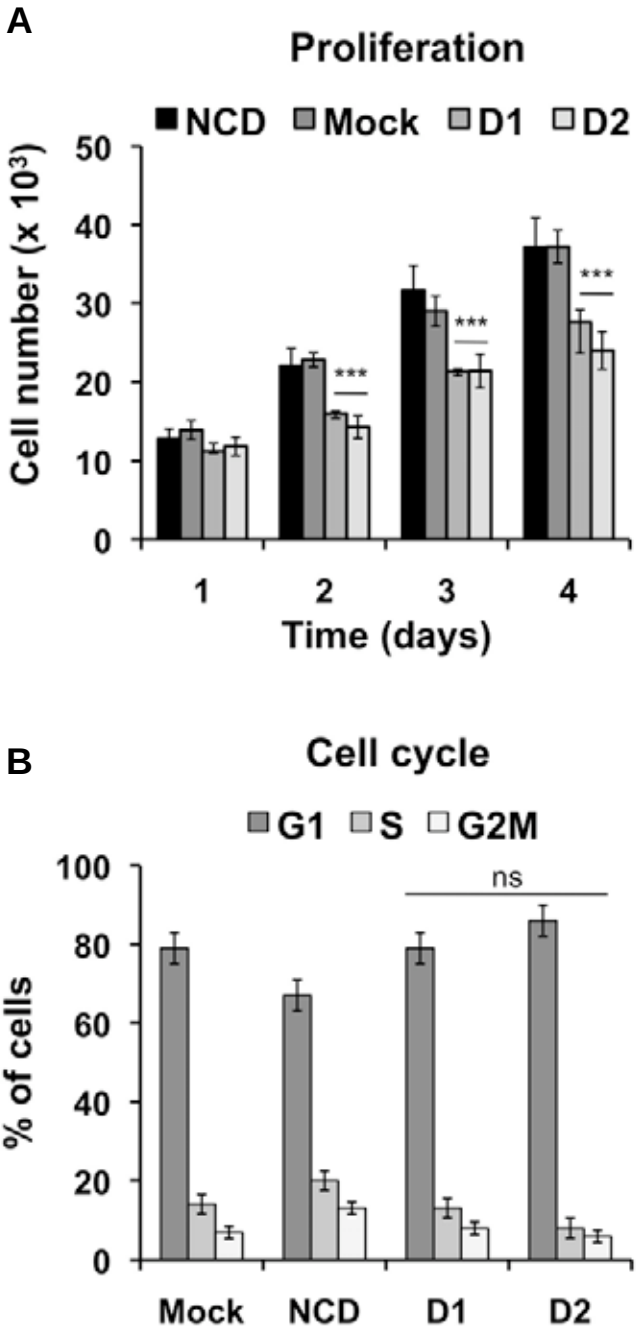
A
Proliferation
NCD
Mock
D1
D2
Cell number (x 10³)
50
40
30
20
10
0
***
***
***
1
2
3
4
Time (days)
B
Cell cycle
G1
S
G2M
ns
% of cells
100
80
60
40
20
0
Mock
NCD
D1
D2

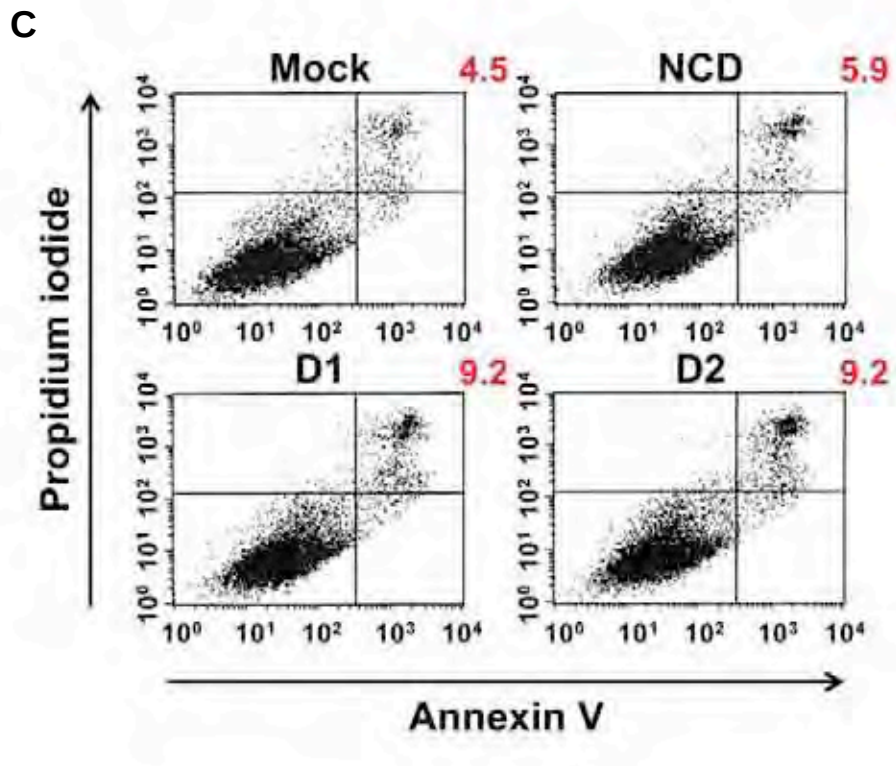

Figure 3.7 Reduced cell growth and increased cell death with RhoJ knockdown. Human umbilical vein endothelial cells were either mock transfected or transfected with negative control duplex (NCD), RhoJ duplex 1 (D1) or RhoJ duplex 2 (D2) at 10 nM. (A) Cell growth was assessed by cell counting 1-4 days after transfection. Values represent the means of one experiment with three replicates. Error bars depict the standard error of the mean of triplicates for each time point. Similar data were obtained in four independent experiments. One-way ANOVA showed a significant reduction of cell proliferation with RhoJ knockdown ($P<0.0001$, days 2-4). Tukey's multiple comparison test was used to compare D1 or D2 with NCD (*** = $P<0.001$). (B) Three days after transfection, cells were stained with propidium iodide and the cell cycle was analysed by an Acumen® eX3 microplate cytometer. Values represent the percentage of cells in G1, S and G2/M stages of the cell cycle from three independent experiments, each with 12 or more replicates. Error bars represent the standard error of the mean. One-way ANOVA showed that RhoJ knockdown did not have a significant effect on cell division (ns: not significant). (C) Three days after transfection, cells were stained with annexin V and propidium iodide and analysed by a fluorescence activated cell scanner. Results are displayed as a bivariate distribution of annexin V (FL1) and propidium iodide (FL3) fluorescence intensity The percentage of cells stained double positive for both annexin V and propidium iodide are indicated in red. Similar data were obtained in three independent experiments.

plasma membrane; making it detectable with annexin V conjugated to fluorescein (FITC), a protein with high affinity for this phospholipid (242). The loss of integrity of the plasma membrane in late apoptosis alters the permeability of the cell, enabling PI to enter and stain the nucleic acid (243).

To determine whether silencing RhoJ induces EC death, RhoJ siRNA treated HUVEC were stained with annexin V and PI and analysed by flow cytometry. The results were displayed as a bivariate distribution of annexin V (FL1) and PI (FL3) fluorescence intensity. Cells in the lower-left quadrant were viable cells that were unstained for both annexin V and PI. Cells in the lower-right quadrant were early apoptotic that stained positive for annexin V but negative for PI. Cells in upper-right quadrant represent the late apoptotic cell population that stained positive for both annexin V and PI. In figure 3.7C, cells found in the upper-right quadrant that were undergoing apoptosis or already dead is displayed as a percentage (in red). RhoJ reduced populations showed a 2-fold increase in cell death (9.2%) compared with mock (4.5%) and NCD transfected (5.9%) populations. However these increases in cell death are still relatively low.

Since knockdown of RhoJ reduces EC motility and increases cell death, it was important to determine whether the reduced motility of RhoJ-depleted cells found in figures 3.5 and 3.6 were due to cells undergoing apoptosis. In order to investigate whether an increase in apoptosis was impeding migration of RhoJ-depleted cells, cells at the wound edge of a scratch wound assay were analysed for apoptosis. Two days after siRNA transfection, scratch wound assays were set up on gelatin-coated glass coverslips. Scratch wounds on glass coverslips were made on a smaller scale due to scraping with a smaller pipette tip. Wounds made on glass coverslips typically healed after nine hours in control cells (not shown). Cells were fixed but not permeabilised and stained with annexin V-FITC in order to visualise apoptotic cells at

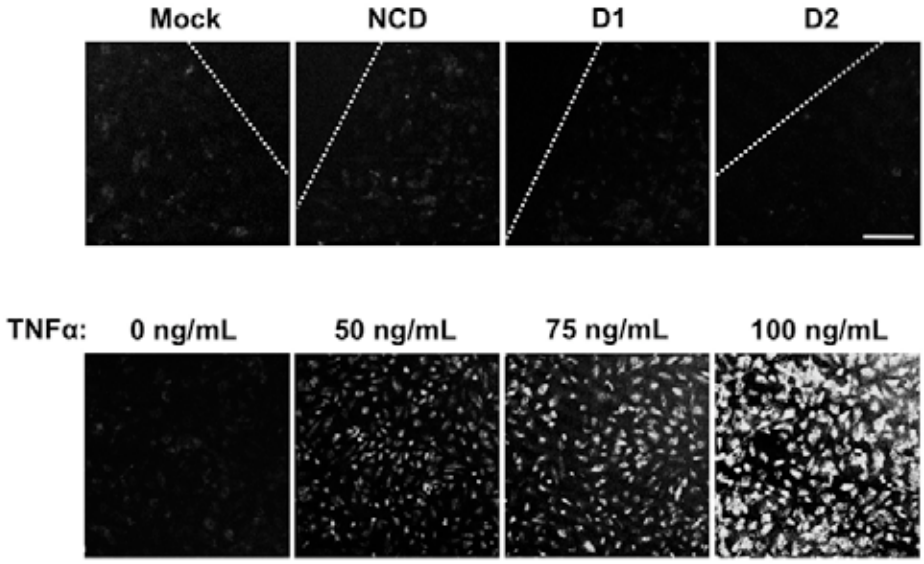

Figure 3.8 Apoptosis was not detected at the wound edge with RhoJ knockdown. Human umbilical vein endothelial cells were either mock transfected or transfected with negative control duplex (NCD), RhoJ duplex 1 (D1) or RhoJ duplex 2 (D2) at 10 nM. Two days after transfection, scratch wound assays were set up on fully confluent glass coverslips. Scratches were allowed to heal for 6 hours before staining with annexin V-FITC to visualise cells undergoing apoptosis. Dotted white lines indicate the wound edge. As a positive control for detecting endothelial apoptosis, wildtype cells were treated with 0, 50, 75 or 100 ng/mL of tumour necrosis factor-alpha (TNFα) for 4 hours and stained with annexin V-FITC. Scale bar = 100 μm. Similar data were obtained in three independent experiments.

the wound margin six hours after the scratches were made. Tumour necrosis factor-α (TNFα) is a potent inducer of EC apoptosis (216, 217). As a positive control for detecting endothelial apoptosis, untransfected HUVEC were treated with varying amounts of TNFα and stained with annexin V-FITC. RhoJ-depleted cells at the wound margin were not found to be apoptotic (figure 3.8). Although there is a weak level of background staining, the cells are negative for annexin V. The cells treated with TNFα showed positive staining for annexin V that increased in intensity as the amount of TNFα increased. This was most likely due to cells gradually losing membrane integrity and annexin V-FITC being able to enter cells and stain intracellular phosphatidylserine as well as extracellular. These data suggest that although siRNA-knockdown of RhoJ does induce a small rise in apoptosis, the motility defects displayed by RhoJ-depleted cells are not apoptosis-related.

3.2.5 Summary

SiRNA mediated silencing of RhoJ in HUVEC cells did not induce an interferon response and knockdown of RhoJ protein continued over 7 days using RhoJ-specific siRNA duplexes at a low concentration of 10 nM. Knockdown of RhoJ in HUVEC impaired tube formation in two and three-dimensional tube formation assays. RhoJ-specific siRNA-treated HUVEC displayed reduced chemokinesis, chemotaxis and cell growth. RhoJ knockdown in human microvascular HMEC-1 cells also resulted in impaired tube formation and cell motility defects. An increase in apoptosis was detected with RhoJ knockdown, with no effect on the cell cycle, but this increase in cell death did not explain the reduced chemokinesis of RhoJ depleted cells.

3.3 Discussion

Impaired tubule formation was observed when RhoJ was silenced in two-dimensional Matrigel tube formation assays (figure 3.2). Reduced connections between branches and

retraction of tubules at later time points were found with silencing of RhoJ in both HUVEC and HMEC-1. In three-dimensional sprouting bead assays, which are more representative of physiological capillary formation, the number of sprouting tubules found when RhoJ expression was knocked down in HUVEC was significantly reduced (figure 3.4). These data suggest that RhoJ GTPase activity is important for *in vitro* endothelial tube formation. This would be consistent with the previous finding of Connolly *et al.* (2002) which showed that inactivating GTPase function of small Rho proteins using toxin B 10463, from *Clostridium difficile* bacterium, inhibited tube formation on Matrigel in a dose-dependant manner (170).

Interestingly, in our Matrigel assays, RhoJ depleted cells were able to align themselves into short cord-like structures but these primitive tube-like structures failed to form extensive branched capillary networks like control cells. Connolly *et al.* (2002) also studied the cellular changes that occurred in HUVEC when in contact with Matrigel (170). They demonstrated that microtubule dynamics and cellular protrusions, such as lamellae and membrane ruffles, were required for the initial alignment of cells into short cord-like aggregates but the extension of these short tube-like structures into interconnected lumen-containing tubules was mainly regulated by tight control of cell migration and actomyosin contractility (170). Thus our data indicates that RhoJ is not required for the initial alignment of ECs into primitive cords through the use of cellular protrusions but is essential for the second stage of differentiation where cells migrate into complex branched tubule networks.

RhoJ knockdown also induced chemokinetic and chemotactic motility defects in HUVEC and HMEC-1 (figure 3.5 and 3.6). In the scratch-wound assay, RhoJ depleted cells displayed reduced migration compared to control cells. In the Boyden chamber assay, RhoJ silencing significantly reduced the number of cells that migrated through filter pores towards the chemoattractant. Since Rho GTPases are mostly known to be involved in regulating

cytoskeletal actin dynamics (139), it was not surprising that RhoJ knockdown impaired cell motility. Moreover, the impaired tube formation found with RhoJ knockdown could be explained by the reduced cell motility. Branching of tubules to form interconnected networks is a process heavily dependent on EC migration (170). Since tubule branching was significantly impaired when RhoJ was knocked down in Matrigel assays, it is reasonable to surmise that the cell migratory defects of RhoJ knocked cells may have caused the ineffective tube formation. Therefore, these data suggest that RhoJ may play a critical role in EC migration, which is not only important for physiological angiogenesis but also vital to the repair of injuries to the endothelium.

EC proliferation and apoptosis are also fundamental aspects of EC biology. Angiogenesis requires quiescent ECs to become proliferative in order to have enough ECs to remodel the vasculature (71). On the other hand, Segura *et al.* (2002) showed that apoptosis occurs inside tubules to create lumens and inhibiting programmed cell death in ECs impairs *in vitro* and *in vivo* angiogenesis (244). Thus angiogenesis requires the subtle balance between EC growth and death. RhoJ knockdown was shown to reduce EC growth and increase apoptosis (figure 3.7). However the cell cycle was not affected suggesting that RhoJ is not required for cell cycle regulation unlike its closely related family member Cdc42 (163). Since RhoJ knockdown did not impair cell division, it is most likely that the reduced number of viable cells found in the cell-counting assays was due to cells apoptosing more.

The increase in apoptosis could be another possible explanation for the defective tube formation found with RhoJ knockdown. The lack of branching and connectivity of RhoJ depleted networks may have been due to too many cells apoptosing. However, the increase in apoptosis was only a small degree more than control cells. In line with what is already known about the functions of Rho GTPase proteins, it is probable that RhoJ is regulating cell

locomotion, by modulating actin reorganisation, than apoptosis. Thus RhoJ signalling may not be directly regulating apoptosis but may occur as a secondary phenotype to accumulated cytoskeletal problems. Consistent with this theory, RhoJ-depleted cells at the wound edge of a scratch-wound assay were not found to be undergoing apoptosis (figure 3.8). This suggests that RhoJ knockdown-induced motility defects were not apoptosis-related. However, later time points were not checked and it is possible that apoptosis might have occurred at the late stages of wound healing (due to cytoskeletal defects) thus contributing to the phenotype. In support of this, Chen *et al.* (1997) showed that non-motile cell shape and increased cellular tension is capable of switching proliferative ECs into programmed cell death (245). This may be the case for RhoJ knockdown cells; where changes in cell locomotion induce some cells but not all to apoptose. In summary, the increase in cell death may not be directly modulated by RhoJ but may be an independent motility-induced phenotype. The combination of both impaired motility and the small increase in apoptosis are likely to contribute to the profound defective tube formation in the Matrigel and sprouting bead assays.

In previous studies, the overexpression of dominant active RhoJ in REF-52 fibroblasts was found to induce the production of dynamic actin-rich dorsal ruffles across the top surface of the cell (197). Dorsal ruffles are dynamic actin ‘waves’ that have been shown to mediate the disassembly of actin stress fibers and prepare static cells for subsequent movement (246, 247). Similarly in another study, immortalised porcine aortic endothelial (PAE) cells expressing constitutively active RhoJ were found to display lamellipodia and focal adhesion-like structures at the cell periphery (204). More recently, dominant active overexpression of RhoJ in immortalised PAE cells promoted the formation of podosomes (205). Podosomes are dynamic actin-rich cell-matrix adhesion structures found on the ventral surface of highly motile cells. They are thought to stimulate the activity of matrix metalloproteinases and cell invasion (248, 249). These data all show that RhoJ activity induces reorganisation of

filamentous actin and cell-matrix adhesions. The present study is consistent with and extends past findings since we have shown that knocking down RhoJ interferes with EC migration, which is a process extremely reliant on the normal control of actin reorganisation and cell-matrix adhesions. Furthermore, we have shown that RhoJ's role in EC migration is important for *in vitro* tubulogenesis.

Most previous studies performed on RhoJ used ectopic overexpression of wild type or mutant RhoJ (197, 198, 204). However, in 2003, de Toledo group used siRNA technology to knock down RhoJ in HeLa cells (203), and RNAi was also used to knockdown RhoJ in immortalised mouse preadipocyte cells (3T3 L1) by Kawaji and colleagues in 2010 (202). Although we are not the first to knockdown RhoJ using siRNA, our studies are unique compared to previous research since we have assessed the impact of RhoJ reduction in primary human ECs, which are cells that endogenously express relatively high levels of RhoJ. The use of primary cells instead of immortalised cell lines provides a more normal physiological system to study the effects of gene silencing on cell behaviour.

Using RhoJ specific siRNA duplexes, we were able to successfully transfect primary human umbilical vein ECs (HUVEC) and knockdown RhoJ message/protein using a low dose of 10 nM (figure 3.1). Additionally, using RhoJ specific duplexes at this concentration did not induce expression of interferon response genes and protein knockdown persisted over 7 days. In the present study, sufficient controls were utilised to ensure that phenotypic changes observed with RhoJ knockdown were specific to loss of RhoJ function. For example, cells were transfected with a negative control siRNA duplex (NCD) that did not have sequence homology to any human gene. This duplex was used at the same concentration used for RhoJ specific duplexes in all experiments and was also shown not to upregulate the expression of interferon response genes (figure 3.1). In addition, two different siRNA duplexes (D1 and

D2) that targeted two different regions of RhoJ coding region were used. Both D1 and D2 duplexes induced the same phenotypes, which implied that effects found were specific to reduction of RhoJ and not off-target effects. Moreover, transfection of NCD did not induce the same phenotypes as RhoJ specific duplexes, further supporting that these effects were specific to loss of RhoJ. Although, using multiple siRNA duplexes to one target is the most widely accepted control to enhance confidence in RNAi data (250), future work could include siRNA rescue experiments to provide final confirmation that the observed effects are due to specifically knocking down RhoJ. This can be achieved by expressing wild type RhoJ with one or more silent point mutations within the target regions of the RhoJ specific duplexes to create a form resistant to RNAi knockdown.

The main limitation of the methodology used in this chapter is the use of HUVEC since angiogenesis occurs only in microvascular ECs and HUVEC are macrovascular. The most appropriate cell type to use in angiogenesis research are human microvascular ECs (HMEC) since these are capillary ECs and of human origin, however these cells are costly to maintain and often difficult to source. Umbilical cords were easy to obtain and isolate by our group and for these reasons, HUVEC were used routinely in our laboratory. However, it was important for us to confirm the physiological relevance of RhoJ and investigate whether RhoJ knockdown had the same effect in microvascular ECs as in HUVEC. Thus key aspects of angiogenesis such as tube formation and migration were also assessed in an immortalised human microvascular EC line (HMEC-1). The phenotypic changes that were observed in HUVEC after loss of RhoJ were also found in HMEC-1 cells. Since the phenotypes were repeated in capillary ECs, this suggests that RhoJ may function in ECs from different vascular beds.

In conclusion, since Rho GTPase proteins are well known for their regulatory effects on cell motility, and the data described in this chapter suggest that RhoJ may play a critical role in EC migration, the function of RhoJ in aspects of cell locomotion were examined in detail and this work is described in chapter 4.

Chapter four

RhoJ modulation of actomyosin contractility and focal adhesion numbers

4.1 Introduction

Cell migration can be thought of as a cyclic process. The initial response of a cell to a migration-promoting stimulus is to polarise and extend protrusions, either as filopodia or lamellipodia, in the direction of migration. Cell polarity and filopodia formation is known to be regulated by Cdc42 while lamellipodia formation has been shown to be under the control of Rac1 (163). The formation of these protrusions is driven by actin polymerisation and is stabilised by adhering to the ECM through focal adhesions. Focal adhesions are large, dynamic protein complexes that are often heterogeneous structures, varying in size, strength and organisation (108). Focal adhesions act at traction sites for migration as the cell moves forward over them and are dissembled at the cell rear, allowing the cell to detach (251). Thus, focal adhesions play a critical role in mechanotransduction and their coordinated assembly and turnover are essential to cell locomotion.

The turnover of focal adhesions requires myosin-induced contractility. Migrating cells must be able to detach from the ECM. The ends of stress fibres are attached to focal adhesion sites and are composed of actin and myosin bundles, known as actomyosin (252). To retract the trailing edge, cells need to exert force to focal adhesion sites at the cell rear to disassemble adhesions through coordinated contraction of actomyosin bundles (253). Actomyosin contraction is mediated primarily by myosin II activity, which is regulated by phosphorylation of myosin light chain (MLC). Rho kinase (ROCK) acts downstream of RhoA and is known to phosphorylate a number of targets including MLC (134). Therefore, RhoA is known to positively regulate stress fibre formation via activation of ROCK (161, 162, 254).

Small Rho GTPases are key regulators of cell migration. Cdc42 and Rac1 are generally proposed to function at the leading edge to induce cell polarisation and actin protrusions, whereas RhoA is believed to mainly act at the cell body to facilitate contraction (101).

RhoJ was previously shown to modulate filamentous actin formation through overexpression of dominant active or inactive RhoJ (197, 198, 204). In addition, siRNA-mediated knockdown of endogenous RhoJ protein in human ECs was shown to impair endothelial tube formation and migration (chapter 3). The aim of the experiments described in this chapter was to investigate how RhoJ causes defects in cell motility in human ECs. To study this, aspects of cell locomotion were examined in detail. HUVEC were either treated with RhoJ-specific siRNA to knockdown RhoJ or transduced with lentivirus constructs to overexpress dominant active or wild type RhoJ. The role of RhoJ in EC polarisation, cell-matrix and cell-cell adhesion and stress fibre formation was assessed using immunofluorescence and confocal microscopy. To analyse the morphology of cells during chemotaxis when silencing or overexpressing RhoJ, Dunn chemotaxis chamber assays were performed using time-lapse microscopy. The effect of RhoJ knockdown and overexpression on endothelial actomyosin contraction was measured using collagen type I gel contraction assays and pharmacological inhibition of ROCK and myosin II.

In summary, this chapter aims to explore the molecular mechanism by which RhoJ is regulating human EC migration.

4.2 Results

4.2.1 RhoJ regulation of focal adhesion formation

Focal adhesions are large, dynamic protein complexes through which the intracellular cytoskeleton connects to the ECM. The dynamic assembly and disassembly of focal adhesions plays a central role in cell migration (108). Vinculin is a cytoskeletal focal adhesion protein that binds to actin directly. Paxillin binds to the tail domain of vinculin (122) and provides a platform for protein tyrosine kinases such as FAK. FAK phosphorylates paxillin at Tyr118, providing a docking site for recruitment of other signalling molecules to focal adhesions, leading to their maturation (126). FAK Y397 autophosphorylation site is required for adhesion strengthening (255).

To elucidate the underlying cause for reduced movement in cells lacking RhoJ (chapter 3), focal adhesion markers, vinculin, phospho-paxillin and phospho-FAK, were used to investigate the effects of RhoJ knockdown on focal adhesion formation. HUVEC were either mock transfected, transfected with NCD, RhoJ specific D1 or D2. After two days, cells were adhered to gelatin-coated glass coverslips at a low density and were stained with anti-vinculin, anti-phospho paxillin (Tyr118) and anti-phospho FAK (Y397) antibodies to visualise focal adhesions. To quantify focal adhesion formation, the numbers of focal adhesions per cell were counted for each focal adhesion marker. Cells with reduced RhoJ expression displayed more vinculin, phospho-paxillin and phospho-FAK positive focal adhesions that also appeared slightly denser than control transfected HUVEC (figure 4.1). The quantitation confirmed that RhoJ-depleted cells had significantly increased numbers of vinculin, phospho-paxillin and phospho-FAK stained focal adhesions (figure 4.1B). This increase in focal adhesions may account for the impediment in cell motility in the RhoJ knockdown cells (chapter 3).

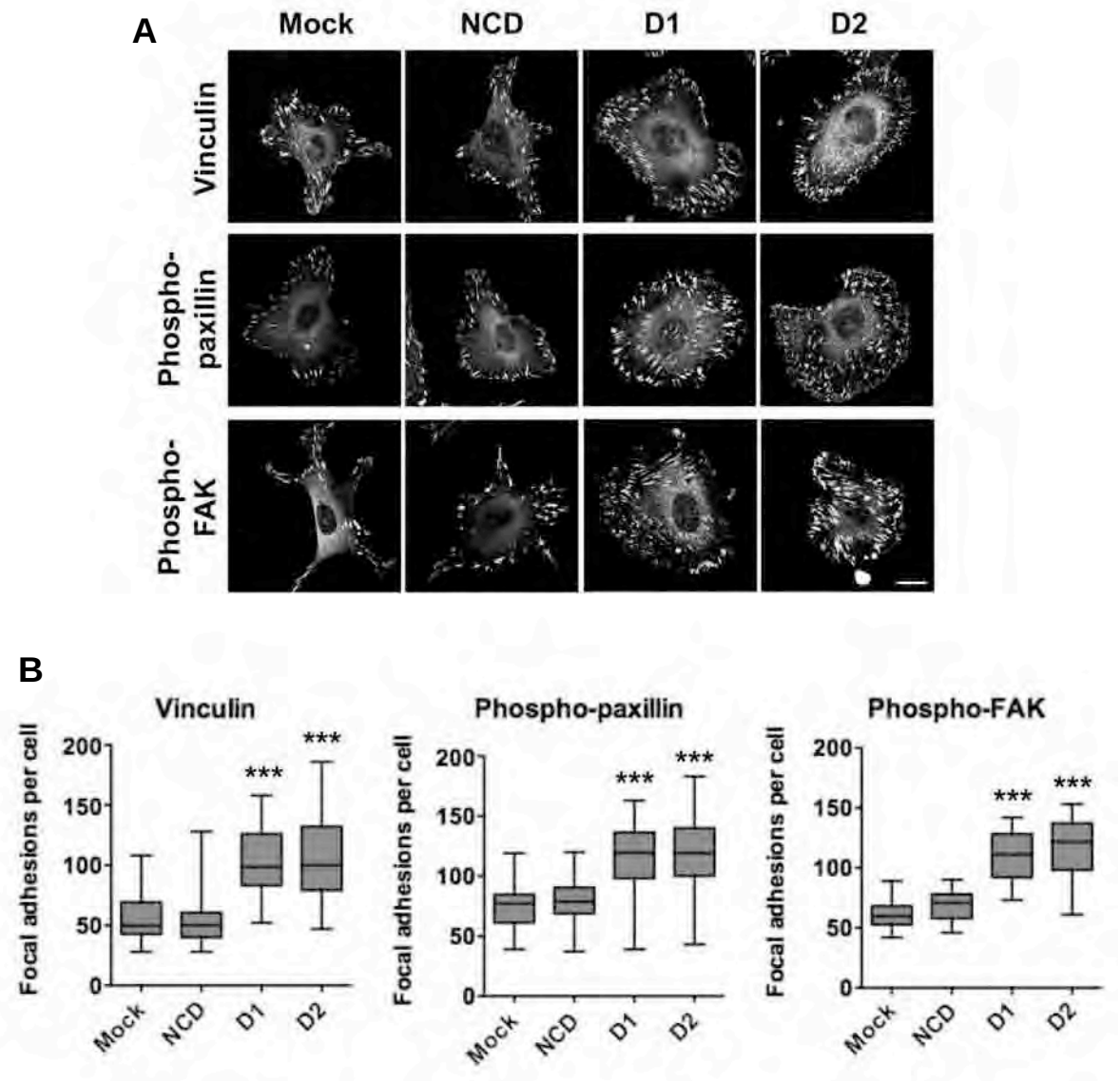

Figure 4.1 RhoJ knockdown increases focal adhesion numbers in sparsely plated cells. Human umbilical vein endothelial cells were either mock transfected or transfected with negative control duplex (NCD), RhoJ duplex 1 (D1) or RhoJ duplex 2 (D2) at 10 nM. (A) Two days later, cells were plated at low density on to glass coverslips and stained to visualise focal adhesions using vinculin, phospho-paxillin (Try118) and phospho-FAK (Y397) antibodies. Scale bar = 20 μm. (B) The numbers of focal adhesions found per cell were quantified for 30 cells from three independent experiments and displayed as box and whisker plots. The box contains the middle 50% of the data and the median is shown by the line in the box. The upper edge of the box represents the 75th percentile (upper quartile) and the lower edge of the box indicates the 25th percentile (lower quartile) of the data. The whiskers represent the maximum and minimum values of the data. One-way ANOVA showed a significant increase of focal adhesion numbers with RhoJ knockdown ($P<0.0001$ in each case). Tukey's multiple comparison test was used to compare D1 or D2 with NCD (*** = $P<0.001$).

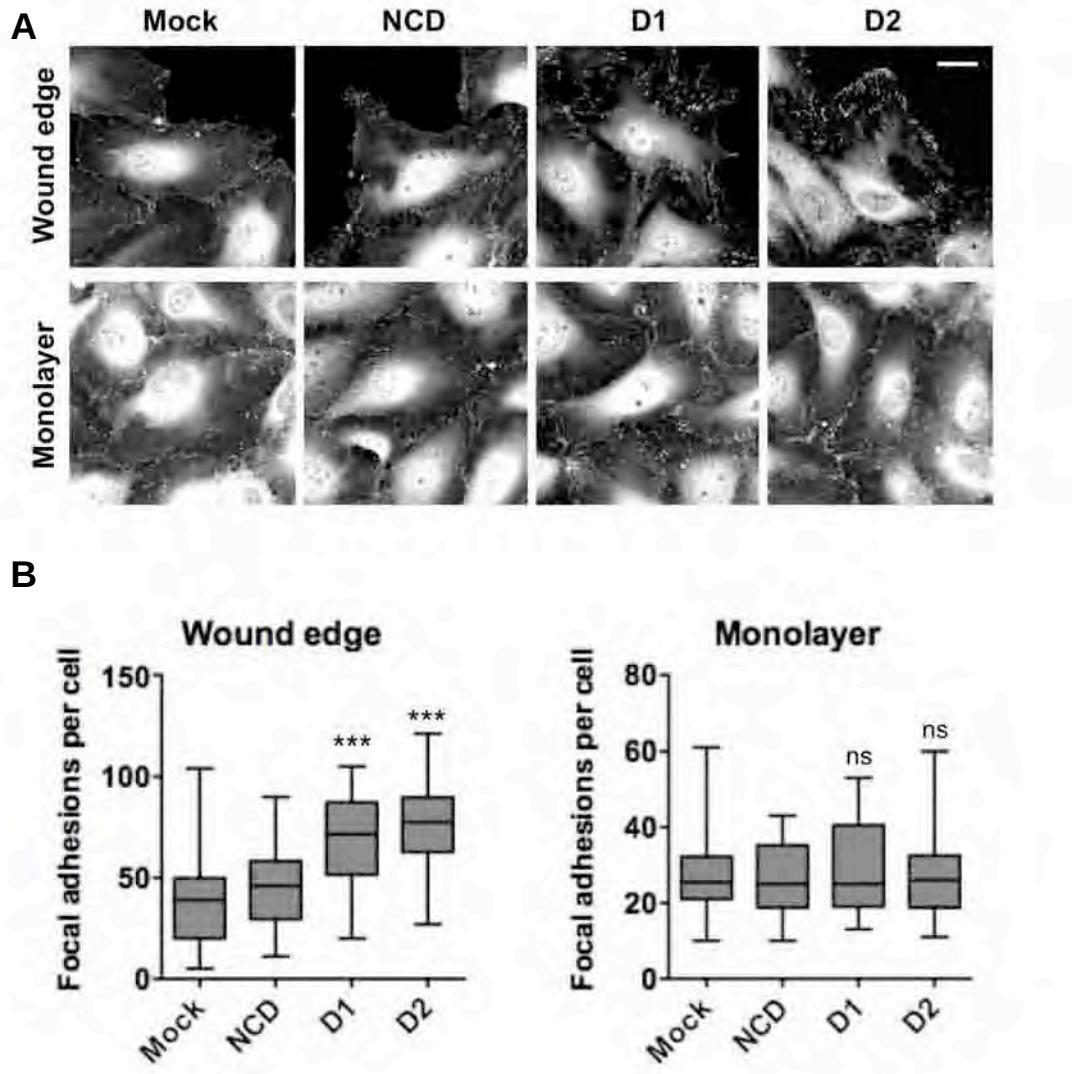

Figure 4.2 Knockdown of RhoJ increases the number of focal adhesions at the wound edge but not in the monolayer. Human umbilical vein endothelial cells were either mock transfected or transfected with negative control duplex (NCD), RhoJ duplex 1 (D1) or RhoJ duplex 2 (D2) at 10 nM. (A) Two days after transfection, scratch wound assays were set up on fully confluent glass coverslips and wounds were allowed to heal for 6 hours before staining with anti-vinculin to visualise focal adhesions. Scale bar = 10 µm. (B) The numbers of focal adhesions in cells at the wound edge or in the monolayer were quantified for at least 30 cells from three independent experiments and displayed as a box and whisker plots. The box contains the middle 50% of the data and the median is shown by the line in the box. The upper edge of the box represents the 75^{th} percentile (upper quartile) and the lower edge of the box indicates the 25^{th} percentile (lower quartile) of the data. The whiskers represent the maximum and minimum values of the data. One-way ANOVA showed a significant increase of focal adhesion numbers with RhoJ knockdown at the wound edge ($P<0.0001$) but not in the monolayer (ns: not significant). Tukey's multiple comparison test was used to compare D1 or D2 with NCD (*** = $P<0.001$).

ECs in vessels are normally found as a monolayer surrounded by other ECs. Hence it was important to know whether focal adhesion numbers were also affected with RhoJ knockdown in an endothelial monolayer. However, to form a new microvessel ECs can differentiate to become tip cells, which guide newly formed sprouts towards a chemoattractant gradient. Tips cells are not completely surrounded by other ECs and have now been shown to have distinct signalling pathways controlling their migration (256).

To assess whether RhoJ knockdown differentially affected focal adhesion numbers in ECs depending on their cellular context, cells at the wound edge of a scratch wound were compared to those found within a monolayer. HUVEC were siRNA transfected with NCD, RhoJ specific D1 or D2 or mock transfected. Two days later, scratch wound assays were set up on gelatin-coated glass coverslips. Six hours after the scratches were made, cells were fixed, permeabilised and stained with anti-vinculin antibodies. To quantify focal adhesion numbers, the number of focal adhesions found per cell either at the wound edge or in the monolayer was counted. SiRNA mediated knockdown of RhoJ resulted in increased focal adhesion numbers in cells at the edge of a scratch compared with control transfected cells (figure 4.2A). However no differences were observed in cells within the monolayer. Counting focal adhesions confirmed that RhoJ knockdown significantly increased the number of focal adhesions per cell at the migrating front of a scratch wound but RhoJ knockdown did not significantly affect focal adhesion formation of cells in the monolayer (figure 4.2B).

4.2.2 RhoJ regulation of stress fibre formation and actomyosin contractility

Since Rho GTPases have been shown to control the actin cytoskeleton and focal adhesions are physically linked to the actin cytoskeleton, experiments were performed to investigate how RhoJ knockdown might affect filamentous actin (f-actin) organisation in sparsely plated ECs.

Two days after siRNA transfection, HUVEC were adhered to gelatin-coated glass coverslips at a low density and were stained with phalloidin-TRITC to detect f-actin. Control transfected HUVEC displayed actin protrusions and moderate numbers of stress fibres (figure 4.3A). However, cells with reduced RhoJ expression appeared to have less protrusions and more stress fibres. To quantify stress fibre formation, LSM 510 confocal software was used to obtain the mean fluorescent intensity of the phalloidin-TRITC staining per cell. RhoJ knockdown significantly increased actin staining intensity indicating that RhoJ-depleted cells have increased numbers of stress fibres (figure 4.3B).

As mentioned earlier, ECs exist *in vivo* as a monolayer, except for when endothelial tip cells are leading the end of an angiogenic sprout. To assess whether RhoJ knockdown affected stress fibre formation in ECs depending on their cellular setting, cells at the wound edge of a scratch wound were compared to those found within a monolayer. HUVEC were either mock transfected, transfected with NCD, RhoJ specific D1 or D2. Two days later, scratch wound assays were set up on gelatin-coated glass coverslips. Six hours after the scratches were made, cells were fixed, permeabilised and stained with phalloidin-TRITC. To quantify stress fibres, the mean fluorescent intensity of the phalloidin-TRITC staining per cell either at the wound edge or in the monolayer was measured. SiRNA-mediated knockdown of RhoJ resulted in increased stress fibres in cells at the edge of a scratch compared with control transfected cells (figure 4.4A).

As before, no differences were observed in cells within the monolayer. RhoJ knockdown significantly increased actin intensity at the migrating front of a scratch wound but RhoJ knockdown did not significantly affect stress fibre formation of cells in the monolayer (figure 4.4B). These data suggest that increased stress fibres in RhoJ-depleted cells may be the cause for the motility defects found in RhoJ knockdown cells.

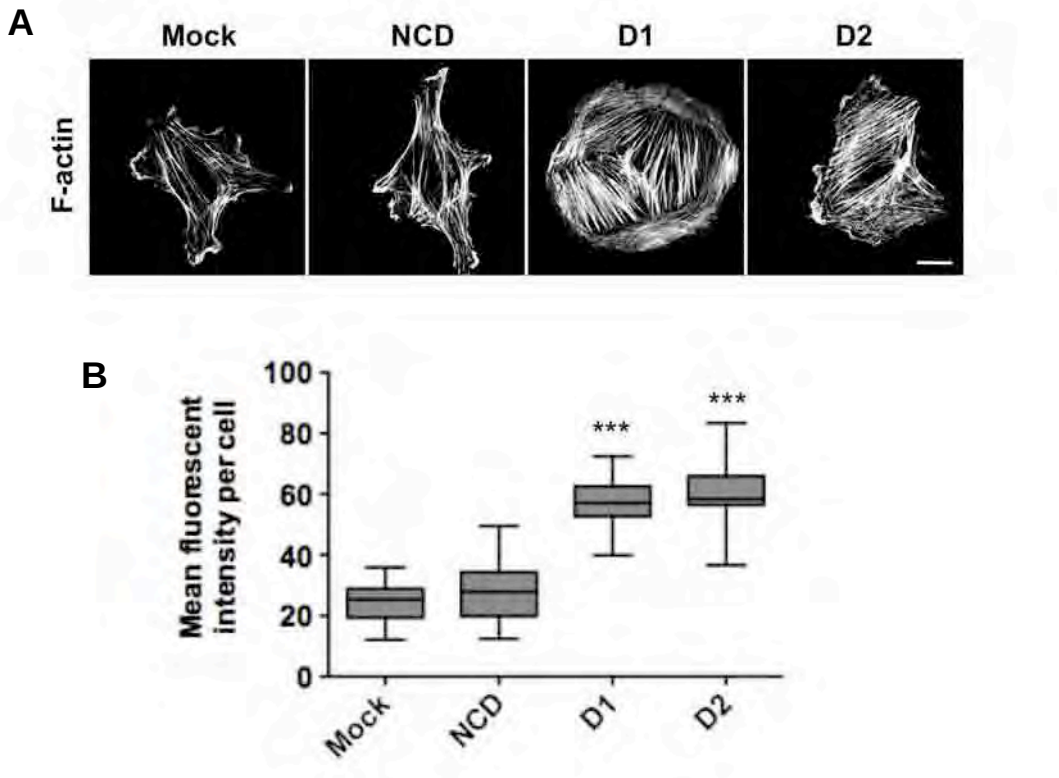

Figure 4.3 RhoJ knockdown increases stress fibre formation in sparsely plated cells. Human umbilical vein endothelial cells were either mock transfected or transfected with negative control duplex (NCD), RhoJ duplex 1 (D1) or RhoJ duplex 2 (D2) at 10 nM. (A) Two days after transfection, cells were plated at low density on to glass coverslips and stained with phalloidin-TRITC to visualise filamentous actin (f-actin). Scale bar = 20 μm. (B) The mean fluorescent intensity of f-actin staining per cell were quantified for 30 cells from three independent experiments and displayed as box and whisker plots. The box contains the middle 50% of the data and the median is shown by the line in the box. The upper edge of the box represents the 75th percentile (upper quartile) and the lower edge of the box indicates the 25th percentile (lower quartile) of the data. The whiskers represent the maximum and minimum values of the data. One-way ANOVA showed a significant increase in the intensity of f-actin staining in RhoJ-depleted cells ($P<0.0001$). Tukey's multiple comparison test was used to compare D1 or D2 with NCD (*** = $P<0.001$).

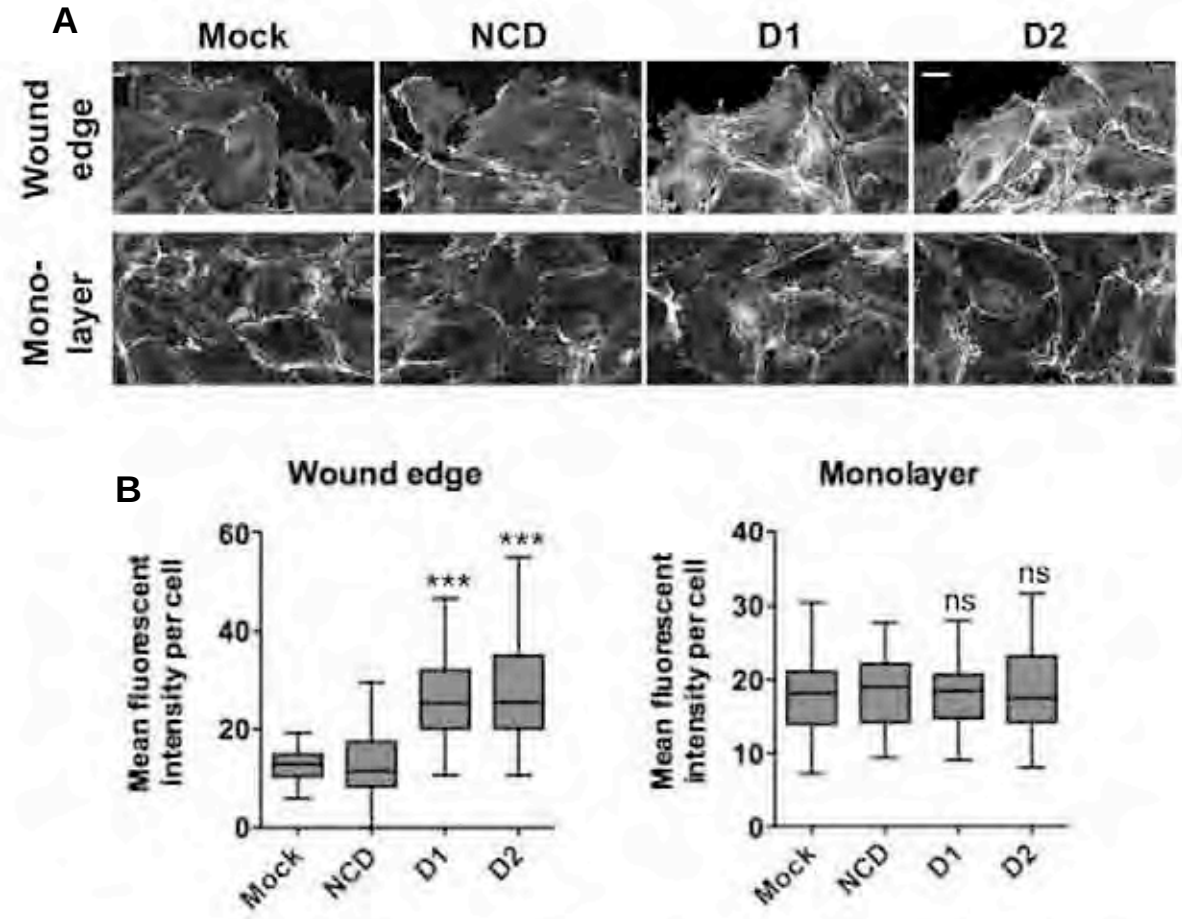

Figure 4.4 Knockdown of RhoJ increases stress fibre formation at the wound edge but not in the monolayer. Human umbilical vein endothelial cells were either mock transfected or transfected with negative control duplex (NCD), RhoJ duplex 1 (D1) or RhoJ duplex 2 (D2) at 10 nM. (A) Two days after transfection, scratch wound assays were set up on fully confluent glass coverslips and allowed to heal for 6 hours before staining with phalloidin-TRITC to visualise filamentous actin. Scale bar = 10 μm. (B) The mean fluorescent intensity of filamentous actin staining per cell of cells at the wound edge or in the monolayer were quantified for at least 30 cells from three independent experiments and displayed as a box and whisker plots. The box contains the middle 50% of the data and the median is shown by the line in the box. The upper edge of the box represents the 75th percentile (upper quartile) and the lower edge of the box indicates the 25th percentile (lower quartile) of the data. The whiskers represent the maximum and minimum values of the data. One-way ANOVA showed a significant increase in the intensity of filamentous actin staining in RhoJ-depleted cells at the wound edge ($P<0.0001$) but not in the monolayer (ns: not significant). Tukey's multiple comparison test was used to compare D1 or D2 with NCD (*** = $P<0.001$).

In order to visualise the migratory behaviour of cells lacking RhoJ in response to a chemoattractant gradient during chemotaxis, a Dunn chemotaxis chamber assay was set up where the cells could be observed microscopically in real time, something that could not be done with a Boyden chamber. The Dunn chamber consists of two concentric circles ground into one face of a glass slide, referred to as the inner and outer wells. A ring-shaped ridge, referred to as the bridge, separates the two wells. The bridge is 20 μm lower than the rest of the glass slide. The outer well contains the chemoattractant and the inner well contains control media. A linear gradient of the chemoattractant forms by diffusion across the bridge between the two wells. Cells seeded onto a glass coverslip are inverted onto the slide. The cells that lie directly over the bridge of the chamber between the two wells can be observed using live imaging microscopy and their migratory paths towards the gradient can be mapped.

Two days after HUVEC were siRNA transfected, cells were plated sparsely onto coverslips and left to adhere for 1 hour in low-serum media before loading on to the Dunn chamber. The outer wells were filled with media containing 10% FCS supplemented with bovine brain extract. Inner wells were filled with 1% FCS media. The Dunn chamber was placed in a humidified chamber on a heated stage at 37°C in 5% CO_2 using an inverted microscope setup. Time-lapse images were digitally captured every minute for 4 hours. Migratory paths of individual cells were tracked and plotted as direction plots. The majority of the mock and NCD transfected cells migrated towards the chemoattractant, which is located at the top of the plots (figure 4.5A). However RhoJ knocked down cells did not migrate towards the direction of the chemoattractant and did not considerably move away from their point of origin. The time-lapse images in figure 4.5B show that the control-transfected cells were polarised, elongated and migrated towards the chemoattractant. However RhoJ-depleted cells were round in shape, unpolarised and displayed dynamic blebbing of their plasma membrane, which occurred constantly throughout the 4-hour period. Blebs arise from rapid detachment of

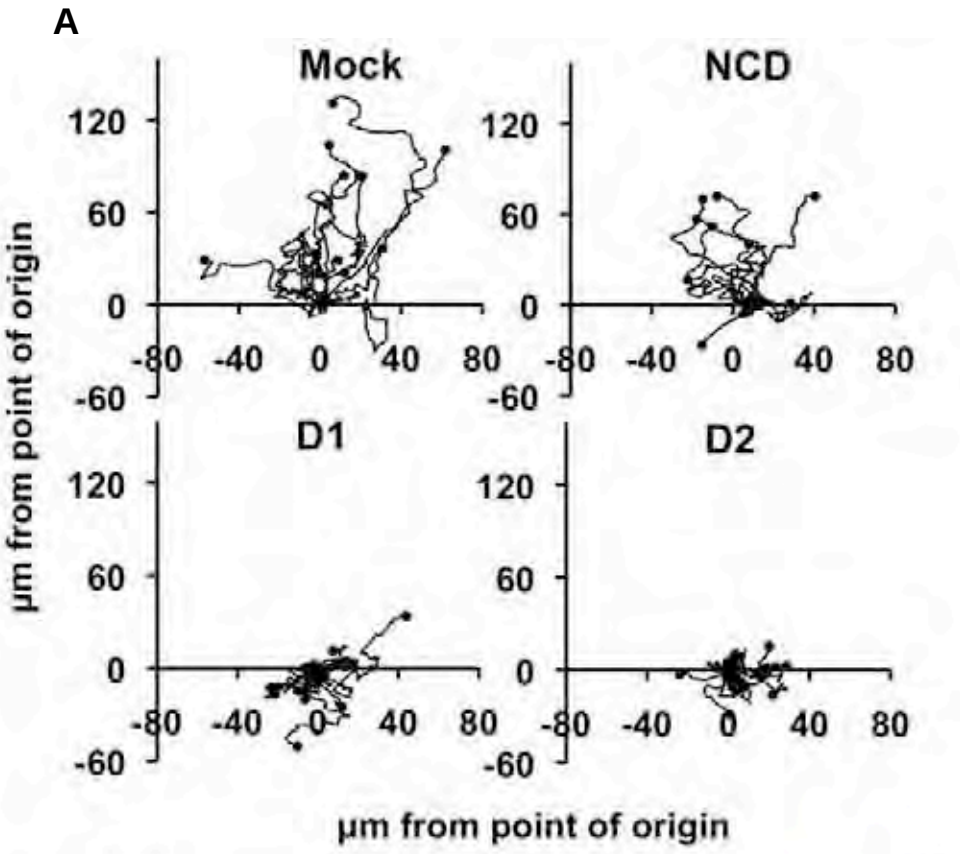
A
Mock
NCD
D1
D2
120
60
0
-60
-80
-40
0
40
80
µm from point of origin
µm from point of origin

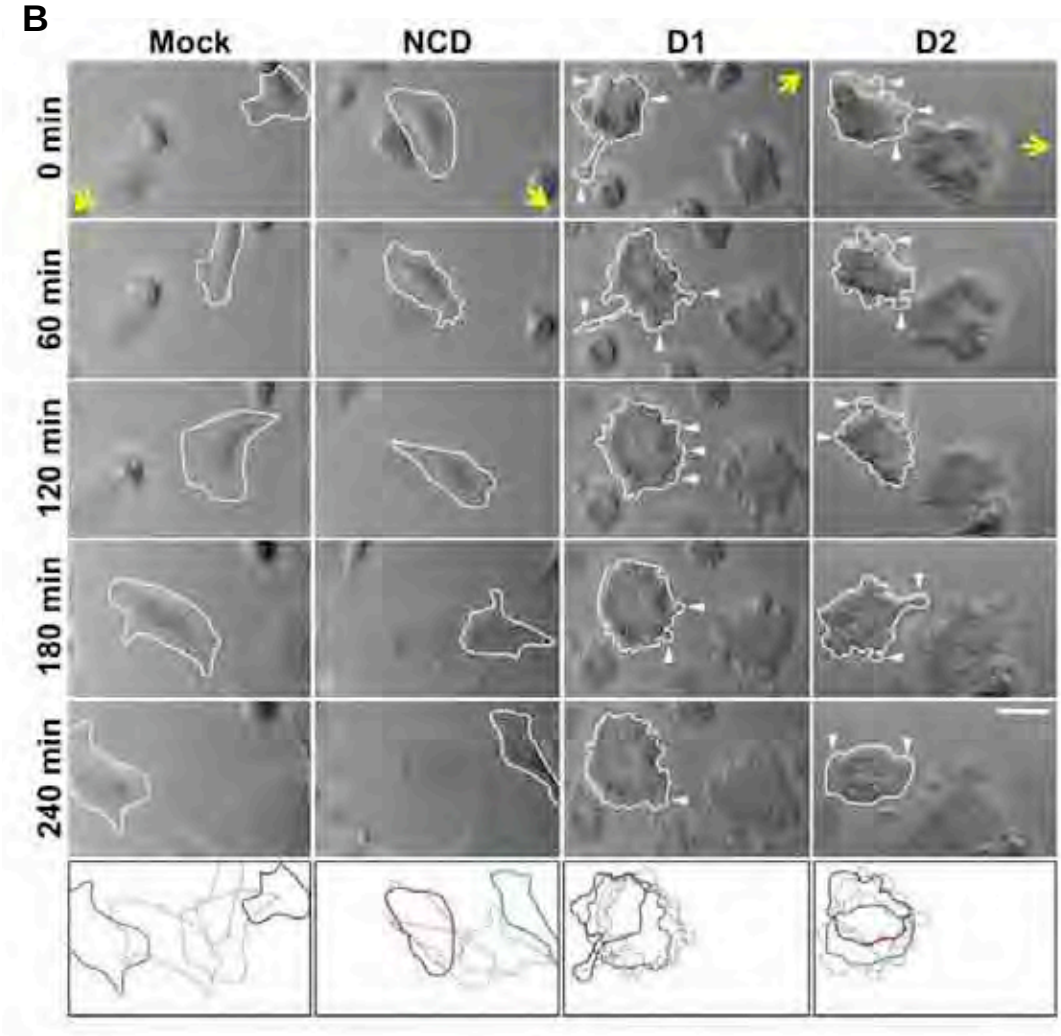

Figure 4.5 Cells with reduced RhoJ expression demonstrate defective morphological polarisation and bleb-like membrane protrusions in the presence of a chemoattractant gradient. Human umbilical vein endothelial cells were either mock transfected or transfected with negative control duplex (NCD), RhoJ duplex 1 (D1) or RhoJ duplex 2 (D2) at 10 nM. Two days after transfection, cells were plated onto gelatin-coated coverslips and inverted onto the Dunn chemotaxis chamber. Cell polarisation and migration towards 10% fetal calf serum and bovine brain extract was monitored over 4 hours using time-lapse microscopy. (A) The migratory tracks of 10 or more cells are displayed as direction plots with the source of the chemoattractant located at the top of the plots. (B) Frames of cells at 0, 60, 120, 180 and 240 min are shown. Outlines of the cells at 0 (red), 60-180 (grey) and 240 (green) min reveal the migratory paths of the cells outlined in white. Yellow arrows indicate the source of the chemoattractant and white arrowheads indicate bleb-like protrusions. Scale bar = 10 μm. Similar data were obtained in three independent experiments.

the actomyosin cortex from the plasma membrane. Blebs inflate over ~30 seconds to form spherical protrusions that are filled with cytosol (257, 258). When blebs stop expanding, blebs are retracted as the contractile actin cortex reassembles under the membrane (259). Membrane detachment from the actin cortex and bleb inflation are thought to occur as a result of increased intracellular pressure generated by increased actomyosin contraction since blebbistatin-mediated inhibition of myosin II ATPase was shown to prevent bleb formation (260).

Since membrane blebbing is driven by actomyosin contractility and RhoJ knockdown was shown to increase stress fibre formation, the effect of RhoJ depletion on contractility was investigated by measuring endothelial contractility using a gel contraction kit. The use of cell-populated collagen type I gels to measure contractility of human fibroblasts was first described by Bell *et al.* (1979) (219). Vernon and Sage in 1996 then demonstrated that ECs also have the ability to contract collagen type I gels (220). In order to assay cell contraction, siRNA transfected HUVEC were harvested and embedded into type I collagen gels. Two days later, when stress had developed in the collagen matrices, the collagen gels were gently released from the sides of the culture dishes using a sterile pipette tip to initiate cell contraction. The degree of cell contraction was evaluated by measuring the diameter of the free-floating collagen gels after five days. Blebbistatin is an inhibitor of myosin II ATPase activity and binds specifically to the ATP binding region of myosin II heads and blocks the release of P_i hence inhibiting actomyosin contractility (261, 262). Thus for each condition, a negative control was added where blebbistatin was used to inhibit actomyosin contractility. RhoJ knockdown significantly decreased the diameter of collagen gels indicating that cells with reduced RhoJ expression have increased actomyosin contractility (figure 4.6A). Contraction of the collagen gels was reversed by adding blebbistatin, thus providing further

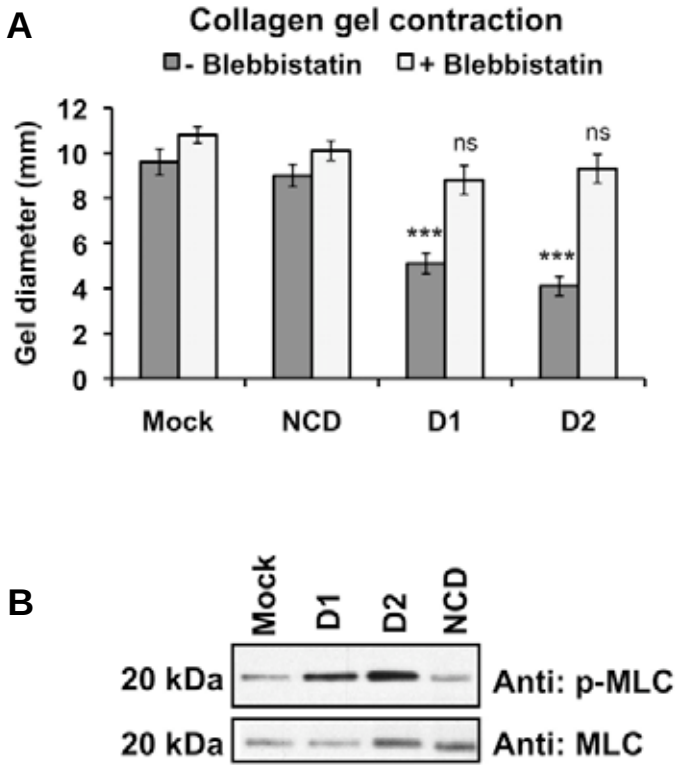

Figure 4.6 RhoJ knockdown increases actomyosin contractility. Human umbilical vein endothelial cells were either mock transfected or transfected with negative control duplex (NCD), RhoJ duplex 1 (D1) or RhoJ duplex 2 (D2) at 10 nM. (A) Two days after transfection, collagen gel contraction assays were set up and the diameters of cell-populated collagen gels were measured 7 days later. For each condition a control was added where non-muscle myosin II was inhibited by blebbistatin. Values represent the means of three independent experiments. Error bars depict the standard error of the mean. One-way ANOVA showed that knockdown of RhoJ significantly decreased the diameter of collagen gels ($P<0.0001$), which was reversed with blebbistatin (ns: not significant). Tukey's multiple comparison test was used to compare D1 or D2 with NCD (*** = $P<0.001$). (B) One day after transfection, cells were replated on to Matrigel. 24 hours later, cell lysates were prepared and blotted for phospho and total myosin light chain (MLC). Performed by Dr. Sabu Abraham and Dr. Georgia Mavria (Institute of Molecular Medicine, Leeds, UK and Institute of Cancer Research, London, UK). Permission for the use of their figure in this thesis was given. Similar data were obtained in three independent experiments

evidence that RhoJ-depleted cells contracted the collagen gels via increased actomyosin contractility.

Rho-kinase (ROCK) is a serine/threonine kinase and is an effector molecule of RhoA (263). ROCK phosphorylates myosin light chain (MLC), which in turn increases actomyosin contractility (263). Cells undergoing actomyosin contraction would be expected to have increased levels of phosphorylated MLC. Dr. Sabu Abraham and Dr. Georgia Mavria (collaborators from the Institute of Molecular Medicine, Leeds, UK and Institute of Cancer Research, London, UK) checked the levels of phospho-MLC in RhoJ knockdown cells undergoing differentiation on Matrigel. This experiment involved knocking down RhoJ and plating cells on to Matrigel for 24 hours before harvesting and lysing the cells. Western blotting was performed using phospho-MLC (ser19/thr18) antibodies to detect the levels of phosphorylated MLC or pan-MLC antibodies to detect total levels of MLC. Knockdown of RhoJ increased phospho-MLC levels in cells plated on to Matrigel, indicating that these cells have increased actomyosin contractility (figure 4.6B). This data was included in this thesis to further support the data in figure 4.6A showing that RhoJ knocked down cells have increased actomyosin contractility. Dr. Sabu Abraham and Dr. Georgia Mavria gave full consent for the use of their data in this thesis.

The effects of overexpressing wild type RhoJ or constitutively active RhoJ (permanently locked in the GTP-bound active form) on cell motility and contractility was also assessed. Cells that expressed GFP, GFP-tagged wild type RhoJ (GFP-wtRhoJ) or GFP-tagged dominant active mutant (Q79L) of RhoJ (GFP-daRhoJ) were generated by Mrs. Katarzyna Leszczynska (University of Birmingham, UK). Recombinant lentiviral particles containing

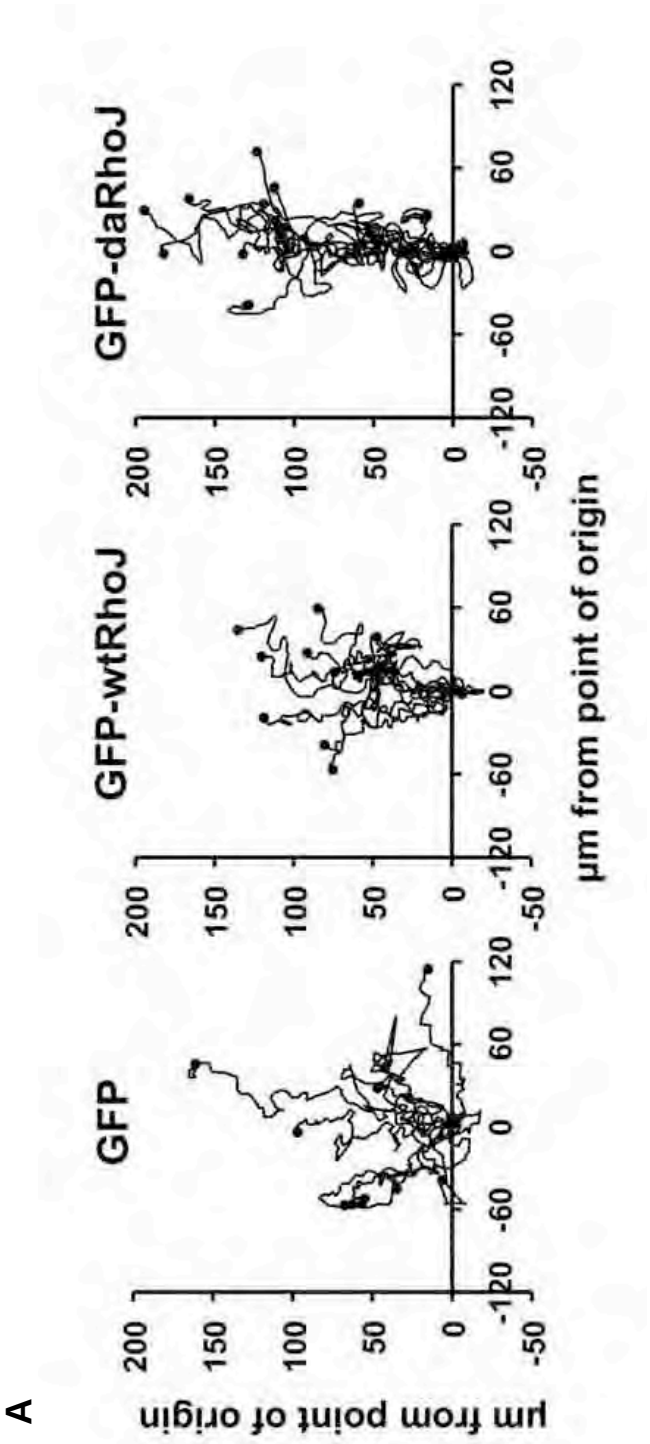
A
GFP
GFP-wtRhoJ
GFP-daRhoJ
µm from point of origin
µm from point of origin
200
150
100
50
0
-50
-120
-60
0
60
120

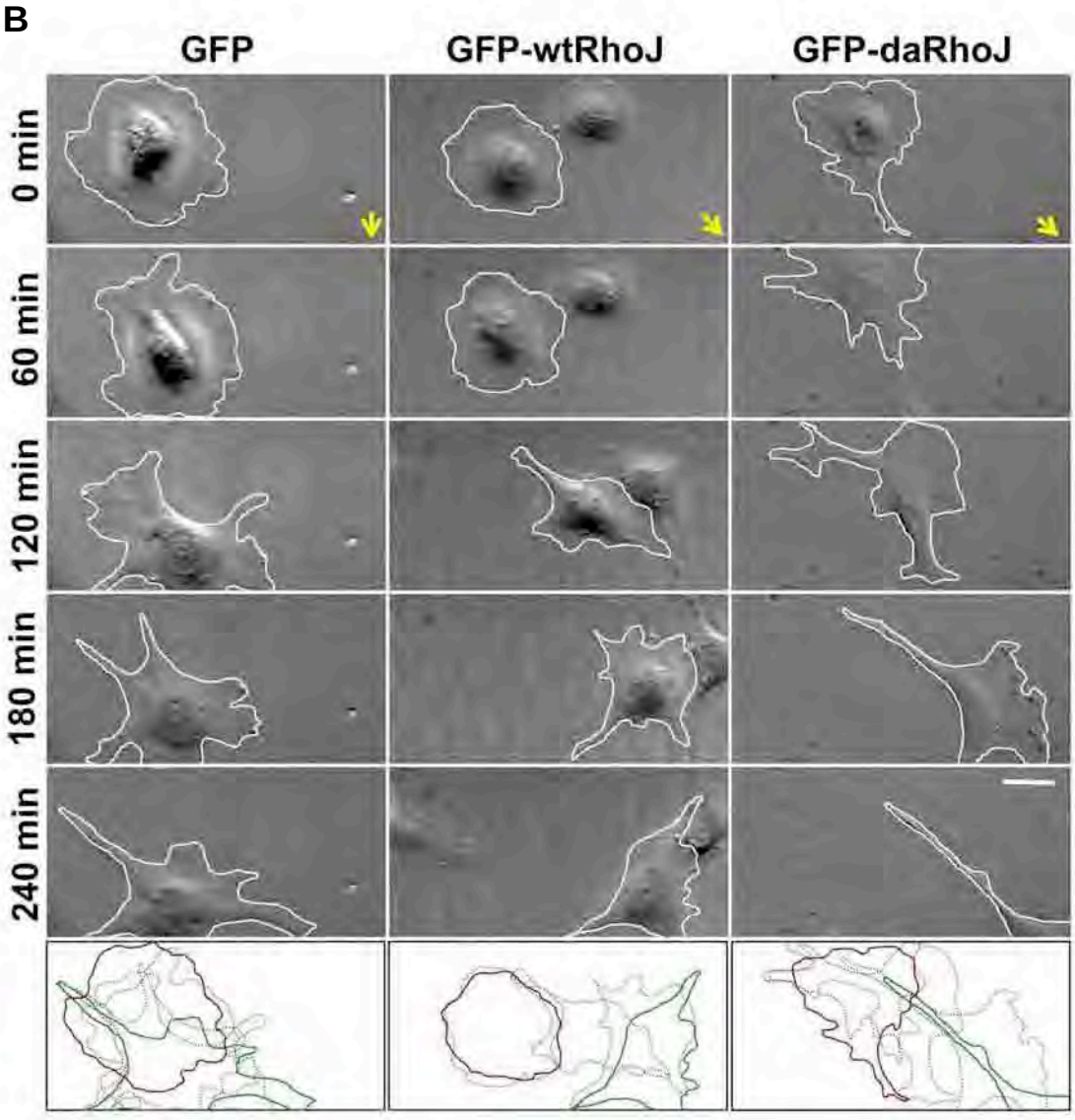
B
GFP
GFP-wtRhoJ
GFP-daRhoJ
0 min
60 min
120 min
180 min
240 min

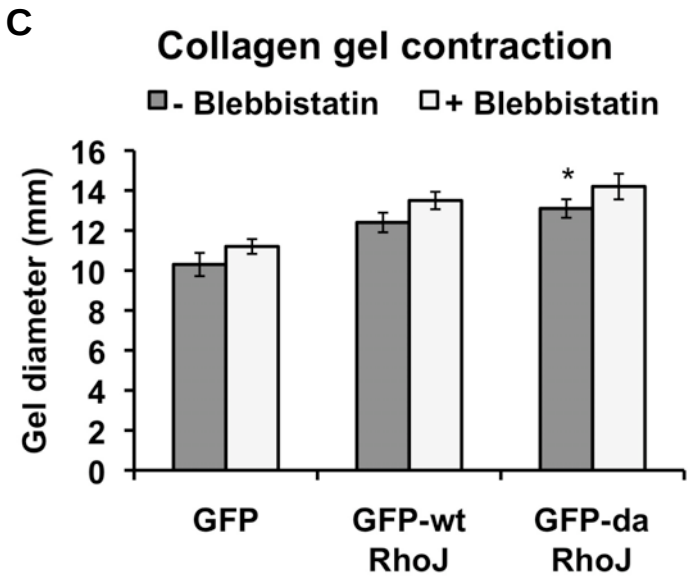
C
Collagen gel contraction
- Blebbistatin
+ Blebbistatin
Gel diameter (mm)
16
14
12
10
8
6
4
2
0
*
GFP
GFP-wt RhoJ
GFP-da RhoJ

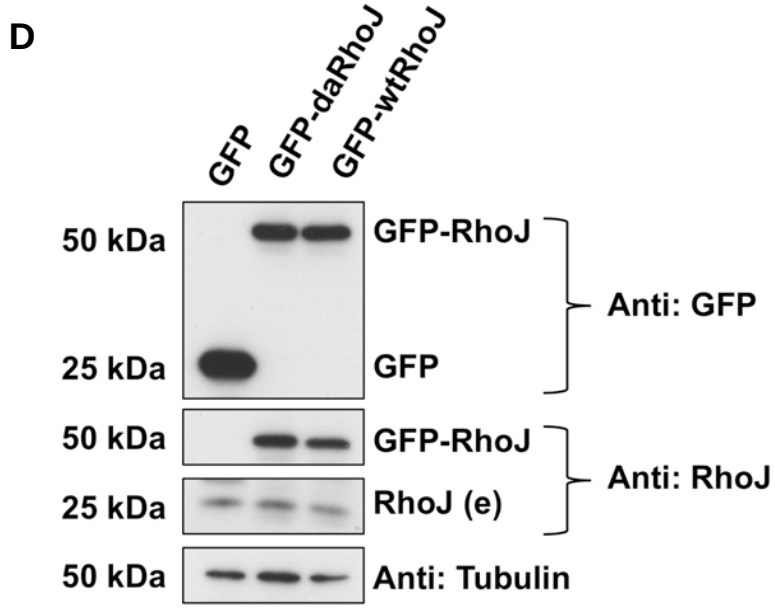

Figure 4.7 Overexpression of dominant active RhoJ increases cell motility and reduces actomyosin contractility. Human umbilical vein endothelial cells were lentivirally transduced to express GFP, GFP-wtRhoJ or GFP-daRhoJ (A) Cells were plated onto gelatin-coated coverslips and inverted onto the Dunn chemotaxis chamber. Cell polarisation and migration towards 10% fetal calf serum and bovine brain extract was monitored over 4 hours using time-lapse microscopy. The migratory tracks of 10 or more cells are displayed as direction plots with the source of the chemoattractant located at the top of the plots. (B) Frames of cells at 0, 60, 120, 180 and 240 min are shown. Outlines of the cells at 0 (red), 60-180 (grey) and 240 (green) min reveal the migratory paths of the cells outlined in white. Yellow arrows indicate the source of the chemoattractant. Scale bar = 10 μm. Similar data were obtained in three independent experiments. (C) Collagen gel contraction assays were set up and the diameter of cell-populated collagen gels were measured 7 days later. For each condition a control was added where non-muscle myosin II was inhibited by blebbistatin. Values represent the means of three independent experiments. Error bars depict the standard error of the mean. One-way ANOVA showed that overexpression of dominant active RhoJ significantly increased the diameter of collagen gels ($P<0.0183$). Tukey's multiple comparison test was used to compare GFP-wtRhoJ or GFP-daRhoJ with GFP control (* = $P<0.05$). (D) Western blots of GFP, GFP-wtRhoJ and GFP-daRhoJ cell lysates blotted with GFP, RhoJ and tubulin antibodies. (e): endogenous. Performed by Mrs. Katarzyna Leszczynska from The University of Birmingham, UK. Full consent for the use of this figure was given.

either GFP, GFP-wtRhoJ or GFP-daRhoJ were produced by transient transfection of HEK293T cells. The lentiviral supernatants were collected and concentrated before stably transducing into HUVEC. Cells from each condition were then purified by selection of GFP positive cells using flow cytometric sorting to ensure that every cell used in assays were successfully infected with either GFP, GFP-wtRhoJ or GFP-daRhoJ lentivirus vectors.

In order to observe the morphology and the chemotactic response of cells overexpressing wild type or dominant active RhoJ during live chemotaxis, a Dunn chemotaxis chamber assay was set up. GFP, GFP-wtRhoJ and GFP-daRhoJ cells were plated sparsely onto coverslips and left to adhere for 1 hour in low-serum media before loading on to the Dunn chamber. The outer wells were filled with media containing 10% FCS supplemented with bovine brain extract and inner wells were filled with 1% FCS media. Time-lapse images of cells that lay directly over the bridge between the two wells at 37°C in 5% CO_2 were digitally captured every minute for 4 hours. Most of the cells expressing GFP alone migrated towards the FCS gradient (figure 4.7A). Cells expressing GFP-wtRhoJ and GFP-daRhoJ also migrated successfully towards the chemoattractant however GFP-daRhoJ cells moved a greater distance towards the FCS suggesting that these cells have increased motility. GFP-wtRhoJ and GFP-daRhoJ cells polarised and extended towards the chemoattractant in a similar way to control cells (figure 4.7B). Moreover, GFP-daRhoJ cells generally extended out long cellular protrusions in an attempt to connect to one another in similar way to how ECs connect in tube forming assays on Matrigel.

To investigate the effect of wild type RhoJ or constitutively active RhoJ overexpression on actomyosin contraction, cells expressing either GFP, GFP-wtRhoJ or GFP-daRhoJ were embedded into type I collagen gels. Two days later, gel contraction was initiated by pulling away the collagen gels from the sides of the culture dishes with a sterile pipette tip. The

degree of cell contraction was evaluated by measuring the diameter of the free-floating collagen gels after five days. For each condition, a negative control was added where blebbistatin was used to inhibit actomyosin contractility. Overexpression of dominant active RhoJ significantly increased the diameter of collagen gels in comparison to control indicating that GFP-daRhoJ cells have decreased actomyosin contractility (figure 4.7C). Although the mean diameter of the collagen gels containing GFP-wtRhoJ cells was higher than GFP control, the means were not statistically different from each other. The expression of the GFP, GFP-wtRhoJ and GFP-daRhoJ was confirmed by western blotting (figure 4.7D). Cell lysates from HUVEC expressing GFP, GFP-wtRhoJ or GFP-daRhoJ were blotted with GFP, RhoJ or tubulin antibodies. This Western blot was performed by Mrs. Katarzyna Leszczynska (The University of Birmingham, UK) and full consent for the use of figure 4.7D in this thesis was given.

Data in figure 4.8 shows that cells with reduced RhoJ expression did not polarise their cell shape in the direction of migration indicating that these cells may not have the ability to detect chemoattractant stimuli in order to migrate directionally. Polarised cells reorganise the position of the Golgi apparatus towards the direction of movement (103). Nobes and Hall (1999) showed that Cdc42 activity is required for Golgi reorientation and that the reorientation of the Golgi towards the direction of migration is an essential process for directional cell movement (165). To determine whether knocking down RhoJ affects cell polarisation, the position of the Golgi apparatus in RhoJ-depleted cells at the wound edge was assessed. Two days after transfection, scratch wound assays were set up on fully confluent glass coverslips. Six hours later, cells were fixed, permeabilised and stained with anti-GM130 (a cis-Golgi matrix protein (264)) and DAPI. To quantify the number of polarised wound edge cells, cells were divided up into three 120° sectors centering on the nucleus, one of which faced the edge of the wound. Cells in which the Golgi apparatus was found within the

sector facing the wound were scored positive and counted. Staining of the Golgi in cells at the wound edge and an example of how cells were scored as positive are shown in figure 4.8A. Quantitation of the the wound edge cells revealed that RhoJ-depletion did not alter the reorientation of the Golgi apparatus which suggests that cells with reduced RhoJ expression are capable of sensing the edge of a scratch (figure 4.8B).

ECs are connected to one another through cell-cell adherens junctions, which are important for contact inhibition regulation, permeability and the organisation of new vessels during angiogenesis (265). VE-Cadherin is expressed at adherens junctions and is known to modulate endothelial permeability and barrier function downstream of RhoA and Rac1. RhoA inhibition has been shown to increase junctional localisation of VE-Cadherin whereas inhibition of Rac1 shows the converse (177). The effect of RhoJ knockdown on cell-cell junctions was also investigated by analysing the expression of VE-Cadherin at cell-cell junctions. HUVEC were transfected with NCD, RhoJ specific D1 or D2 or mock transfected. Cells were grown to confluence on glass coverslips and seven days later, cells were fixed, permeabilised and stained with anti-VE-Cadherin and DAPI. Expression of VE-Cadherin at cell-cell junctions did not appear to be altered by RhoJ knockdown (figure 4.9).

4.2.3 Rescue of motility defects in RhoJ siRNA-treated cells

4.2.3.1 Inhibition of Rho-kinase activity

The activation of ROCK, which is downstream of RhoA, modulates the rearrangement of the actin cytoskeleton and focal adhesions by inducing contraction of actomyosin fibres (134, 159). Since RhoJ knockdown was shown to increase stress fibre formation (figure 4.3), actomyosin cell contraction and MLC phosphorylation (figure 4.6), it was hypothesised that knockdown of RhoJ causes an increase in ROCK activity, which in turn increases phospho-

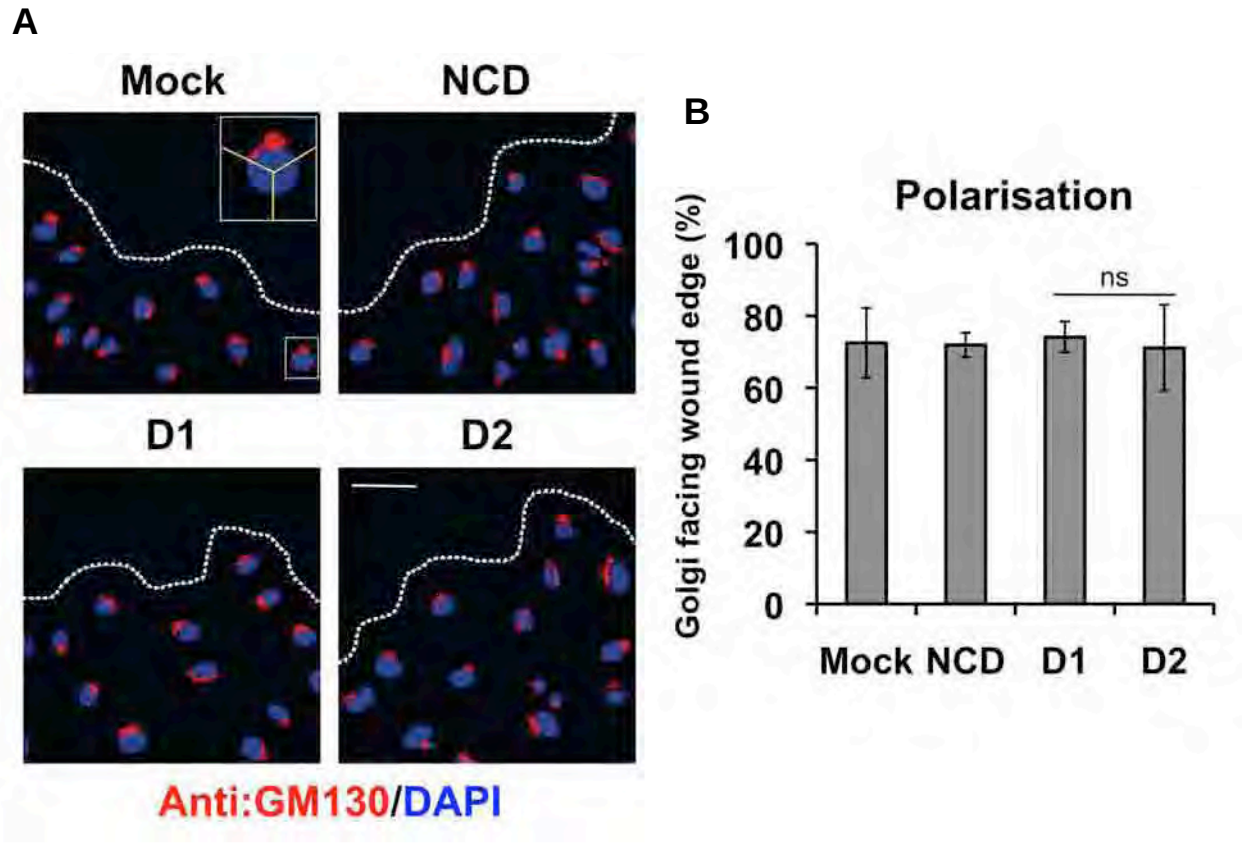

Figure 4.8 Knockdown of RhoJ does not affect polarisation of the Golgi apparatus in a scratch wound assay. Human umbilical vein endothelial cells were either mock transfected or transfected with negative control duplex (NCD), RhoJ duplex 1 (D1) or RhoJ duplex 2 (D2) at 10 nM. Two days after transfection, scratch wound assays were set up on fully confluent glass coverslips and allowed to heal for 6 hours before fixing and staining with anti-GM130 and DAPI. The white boxes represent a polarised cell with the Golgi apparatus located within the 120° sector facing the wound edge. Dotted white lines indicate the edge of the scratch. Scale bar = 20 μm. (B) The percentage of cells at the scratch margin with the Golgi apparatus facing the wound edge was calculated from 50 cells from three independent experiments. Error bars show the standard error of the mean. Analysis using one-way ANOVA showed that knockdown of RhoJ did not affect Golgi reorientation in migrating cells (ns: not significant).

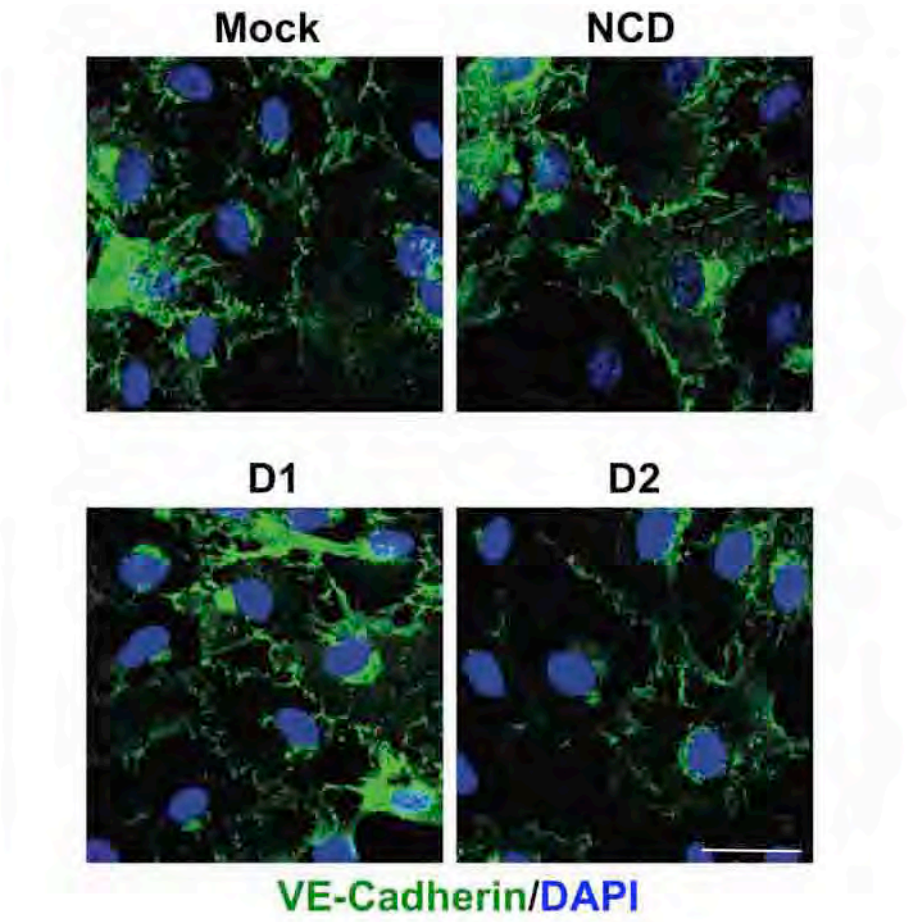

Figure 4.9 Knockdown of RhoJ does not affect the localisation of VE-Cadherin at cell-cell junctions. Human umbilical vein endothelial cells were either mock transfected or transfected with negative control duplex (NCD), RhoJ duplex 1 (D1) or RhoJ duplex 2 (D2) at 10 nM. Transfected cells were grown to confluence on glass coverslips and were then stained with anti-VE-Cadherin and DAPI. Scale bar = 50 μm. Similar data were obtained in three independent experiments

MLC levels and actomyosin contractility resulting in impaired tube formation and motility defects. Thus it was thought that inhibition of ROCK would ameliorate the RhoJ knockdown-mediated defects in cell motility and tube formation. To test this hypothesis, ROCK was inhibited using a selective ROCK inhibitor, Y27632 (266), in RhoJ knocked down cells. These cells were then assayed in Matrigel tube formation, scratch wound and Boyden chamber chemotaxis assays. Assays were set up as previously described except where required Y27632 was added to the media at 10 μM at the beginning of every assay.

Twenty-four hours post seeding on to Matrigel, cells with reduced RhoJ expression treated with Y27632 produced well-connected and stable capillary-like networks (figure 4.10A). These tubule networks displayed reduced numbers of unconnected branches and increased numbers of complex nodes (nodes with 3 or more branch points) to similar levels found in NCD control (figure 4.10B). In wound healing, ROCK inhibited RhoJ-depleted cells completely closed the scratch by 24 hours at a similar rate to NCD treated cells (figure 4.10C). The significant reduction in chemokinetic migration with RhoJ knockdown at 24 hours was reversed with inhibition of ROCK (figure 4.10D). In the Boyden chamber assay, as expected, knockdown of RhoJ alone resulted in a significant reduction in chemotactic migration towards serum-rich media. However with ROCK inhibition in RhoJ knocked down cells, the migratory response towards the chemoattractant gradient was similar to NCD control (figure 4.10E).

ROCK was also inhibited using H1152 (267), which is an inhibitor that has an unrelated chemical structure to Y27632. Although Y27632 is known to inhibit ROCK with high potency, like all pharmacological inhibitors, it can exhibit off-target effects (268). To confirm that the phenotypic effect of Y27632 in the assays above was due to ROCK inhibition, it was

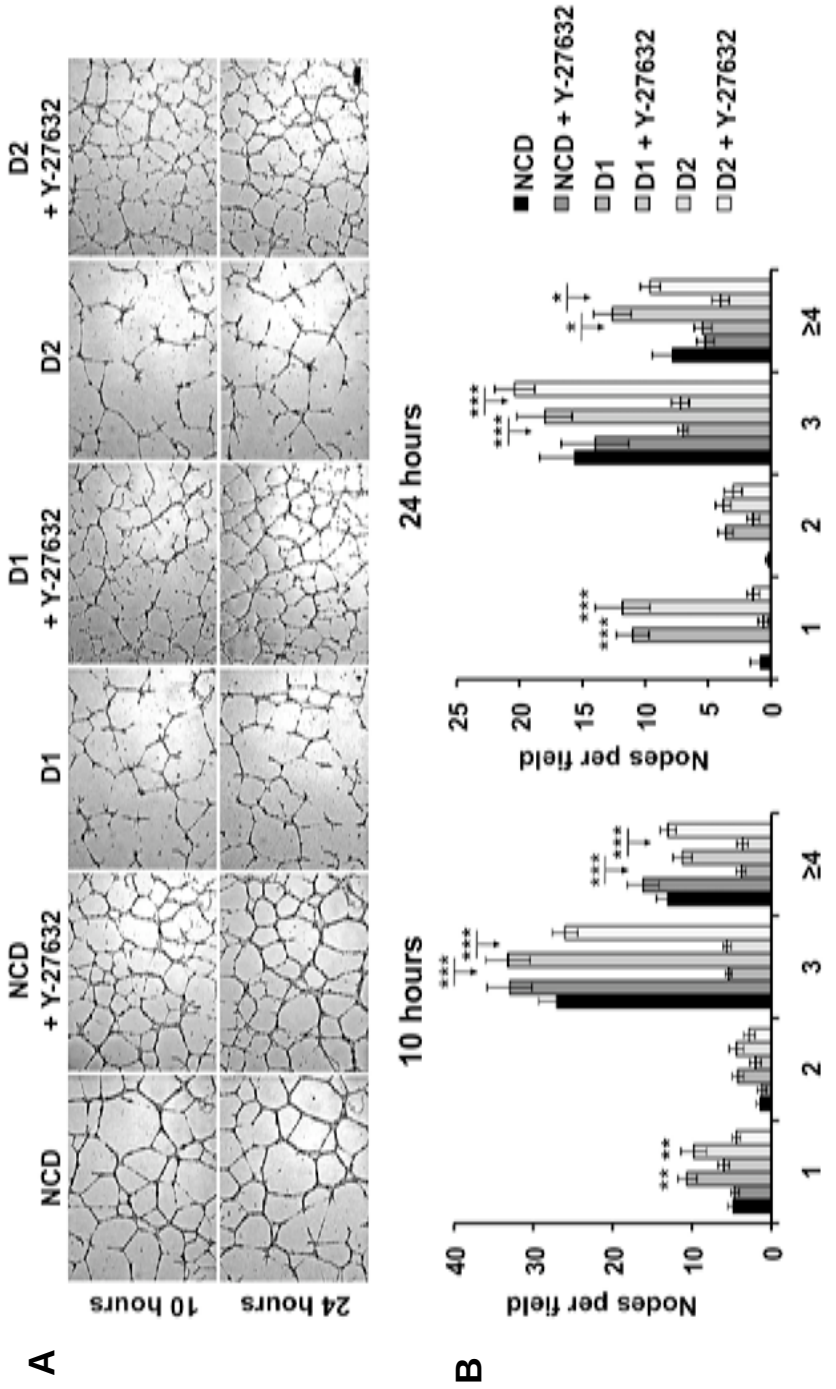
A
NCD
NCD + Y-27632
D1
D1 + Y-27632
D2
D2 + Y-27632
10 hours
24 hours
B
10 hours
24 hours
Nodes per field
NCD
NCD + Y-27632
D1
D1 + Y-27632
D2
D2 + Y-27632
1
2
3
≥4

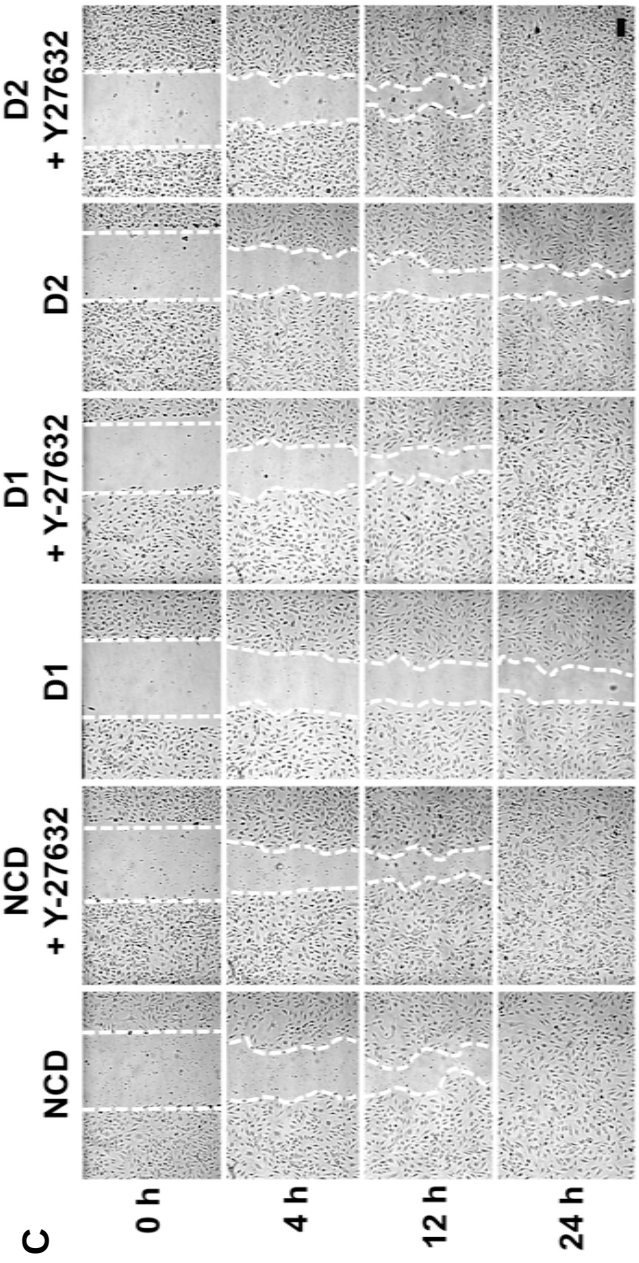
C
0 h
4 h
12 h
24 h
NCD
NCD
+ Y-27632
D1
D1
+ Y-27632
D2
D2
+ Y27632

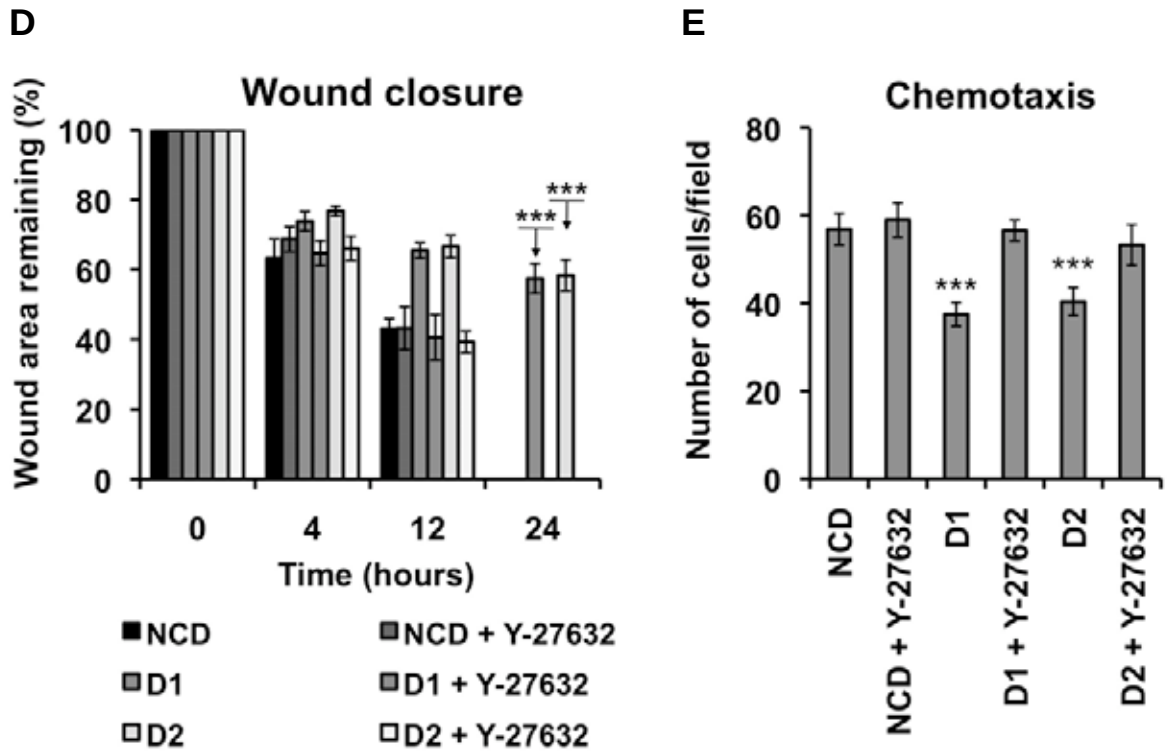

Figure 4.10 Inhibition of ROCK using Y27632 restores tube forming and motility defects in cells with reduced RhoJ expression. Human umbilical vein endothelial cells were either mock transfected or transfected with negative control duplex (NCD), RhoJ duplex 1 (D1) or RhoJ duplex 2 (D2) at 10 nM. Two days after transfection, cells were either treated with or without Y27632 (A) Pictures of Matrigel assay at 10 and 24 hours. Scale bar = 200 μm. (B) Matrigel assays were quantified by counting the number of nodes with 1, 2, 3 or ≥4 branches from five random fields of view. Values represent the means from three independent experiments. Error bars depict the standard error of the mean. One-way ANOVA showed that RhoJ knockdown significantly impaired two-dimensional tubule formation ($P<0.0001$ for all nodes except node 2), which was reversed with Y27632 treatment. Tukey's multiple comparison test was used to compare D1 or D2 with NCD (* = $P<0.05$, ** = $P<0.01$, *** = $P<0.001$). (C) Scratch wounds at 0, 4, 12 and 24 hours. Scale bar = 200 μm. (D) The percentage of wound remaining was measured and plotted. Values represent the means from three independent experiments. Error bars depict the standard error of the mean. One-way ANOVA showed a significant reduction of chemokinesis at 24 hours with RhoJ knockdown ($P<0.0001$), which was reversed with inhibition of ROCK. Tukey's multiple comparison test was used to compare D1 or D2 with NCD (*** = $P<0.001$). (E) Quantitation of cell migration using Boyden chemotaxis chamber. Values represent the means from three independent experiments with nine or more replicates in each experiment. Error bars depict the standard error of the mean. One-way ANOVA showed a significant reduction of chemotaxis to fetal calf serum in RhoJ-depleted cells ($P<0.0001$), which was reversed with ROCK inhibition. Tukey's multiple comparison test was used to compare D1 or D2 with NCD (*** = $P<0.001$).

important to use another ROCK inhibitor from a structurally distinct chemical series. Inhibitors of different structure that share one target are predicted to have different off-target effects. Therefore if using inhibitor H1152 resulted in the same phenotypic effects as Y27632, it can be assumed that it is due to the fact that they both inhibit ROCK.

With H1152 treatment tube formation and cell motility defects observed with RhoJ knockdown were restored in a similar way to Y27632 treatment (figure 4.11). These data suggest that the RhoJ knockdown mediated effects on tube formation and motility are due to increased ROCK activity.

4.2.3.2 Inhibition of myosin II ATPase activity

Activated ROCK increases myosin II ATPase activity in two ways, phosphorylation of MLC and inactivation of MLC phosphatase. Non-muscle myosin II interacts with actin filaments in an ATP-dependant manner. At the start of the cycle, myosin heads lacking a bound nucleotide are locked onto actin filaments. ATP binds to the myosin head and induces a conformational change that reduces the affinity of the myosin head for actin and allows it to move along the filaments. ATP is then hydrolysed into ADP and inorganic phosphate (P_i), which results in myosin weakly binding to a new site on the actin filament. P_i release increases the strength of myosin binding to actin and ADP is dissociated leaving the myosin head again locked tightly to the actin filament, generating actomyosin contractility (132).

Blebbistatin is an inhibitor of myosin II ATPase activity (261, 262). Blebbistatin binds specifically to the ATP binding region of myosin II heads and blocks the release of P_i hence inhibiting actomyosin contractility. The tube forming and motility defects found in RhoJ knockdown cells were rescued when ROCK was inhibited (figures 4.10 and 4.11). These experiments demonstrated that RhoJ-siRNA treated cells have increased ROCK activity but

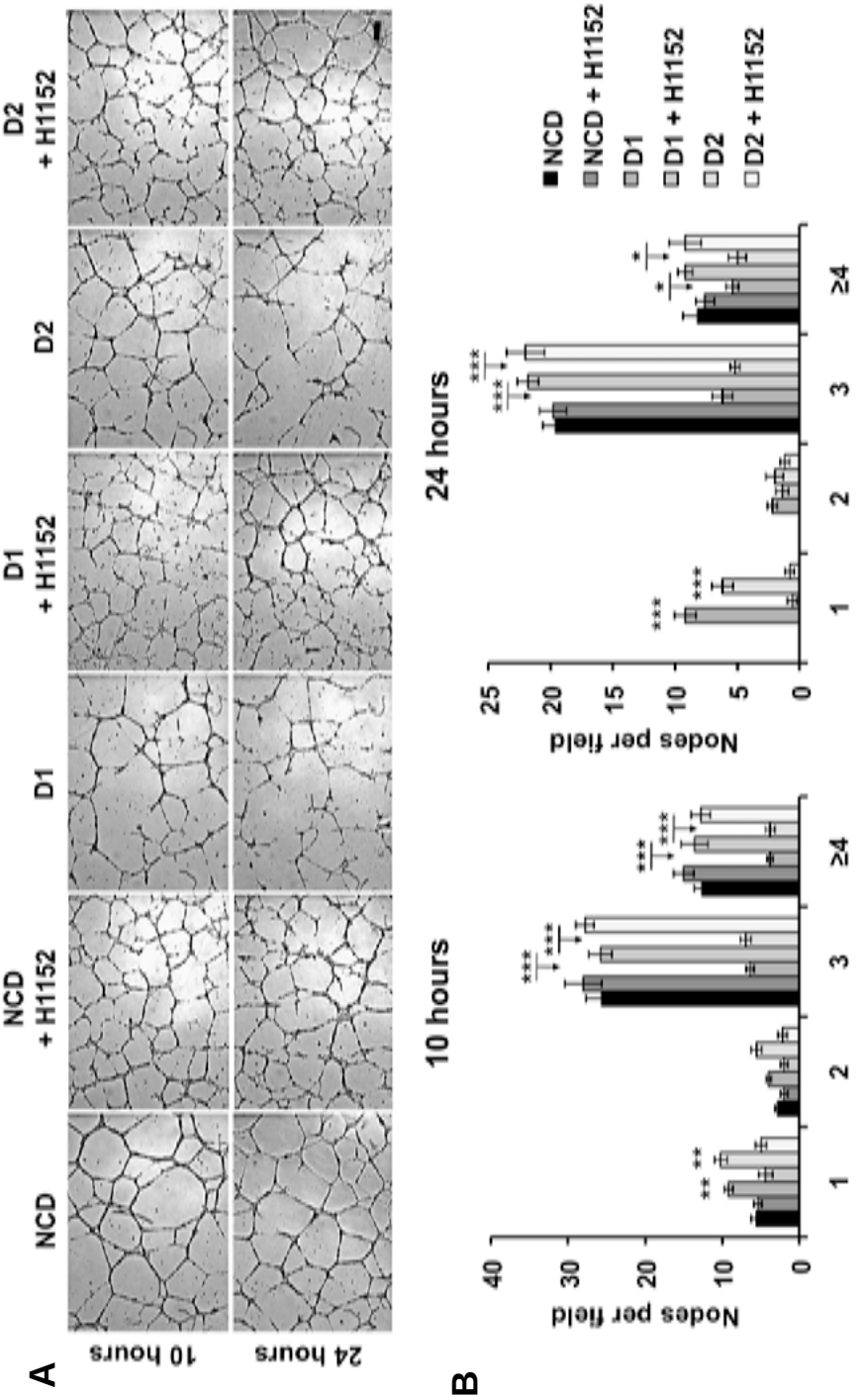
A
NCD
NCD + H1152
D1
D1 + H1152
D2
D2 + H1152
10 hours
24 hours
B
10 hours
24 hours
Nodes per field
NCD
NCD + H1152
D1
D1 + H1152
D2
D2 + H1152
1
2
3
≥4

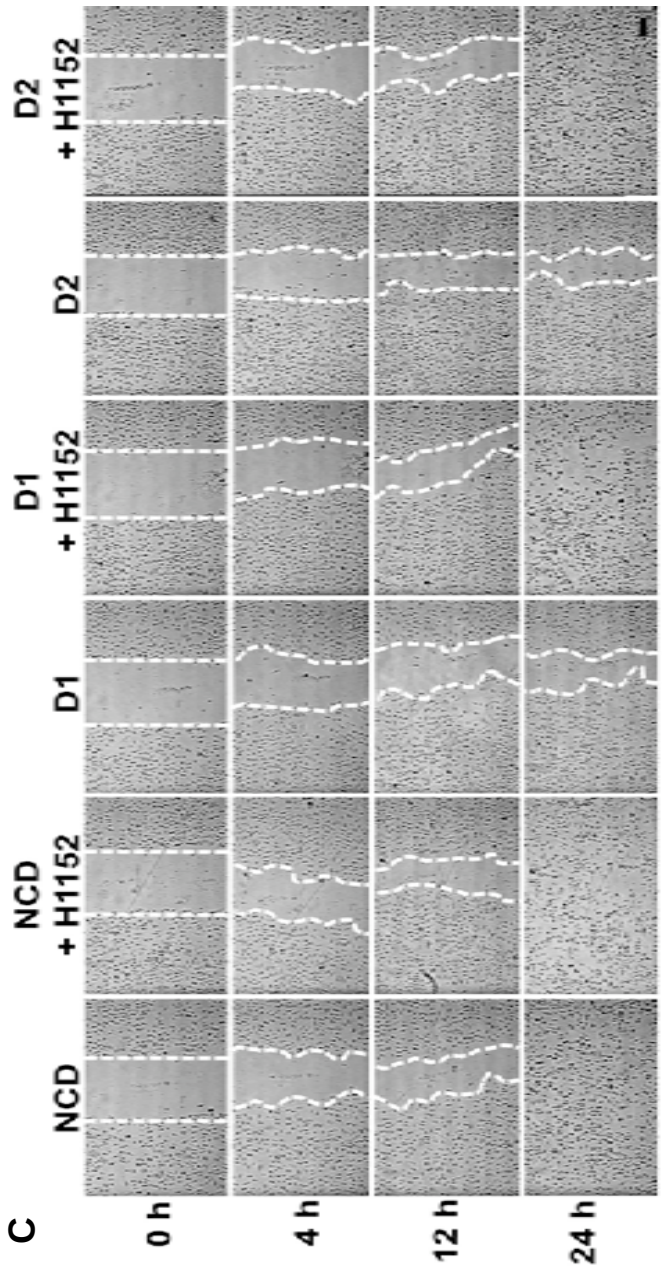
C
NCD
NCD + H1152
D1
D1 + H1152
D2
D2 + H1152
0 h
4 h
12 h
24 h

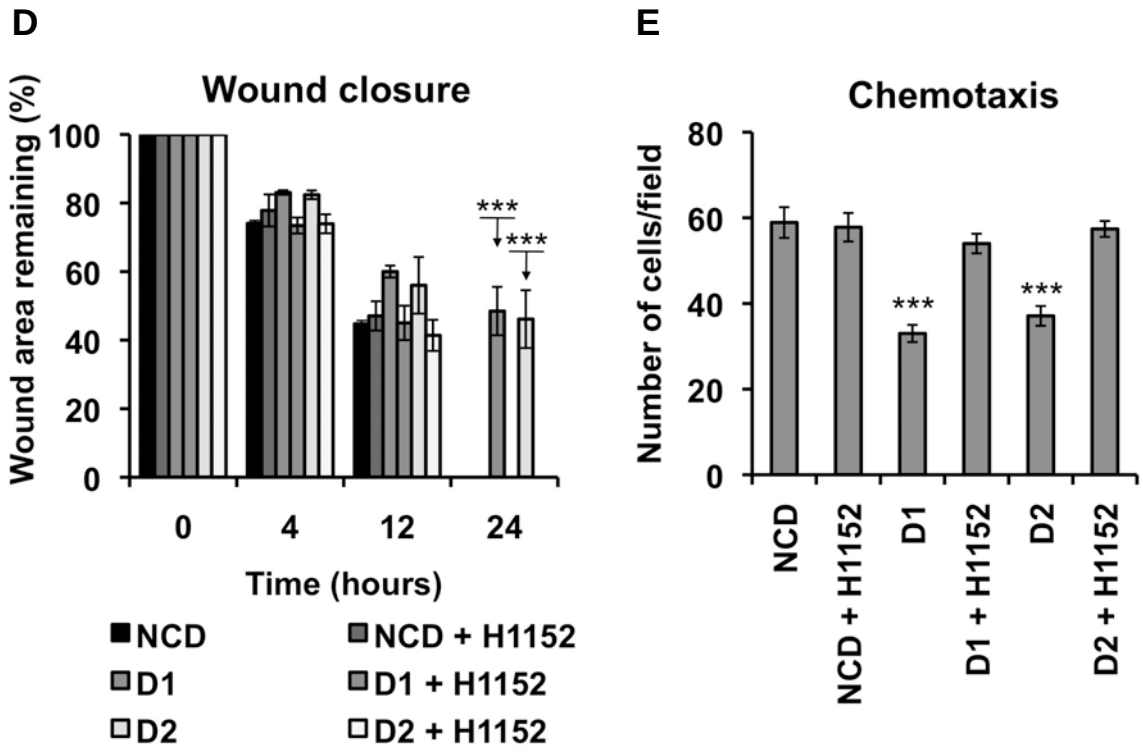

Figure 4.11 Inhibition of ROCK using H1152 restores tube forming and motility defects in RhoJ-depleted cells. Human umbilical vein endothelial cells were either mock transfected or transfected with negative control duplex (NCD), RhoJ duplex 1 (D1) or RhoJ duplex 2 (D2) at 10 nM. Two days later, cells were either treated with or without H1152 (A) Pictures of Matrigel assay at 10 and 24 hours. Scale bar = 200 μm. (B) Matrigel assays were quantified by counting the number of nodes with 1, 2, 3 or ≥4 branches from five random fields of view. Values represent the means from three independent experiments. Error bars depict the standard error of the mean. One-way ANOVA showed that RhoJ knockdown significantly impaired two-dimensional tubule formation ($P<0.0001$ for all nodes except node 2), which was reversed with H1152 treatment. Tukey's multiple comparison test was used to compare D1 or D2 with NCD (* = $P<0.05$, ** = $P<0.01$, *** = $P<0.001$). (C) Scratches wounds at 0, 4, 12 and 24 hours. Scale bar = 200 μm. (D) The percentage of wound remaining was measured and plotted. Values represent the means from three independent experiments. Error bars depict the standard error of the mean. One-way ANOVA showed a significant reduction of chemokinesis at 24 hours with RhoJ knockdown ($P<0.0001$), which was reversed with inhibition of ROCK. Tukey's multiple comparison test was used to compare D1 or D2 with NCD (*** = $P<0.001$). (E) Quantitation of cell migration using Boyden chemotaxis chamber. Values represent the means from three independent experiments with nine or more replicates in each experiment. Error bars depict the standard error of the mean. One-way ANOVA showed a significant reduction of chemotaxis to fetal calf serum in RhoJ-depleted cells ($P<0.0001$), which was reversed with ROCK inhibition. Tukey's multiple comparison test was used to compare D1 or D2 with NCD (*** = $P<0.001$).

different substrates can be phosphorylated by ROCK as well as MLC. To elucidate whether the defects found in RhoJ knockdown cells were directly due to an increase in actomyosin contractility, blebbistatin was used to specifically inhibit the ATPase activity of myosin II. These experiments were carried out in a similar fashion to the ROCK inhibition assays described previously except blebbistatin was added at a concentration of 5 μM.

In tube formation, cells with reduced RhoJ expression treated with blebbistatin produced well-linked and stable tubule networks (figure 4.12A). These networks no longer appeared weak and unconnected as shown with RhoJ knockdown alone and instead were similar to the tubule networks created by NCD cells. Blebbistatin treatment in RhoJ-depleted cells reduced the number of unconnected branches and increased the number of nodes with 3 or more branch points at 10 and 24 hours to similar levels found in NCD control. In wound healing, blebbistatin treatment in RhoJ-depleted cells resulted in complete closure of the wound at 24 hours at a similar rate to NCD treated cells (figure 4.12C). The significant reduction in migration with RhoJ knockdown alone was fully restored when myosin II ATPase activity was inhibited (figure 4.12D). In the Boyden chamber assay, knockdown of RhoJ alone resulted in a significant reduction in chemotactic migration towards serum-rich media (figure 4.12E). However with blebbistatin treatment in RhoJ knocked down cells, the migratory response towards the chemoattractant gradient was restored back to normal.

Inhibition of actomyosin contractility ameliorated the cell motility and tube formation defects found in RhoJ knocked down cells. These data produced similar results to when ROCK was inhibited in RhoJ-depleted cells (figures 4.10 and 4.11). These data suggest that tube formation and motility defects found with RhoJ knockdown are due to increased ATPase activity of myosin II resulting in increased actomyosin contractility, which is a downstream effect of increased ROCK activity.

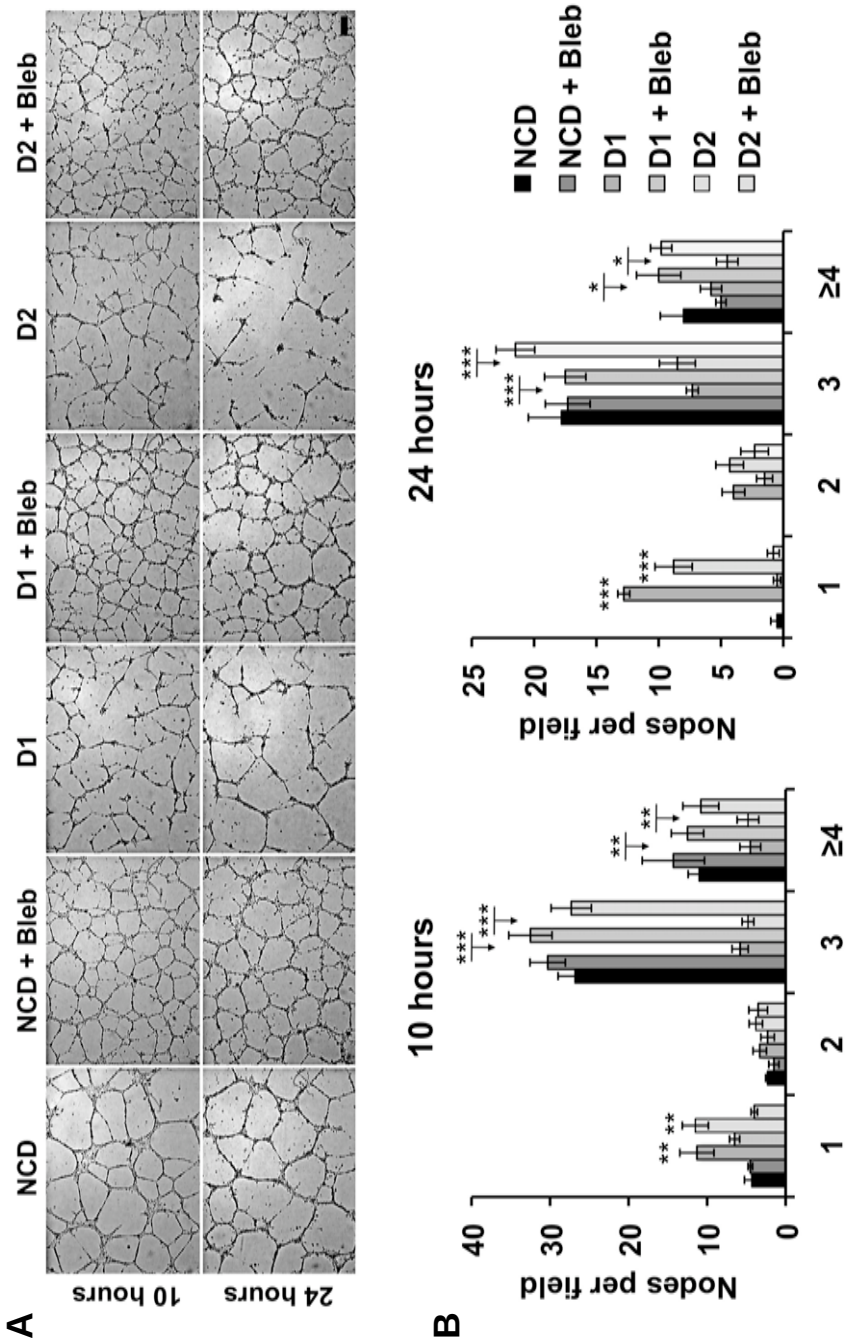
A
NCD
NCD + Bleb
D1
D1 + Bleb
D2
D2 + Bleb
10 hours
24 hours
B
10 hours
24 hours
Nodes per field
NCD
NCD + Bleb
D1
D1 + Bleb
D2
D2 + Bleb
1
2
3
≥4

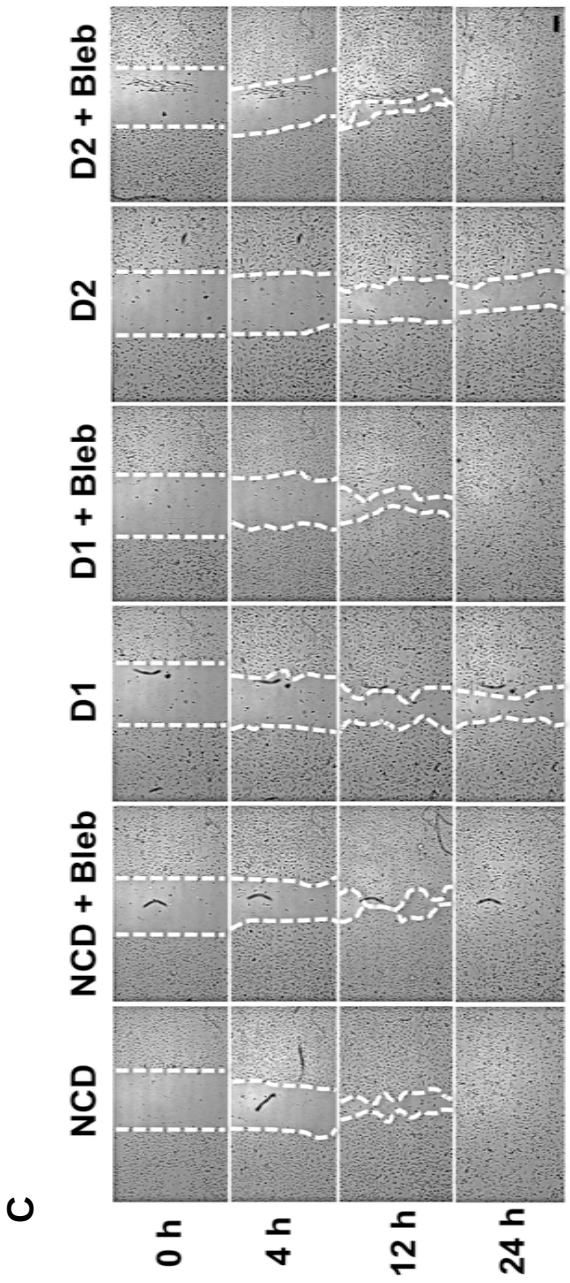
C
NCD
NCD + Bleb
D1
D1 + Bleb
D2
D2 + Bleb
0 h
4 h
12 h
24 h

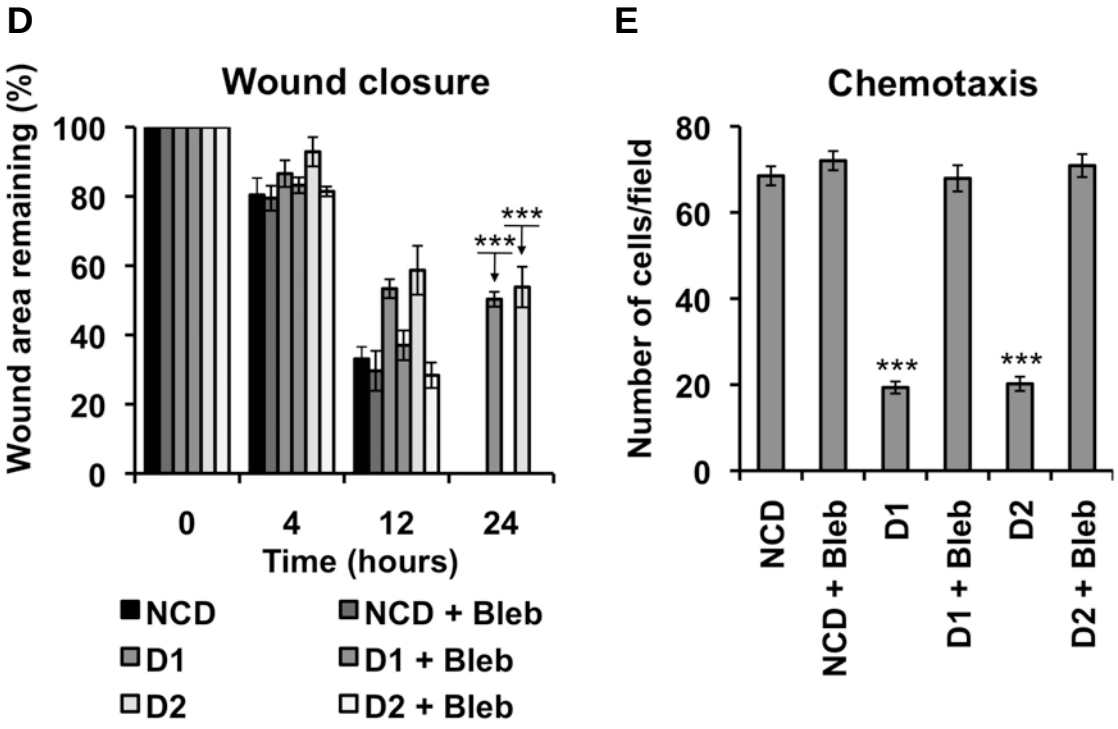

Figure 4.12 Inhibition of myosin II using blebbistatin restores tube forming and motility defects in RhoJ-depleted cells. Human umbilical vein endothelial cells were either mock transfected or transfected with negative control duplex (NCD), RhoJ duplex 1 (D1) or RhoJ duplex 2 (D2) at 10 nM. Two days after transfection, cells were either treated with or without blebbistatin (A) Pictures of Matrigel assay at 10 and 24 hours. Scale bar = 200 μm. (B) Matrigel assays were quantified by counting the number of nodes with 1, 2, 3 or ≥4 branches from five random fields of view. Values represent the means from three independent experiments. Error bars depict the standard error of the mean. One-way ANOVA showed that RhoJ knockdown significantly impaired two-dimensional tubule formation ($P<0.0001$ for all nodes except node 2), which was reversed with blebbistatin treatment. Tukey's multiple comparison test was used to compare D1 or D2 with NCD (* = $P<0.05$, ** = $P<0.01$, *** = $P<0.001$). (C) Scratch wounds at 0, 4, 12 and 24 hours. Scale bar = 200 μm. (D) The percentage of wound remaining was measured and plotted. Values represent the means from three independent experiments. Error bars depict the standard error of the mean. One-way ANOVA showed a significant reduction of chemokinesis at 24 hours with RhoJ knockdown ($P<0.0001$), which was reversed with blebbistatin treatment. Tukey's multiple comparison test was used to compare D1 or D2 with NCD (*** = $P<0.001$). (E) Quantitation of cell migration using Boyden chemotaxis chamber. Values represent the means from three independent experiments with nine or more replicates in each experiment. Error bars represent standard error of the mean. One-way ANOVA showed a significant reduction of chemotaxis to fetal calf serum in RhoJ-depleted cells ($P<0.0001$), which was reversed with blebbistatin treatment. Tukey's multiple comparison test was used to compare D1 or D2 with NCD (*** = $P<0.001$).

4.2.4 Summary

RhoJ silencing increased the number of focal adhesions and stress fibres in wound edge cells but not in cells found in the monolayer. In the presence of a chemoattractant gradient, RhoJ-depleted cells produced bleb-like membrane protrusions and showed impaired cellular morphology. In contrast, cells overexpressing RhoJ, either wild type or dominant active, were highly motile in the Dunn chamber chemotaxis assay. RhoJ knockdown increased cellular contraction and the converse was seen with cells overexpressing dominant active RhoJ. Furthermore, increased levels of phospho-MLC were detected in cells lacking RhoJ on Matrigel. RhoJ knockdown did not affect directional sensing or the expression of VE-Cadherin at cell-cell junctions in the monolayer. Tube forming and migration phenotypes (introduced in chapter 3) were reversed when ROCK or myosin II ATPase activity was inhibited in cells with reduced RhoJ expression.

4.3 Discussion

SiRNA-mediated knockdown of RhoJ in primary ECs was found to impede EC motility in chapter 3. Subsequently, cells lacking RhoJ were found to display more focal adhesions than mock or NCD-transfected cells (figure 4.1). It is likely that the significant increase in focal adhesion numbers perturbed the normal cyclic process of focal adhesion assembly and disassembly, thereby causing motility to become impaired in RhoJ depleted cells. In addition, the increase in focal adhesions may have induced tighter adhesion to the matrix substrate rendering RhoJ knocked down cells immobile. Studies have shown that activation of FAK increases cell-matrix adhesion strength (255, 269). Since RhoJ siRNA treated cells displayed increased numbers of phospho-FAK containing focal adhesions, it is likely that these cells had stronger adherence to the ECM. Moreover, the focal adhesions in RhoJ knocked down cells were vinculin, phospho-paxillin and phospho-FAK positive (figure 4.1) showing that RhoJ

knockdown did not affect the assembly of these proteins into focal adhesion complexes. However, the increase in their numbers is indicative of problems with disassembly and turnover. Thus RhoJ may have an important role in focal adhesion turnover in ECs but in order to confirm this theory, the rate of focal adhesion turnover would need to be measured.

Stress fibers are physically linked to focal adhesions via the actin binding site on the vinculin tail domain (121). Forces generated in stress fibres, by the pulling of myosin II on actin filaments, are exerted on focal adhesions in order for cells to move (270). Considering their connection, it was not surprising that RhoJ knockdown also induced an increase in stress fibres (figure 4.3). Stress fibres are bundles of actin and non-muscle myosin II filaments, which have contractile activity and regulate tension within cells (129-131). Therefore since RhoJ siRNA treated cells had increased stress fibres, it was logical to assume that these cells would also have increased actomyosin contractility. As expected, cells with reduced RhoJ expression were found to contract collagen gels significantly more than controls cells (figure 4.6A). Conversely, cells expressing dominant active RhoJ contracted the collagen gels significantly less than control cells (figure 4.7C).

In line with our findings, RhoJ-silenced cells on Matrigel were also found to have increased levels of phosphorylated MLC (figure 4.6B). MLC can be phosphorylated by a number of kinases including RhoA-dependent ROCK and calcium-dependent MLC kinase, which result in increased myosin II ATPase activity and stress fiber contractility (127, 254). Using two structurally unrelated inhibitors of ROCK, the tube forming and motility defects of RhoJ siRNA treated cells were reversed to phenotypes equivalent to that seen in negative control duplex treated cells (figures 4.10 and 4.11). These data strongly suggest that the increase in phospho-MLC was due to an increase in ROCK activity, which in turn increased the ATPase activity of myosin II. The present study also demonstrates that the direct inhibition of non-

muscle myosin II using blebbistatin also reversed the effect of RhoJ knockdown on scratch wound closure and tube formation (figure 4.12). Inhibiting the function of non-muscle myosin II in alternative ways resulted in the rescue of RhoJ knockdown phenotypes. This suggests that phenotypes induced by loss of RhoJ were due to increased actomyosin contractility, mediated through increased ROCK activity. These data indicate that RhoJ negatively regulates stress fibre formation and actomyosin contractility.

Interestingly, the increased stress fibre and focal adhesion phenotype was only evident in sparsely plated cells or cells at the migration front of scratch wound assays but not within monolayers (figures 4.1 to 4.4). This suggests that RhoJ plays a critical role in migrating cells but the cells within the monolayer may not be dependent on RhoJ for maintenance of focal adhesions or stress fibres. The lack of phenotype in the monolayer may be due to signalling from neighbouring cells, through intact cell-cell contacts, which suppress the phenotypes of RhoJ knockdown and compensate for the loss of RhoJ.

In chapter 3, the reduced migration of RhoJ depleted cells in the scratch wound assay, was more evident at later time points (figures 3.5A-B and 3.6A-B). RhoJ depleted cells were able to migrate to some extent initially but by 24 hours migration was significantly reduced. Since we have found that cells in a monolayer do not express the RhoJ knockdown phenotype, RhoJ knockdown cells at the wound edge may have retained the ‘monolayer phenotype’ during initial wound closure and migrated normally at first. However, only after the cells started to move and reduced contact with neighboring cells, focal adhesions and stress fibres may have begun to accumulate, which caused motility to slow.

This may also explain why initial tube formation was not largely affected by RhoJ knockdown but the secondary stage was (figures 3.2 to 3.4). Perhaps RhoJ knockdown did not

affect the initial phase since motility is not required (170). However in the secondary phase, when migration is essential, the loss of RhoJ resulted in excessive contractility and focal adhesion numbers, which inhibited migration and the extension of primitive cords. The weak connections made in RhoJ knockdown conditions also appeared to retract by 24 hours (figures 3.2A-B and 3.3A-B), this is consistent with our finding that these cells have increased contractility (figure 4.6A). In addition, the observations that RhoJ knocked down cells on Matrigel have increased levels of phosphorylated MLC (figure 4.6B) and inhibition of ROCK or myosin II ATPase activity ameliorates the motility and tube formation defects, strongly suggest that actomyosin contractility was increased in these cells through increased ROCK activity (figures 4.10 to 4.12). Moreover, it has previously been shown that increased actomyosin contractility is capable of inducing cell death during tube formation (92).

Cell–cell adhesions are essential for normal tube formation (265, 271). Altered cell-cell adhesions could also produce the same effect as RhoJ knockdown on tube formation. Although, we found no mis-localisation of the adherens junctional protein VE-Cadherin in a monolayer of RhoJ siRNA treated cells (figure 4.9), we cannot formally rule out a cell-cell adhesion defect because cells within a monolayer appear to suppress RhoJ knockdown phenotypes. In future studies, it would be interesting to examine the expression of VE-Cadherin in RhoJ knocked down cells on Matrigel.

In agreement with our observations, a past study reported stress fibre loss in mouse fibroblast cells expressing dominant active mutant of RhoJ (198). In further support of our findings, Vignal *et al.* (2000) showed that constitutively active RhoJ expression in rat embryonic fibroblasts induced the formation of actin-rich ruffles on the dorsal membrane (197). These ‘waves’ are known to disassemble stress fibres and promote actin reorganization (246, 247). Therefore, it is possible that RhoJ knockdown might have prevented dorsal ruffling, which

resulted in the accumulation of stress fibre bundles and increased actomyosin contractility. This group also observed a significant increase of stress fibres in fibroblasts expressing dominant negative RhoJ and conversely a reduction in cells expressing dominant active RhoJ (197). Our work agrees with these past studies but we are the first to show a role for endogenous RhoJ in primary ECs. Moreover, dominant active RhoJ induced lamellipodia formation in porcine aortic ECs stably expressing the human platelet-derived growth factor β-receptor (204). In agreement with this finding, our observations were that RhoJ depleted cells were typically more rounded and poorly spread, however, control cells were polarised and presented polygonal protrusions such as lamellipodia. The extension of lamellipodia is stimulated by integrin engagement (106). Perhaps the inhibition of focal adhesion turnover by RhoJ knockdown prevented the spreading of these cells. Moreover, Wakatsuki *et al.* (2003) demonstrated that cell spreading is inversely related to myosin II activity and that increased actomyosin contractility (driven by RhoA) hinders lamellipodia and filopodia formation. (99). Additionally, they showed that during cell spreading, RhoA activity is low while the activity of Rac1 and Cdc42 is high. Low RhoA activity has also been shown to induce high turnover of focal adhesions in fibroblast cells (106, 272). Therefore, perhaps the lack of RhoJ signalling triggered circular, non-polarised cell shapes due to these cells having increased RhoA signalling. Thus it may be possible for RhoJ activity to be conversely correlated to that of RhoA, whereby high RhoJ activity could increase focal adhesion turnover rate and reduce actomyosin contractility, and visa versa. Our data suggests that RhoJ may negatively regulate the RhoA signalling pathway.

Consistent with chapter 3, RhoJ knockdown diminished cell migration toward a gradient of chemoattractant in the Dunn chemotaxis chamber (figure 4.5A). Conversely, cells overexpressing wild type or dominant active RhoJ were capable of moving toward the chemical stimuli and migrated further than control cells toward the chemoattractant (figure

4.7A). These data further support the data in chapter 3, which suggest that RhoJ is important for EC motility. Consistently, RhoJ siRNA treated cells were also non-polarised, poorly spread and had circular cell shapes in the Dunn chamber. Intriguingly however, cells lacking RhoJ also constantly produced and retracted bleb-like plasma membrane protrusions (figure 4.5B). This was not observed in other situations such as in the scratch wound or Matrigel assays suggesting that perhaps the presence of a serum gradient may have somehow induced the cells to bleb. Cells overexpressing wild type or constitutively active RhoJ demonstrated the opposite morphology, whereby cells were polarised, elongated and extended long cellular protrusions (figure 4.7B), suggesting that these cells were highly motile. In addition, in normal cell culture conditions, cells expressing dominant active RhoJ were also found to undergo extensive tubulogenesis (data not shown). This is compatible with a recent study that shows that reduced contractility results in high EC motility and morphogenesis (174).

Bleb formation corresponds with high myosin II activity and myosin II inhibition prevents blebbing (260, 273, 274). Blebs are thought to be a mechanical response to a localised increase in intracellular pressure, which is exerted through actomyosin contractility (257, 275). During the last decade, it has started to emerge that cell movement does not exclusively involve the extension of lamellipodia but can also require membrane blebbing (260). Normal blebbing occurs at the leading edge of a cell and the cell is then thrust forward by a subsequent contraction of the cell body (260). Many types of cells have been shown to utilise polarised blebbing as an alternative to lamellipodial migration such as zebrafish germ cells, tumour cells and depending on their environment, neutrophils and leukocytes (273, 274, 276). Moreover, zebrafish germ cells have been shown to display blebbing at the leading edge following stimulation by a chemoattractant gradient (276).

Our hypothesis is that increased contractility in RhoJ siRNA treated cells may have hindered spreading and by compensating for the lack of lamellipodia, these cells may then have attempted to migrate through blebbing in response to the chemoattractant gradient. However, due to unlocalised and sustained actomyosin contractility, the blebbing was not polarised but apparent all round the cell circumference. Moreover, RhoJ depleted cells were found to successfully reorientate their Golgi apparatus toward the wound edge in scratch wound assays (figure 4.8), indicating that these cells had the ability to sense direction and migration-promoting stimuli but were unable to physically polarise their cell shape to move. Moreover, cells lacking RhoJ did not move a great deal from their points of origin and from our findings we can argue that this may have been due to these cells having increased adherence to the ECM as well as too much widespread intracellular tension. Many studies have shown that increased RhoA-ROCK-myosin signalling is essential for blebbing (277, 278). This coincides with our theory that RhoJ may be negatively regulating the RhoA pathway in some way, thus loss of RhoJ leads to accumulated contractile tension that spreads across the entire cell.

In conclusion, RhoJ negatively modulates focal adhesion numbers and actomyosin contractility in ECs *in vitro* and may be essential for endothelial motility and angiogenesis *in vivo*. However, there is a complex interplay and reciprocal regulation between focal adhesion maturation, turnover, and actomyosin contractility. Studies have shown that focal adhesion disassembly, size and distribution is dependent on the controlled activity of myosin II (116, 279). Conversely, components of focal adhesions have been shown to regulate contractility. At present, we do not know which process RhoJ affects directly. To determine whether increased contractility is the cause or consequence of defective focal adhesion turnover, the downstream effector proteins that GTP-bound RhoJ binds to would need to be identified.

To assess the biological relevance of RhoJ function in angiogenesis, it is necessary to study the role of RhoJ *in vivo*. By understanding the function of RhoJ *in vivo*, insights can be gained on the role of RhoJ in pathological angiogenesis in diseases such as psoriasis, arthritis, atherosclerosis and cancer metastasis. Future *in vivo* experiments may include knockdown or overexpression of RhoJ in murine Matrigel plug or sponge assays and the use of tumour models to assess the role of RhoJ in tumour angiogenesis. Currently, our group is in the process of generating a RhoJ knockout mouse. It would be interesting to see if these mice display any vascular defects and also to analyse the ECs from these mice at the cellular level. Furthermore, the role of RhoJ in zebrafish was already explored and this work is described in chapter 5.

Chapter five

RhoJ in zebrafish development

5.1 Introduction

Zebrafish, *danio rerio*, are small teleost tropical fish that are often used as model systems for studying aspects of developmental biology including *in vivo* angiogenesis. The advantages of using zebrafish are that protein expression can be easily knocked down using morpholino technology and the transparency of the embryos greatly facilitates visualisation of blood vessel formation (95).

Zebrafish embryonic development is described in six broad periods of embryogenesis and each period is subdivided into stages, which are named according to their morphological features: the zygote (1-cell), cleavage (2-cell to 64-cell), blastula (128-cell to 30% epiboly), gastrula (50% epiboly to bud), segmentation (1-4 somites to 26+ somites) and pharyngula (prim-5 to long-pec) periods. In segmentation, somitogenesis occurs, which is the formation of somites from the presomitic mesoderm. At the final stages of the segmentation period, the primary vessels, the dorsal aorta and cardinal vein begin to form. During pharyngula period, angiogenesis occurs and the circulatory system begins to develop (280). The sprouting of the intersegmental arteries from the dorsal aorta occurs around 22 hours post fertilisation (hpf). These arteries sprout dorsally and once reached the level of the dorsal neural tube, the vessels connect from anterior and posterior sides to form the future dorsal longitudinal anastomotic vessel (DLAV) (224).

Having discovered that RhoJ is both highly expressed in human ECs and regulates endothelial motility and tube formation *in vitro* (chapters 3 and 4), it was important to discover the role of RhoJ *in vivo*, and zebrafish were chosen initially for this purpose. With zebrafish RhoJ being a hypothetical protein, the sequence and expression of RhoJ in zebrafish was firstly validated. The expression profile of RhoJ was also examined using reverse transcription PCR to

determine the temporal regulation of RhoJ expression, which would give an insight into the possible functions of RhoJ during zebrafish development. Furthermore, the tissue distribution profile of zebrafish RhoJ during normal embryonic angiogenesis was determined using whole-mount *in situ* hybridization experiments. Morpholinos are synthetic complementary antisense oligonucleotides that can either block translation or modify pre-mRNA splicing in order to knockdown gene function (98). Thus in order to investigate the function of RhoJ in zebrafish embryos, morpholino antisense oligonucleotides were used to knockdown RhoJ function *in vivo*.

To conclude, this chapter aims to investigate the expression profile and function of RhoJ during zebrafish embryonic development.

5.2 Results

5.2.1 Validation of RhoJ mRNA expression and sequence in zebrafish

Zebrafish RhoJ was a hypothetical protein and its sequence had been predicted by homology with mammalian RhoJ. Figure 5.1 shows the alignment of RhoJ's amino acid sequence in human, mouse and zebrafish. The proteins have conserved exon structures and highly conserved primary sequences, which diverge only at the N- and C-termini. Protein sequence analysis by ClustalW program (Network Protein Sequence Analysis tool) showed that human and mouse RhoJ amino acid sequences were 93% identical and human and zebrafish RhoJ amino acid sequences were 76% identical.

With zebrafish RhoJ expression and sequence being hypothetical, it was thus important to determine if RhoJ was expressed in zebrafish and to confirm its sequence and exon structure. To validate this prediction, zebrafish were mated and embryos at 23, 24 and 26 hours post

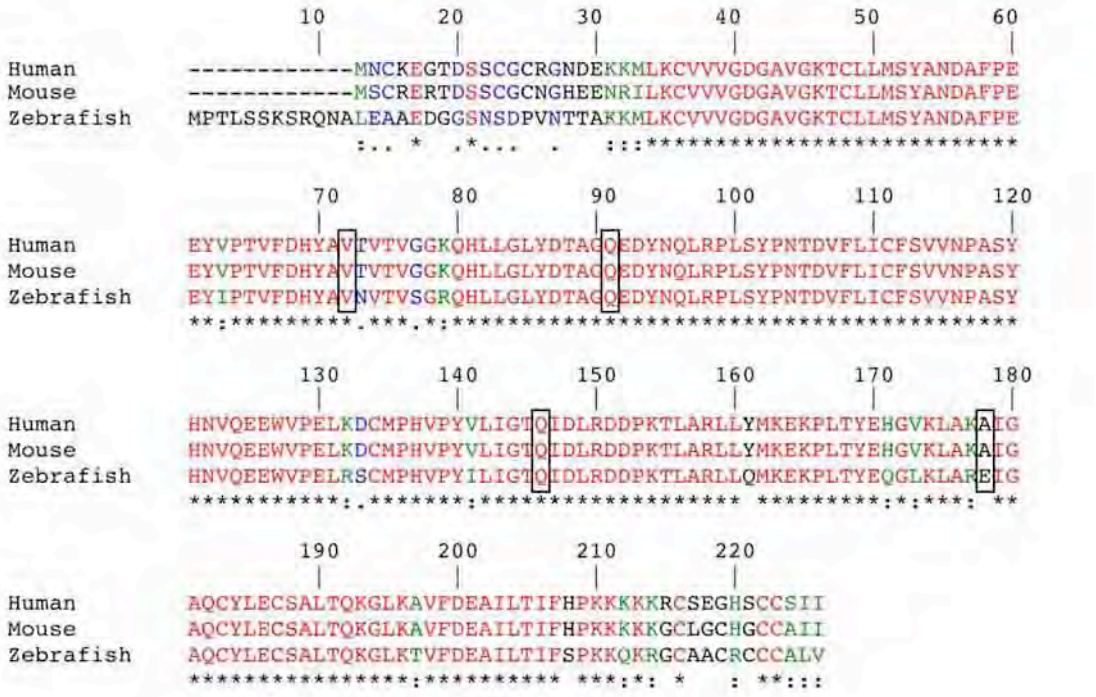

Figure 5.1 Predicted amino acid sequences of RhoJ in human, mouse and zebrafish. The alignment of human, mouse and zebrafish RhoJ amino acid sequences were generated by using ClustalW program available at Network Protein Sequence Analysis (NPS@) web server: http://npsa-pbil.ibcp.fr/NPSA/npsa_clustalw.html. The boxes highlight the exon boundaries in each organism. Underneath the alignment, identical residues (red) are indicated by asterisks (*), strongly similar residues (green) are indicated by colons (:), weakly similar residues (blue) are represented by dots (.) and different residues (black) are left blank. Human and mouse RhoJ sequences are 93% identical, human and zebrafish RhoJ sequences are 76% identical.

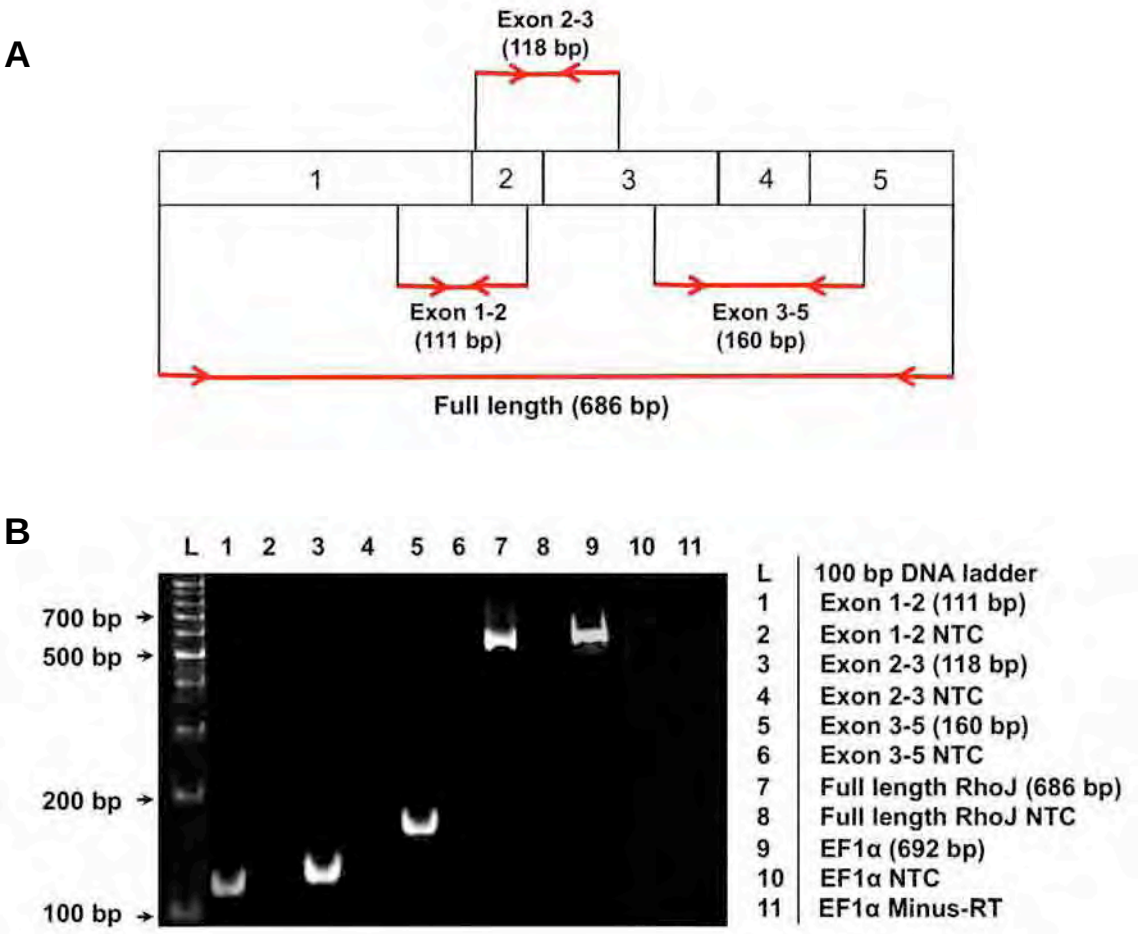

Figure 5.2 Full length RhoJ is expressed in zebrafish embryos. (A) Schematic showing the exon structure of zebrafish RhoJ and the fragments amplified by reverse transcription PCR (RT-PCR). To distinguish between expressed exons and spliced-out exons, primers were designed to cross exon boundaries (indicated by red arrows). (B) Non-denaturing polyacrylamide gel demonstrates the amplification of zebrafish RhoJ from cDNA obtained from a mixture of embryos at 23, 24 and 26 hours post fertilisation (hpf) using different primer pairs. EF1α was used as a positive control. A minus reverse transcriptase enzyme control (minus-RT) was used with EF1α primers. No template controls (NTC), containing water instead of cDNA, were added for each reaction.

fertilisation (hpf) were collected, removed from their chorions and lysed with trizol. From this lysate, RNA was extracted and cDNA was generated. This cDNA template was then used in reverse transcription PCR experiments to amplify the predicted coding region of zebrafish RhoJ. To confirm that none of the five exons were spliced out, PCRs were also performed using primers that were designed to cross various exon boundaries (figure 5.2A). No template controls were added for each primer pair where the reaction contained all the PCR reagents except the cDNA template. Elongation factor 1 alpha (EF1α) is a zebrafish housekeeping gene (281) and was used as a positive control.

Full length RhoJ was found to be expressed in 23-26 hpf zebrafish cDNA with all five exons present (figure 5.2B). The full length coding sequence of zebrafish RhoJ was then cloned into pCR®-Blunt II-TOPO® (see section 2.4 DNA Constructs) and sequencing was found to match the predicted sequence.

5.2.2 RhoJ mRNA expression during zebrafish stages of development

At different developmental stages, the expressions of different proteins are regulated. Therefore it was interesting to investigate when RhoJ was expressed during zebrafish development. To investigate the expression of RhoJ during zebrafish embryogenesis, embryos from the stages of the main developmental periods were analysed for RhoJ expression; 8-cell (cleavage), 30% epiboly (blastula), 5-somite (segmentation), prim-5 and long-pec (pharyngula). The morphology of zebrafish embryos at these stages are illustrated in figure 5.3A. The onset of embryonic transcription and the degradation of maternal transcripts is a gradual process from 1-cell to 16-cell stage of embryogenesis. Thus in 8-cell stage, the embryo is still carrying mRNA from the mother (282). At 30% epiboly, the embryo is preparing for gastrulation. Hemangioblasts, precursor cells to endothelial and pluripotent

hematopoietic cells, are known to exist in the blastodisc at this stage (283). At the 5-somite stage of the segmentation period, the first five somites develop. Neovascularisation is known to occur in the late stages of segmentation and then angiogenesis is prevalent from prim-5 to long-pec stages of the pharyngula period (280, 284).

Embryos from various stages were collected and lysed. From these lysates, RNA was extracted and cDNA was generated. The same amount of RNA was used to generate each cDNA template. The cDNAs were then used in PCR experiments to amplify full length RhoJ and zebrafish housekeeping control, EF1α. No template and minus-RT controls were added as controls for genomic or cDNA template contamination and were set up as previously described.

RhoJ was expressed in all five stages; 8-cell, 30% epiboly, 5-somite, prim-5 and long-pec (figure 5.3B). The expression level of RhoJ at 8-cell and 30% epiboly was relatively similar. However, at 5-somite, RhoJ expression was slightly downregulated. RhoJ expression was slightly increased at the prim-5 and long-pec stages of pharyngula. These data show that RhoJ transcripts are being made in all five embryonic stages of development however mRNA RhoJ expression was highest at the stage when angiogenesis is known to be occurring.

5.2.3 RhoJ mRNA expression during zebrafish embryonic angiogenesis

To further investigate the expression of zebrafish RhoJ, its tissue distribution was investigated by whole-mount *in situ* hybridization. Human RhoJ is highly expressed in ECs (206), and so it was important to determine whether zebrafish RhoJ also showed the same expression pattern. If so zebrafish would be a suitable model to study *in vivo* angiogenesis.

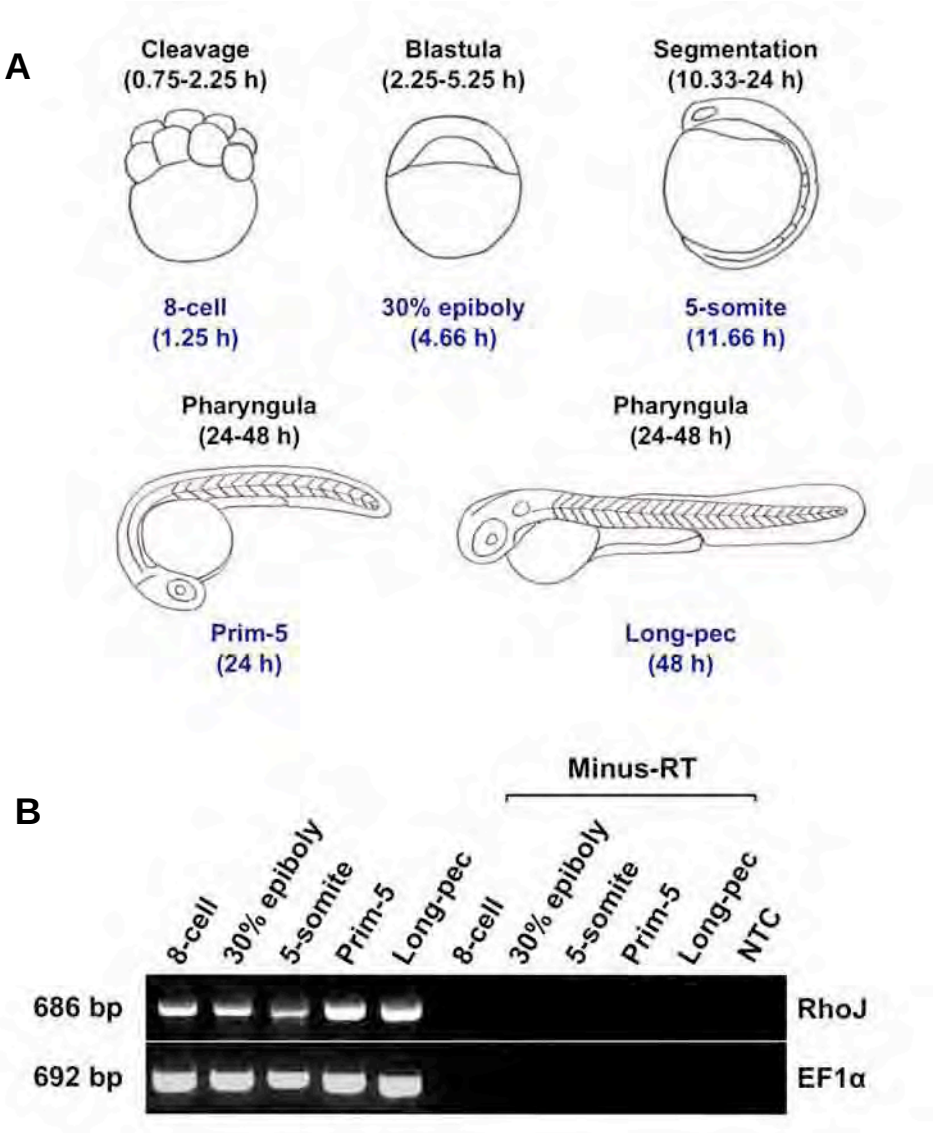

Figure 5.3 RhoJ is expressed in cleavage, blastula, segmentation and pharyngula stages of zebrafish development. (A) Lateral view drawings of the zebrafish embryonic developmental stages that were analysed for RhoJ mRNA expression. Development periods are labelled in black and stages are shown in blue. (B) Full length RhoJ was amplified by reverse transcription PCR from cDNA obtained from zebrafish embryos at 8-cell, 30% epiboly, 5-somite, prim-5 or long-pec stage. The same amount of RNA was used to generate each cDNA template. EF1α was used as a housekeeping control. Minus reverse transcriptase enzyme controls (minus-RT) and no template controls (NTC) were added for each reaction.

To analyse RhoJ mRNA expression in zebrafish embryos, antisense and sense riboprobes labeled with digoxigenin were generated from the pCR®-Blunt II-TOPO-zebrafish RhoJ cloned construct (see section 2.4 DNA Constructs). Whole-mount *in situ* hybridization experiments were performed on paraformaldehyde-fixed prim-5 (24 hpf) zebrafish embryos, since this is when embryonic angiogenesis is known to occur. A simplified diagram of the anatomy of a 24 hpf zebrafish embryo is shown in figure 5.4. At this stage, blood circulates in a closed circuit by leaving the heart and entering the dorsal aorta and caudal artery before returning through the caudal and posterior cardinal vein. The intersegmental arteries, which at this stage do not carry circulation, sprout from the dorsal aorta via angiogenesis.

For the *in situ* hybridization experiments, embryos were digested with proteinase K to allow entry of the probes before being re-fixed with PFA. The probes were then hybridized to the complementary mRNA sequences *in situ*. The probes used were sense and antisense riboprobes for RhoJ and Friend leukemia virus integration 1 (Fli1) which is a transcription factor specifically found in artery and vein ECs in zebrafish embryos (285). Fli1 probes were generated by Dr. Rajeeb Swain (University of Birmingham, UK) and were used as a positive control for endothelial expression. An anti-digoxigenin antibody conjugated to alkaline phosphatase was then used before adding BM purple, a substrate for alkaline phosphatase, which develops a purple colour. The purple colour indicates the location of the gene of interest in the whole-embryo.

Embryos probed with Fli1 antisense riboprobes revealed a clear vascular pattern with the main vessels stained purple such as the dorsal aorta, posterior cardinal vein and the intersegmental arteries (figure 5.5). However RhoJ appeared to be expressed in the somites of the embryo, which lie in between the intersegmental arteries. This expression was confirmed

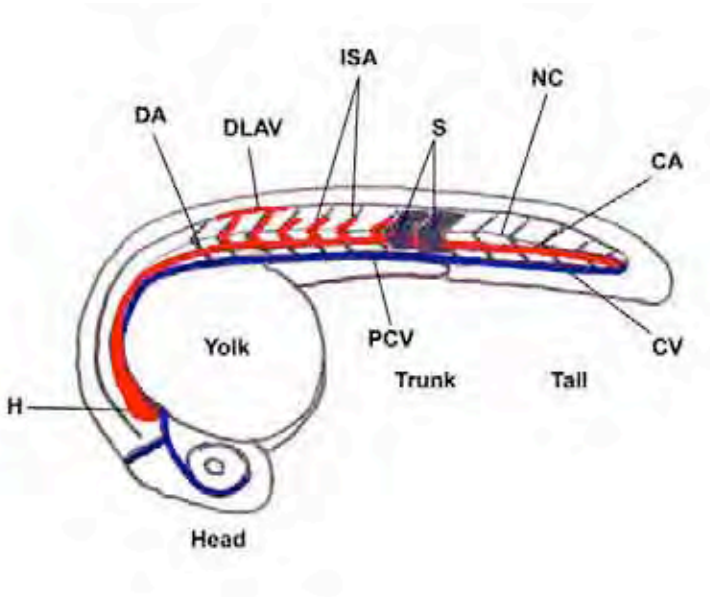

Figure 5.4 Anatomy of zebrafish embryo. Lateral view drawing of a 24 hours post fertilisation (hpf) zebrafish embryo. At this stage, blood leaves the heart (H) and enters the dorsal aorta (DA). The circulation progresses into the caudal artery (CA) where blood empties into the caudal vein (CV) and the posterior cardinal vein (PCV) before returning to the heart. At this time, intersegmental arteries (ISA) are sprouting from the dorsal aorta, but do not yet carry circulation. At around 30 hpf, the ISA begin to connect with one another to form the dorsal longitudinal anastomotic vessel (DLAV). The somites (S) are muscle segments that lie between the intersegmental vessels. NC; notochord.

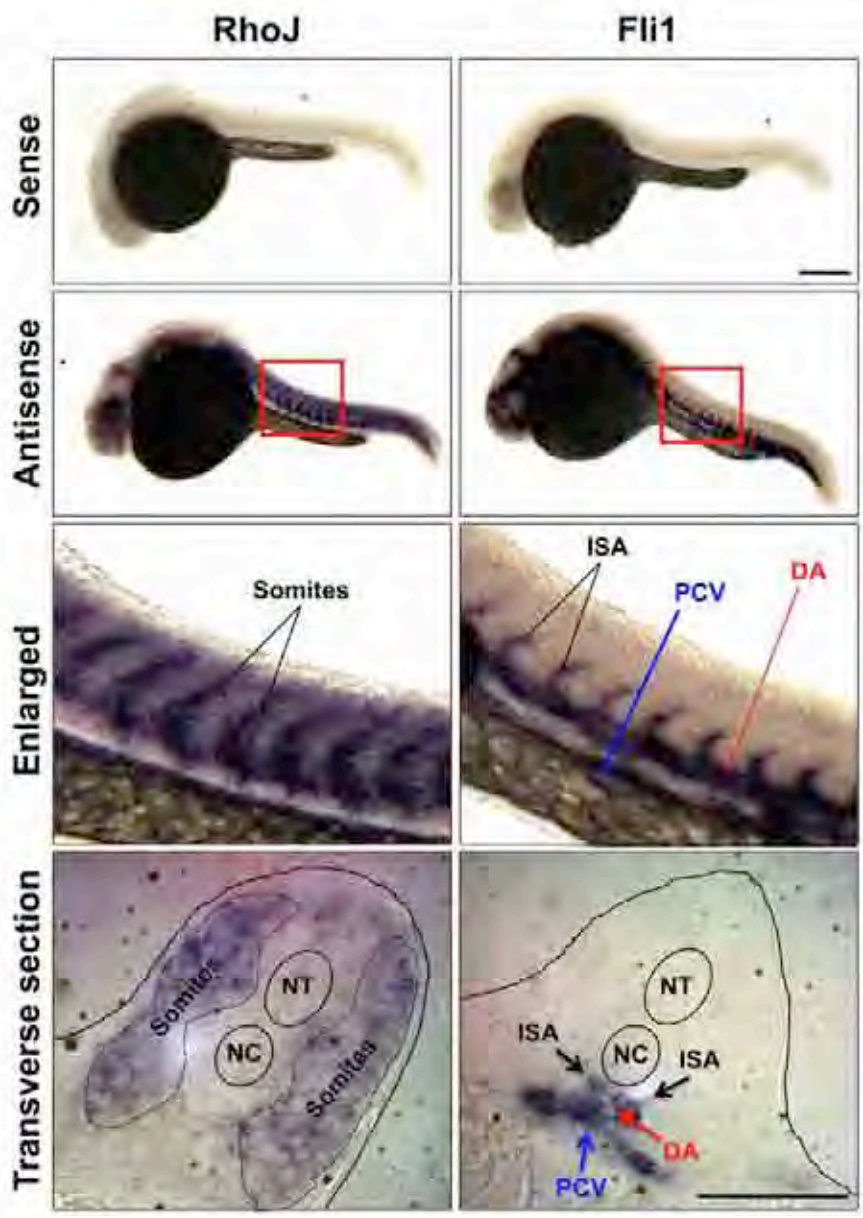

Figure 5.5 RhoJ mRNA is expressed in the somites of 24 hpf zebrafish embryos. Whole-mount *in situ* hybridization experiments were performed on 24 hours post fertilisation (hpf) embryos using full length zebrafish RhoJ sense and antisense riboprobes. Friend leukemia virus integration 1 (Fli-1) riboprobes were also used as a control for endothelial cell expression. The embryos are shown laterally and the red boxes represent the regions enlarged. The embryos used in the *in situ* hybridization experiments were formalin fixed, paraffin wax embedded cut into 1 µm transverse sections by Cancer Research UK. The transverse sections were made through the trunk with the dorsal side up. ISA: intersegmental arteries; DA: dorsal aorta; PCV: posterior cardinal vein; NT: neural tube; NC: notochord. Scale bars = 250 µm. Similar data were obtained in three independent experiments

by sectioning the trunk of the embryos into 1 μm transverse sections (figure 5.5). RhoJ expression was only found on either sides of the neural tube and notochord, where somites are distributed. Thus these data confirm that RhoJ does not have vascular expression during prim-5 stage of angiogenesis and that RhoJ may have a function in muscle cells in zebrafish and not in the endothelium.

The expression pattern of RhoJ at a later stage of the pharyngula period, long-pec (48 hpf), was also examined using whole-mount *in situ* hybridization experiments. Interestingly, RhoJ mRNA expression was not found in the somites of 48 hpf embryos but in the cephalic (head) region (figure 5.6). In order to gain further insight into what tissue type(s) RhoJ may be expressed in at this stage, the Zebrafish Information Network (ZFIN) gene expression database was used to find zebrafish genes (at 48 hpf) that had a similar expression pattern to RhoJ.

Zebrafish genes, Rtn3 (reticulon 3) and Aldh7a1 (aldehyde dehydrogenase 7 family member A1), were found to have similar but not identical cephalic expression patterns to RhoJ (figure 5.6). Thisse *et al.* (2004) identified the expression patterns of Rtn3 and Aldh7a1. They reported that Rtn3 is expressed in the somites, cranial ganglia, retinal ganglion, brain marginal zone, pectoral fin muscles and head muscles (286). In addition, Aldh7a1 was reported to be expressed in the retina, posterior and dorsal tectum, somites, pectoral fin muscles and head muscles. RhoJ-stained embryos showed expression that was similar to the pectoral fin muscle and cephalic muscle expression of Rtn3. Moreover, RhoJ expression was found to resemble the posterior and dorsal tectum, pectoral fin muscle and head muscle expression of Aldh7a1. Thus RhoJ may be expressed in cephalic musculature, pectoral fin muscles and posterior and dorsal tectums of 48 hpf zebrafish embryos.

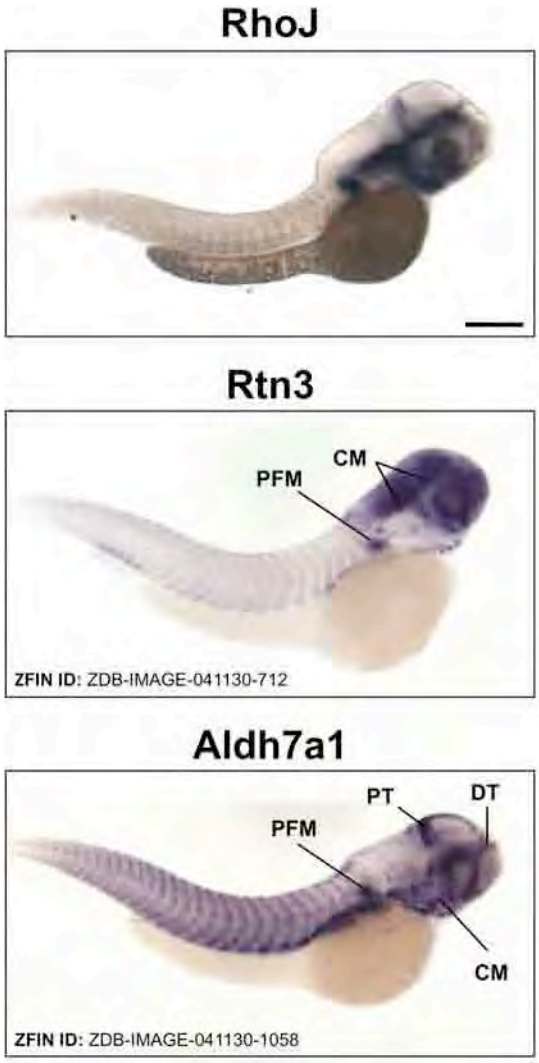

Figure 5.6 RhoJ mRNA is expressed in the cephalic region of 48 hpf zebrafish embryos but not in somites. Whole-mount *in situ* hybridization experiments were performed on 48 hours post fertilisation (hpf) embryos using full length zebrafish RhoJ antisense riboprobes. Images of 48 hpf embryos stained with Rtn3 (reticulon 3) and Aldh7a1 (aldehyde dehydrogenase 7 family member A1) were obtained from the Zebrafish Information Network database (ZFIN: **http://zfin.org**) (286). The expression pattern of RhoJ was found to resemble the expression patterns of Aldh7a1 and Rtn3 to some extent and these similarities are annotated as follows: CM: cephalic musculature; PFM: pectoral fin muscle; PT: posterior tectum; DT: dorsal tectum. Scale bar = 250 µm.

5.2.4 *In vivo* knockdown of RhoJ in zebrafish

Although zebrafish RhoJ was not expressed in the endothelium, the effect of RhoJ *in vivo* knockdown on vessel formation was still investigated since RhoJ had upregulated expression during angiogenesis (figure 5.3). Synthetic antisense morpholino oligonucleotides have been successfully used in zebrafish to knockdown gene function by gene-specific inhibition of mRNA translation or by modifying pre-mRNA splicing (287, 288). Morpholinos have a similar base structure to RNA and DNA but have a morpholine ring instead of a ribose sugar. In addition, morpholinos have altered backbone linkages compared to RNA and DNA that are nonionic. Together, these modifications form a highly soluble analogue of RNA and DNA capable of hybridizing to specific single-stranded nucleic acid sequences by Watson-Crick base pairing (289). Advantages of using morpholinos over DNA or RNA oligomers are that the backbones are resistant to enzymatic degradation and are less likely to interact nonspecifically with cellular components since the backbones lack negative charge (290).

Morpholinos that block translation of proteins work by binding to the 5'-untranslated region of mRNA through to the first 25 bases of the coding sequence. Hybridization of the morpholino at these regions prevents the ribosomal initiation complex (translation machinery) from binding. This prevents translation of the transcript resulting in knockdown of the protein. A translation blocker morpholino was designed to target the first 25 bases of the coding sequence of RhoJ mRNA.

Splicing of pre-mRNA to make mature mRNA occurs through the activity of spliceosome complexes. Spliceosomes are directed where to make cuts by small nuclear ribonuclear proteins (snRNP) that bind to sequences in the pre-mRNA, flanking the positions of splice junctions. Morpholino oligos are able to enter the nucleus and interfere with pre-mRNA

splicing by targeting splice junctions to inhibit the binding of snRNPs that mark the splice sites for the splicesome. For knockdown of gene function, morpholinos are typically used to modify splicing to produce non-functional proteins. By targeting internal splice sites, an exon that encodes for one of the protein's functional moieties can be spliced out from the mature mRNA (288). Thus to knockdown RhoJ function, a splice blocker morpholino was designed to bind specifically to the exon2-intron2 splice junction of RhoJ pre-mRNA, as illustrated in figure 5.8A. Blocking this splice site results in exon 2 not being in the final mRNA transcript for RhoJ and the lack of exon 2 results in the production of non-functional RhoJ protein.

To control for non-specific effects, control morpholinos, which are not complementary to any known gene sequence were used. Using high concentrations of morpholinos can cause toxicity in embryos causing unspecific phenotypes and embryo lethality (291). Dose response assays determine the margin between the induction of a specific phenotype and the onset of toxicity. Thus it was necessary firstly to test the toxicity of the morpholinos at various concentrations and determine the lowest effective concentration. This was tested by treating embryos with translation blocker or splice blocker morpholinos at a range of doses and the dose that did not induce embryonic fatality was chosen. Embryo lethality was not found by using translation blocker morpholino at 1 mM and splice blocker morpholino at 0.5 nM (see appendix 5). In order to accurately compare between the conditions, control morpholinos were also injected at both these concentrations.

In order to investigate the knockdown of RhoJ on angiogenesis in zebrafish, it was first important to determine whether the translation and splice blocker morpholinos were successfully knocking down and altering splicing of RhoJ respectively. RhoJ specific and control morpholinos were injected into zebrafish embryos at zygotic stages (1-8 cell stage) of embryogenesis. Embryos injected with translation blocker or control morpholino were grown

to 26 hpf and were then lysed in NP40 lysis buffer. To investigate whether translation blocker morpholino successfully knocked down RhoJ protein, embryo lysates were blotted with anti-RhoJ antibodies and anti-β actin antibodies as a control for loading. Translation blocker morpholino was found to successfully knock down the expression of RhoJ in zebrafish embryos (figure 5.7).

Fish injected with splice blocker or control morpholino were cultured until 26 hpf. These embryos were lysed in trizol, RNA was extracted and then cDNA was generated. To determine whether splicing at exon2-intron2 splice junction was successfully blocked by splice blocker morpholino, PCR was performed using primers designed to cross exon 1-3 boundaries, indicated by red arrows in figure 5.8A. The amplified fragment of exon 1-3 using control cDNA would produce a band size of 175 base pairs (bp) in length. However, if the splice blocker morpholino was successful and exon 2 was not spliced into the mature mRNA, the band size would shift to 116 bp in length. The zebrafish housekeeping gene EF1α was used as a positive control. No template and minus-RT controls were set up as described previously to check for genomic DNA or cDNA template contamination. Splice blocker morpholino successfully modified splicing of the pre-mRNA transcript of RhoJ as there was a 116 bp band detected in morpholino-treated fish cDNA (figure 5.8B). However there was also a 175 bp band found, which suggests that the morpholino was not completely efficient. This may be due to there being maternal transcripts of RhoJ being present at the zygotic stages of zebrafish embryogenesis, which cannot be modified as maternal transcripts are already spliced. Knowing the limitations of RhoJ splice blocker, this morpholino was still used in RhoJ knockdown studies.

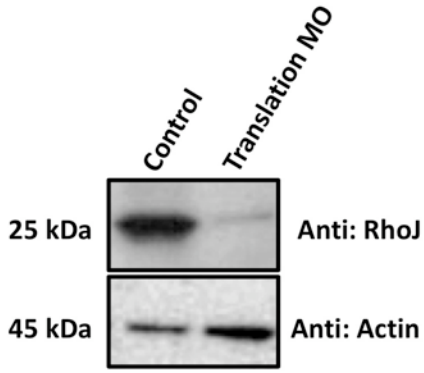

Figure 5.7 Translation blocker morpholino successfully knocks down RhoJ protein. Embryos were injected with translation blocker or control morpholino at 1 mM. Embryos were then lysed with NP40 lysis buffer and were blotted with anti-RhoJ antibodies and anti-β actin antibodies (as a control for loading) to determine successful knockdown of RhoJ protein expression.

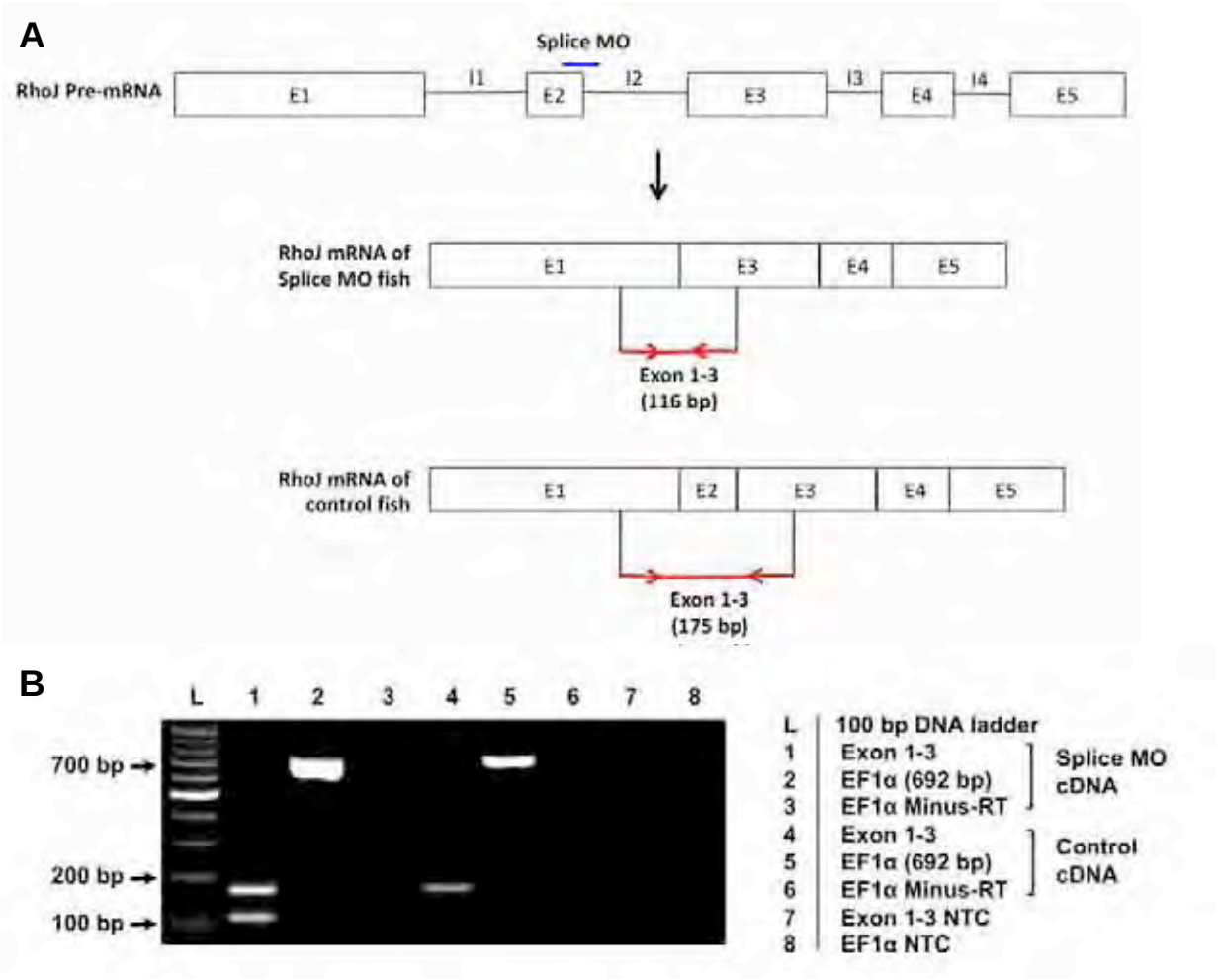

Figure 5.8 Splice blocker morpholino modifies RhoJ splicing. (A) Schematic displaying the splicing modification of splice blocker morpholino (splice MO) on RhoJ pre-mRNA by binding complementary to exon2-intron2 splice junction in the pre-mRNA transcript. To distinguish whether splicing at this junction was blocked, primers were designed to cross exon 1-3 boundaries (indicated by red arrows). When amplifying this region by PCR, the splice blocker morpholino injected fish amplify shorter fragments due to exon 2 being spliced out. (B) Embryos injected with 0.5 nM splice blocker morpholino or control morpholino were lysed with trizol, cDNA templates were generated using the same amount of RNA and reverse transcription PCR was performed using primers to cross exon boundaries 1-3. EF1α was used as a positive control. Minus reverse transcriptase enzyme controls (minus-RT) were used with EF1α primers and no template controls (NTC) were added for each primer pair.

In 2002, a zebrafish transgenic line that expresses green fluorescent protein (GFP) specifically in all blood vessels throughout embryogenesis under the control of vascular-specific Fli1 promoter was generated by Lawson and colleagues (292). This transgenic line allows detailed analysis of both wildtype and mutant embryonic vasculature, facilitating the identification of new mutants affecting *in vivo* angiogenesis. Fli1-GFP transgenic fish are commonly chosen to visualise the development of blood vessels over other methods such as confocal microangiography since this method only permits the visualisation of vessels that are connected to the active circulatory network. Thus the effect of RhoJ protein knockdown or splice modification on embryonic vessel formation was assessed using Fli1-GFP transgenic fish.

Fish were injected with RhoJ specific or control morpholinos, cultured until 26 hpf and fixed. Uninjected transgenic fish were also fixed as a control for morpholino injection. The Fli1-GFP transgenic fish were then fluorescently imaged for their EC specific GFP expression. Fish were fixed at 26 hpf since this is the stage when most of the intersegmental arteries have fully sprouted and reached the level of the dorsal neural tube being able to then merge with their neighbours from anterior and posterior segments to form the DLAV at 30 hpf (97).

Following injection of translation or splice blocker morpholino, the development of the main vessels (dorsal aorta and posterior cardinal vein) were unaffected but the growth of the intersegmental arteries appeared to be either stunted or delayed in comparison to control morpholino injected fish (figure 5.9A). Affected embryos injected with RhoJ-specific morpholinos displayed under-developed intersegmental arteries, which did not reach the level of the dorsal neural tube. In order to quantify the effect of RhoJ knockdown on vessel formation, the embryos were analysed for impaired sprouting of the intersegmental arteries. Translation and splice blocker morpholino groups were found to have increased numbers of

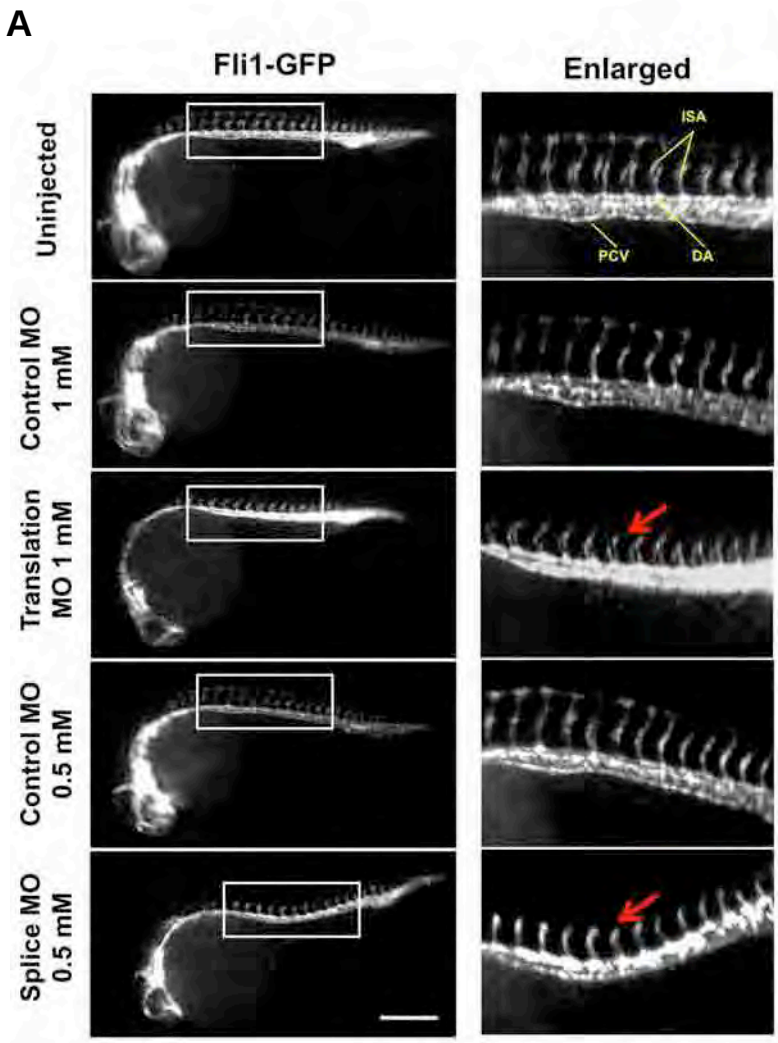
A
Fli1-GFP
Enlarged
Uninjected
Control MO 1 mM
Translation MO 1 mM
Control MO 0.5 mM
Splice MO 0.5 mM
ISA
PCV
DA

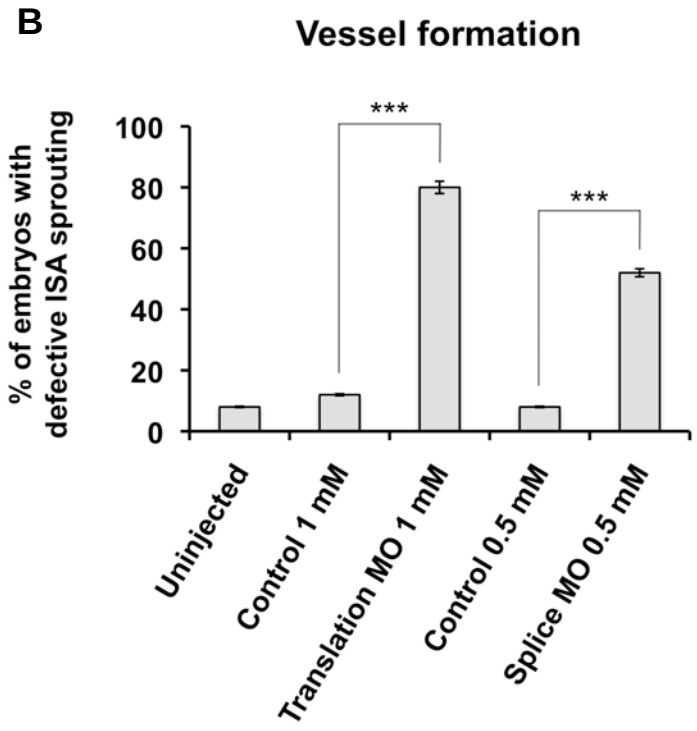

Figure 5.9 RhoJ knockdown impairs growth of intersegmental arteries in Fli1-GFP zebrafish embryos. At embryonic stage, 1-8 cell, Fli1-GFP transgenic zebrafish embryos were injected with translation blocker (translation MO), splice blocker (splice MO) or control morpholino (control) or uninjected and cultured until 26 hours post fertilisation (hpf). Embryos were then fixed and viewed under a fluorescent microscope. The white boxes represent the regions enlarged. Arrows point to under-developed intersegmental arteries (ISA). PCV: posterior cardinal vein, DA: dorsal aorta. Scale bar = 250 μm. (B) The effect of RhoJ knockdown on vessel formation was quantified by calculating the percentage of embryos with defective ISA sprouting. Values represent the means from three independent experiments (35 embryos from each experiment were scored). Error bars depict the standard error of the mean. One-way ANOVA showed a significant effect of RhoJ knockdown on ISA formation ($P<0.0001$). Tukey's multiple comparison test was used to compare translation MO with control 1 mM or splice MO with control 0.5 nM (*** = $P<0.001$).

embryos with impaired intersegmental artery formation in comparison to control groups (figure 5.9B). The percentage of affected embryos injected with splice blocker morpholino was around 30% less than that of translation blocker morpholino. This can be explained by the fact that the RhoJ splice blocker does not modify all RhoJ transcripts, and is not as efficient as blocking RhoJ translation.

Since RhoJ is expressed in the somites and not the vasculature (figure 5.5), it was essential to know whether the vascular defects found with RhoJ knockdown was a secondary effect of impaired somite formation. Thus to analyse somite morphology in morpholino injected fish, whole-mount *in situ* hybridization experiments were performed using myogenic differentiation 1 (MyoD) riboprobes, a zebrafish somite marker (293). Embryos that were injected with translation or splice blocker morpholinos displayed alterations in somite morphology where the somites were not uniformly arranged into V-shaped segments and did not have clear boundaries between the somites (figure 5.10A). RhoJ mutant embryos were found to have a range of phenotypic severity and were categorised into normal, moderate and severe phenotypes according to morphological characteristics. Moderately affected morphant embryos were found to have no more than 5 weak or undefined somite boundaries. More severely affected embryos displayed more than 5 weak or undefined somite boundaries and sometimes missing somites and bent tails. Normal embryos displayed normal 26 hpf somite morphology. The frequency of moderate and severe phenotypes was found to increase with injection of translation or splice blocker morpholinos (figure 5.10B).

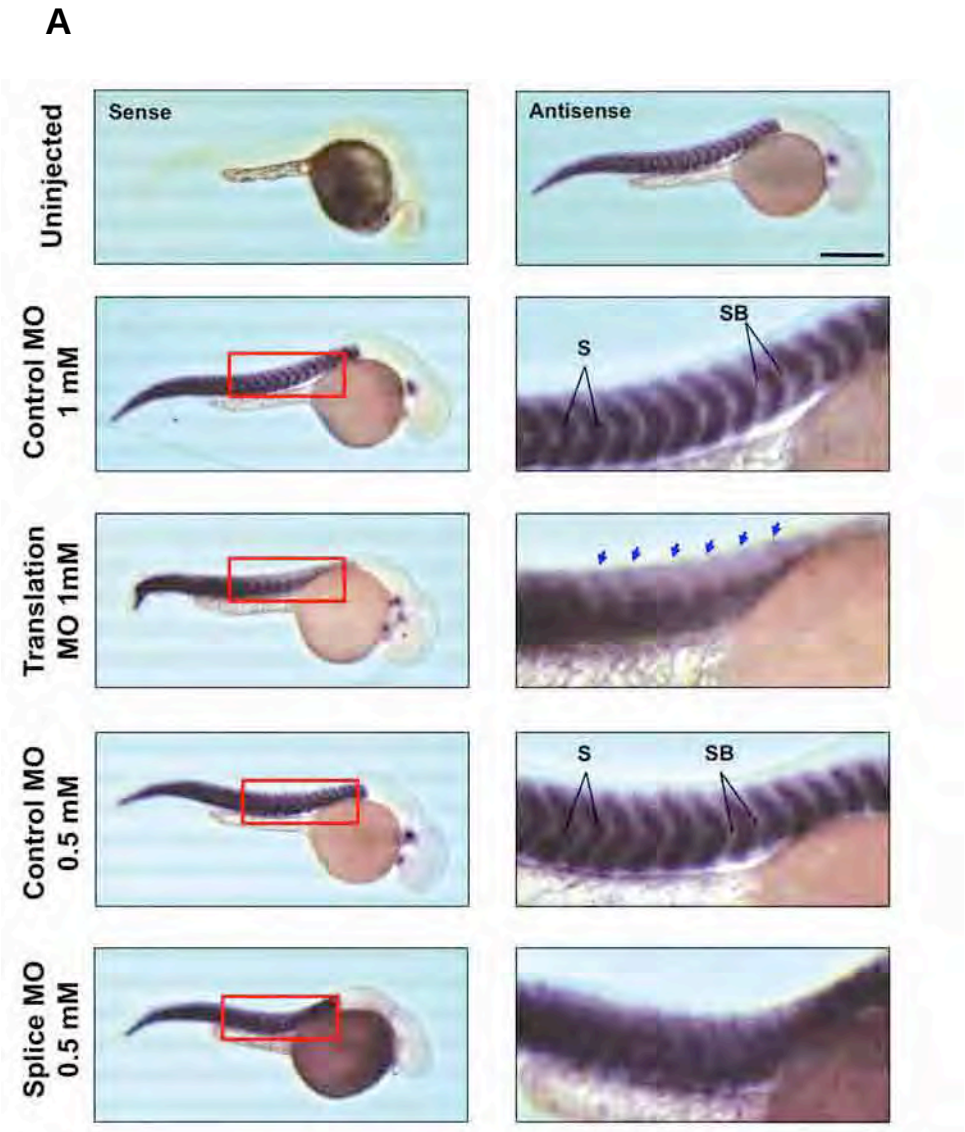
A
Uninjected
Sense
Antisense
Control MO 1 mM
S
SB
Translation MO 1mM
Control MO 0.5 mM
S
SB
Splice MO 0.5 mM

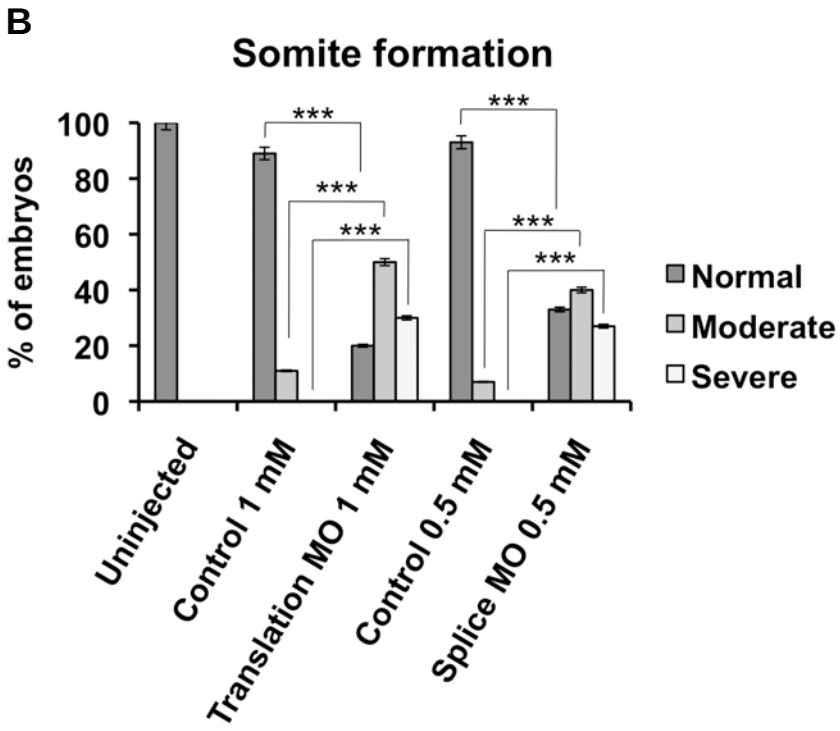

Figure 5.10 RhoJ knockdown impairs somite formation in Fli1-GFP zebrafish embryos. (A) To analyse somite morphology, whole-mount *in situ* hybridization experiments were performed on morpholino-injected Fli1-GFP embryos using a somite muscle specific marker, myogenic differentiation 1 (MyoD). Red boxes represent the regions enlarged. Blue arrows point to missing somites (S). Embryos injected with translation blocker (translation MO) or splice blocker (splice MO) morpholinos displayed impaired somite patterning and weak or undefined somite boundaries (SB). Scale bar = 250 µm. (B) Somite morphology was scored according to the following criteria: normal (embryos have normal 26 hpf somite morphology); moderate disruption (embryos display ≤5 weak or undefined somite boundaries); severe disruption (embryos have >5 weak or undefined somite boundaries). Values represent the means from three independent experiments (35 embryos from each experiment were scored). Error bars depict the standard error of the mean. One-way ANOVA showed a significant effect of RhoJ knockdown on somite boundary formation ($P<0.0001$). Tukey's multiple comparison test was used to compare translation MO with control 1 mM or splice MO with control 0.5 nM (*** = $P<0.001$).

5.2.5 Summary

Zebrafish RhoJ was a hypothetical protein and its sequence had been predicted by homology with mammalian RhoJ and conserved exon sequences. Full length RhoJ was amplified from zebrafish cDNA and the sequence of this amplicon was found to match the predicted sequence. RhoJ mRNA was detected in all periods of embryonic development (cleavage, blastula, segmentation and pharyngula). The localisation of RhoJ mRNA expression during pharyngula was investigated. At 24 hpf, RhoJ expression was found in the somites. However, at 48 hpf, expression of RhoJ was not detected in the somites but was found in the head region instead. By comparing expression of RhoJ to other known zebrafish genes, this expression pattern resembles the posterior and dorsal tectums and cephalic and pectoral fin musculature. When RhoJ function was knocked down using antisense oligonucleotide morpholinos, angiogenic sprouting of the intersegmental arteries was impaired and somite patterning was disorganised, due to loss of proper somite boundaries.

5.3 Discussion

The mRNA expression of RhoJ at different embryonic stages of zebrafish development was assessed in 8-cell, 30% epiboly, 5-somite, prim-5 and long-pec embryos (figure 5.3). RhoJ was expressed in all stages with low expression in 5-somite, when somites are forming and high expression in prim-5 and long-pec, when angiogenesis is occurring (280). This suggested that RhoJ might be playing a role in vessel formation. However, *in situ* hybridization studies revealed that the mRNA expression of RhoJ in prim-5 embryos was not localised to the vasculature but was found in the somites (figure 5.5). With RhoJ being highly expressed in human ECs (206), it was surprising for zebrafish RhoJ not to be expressed in the endothelium.

Despite zebrafish RhoJ not being expressed in the vasculature, knocking down RhoJ function by interfering with the translation or splicing of RhoJ still impaired intersegmental artery development in Fli1-GFP transgenic fish (figure 5.9). Although the sprouting of the intersegmental arteries was impeded, the main vessels were unaffected, indicating that RhoJ knockdown affected only angiogenesis and not vasculogenesis. The high expression of RhoJ during embryonic angiogenesis in figure 5.3 and RhoJ knockdown resulting in impaired vessel formation might be explained by RhoJ downstream signalling being responsible for guiding the growth of angiogenic intersegmental vessels in between muscle segments. However subsequent experiments revealed that embryos injected with translation blocker or splice blocker morpholinos displayed defects in somite boundary morphology (figure 5.10). The somites were shown to have weak or absent somite boundaries with the gaps in between somites irregularly spaced, causing the somites to be very close to one another. This somite-patterning defect may have in turn affected the migration of the intersegmental arteries. Thus the vascular defect found with RhoJ knockdown may have been due to loss of RhoJ function as a regulator of somite boundary formation. These data promote the notion that RhoJ does not play a role in EC biology in zebrafish as it does in mammals.

Consistent with our data, Shaw *et al.* (2006) showed that a class of zebrafish somite morphogenesis mutants also displayed defects in trunk angiogenic vessel patterning due to lack of proper somite boundary formation. This group also showed that somite patterning defects are accompanied by mispatterned segmental expression of vascular guidance molecules such as semaphorin 3A1 (294). Semaphorin 3A1 is expressed in somites of zebrafish and is known to guide the patterning of the developing vasculature in between the somites by binding to PlexinD1, a receptor expressed on ECs (295). Therefore it is a possibility that breakdown of somite morphology in RhoJ morphants leads to the failure to properly express vascular guidance cues in somites/somite boundaries which causes the

impaired development of the intersegmental arteries. In summary, RhoJ knockdown studies showed that RhoJ plays a role in the development of somites boundaries, which are vital structures for the normal sprouting of angiogenic vessels.

Embryogenic morphogenesis is a result of coordinated cell motility and cell-shape changes, which involves actin reorganisation and focal adhesion formation. Focal adhesion kinase (FAK), a nonreceptor tyrosine kinase, is a vital intracellular constituent of focal adhesions. Phosphorylation of FAK has been shown to promote both cell motility and cell adhesion. Ilić *et al.* (1995) demonstrated that FAK null embryos were able to initiate gastrulation normally but formed no somites during mouse embryogenesis. Cells isolated from these mice also had reduced motility and increased focal adhesions compared to control cells (296). These results are similar to the *in vitro* loss of RhoJ function data shown in chapters 3 and 4, which implies that RhoJ is involved in focal adhesion turnover during cell migration. It was also reported by Henry *et al.* (2001) that FAK is highly concentrated at the somite boundaries of zebrafish embryos (297), suggesting a role for FAK in the formation and stabilisation of somite borders. Studies performed by Crawford *et al.* (2003) showed that paxillin, a focal adhesion-associated adaptor protein that binds to FAK, colocalises with phosphorylated FAK at the boundaries of somites in zebrafish (298). These data demonstrate that cell-matrix adhesions at somite boundaries are important in stabilising somite boundaries. Since we have shown that RhoJ plays a role in focal adhesion formation in mammalian cells (chapter 4), RhoJ may stabilise somite borders by directly or indirectly regulating focal adhesion formation at somite boundaries during zebrafish development. However, we have not investigated the subcellular localisation of RhoJ in zebrafish muscle cells and so we do not know if zebrafish RhoJ is expressed in focal adhesions. Zebrafish RhoJ is quite divergent to human RhoJ at the N- and C-terminal ends so may not have the same localisation in zebrafish (this could be investigated in future studies).

Two different RhoJ-specific morpholinos with non-overlapping sequences were used as controls for non-specific effects in the RhoJ loss-of-function studies. Both morpholinos produced the same phenotypes. This supports the hypothesis that the observed phenotypes were due to knockdown of RhoJ and not an interaction with an off-target mRNA, since morpholinos with different sequences do not generally elicit the same nonspecific effects. In addition, a control morpholino was also injected at the same concentration as the RhoJ-specific morpholinos to show that the phenotypes found were specific to knockdown of RhoJ. However, it would also be informative to perform mRNA rescue experiments to further confirm the specificity of the RhoJ knockdown phenotype. This can be carried out by co-injecting RhoJ mRNA that is not recognised by the translation blocker morpholino by creating silent mutations in the region of the coding sequence that the morpholino would bind to. In the case of the splice blocker morpholino, wild type RhoJ mRNA can be co-injected (299).

Furthermore, the expression of RhoJ in long-pec embryos was not found in the somites but restricted to the head region (figure 5.6). Analysis of this expression pattern revealed that RhoJ may be expressed in the head muscles, pectoral fin muscles and posterior and dorsal tectums of 2 day old zebrafish embryos. There are different subtypes of cephalic muscles and RhoJ may not be expressed in all the head muscles. Co-ordinated contraction of these various cephalic muscles in zebrafish mediates the expansion and compression of the jaw and gills during feeding and respiration. The pectoral fins aid swimming and maneuvering in adult fish and begin to develop at around 40 hpf when somites 2-4 migrate to form the pectoral fin musculature (300). The tectums are regions of the midbrain that control vision. Thus RhoJ may have varying functions in zebrafish and to investigate these functions, further work would need to be carried out to see what happens when RhoJ is knocked down at long-pec stage. The downregulation of RhoJ expression in the somites and the upregulation of RhoJ

expression in cephalic structures at 48 hpf may be controlled at the transcriptional level. For example, epigenetic changes to DNA may be altering the expression of RhoJ by preventing transcription or tissue specific transcription factors may be switching RhoJ transcription 'on' or 'off' depending on the stage of development.

The expression pattern of RhoJ has only been identified in prim-5 and long-pec zebrafish embryos and the localisation of RhoJ at other stages of development still remains to be investigated. Future work could include investigating the expression of RhoJ from fertilisation to adulthood using whole-mount *in situ* hybridization experiments, data from these experiments would provide further insights into the function of RhoJ in zebrafish at different stages of embryogenesis.

The fact that RhoJ is not expressed in vasculature of zebrafish indicates that perhaps the role of RhoJ in actomyosin contractility is not required or that another gene is taking over RhoJ's role in zebrafish. Due to the close homology of Cdc42, TC10 and RhoJ and the fact that they can all bind to the same effector proteins, it is reasonable to suggest that they may substitute for one another. In zebrafish there are three homologues for Cdc42, but in humans there is only one (301). A possible explanation for the lack of RhoJ in the endothelium is that one of the other Cdc42 homologues or TC10 could be taking over RhoJ's role. This hypothesis was tested in our laboratory by Ms Diana Walsh (University of Birmingham) by investigating the mRNA expression patterns of the zebrafish Cdc42 homologues (zebrafish Cdc42, Cdc42 like 1 and Cdc42 like 2) and TC10 by performing whole-mount *in situ* hybridization experiments. Although none of the GTPases were specifically expressed in the endothelium, they were all ubiquitously expressed and Cdc42 like 2 and TC10 showed increased staining intensity at the somite boundaries. Thus, since the other Cdc42 subfamily group members are expressed in

the vasculature at low levels, there is a chance that the other Cdc42 homologues may be taking the endothelial role of RhoJ in zebrafish.

Divergent gene expression across species is extremely common. Variations in gene expression are controlled by *cis*-regulatory DNA sequences (promoters or enhancers) that contain binding sites for *trans*-acting regulatory proteins such as transcription factors (302). The specific combination of transcription factor binding sites within an enhancer determines its activity and specifies the timing, location and abundance for the gene it regulates. Many genes are controlled by multiple enhancers, and each of these control a subset of the gene's expression pattern (303). Studies have shown that non-coding sequences upstream of genes and in intron regions have low conservation across species, indicating that these sequences drive gene expression variation in different species (304). The fact that zebrafish and human RhoJ amino acid sequences are 76% identical but are expressed in different tissues and may have completely different functions may be due to zebrafish and human RhoJ having variations in their *cis*-regulatory elements either in their promoter or enhancer regions. The *cis*-regulatory sequences controlling the expression of zebrafish RhoJ may have changed over evolutionary time through the process of mutation, causing RhoJ to have an altered expression profile. In order to understand more about what controls the expression of RhoJ in zebrafish and in mammals, the *cis*-regulatory DNA sequences that control RhoJ expression in each species could be examined.

To summarise, although the amino acid sequences of human, mouse and zebrafish RhoJ were highly conserved, RhoJ mRNA expression was found in the somites of developing zebrafish embryos. Knockdown of zebrafish RhoJ impeded proper vasculature development, which was found to be due to impaired somite boundaries. Thus we hypothesise that RhoJ may be

involved in somitogenesis and/or maintenance of somite boundaries in 24 hpf zebrafish embryos but its function may also change according to its stage-specific expression.

Since zebrafish RhoJ was surprisingly not expressed in ECs, it was then necessary to determine the expression profile of RhoJ in mammals. Preliminary studies were carried out to investigate the localisation of RhoJ expression in humans and mice and this work is described in chapter 6.

Chapter six

Expression profile of mammalian RhoJ

6.1 Introduction

Bioinformatic analyses of endothelial cDNA libraries using publically available serial analysis of gene expression (SAGE) and expressed sequence tag (EST) libraries identified the small Rho GTPase, RhoJ, as being highly expressed by ECs. This prediction was further validated using reverse transcription and quantitative PCR in a range of primary cell isolates. RhoJ was highly expressed in human umbilical ECs (HUVEC) and human dermal microvascular ECs (HDMEC) but had little or no expression in fibroblasts, hepatocytes, lymphocytes or keratinocytes (206). Although Vignal *et al.* (2000) reported that mouse RhoJ expression is high in heart and moderate in lung and liver (197), the types of cells expressing RhoJ in these organs was unknown.

The aim of this chapter is to map the expression of mammalian RhoJ as precisely as possible using the available tools. Since a RhoJ antibody suitable for immunohistochemistry or immunofluorescence had not been generated at the time of this research, whole-mount or fluorescent *in situ* hybridizations were performed using complementary digoxigenin-labelled RNA probes.

Since RhoJ is highly expressed in ECs *in vitro*, it was necessary to determine whether RhoJ is also expressed in the endothelium *in vivo* and expressed during physiological angiogenesis. To visualise mouse RhoJ mRNA expression, whole-mount *in situ* hybridization experiments were performed on mouse embryos, at a stage when normal embryonic angiogenesis is known to occur. To determine whether RhoJ is expressed specifically in ECs, the tissue distribution profile of RhoJ in adult mice was assessed at the mRNA and protein level using quantitative PCR and Western blotting. To visualise the localisation of RhoJ in normal human tissues and to determine whether RhoJ is expressed in the endothelium of human cancerous tissues, the

mRNA expression of RhoJ in various human normal and cancerous tissues was examined using fluorescent *in situ* hybridization technology.

In summary, this chapter aims to characterise the expression profile of mammalian RhoJ and to confirm the hypothesis that RhoJ is highly upregulated in ECs.

6.2 Results

6.2.1 RhoJ mRNA expression during mouse embryonic angiogenesis

In order to localise the expression of RhoJ during normal embryonic angiogenesis, whole mount *in situ* hybridization was performed on developing mouse embryos at embryonic day (E) 9.5, the stage at which the vasculature is developing and angiogenesis is actively occurring (305). Digoxigenin labelled, complementary riboprobes were generated to mouse RhoJ and von Willebrand Factor (vWF), an endothelial specific expressed gene (306) from pGEM-3z mouse vWF and pGEM-3z mouse RhoJ cloned constructs (see section 2.4 DNA constructs). Sense riboprobes were also synthesised as negative controls. In brief, mouse embryos were digested with proteinase K to allow probe penetration. Riboprobes were then applied to allow hybridization to their specific mRNA sequences *in situ*. Anti-digoxigenin antibodies conjugated to alkaline phosphatase were used to locate the region of hybridization. A substrate for alkaline phosphatase, BM purple, was then added to develop a purple colour, revealing the location of the gene of interest's mRNA expression. Figure 6.1 shows the mRNA expression pattern of RhoJ and vWF at E9.5. The expression pattern of RhoJ was similar to the vascular expression of the positive control, vWF. The enlarged regions reveal a clear vascular pattern with the main trunk vessel, dorsal aorta (red arrows), and the intersegmental vessels (yellow arrows) stained blue/purple. This data shows that RhoJ mRNA has endothelial expression during normal embryonic angiogenesis in mice at E9.5.

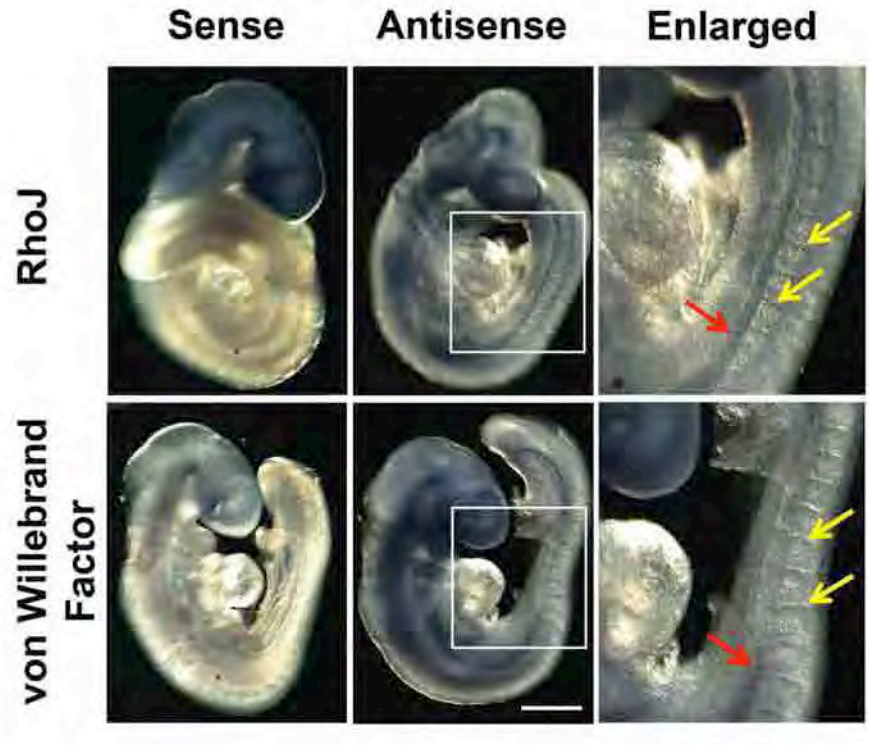

Figure 6.1 RhoJ mRNA is expressed in the vasculature of E9.5 mouse embryos. Whole-mount *in situ* hybridization experiments were performed on E9.5 mouse embryos using full-length mouse RhoJ sense and antisense riboprobes. Von Willebrand Factor riboprobes were used as a positive control for endothelial cell expression. The white boxes represent the areas enlarged. The yellow arrows indicate the intersegmental vessels and the red arrows mark the dorsal aorta. Similar data were obtained in four independent experiments. Scale bar = 200 µm.

6.2.2 Tissue distribution pattern of RhoJ at the protein and mRNA level in adult mice

Since RhoJ mRNA expression was found in the endothelium of developing mouse embryos (figure 6.1), it was necessary to determine whether expression of RhoJ was specific to ECs. Immunohistochemistry or immunofluorescence is commonly used to visualise the expression of endogenous proteins in tissue sections. However in the absence of a suitable RhoJ antibody, the expression profile of RhoJ was examined in various adult mouse tissues using quantitative PCR and Western blotting. Expression patterns of RhoJ were compared with that of VE-Cadherin, a gene known to have an endothelial specific tissue distribution (307). Dr. Michael G. Tomlinson from The University of Birmingham, UK kindly provided various tissue lysates and cDNA samples that were obtained from 8-week old C57BL6 mice.

Quantitative PCR was performed to detect mRNA expression levels of RhoJ and housekeeping gene, glyceraldehyde 3-phosphate dehydrogenase (GAPDH) (308, 309) in various adult mouse tissues (thymus, brain, heart, muscle, kidney, spleen, liver, lung). To accurately quantify gene expression, the expression level of RhoJ or VE-Cadherin was normalised to the expression level of GAPDH. RhoJ mRNA expression was found to be high in lung, moderate in spleen and low in liver, kidney, muscle, heart, brain and thymus. VE-Cadherin was also highly expressed in lung but at low levels in liver, spleen, kidney, muscle, heart and thymus. VE-Cadherin mRNA expression was not found in brain (figure 6.2A).

To detect RhoJ expression at the protein level, lysates were blotted with anti-RhoJ antibody, anti-VE-Cadherin antibody and as a control for equal protein loading, anti-tubulin antibody. Consistent with the analysis of RhoJ mRNA expression in figure 6.2A, the expression of RhoJ protein was high in lung, moderate in spleen and low in liver, kidney, muscle, heart and thymus. No RhoJ expression was detected in brain. VE-Cadherin also showed high expression

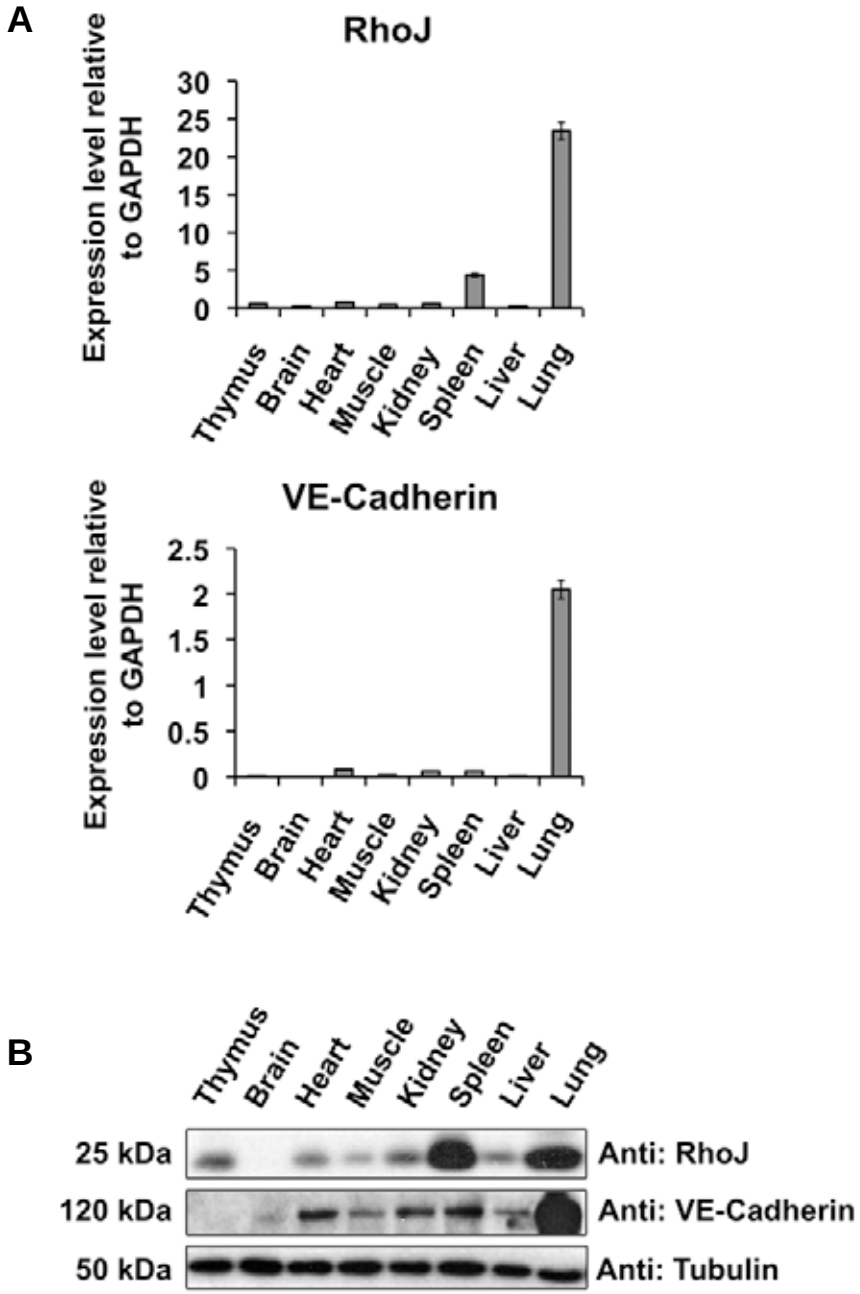

Figure 6.2 RhoJ tissue distribution pattern is similar to that of endothelial specific gene, VE-Cadherin. (A) The mRNA expression levels of RhoJ and VE-Cadherin in a variety of mouse tissues were analysed by using quantitative PCR. The expression levels of RhoJ and VE-Cadherin were normalised to the expression of housekeeping gene glyceraldehyde 3-phosphate dehydrogenase (GAPDH). Values represent the means from three independent experiments using tissues extracted from three different mice. Error bars depict the standard error of the mean. (B) Lysates of various mouse tissues were blotted with anti-RhoJ and anti-VE-Cadherin antibodies. Anti-tubulin antibodies were also used as a loading control. Similar data were obtained in three independent experiments using different donors.

in lung. Low VE-Cadherin expression was found in liver, spleen, kidney, muscle and heart but no expression was found in brain or thymus (figure 6.2B). The protein expression of RhoJ is similar to the expression of VE-Cadherin apart from the relative higher expression of RhoJ in spleen and thymus. The high level of lung expression of RhoJ at both the mRNA and protein level is consistent with an endothelial expression pattern. However, differences in the expression patterns of RhoJ and VE-Cadherin in the spleen and thymus suggest that RhoJ may be expressed in non-ECs in these tissues.

6.2.3 RhoJ expression in mouse spleen and thymus

The spleen is a peripheral lymphoid organ and is rich in B-lymphocytes (B-cells), platelets and megakaryocytes. The spleen serves to provide B-cells, a source of plasma cells, and hence antibodies for the body's immune defences. Blood is filtrated in the spleen, where macrophages phagocytose old or damaged erythrocytes, white blood cells, platelets and bacteria. The spleen also holds a reserve of platelets, which are produced by megakaryocytes, to be supplied to the body in times of emergency clot formation (310).

RhoJ was shown to have high expression in spleen, which was not consistent with endothelial specific expression of VE-Cadherin (figure 6.2). The expression of RhoJ in non-EC types of spleen was investigated by Western blotting. Whole cell lysates of primary mouse B-cells, platelets and megakaryocytes (kindly provided by Alexandra Mazharian and Ying Jie Wang from The University of Birmingham, UK) were blotted with anti-RhoJ antibody and as a control for equal protein loading, anti-tubulin antibody. Since RhoJ is most highly expressed in human ECs (206), the expression of RhoJ in B-cells, platelets and megakaryocytes was compared to the expression of RhoJ in human umbilical vein ECs (HUVEC).

RhoJ protein expression was detected in mouse B-cells and platelets but not in megakaryocytes (figure 6.3A). However, the expression of RhoJ in B-cells and platelets was relatively low compared to the expression of RhoJ in HUVEC. These data explain the high level of RhoJ expression found in mouse spleen seen in figure 6.2 and further confirms that RhoJ is not endothelial specific but is abundantly expressed by ECs.

Thymic T-cell development occurs by pluripotent progenitor cells being released periodically from the bone marrow and migrating into the thymus (311), (312). Thymocytes undergo a number of stromal cell-dependant maturation stages, which are marked by changes in cell-surface molecules. When progenitor cells first enter the thymus, they lack most of the cell surface molecules characteristic of mature T-cells such as co-receptors CD4 and CD8, these thymocytes are known as CD4-CD8- double negative (DN). Double negative thymocytes then mature into CD4+CD8+ double positive (DP), and finally mature into single positive (SP) CD4+ or CD8+ T lymphocytes (313).

Tissue distribution analysis in figure 6.2 showed that RhoJ was expressed at the protein and mRNA level in mouse thymus. However endothelial specific gene, VE-Cadherin, was not detectable at the protein level and had relatively weak mRNA expression in thymus in comparison to RhoJ. In order to determine which non-endothelial thymic cells express RhoJ, quantitative PCR using cDNAs generated from various fetal or adult mouse thymus was performed. cDNA samples of fetal (E15) thymus (whole organ culture), E15 CD45-deoxyguanosine (dGuo)-stroma (thymic stroma, depleted of thymocytes), E15 DN (CD4-CD8-), adult DP (CD4+CD8+), adult SP (CD4+), adult SP (CD8+) and adult CD45+ unfractionated thymocytes (thymic stroma depleted) were kindly provided by Dr. Graham Anderson from The University of Birmingham, UK. In order to determine the level of RhoJ expression in non-endothelial thymic cell types, the expression of RhoJ in these cell types was

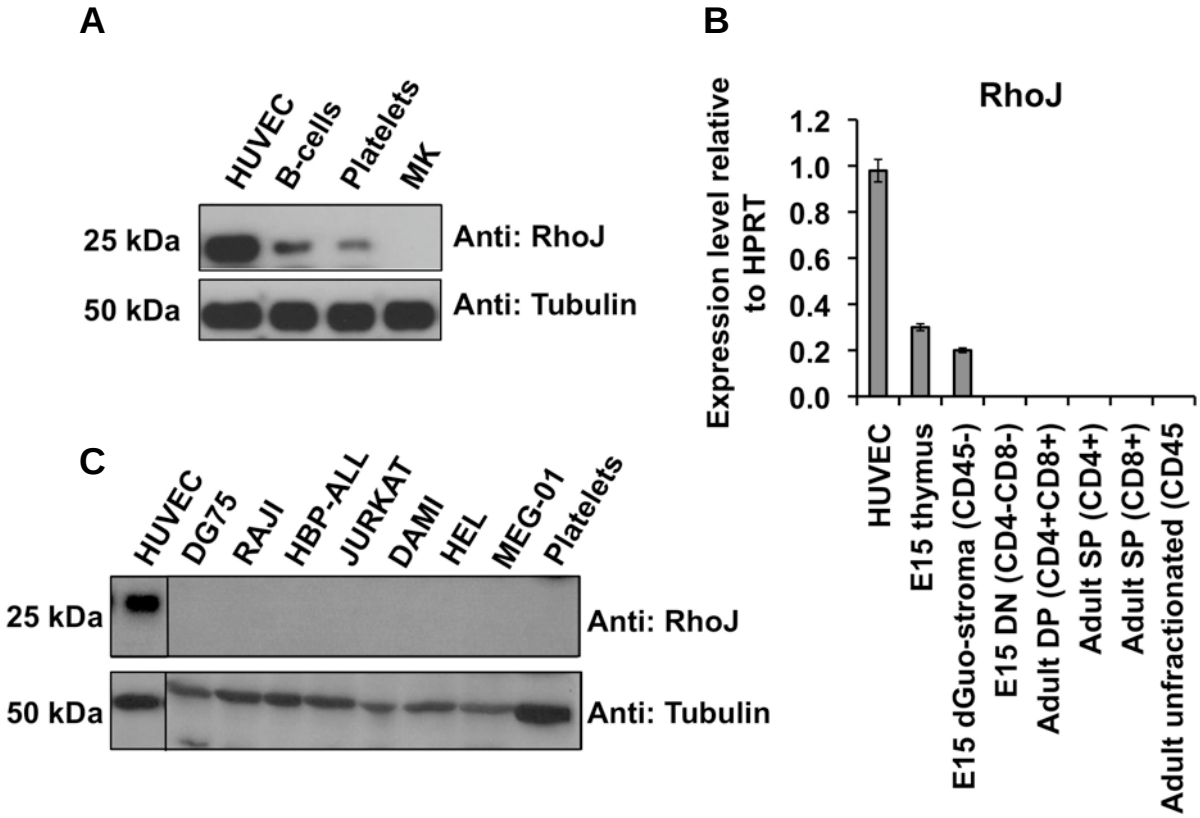

Figure 6.3 RhoJ is expressed in mouse B-cells, platelets and thymic epithelial cells. (A) Lysates of mouse B-cells, platelets and megakaryocytes (MK) were blotted with anti-RhoJ and anti-tubulin antibodies. Similar data were obtained in two independent experiments using cells from different donors. (B) The mRNA expression of RhoJ in mouse thymus-derived cDNA samples were analysed using quantitative PCR. Expression levels of RhoJ were normalised to the expression of housekeeping gene, hypoxanthine phosphoribosyl transferase (HPRT). Values represent the means from three independent experiments using cells derived from different mice. Error bars depict the standard error of the mean. (C) Lysates of various human hematopoietic cell lines and human platelets were blotted with anti-RhoJ and anti-tubulin antibodies. In all cases, the expression of RhoJ at the protein and mRNA level was compared to the expression of RhoJ in human umbilical vein endothelial cells (HUVEC).

compared to the expression of RhoJ in HUVEC. The mRNA expression level of housekeeping gene, hypoxanthine phosphoribosyl transferase (HPRT) (309), was also determined and was used to normalise the expression of RhoJ.

RhoJ mRNA expression was detected in whole fetal thymus and CD45- dGuo-treated thymus (figure 6.3B). dGuo is selectively toxic to lymphocytes, which carry the leukocyte common antigen, CD45 (314), (315). Thus dGuo treatment produces a CD45- population of thymic stroma epithelial cells (316). Consistent with these data, RhoJ expression was not found in DN, DP, CD4+/CD8+ SP or unfractionated CD45+ thymocytes. Although RhoJ was expressed in whole thymus and thymocyte depleted-thymus, the expression of RhoJ was 75-80% greater in HUVEC than in the thymic stroma. These data explain the low expression of RhoJ in thymus in figure 6.2 and suggest that RhoJ may be involved in T-cell development since thymocyte maturation is stromal cell dependant.

In light of RhoJ being expressed in mouse B-cells, platelets and thymic epithelial cells (figure 6.3) it was important to know whether RhoJ was expressed in transformed human hematopoietic cell lines or platelets. Since it was difficult to obtain human thymic epithelial cells and lymphocytes the closet option was to check RhoJ expression in human hematopoietic transformed cell lines. Western blot analysis was performed on various human B and T lymphoblast, megakaryoblast, erythroblast and platelet cells. Whole cell lysates of cell lines of DG75 and RAJI (B lymphoblast cells derived from Burkitt's lymphoma); HPB-ALL and JURKAT (T cell lines of acute lymphoblastic leukaemia); DAMI and MEG-01 (megakaryoblastic cell lines derived from chronic myelogenous leukaemia); HEL (human erythroleukaemia cell line) and platelets were kindly provided by Dr. Michael G. Tomlinson from The University of Birmingham, UK. The lysates were blotted with anti-RhoJ antibody and as a control for loading, anti-tubulin antibody. HUVEC lysate was also blotted as a

positive control and for expression comparison. RhoJ protein was not detected in human B or T lymphoblasts, megakaryoblasts, erythroblasts or platelets (figure 6.3C).

6.2.4 RhoJ mRNA expression in normal and cancerous human tissues

As mentioned earlier, at the time of these studies a RhoJ-specific antibody was not available to use in immunohistochemistry or immunofluorescence to detect the localisation of endogenous RhoJ protein. Thus to determine the expression profile of RhoJ in a variety of human tissue sections, fluorescent *in situ* hybridization technology was developed to localise the mRNA expression of RhoJ instead. Sections from a variety of normal tissues were provided by the histology service of Cancer Research, UK and purchased from SuperBiochips Inc, Korea. Additionally, a small subset of cancerous tissue sections were also used in the fluorescent *in situ* hybridization experiments in order to determine whether RhoJ was expressed during pathological angiogenesis.

RhoJ was localised using digoxigenin labelled RhoJ specific riboprobes generated from pGEM-3z human RhoJ cloned constructs (see section 2.4 DNA constructs). Once RhoJ specific riboprobes had hybridized to their complementary mRNA sequence *in situ*, sections were probed with an anti-digoxigenin antibody conjugated to rhodamine to reveal the location of RhoJ mRNA expression. *Ulex europeaus* agglutinin I (UEAI) is commonly used as a marker of ECs, since it recognises an endothelial specific glycosylation (317). Sections were stained with UEAI conjugated to fluorescein isothiocyanate (FITC) as a positive control for endothelial expression.

RhoJ mRNA expression was found in ECs, with clear co-localisation with UEAI in a number of normal tissues such as adrenal gland, pancreas, heart, liver, lymph node, lung, muscle and

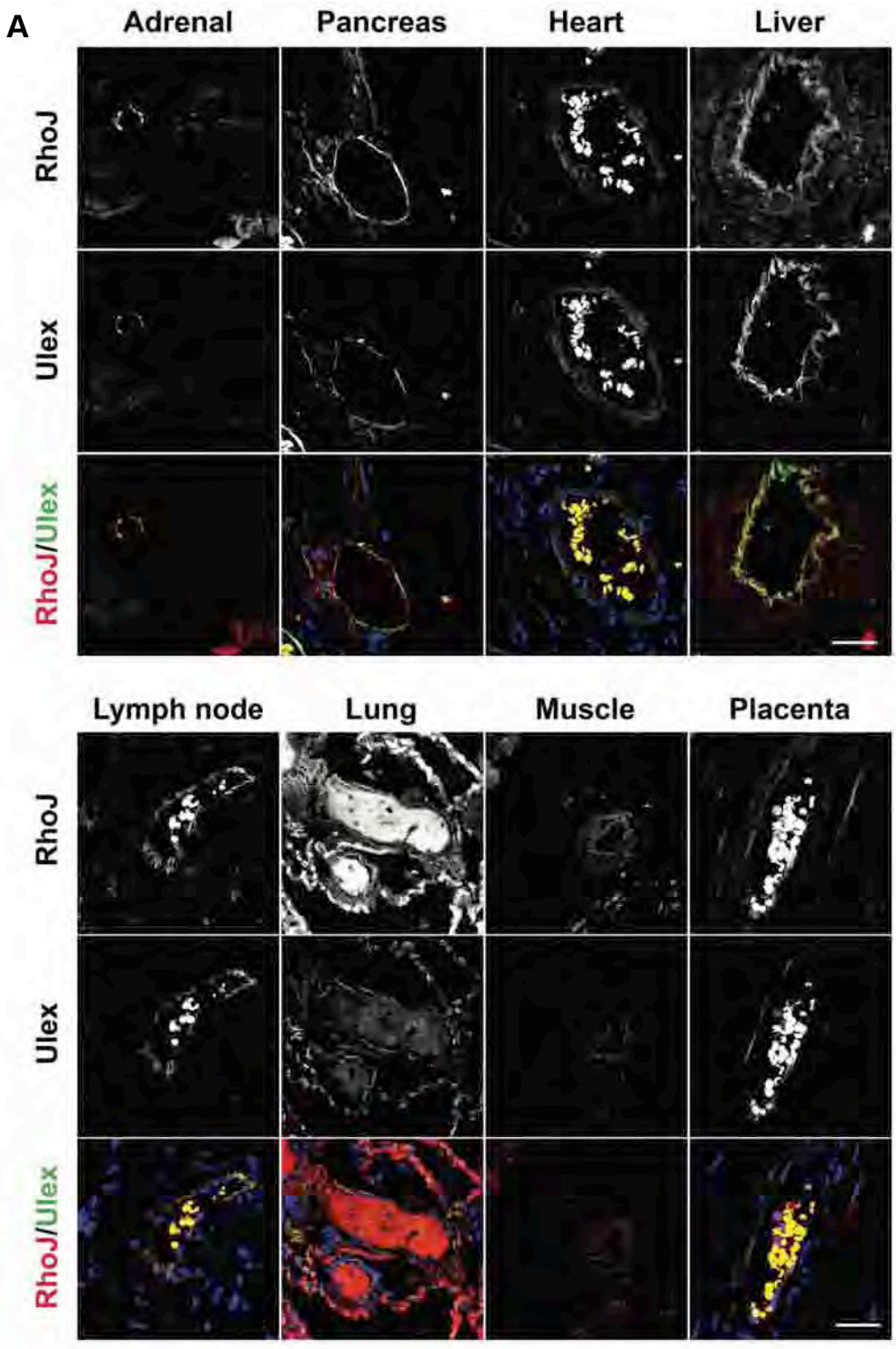
A
Adrenal
Pancreas
Heart
Liver
RhoJ
Ulex
RhoJ/Ulex
Lymph node
Lung
Muscle
Placenta
RhoJ
Ulex
RhoJ/Ulex

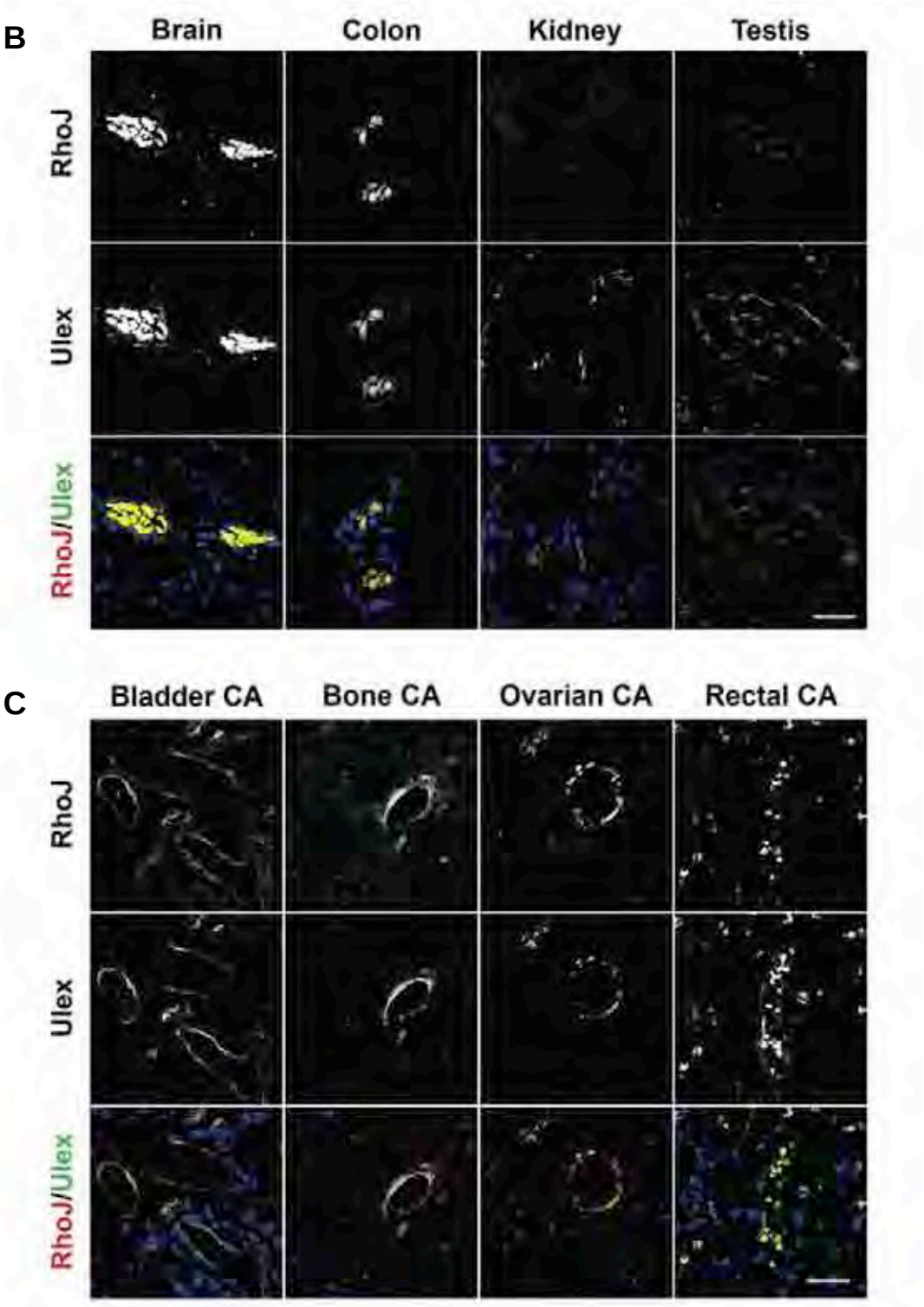

Figure 6.4 Endothelial RhoJ expression is found in normal and cancerous human tissues. Fluorescent *in situ* hybridization was performed on various normal (A-B) and cancerous (C) human tissue sections (CA; carcinoma). An antisense digoxigenin labelled riboprobe and a rhodamine labelled anti-digoxigenin antibody was used to detect RhoJ mRNA expression (red). Fluorescein labelled *Ulex europaeus* agglutinin I (UEAI) was used as an endothelial marker (green). DAPI was used to stain the nuclei (blue). Scale bar = 50 μm.

Human tissue	Endothelial RhoJ expression
Adrenal	+
Pancreas	+
Heart	+
Liver	+
Lung	+
Lymph node	+
Lung	+
Muscle	+
Placenta	+
Brain	-
Colon	-
Kidney	-
Testis	-
Bladder carcinoma	+
Bone tumour	+
Ovarian carcinoma	+
Rectal carcinoma	-

Table 6.1 Distribution of endothelial RhoJ expression in human normal and cancerous tissues.

placenta (figure 6.4A). Although RhoJ expression was found in vessels, RhoJ staining was not restricted to the endothelium in most of these tissues. This is consistent with the data shown in figure 6.2 that although RhoJ expression is endothelial, its expression is not EC specific. Endothelial RhoJ expression was not found in brain, colon, kidney and testis (figure 6.4B). Instead, RhoJ expression was found in non-ECs of kidney and testis. RhoJ expression was found in the endothelium of bladder, bone and ovarian carcinomas but not in rectal carcinoma (figure 6.4C). Erythrocytes that were found in vessels of some tissue sections caused autofluorescence in both the red and green channels. The tissue distribution pattern of RhoJ endothelial expression is summarised in table 6.1. These data show that RhoJ is expressed in normal human vasculature of most organs and is also expressed in the endothelium of some tissues undergoing pathological angiogenesis.

6.2.5 RhoJ expression in human perivascular cells

Once ECs form capillary-like structures *in vivo*, perivascular mural cells (smooth muscle cells and pericytes) are recruited to the abluminal endothelial surface. The ECs of arteries and veins are completely surrounded by single or multiple layers of vascular smooth muscle cells, whereas capillaries are only partially covered by a single layer of pericytes (10). Vascular smooth muscle cells and pericytes have many roles in regulating EC biology but their main functions are to maintain endothelial quiescence, vessel integrity and stability (11, 12).

In section 6.2.4, fluorescent *in situ* hybridization and high-resolution laser scanning confocal microscopy showed that RhoJ highly co-localised with endothelial specific sugar-binding lectin, UEAI (figure 6.4), suggesting that RhoJ is expressed in human ECs *in vivo*. However RhoJ mRNA expression was also observed in vascular smooth muscle cells surrounding the vessel in skeletal muscle in figure 6.4A, suggesting that RhoJ may also be expressed in perivascular cells. In addition, it is also possible that, due to close proximity, expression of RhoJ in other blood vessel associated cell types would result in a localisation pattern similar to that of the endothelial specific glycosylation recognised by UEAI. To address these issues, the expression of RhoJ in perivascular cells at both the mRNA and protein level was determined and compared to endothelial RhoJ expression.

To investigate the mRNA expression level of RhoJ in pericytes and vascular smooth muscle cells, quantitative PCR was performed on primary human placenta-derived pericyte (hPC-PL) and human aortic smooth muscle cell (HASMC) cDNA isolates. To determine whether RhoJ protein was expressed in these cell types, whole cell lysates of hPC-PL and HASMC were blotted with anti-RhoJ antibody and loading control, anti-tubulin antibody. Since RhoJ is highly expressed in ECs (206), the expression of RhoJ in hPC-PL and HASMC at the mRNA

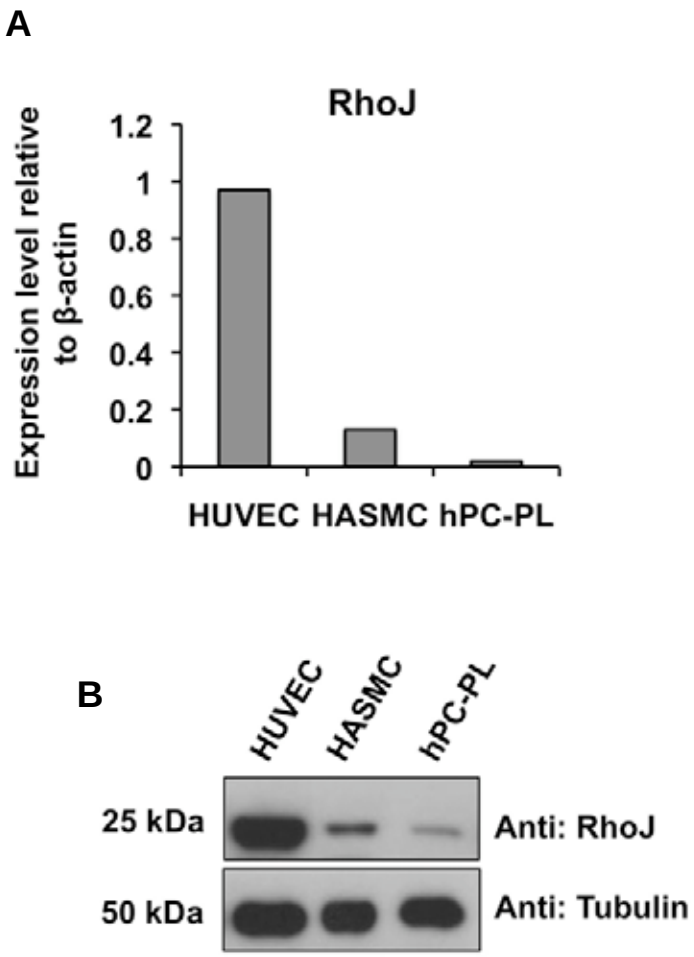

Figure 6.5 RhoJ is expressed in human smooth muscle cells and pericytes. (A) The mRNA expression level of RhoJ was analysed in human umbilical vein endothelial cells (HUVEC), human aortic smooth muscle cells (HASMC) and human placenta-derived pericytes (hPC-PL) using quantitative PCR and normalised to β-actin. (B) Whole cell lysates HUVEC, HASMC and hPC-PL at 10 µg were blotted with anti-RhoJ and anti-tubulin. This experiment was performed using single isolates only. The expression of RhoJ at the mRNA and protein level was compared to the expression of RhoJ in HUVEC.

and protein level was compared to the expression of RhoJ in HUVEC. In both hPC-PL and HASMC a relatively low level of RhoJ mRNA and protein expression was found compared with HUVEC (figure 6.5).

6.2.6 Summary

To summarise, *in vivo* RhoJ expression was found in ECs undergoing physiological angiogenesis during mouse embryonic development. The tissue distribution of mouse RhoJ was found to be similar to an endothelial expression profile but its expression was not restricted to ECs since RhoJ was also detected in mouse B-cells, platelets and the thymic stroma. *In situ* RhoJ expression was found in the endothelium of some but not all normal and pathological human tissue sections. RhoJ expression was also detected in non-ECs including perivascular pericytes and vascular smooth muscle cells. Although the expression of RhoJ is not restricted to ECs, a cell type that expresses RhoJ at higher levels than ECs has not been found in this study.

6.3 Discussion

Since angiogenesis is a process specific to ECs, the expression of RhoJ during normal embryonic angiogenesis was investigated. Whole mount *in situ* hybridization experiments in mouse embryos at E9.5, a stage in development when angiogenesis is occurring were performed. The results revealed a vascular expression of RhoJ in mouse during embryonic angiogenesis (figure 6.1) consistent with the bioinformatic prediction by Herbert *et al.* (2008) that RhoJ is highly upregulated in ECs (206). These data suggest that RhoJ may have a potential role in embryonic angiogenesis. Data presented in chapters 3 and 4 suggest that RhoJ may be promoting EC migration and tube formation through the regulation of focal

adhesion turnover and actomyosin contractility. This data does not tell us whether RhoJ function is important for vasculogenesis or embryonic angiogenesis. However, the RhoJ knockout mouse that is currently being generated by our laboratory may help provide information on this. If no other Rho GTPase compensates for the absence of RhoJ, then these mice may die *in utero*.

Tissue distribution analysis revealed that RhoJ and VE-Cadherin were both highly expressed in lung (figure 6.2), which is a highly vascularised tissue due to its function as a gas-exchange organ (318, 319). However the spleen was shown to have higher expression of RhoJ than VE-Cadherin. Thus cell types of spleen were analysed for RhoJ expression. RhoJ was shown to be expressed in mouse B-cells and platelets but not in platelet precursor cells, megakaryocytes (figure 6.3A). These novel data show that although RhoJ may be primarily expressed in ECs, RhoJ's expression is not specific to the endothelium. However, RhoJ was not found to be expressed in human platelets, B-cell or megakaryocytic hematopoietic transformed cell lines (figure 6.3C) therefore these data suggest that RhoJ may play a role in the functioning of B-cells and platelets in mice. However, the expression of RhoJ in human primary B-cells is still yet to be explored.

In addition, RhoJ expression was found in thymus, which again was not consistent with the expression profile of VE-Cadherin. Thus, various thymus-derived stromal cells and thymocytes were analysed for RhoJ expression (figure 6.3B). Our data showed that RhoJ was not expressed in mouse-derived immature or mature thymocytes or human hematopoietic T-cell transformed cells (figure 6.3C) but was expressed in the stromal epithelial cells of mouse thymus. Griffith *et al.* (2009) have also shown that RhoJ is expressed in the mouse thymic medulla by using a microarray approach to identify stromal gene expression in tissues from microdissected thymic regions (320). These data support our findings and suggests that RhoJ

may be playing a role in T-cell central tolerance development in mouse. The microenvironment of the thymic medulla is where mature single positive T-cells undergo negative selection, rendering T-cells non-reactive to self (321). However, our work and the studies performed by Griffith *et al.* were looking at mouse thymus. The expression profile of RhoJ in human thymus still needs to be investigated. However, it would not be surprising if RhoJ were involved in human T-cell differentiation since different Rho GTPases have been shown to be important for T-cell development. In particular, recent evidence shows that Cdc42 is essential for human T-cell development (322). These data show that although RhoJ expression in ECs is upregulated, the expression of RhoJ is not EC specific and RhoJ may also be important for the functioning of the immune system. This work is also valuable in predicting and understanding the phenotypes that may arise in the RhoJ knockout mouse.

Vignal *et al.* (2000) previously examined the pattern of RhoJ mRNA expression in various murine tissues using Northern blotting (197). Vignal *et al.* reported that RhoJ mRNA is expressed at high levels in heart and at moderate levels in lung and liver. This result differs from what we have found, which is high expression (protein and mRNA) in lung and spleen. The difference in findings could be explained by differences in the age of the mice from which the tissues were extracted. Additionally, there are variations in the signal of the housekeeping control between tissues in the Northern blot shown by Vignal *et al.*, which could explain the slight contrast in our findings. Furthermore, Vignal *et al.* have studied the expression profile of RhoJ at the mRNA level only, whereas we have studied the expression pattern of RhoJ at both the protein and mRNA level with similar results.

To visualise the localisation of RhoJ mRNA expression in human normal and pathological tissues, fluorescent *in situ* hybridization experiments were performed using digoxigenin labelled riboprobes complementary to human RhoJ. RhoJ was expressed predominantly in the

vessels of most normal and cancerous tissues (figure 6.4), suggesting that RhoJ may have a potential role in maintaining vessel integrity. It has been shown that regulation of endothelial barrier integrity, which is disrupted in many vascular diseases, involves RhoA, Rac1, Cdc42 activity (1, 323). It has been documented that breakdown of endothelial integrity is due to increased endothelial tension created by increased actomyosin contractility and disassembly of cell-cell adhesions (323). In addition, evidence shows that individual Rho GTPases can positively and negatively regulate endothelial integrity, depending on their activation and cellular context (324). In sight of these observations, RhoJ may be playing a significant role in the maintenance of the endothelial barrier by working in conjunction with other Rho GTPases.

Moreover, RhoJ mRNA was not detected in sections of the brain, gut (normal and cancerous), kidney and testis (figure 6.4). ECs can display great heterogeneity in their structure and protein expression between and within tissues due to vascular networks having specialised functions depending on their location (5). Therefore the lack of expression in the vessels of some tissues suggests that RhoJ may not be important for the maintenance of all blood vessels but only vessels of certain organs that have specialised requirements. Furthermore, in the blood vessels of organs where RhoJ is absent other Rho GTPases could be functionally substituting RhoJ.

Tissue specific expression of RhoJ mRNA is most likely regulated at the transcriptional level and this may be regulated in several ways. DNA methylation is known to lock genes into ‘off’ preventing the formation of mRNA transcripts. Briefly, when regions of a gene are methylated, usually within the promoter, the gene is transcriptionally blocked but when these regions are under or non-methylated the gene is transcriptionally active or can be activated. Numerous studies have shown that tissue specific expression of genes is usually achieved

through altered DNA methylation (325, 326). Additionally histone modification such as histone H3 methylation on K9 and K27 and histone deacetylase recruitment to DNA methylation sites can induce chromatin to form into a more compacted state leading to repression of gene transcription. Therefore, DNA methylation and histone modification of RhoJ's promoter region could be causing the lack of vascular RhoJ mRNA expression in some human tissues. Another possibility is that RhoJ transcripts are being processed in ECs of all tissues but may be degraded in some tissues through the natural RNAi mechanism. Or instead, RhoJ may be alternatively spliced in certain tissues providing an explanation for why our *in situ* probe did not detect RhoJ in vessels of some tissues. Alternatively, the promoter region could control RhoJ's tissue expression profile, by controlling the binding of certain transcription factors. For example, in tissues where RhoJ is not expressed, the binding site for EC transcription factors may be missing.

In recent years, several groups of transcription factors have been shown to influence the angiogenic process such as zinger finger, basic helix-loop helix, Hey factor proteins and many more (327). However, increasing evidence suggests that the ETS family of transcription factors play an essential role in angiogenesis since nearly all endothelial enhancers and promoters characterised so far contain multiple ETS binding sites (328-330). ETS-1, Erg, and Net (Elk3) are all members of the ETS family of transcription factors and have all been shown to be involved in angiogenesis *in vitro* and *in vivo* (331-333). Therefore it is likely that members of the ETS transcription factor family may regulate RhoJ transcription.

In the present study, RhoJ expression also differed between human and mouse in some cases although both species displayed endothelial RhoJ expression. However data from chapter 5 showed that zebrafish RhoJ was not detected in ECs at all and instead RhoJ was unexpectedly found in muscle tissue. The difference of RhoJ expression between mammals and zebrafish

could be explained by evolutionary mutations in the *cis*-regulatory sequences of zebrafish RhoJ that regulate its spatial and temporal expression leading to altered localisation and function of RhoJ in fish.

Furthermore, RhoJ is expressed in the lining of blood vessels that are undergoing pathological angiogenesis in cancerous tissues (figure 6.4C). It may be possible for to RhoJ to play a different role in tumour vessels than in normal vessels. RhoJ may operate downstream of distinct stimuli in physiological and pathological angiogenesis, which influences the activity of different GEFs and GAPs. As we know, there is a tilt in the balance of pro- and anti-angiogenic factors in pathological angiogenesis, therefore it is likely that the regulation of RhoJ activity is disrupted in these carcinomas, resulting in RhoJ being constitutively active and contributing to the pathological formation of new vessels. Moreover, it is also possible that RhoJ is not involved in pathological angiogenesis since it is not present in all tumours. However, identifying where RhoJ is does not give an indication to the levels of active RhoJ. Although RhoJ was found in most of the cancerous tissues screened, RhoJ was not found in rectal carcinoma sections, which is consistent with the lack of RhoJ expression in normal gut. This indicates that RhoJ may only be involved in the vascular diseases of tissues that it is expressed in at normal conditions.

RhoJ was also expressed at low levels in human pericytes and aortic smooth muscle cells (figure 6.5). A recent study demonstrated that alterations in Rho GTPase dependent signal transduction specifically modulates pericyte shape and contractility, as well as regulating their ability to control endothelial growth (334). Therefore, RhoJ may also be involved in regulating the actin cytoskeleton of mural cells through its modulation of actomyosin contractility. However mural cells are known to express characteristics specific to their localisation (10). We have investigated the expression of RhoJ in pericytes derived from

human placenta and smooth muscle cells from human aorta only; therefore RhoJ may not be expressed in perivascular cells in all tissues. In addition, *in vitro* expression of RhoJ does not necessarily mean that these cells would express RhoJ *in vivo*. Thus the *in vivo* expression of RhoJ in perivascular cells would need to be investigated in future experiments.

Expression of RhoJ in either human or mouse was not restricted to ECs, which confirmed that RhoJ is not endothelial specific. However, expression of RNA does not result in the presence of protein and this is the main limitation to using this approach. To be certain of human RhoJ's expression profile, the expression of RhoJ protein would also have to be checked in human tissue sections using either immunohistochemistry or immunofluorescence. Additionally, as mentioned earlier the activity of RhoJ in these tissues cannot be determined from these experiments. This means that although RhoJ is expressed in normal non-angiogenic, normal embryonic angiogenic and pathological angiogenic vessels, it is not known whether RhoJ is active or inactive. In future work, the active form of RhoJ could be detected *in situ* by localising a specific effector of RhoJ or using an antibody that binds only the GTP-bound form of this Rho GTPase. These approaches have been successful in detecting the GTP-bound form of Rac1 *in situ* (335, 336). These studies, on the expression profile of mammalian RhoJ, are not exhaustive since access to primary cells and human tissues were limited. Other normal tissues such as human spleen and thymus and other pathological angiogenic tissues are still yet to be explored for RhoJ expression.

Chapter seven

Conclusions and perspectives

The data presented in this thesis demonstrates a novel role for RhoJ in EC motility, tube formation and modulation of the actin cytoskeleton and focal adhesion formation. This work also shows an endothelial expression pattern of RhoJ in mammalian tissues, but a distinct localisation and function in zebrafish. This work advances the Rho GTPase and angiogenesis field since this is the first time that RhoJ has been localised to ECs and shown to be important for angiogenic processes. Most of the data in this thesis has been published in Kaur *et al.* (2011) (337), which is included in appendix 6.

At present, the molecular mechanism by which RhoJ affects focal adhesion numbers and contractility is largely unknown. There is reciprocal communication between focal adhesions and actomyosin contractility (338). Components of focal adhesions have been shown to regulate contractility, and activation of myosin II can accentuate focal adhesion maturation and turnover (116, 338). Recently, our group discovered that endogenous RhoJ is intracellularly localised mainly to focal adhesions and partially to cytoplasmic vesicles (see appendix 6) (337). Considering this, it is likely that RhoJ primarily regulates focal adhesions, which in turn induces changes in contractility (figure 7.1). This hypothesis is consistent with our recent finding that RhoJ interacts with G protein-coupled receptor kinase-interacting protein (GIT1)/PAK interacting exchange factor (βPIX) complex (unpublished data; Mrs. Katarzyna Leszczynska), which also localises to focal adhesions and is known to be important for focal adhesion disassembly (339-341).

Although inhibition of ROCK/myosin II ameliorated RhoJ knockdown phenotypes, it does not necessarily follow that RhoJ affects the RhoA-ROCK pathway. Instead, these inhibitions might have reduced contractility to such an extent that it compensated for the effect of RhoJ on focal adhesion turnover. On the other hand, we cannot reject the hypothesis that RhoJ directly regulates the RhoA-ROCK pathway until the exact mechanism of RhoJ function is

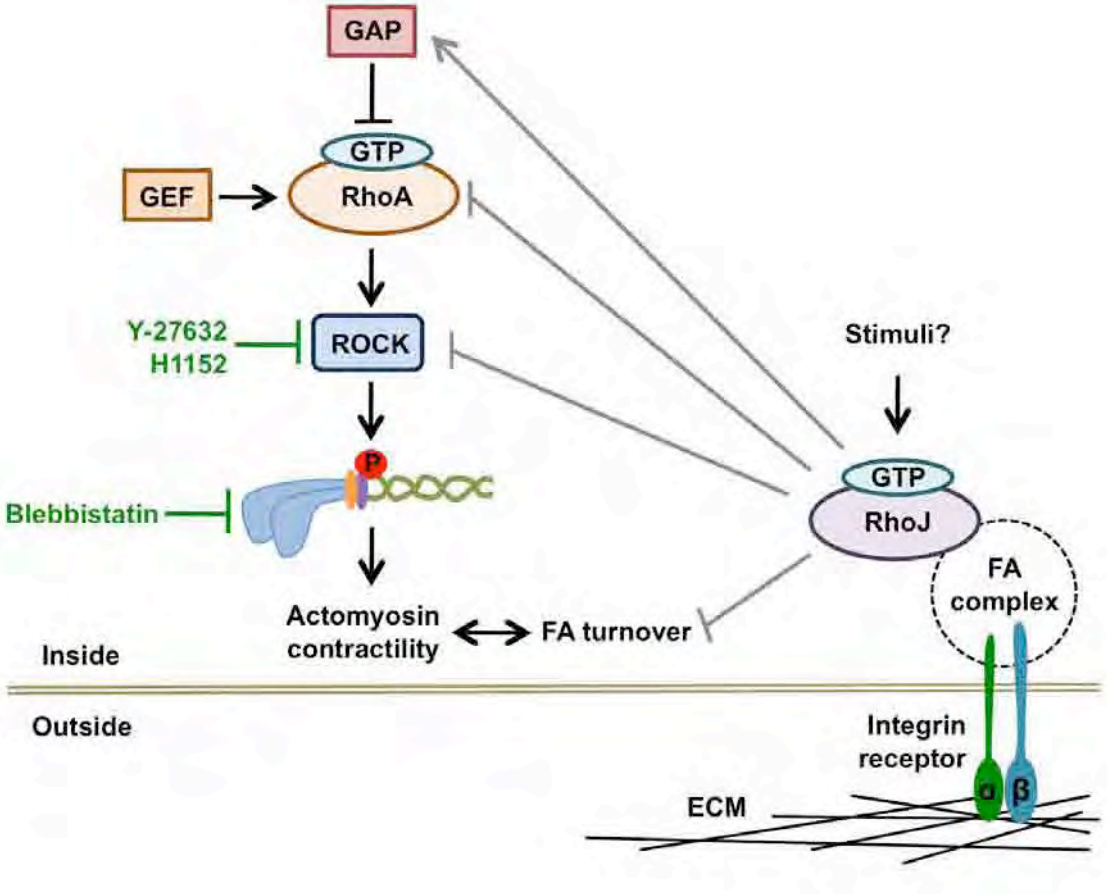

Figure 7.1 Potential mechanisms of RhoJ function in endothelial cells. GTP-bound RhoA activates ROCK, which in turn phosphorylates the regulatory light chain of myosin II and increases actomyosin contractility. RhoJ is localised to focal adhesions in endothelial cells. RhoJ negatively regulates actomyosin contractility and focal adhesion (FA) turnover, which reciprocally regulate each other. Due to the expression of RhoJ in FA, it is most likely that RhoJ regulates these processes by primarily modulating FA turnover. Inhibitory agents that reversed RhoJ knockdown-induced motility defects are shown in green. The use of these agents may have decreased contractility so much that it may have overruled RhoJ's effect on FA turnover. However, it is also possible for RhoJ to interact with RhoA, RhoA GEFs/GAPs and/or ROCK to modulate actomyosin contractility directly.

elucidated. Therefore RhoJ may also negatively regulate contractility by interacting with RhoA, ROCK or RhoA's GEF/GAP proteins (figure 7.1). The link between RhoJ and ROCK would need to be further defined in future work, which could include experiments such as GST pull-down, immunoprecipitation and yeast two-hybrid analyses to investigate whether RhoJ directly interacts with ROCK.

Consistent with the finding that knockdown of RhoJ in ECs negatively regulates tube formation and motility, converse phenotypes have been found in *in vitro* angiogenesis assays with cells expressing dominant active RhoJ (appendix 6) (337). In addition, our collaborators, Dr. Sabu Abraham and Dr. Georgia Mavria, tested the effect of RhoJ knockdown/overexpression in a more physiologically relevant model of angiogenesis, named the organotypic assay, which involved co-culturing HUVEC with human dermal fibroblasts. The interaction of these cell types (in naturally produced ECM) results in the formation of tubules that are highly reminiscent of capillaries formed during *in vivo* angiogenesis (342, 343). Knockdown of RhoJ in this assay reduced capillary branching whereas overexpression of active RhoJ resulted in excessive sprouting, which resembled the unstructured appearance of tumour vessels (appendix 6) (337). Thus these data further reinforce our conclusions about the roles RhoJ plays in ECs. However, it is important to determine if our *in vitro* observations are also present in *in vivo* models of angiogenesis. Future *in vivo* studies could include knockdown or overexpression of RhoJ in mouse Matrigel plug or sponge assays. Also, a way to see if RhoJ knockdown affects focal adhesion numbers and actomyosin contractility *in vivo* could involve setting up a Matrigel plug assay with ECs stably silencing RhoJ and staining the cells for actin and focal adhesion markers in sections of the plug. Furthermore, it would be interesting to see if the RhoJ knockout mouse displays any vascular defects or if ECs from these mice have impaired focal adhesion numbers and actomyosin contractility.

We have also shown that RhoJ is expressed in both physiological and pathological angiogenic vessels. During angiogenesis, endothelial tip cells must lose contact with surrounding cells in order to lead an angiogenic sprout (15, 344). In this situation, the breakdown of cell-cell junctions (triggered by angiogenic stimuli) may activate RhoJ signalling, which induces EC migration and morphogenesis. RhoJ signalling may therefore be important for the migration of endothelial tip cells. Moreover, RhoJ was also expressed in mature vessels. Like other Rho GTPases, RhoJ may be involved in maintaining vessel integrity. The disruption of intercellular junctions during permeability may trigger RhoJ activation, which might in turn induce cell spreading and motility to close intercellular gaps and restabilise vessel integrity. This hypothesis is consistent with the finding that RhoJ is latently activated (around 30 minutes later) by thrombin stimulation (unpublished data; Mrs. Katarzyna Leszczynska). To test the role of RhoJ in regulating the endothelial barrier, firstly the effects of RhoJ on vascular permeability need to be examined. In addition, the activity levels of RhoJ during basal state, disruption and repair of the endothelial barrier need to be investigated. To gain insights into how RhoA, Rac1, Cdc42 and RhoJ may be working together in the maintenance of vessel integrity, it would be interesting to analyse the activity levels of RhoA, Rac1 and Cdc42 when RhoJ is active or inactive.

The fact that RhoJ is not found in all vessels suggests that RhoJ is not important for all ECs and that it has specialised functions for certain tissues. Since RhoJ is not expressed in vessels of all solid tumours, it is also possible that angiogenesis is not dependant on RhoJ function. In the vessels where RhoJ is absent, an alternative member of the Rho family could be taking the role of RhoJ. To determine the mechanism behind the tissue specific expression of RhoJ in ECs; DNA methylation, histone modification, mRNA degradation, pre-mRNA splicing and promoter region analysis would need to be performed in ECs where RhoJ is expressed and compared to ECs where RhoJ is not expressed. The expression of RhoJ also differs across

species; RhoJ is not expressed in ECs in zebrafish and there are also differences in RhoJ expression between human and mouse. In order to understand the large differences in expression of RhoJ across species, it is necessary to examine the *cis*-regulatory sequences that control RhoJ expression in future experiments. Since RhoJ is not restricted to ECs, this highlights the notion that RhoJ may have a wide array of functions depending on species and cell type.

Our findings are largely consistent with past studies that have shown a role for RhoJ in actin reorganisation (197, 198, 204). A previous report showed that RhoJ co-localised with early/sorting endosome markers in HeLa cells, where it played a role in early endocytosis (203). Indeed, this localisation was also observed in our laboratory in cells overexpressing RhoJ, however endogenous RhoJ localised mainly to focal adhesions (337). Evidence shows that during focal adhesion turnover, components such as paxillin are intracellularly trafficked and recycled to focal complexes from the back of the cell to the front through endocytosis (345-348). Therefore it may be possible for RhoJ to regulate the endocytosis of integrins and focal adhesion proteins during turnover. However, future studies would be required to test whether RhoJ is involved in the endocytic machinery that mediate focal adhesion turnover. Previous studies have also demonstrated that Rho GTPases are spatiotemporally activated during tube formation (349). Rac1 and Cdc42 activation is found during the early stages when cell-cell contacts form whereas RhoA activity is prominent during the later stages, which results in branching (349). In future experiments, it would also be interesting to analyse the temporal and spatial activation of RhoJ during specific stages of tube formation such as initial EC alignment, branching and lumen formation. In light of our data, our predictions are that RhoJ activation may occur during branching stages of *in vitro* tubulogenesis.

The present study shows a role for RhoJ in the migration of ECs however many aspects of EC biology still need to be explored. For example, ECs line the inner surface of blood vessels and are directly exposed to blood flow. Previous reports have shown that the mechanical forces generated by blood flow induce the redistribution of stress fibres and focal adhesions (350, 351). For these reasons, it would be interesting to examine the effects of shear stress on RhoJ activity or knockdown phenotypes in future experiments. Also, in order to clarify the precise role of RhoJ in EC migration, it is vital to establish which upstream pathway drives RhoJ to focal adhesions. Recently, our laboratory demonstrated that RhoJ is activated by two major angiogenic factors VEGF-A (appendix 6) (337) and FGF-2 (unpublished data; Mrs. Katarzyna Leszczynska), which implies that RhoJ mediates its effects in EC motility and tube formation downstream of the VEGF-A and FGF-2 signalling pathways. However, it is necessary to investigate the exact signalling pathway upstream and downstream of this activation in future experiments.

Appendix

Appendix 1: Titration of siRNA duplexes

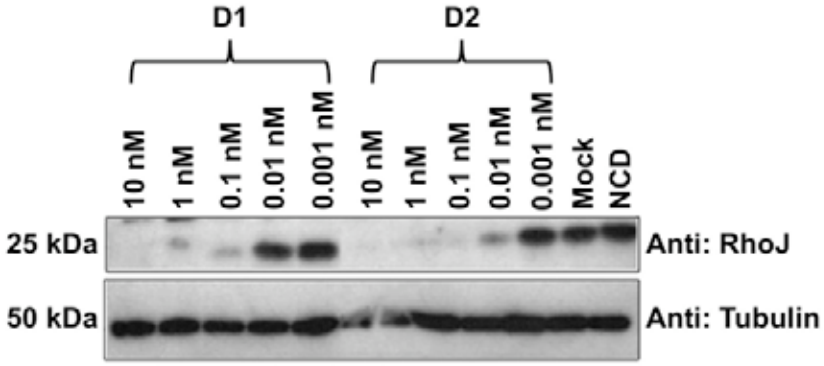

The lowest siRNA concentration to completely knockdown RhoJ protein in RhoJ-specific siRNA transfected cells is 10 nM. Human umbilical vein endothelial cells were either mock transfected or transfected with negative control duplex (NCD), RhoJ duplex 1 (D1) or RhoJ duplex 2 (D2) at 10-fold titrated concentrations. Cells were harvested and lysed 2 days after transfection and Western blotting was performed using anti-RhoJ and anti-tubulin antibodies to determine the lowest concentration of siRNA to completely knockdown RhoJ protein.

Appendix 2: Matrigel tube formation assay set-up and quantitation

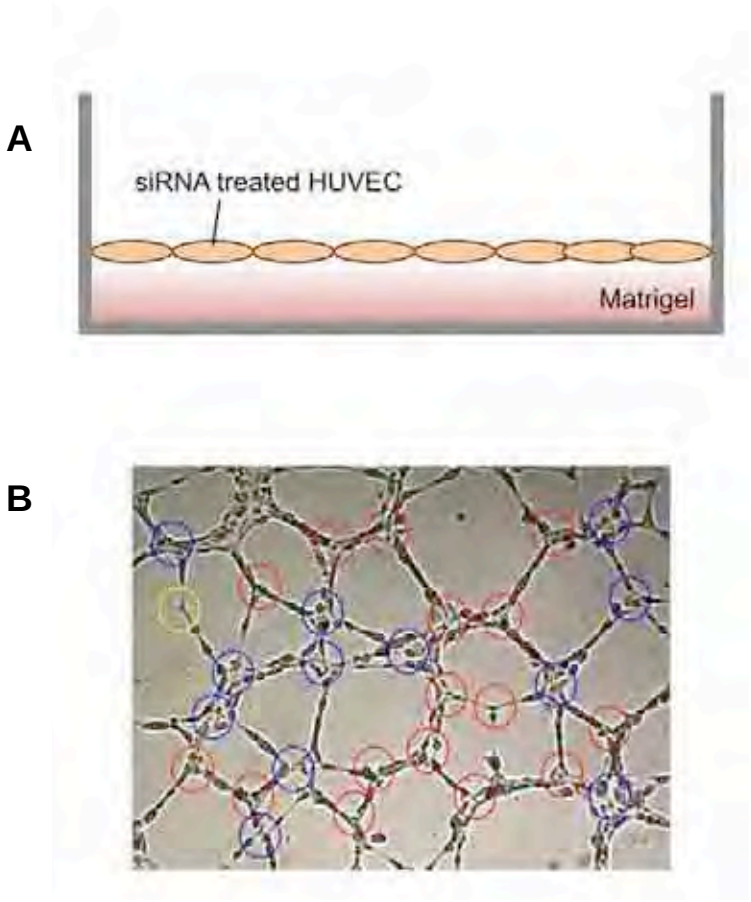

Diagram of Matrigel tube formation assay and node-counting quantitation. (A) The well of a 12 well plate was wetted with PBS prior to adding 70 µL of Matrigel. The Matrigel was allowed to solidify and cells were then harvested and seeded on top. Cells were incubated in 1 mL of culture medium for a further 24 hours. (B) Image represents wild type HUVECs on Matrigel 10 hours post seeding. Nodes are circled according to the number of branches that are extending from the node-junction. Yellow: 2 branch points, Red: 3 branch points, blue; ≥4 branch points.

Appendix 3: Boyden chamber assay set-up and optimisation

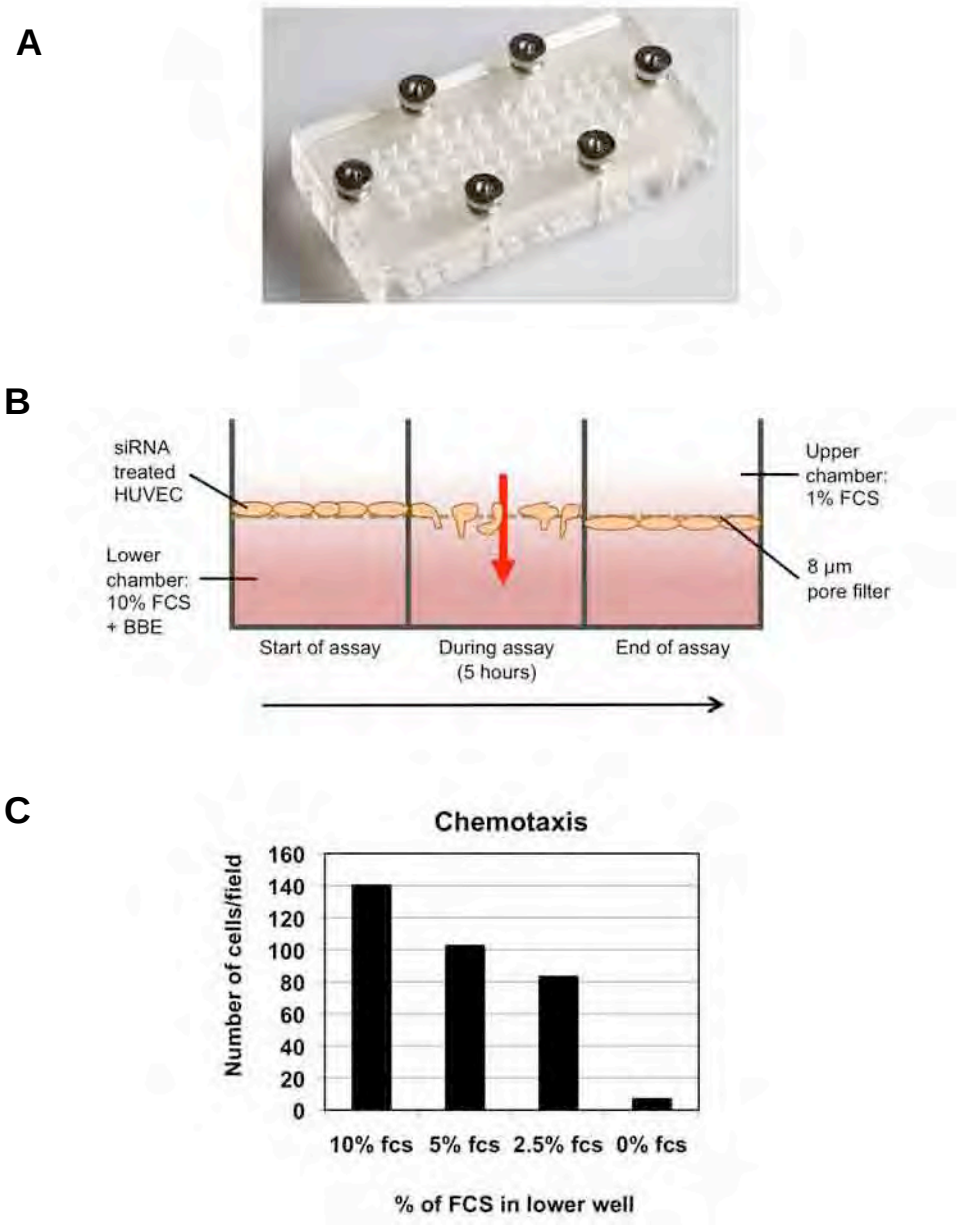

Boyden chamber assay set-up and chemoattractant optimisation. (A) Photograph of 48-well Boyden chamber: Boyden chambers consist of upper and lower wells separated by a micro-porous membrane filter. The chemoattractant is placed in the lower wells and cells are added to the top wells. After a period of incubation, cells that migrated towards the chemoattractant are counted on the lower surface of the membrane. (B) The lower chamber wells contained the chemoattractant (10% FCS (fetal calf serum) and BBE (bovine brain extract)). In the upper wells, cells were seeded in control media (1% FCS) and incubated for 5 hours at 37 °C and 5% CO_2. The cells that were attracted to the chemoattractant, migrated through the porous filter and adhered to the other side, where they could be stained with DAPI and counted. (C) To determine the highest migratory response to the chemoattractant, a 2-fold titration of FCS was performed and the percentage of FCS that produced the greatest migratory response was chosen. Cells were all seeded in 1% FCS media.

Appendix 4: Schematic of Dunn chamber

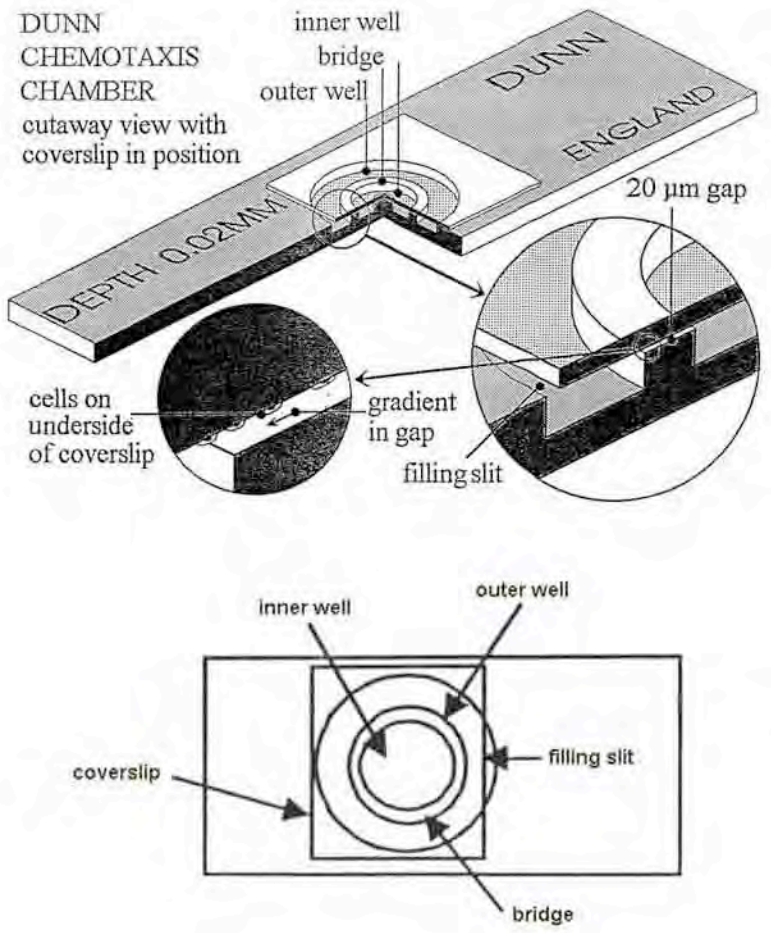

Schematic of Dunn chamber. The Dunn chamber consists of two concentric circles ground into one face of a glass slide, referred to as the inner and outer wells. A ring-shaped ridge, referred to as the bridge, separates the two wells. The bridge is 20 µm lower than the rest of the glass slide. The outer well contains the chemoattractant and the inner well contains control media. A linear gradient of the chemoattractant forms by diffusion across the bridge between the two wells. Cells seeded onto a glass coverslip are inverted onto the slide. The cells that lie directly over the bridge of the chamber between the two wells can be observed using live imaging microscopy and their migratory paths towards the gradient can be mapped. Diagrams obtained from Hawksley's Dunn chamber manual: **www.hawksley.co.uk**.

Appendix 5: Morpholino toxicity test

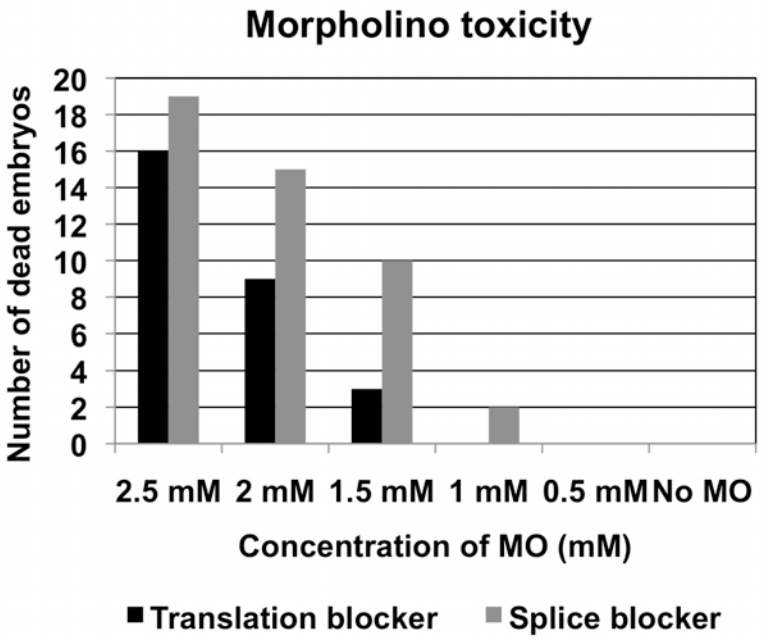

Morpholino toxicity. To determine the toxicity of RhoJ-specific morpholinos, wild type zebrafish embryos (at cleavage stage) were injected with translation blocker or splice blocker morpholinos at various concentrations and the number of embryonic fatalities (at 24 hpf) were counted. A total of 25 embryos were injected for each condition. Embryo lethality was not found at 1 mM translation blocker and 0.5 nM splice blocker.

Kaur Publications List

Arterioscler Thromb Vasc Biol. 2011 Mar;31(3):657-64. Epub 2010 Dec 9.

RhoJ/TCL regulates endothelial motility and tube formation and modulates actomyosin contractility and focal adhesion numbers.

Kaur S, Leszczynska K, Abraham S, Scarcia M, Hiltbrunner S, Marshall CJ, Mavria G, Bicknell R, Heath VL.

CRUK Molecular Angiogenesis Laboratory, Institute for Biomedical Research, The Medical School, University of Birmingham, Birmingham, United Kingdom.

List of references

1. Vandenbroucke E, Mehta D, Minshall R, Malik AB. Regulation of endothelial junctional permeability. Ann N Y Acad Sci. 2008;1123:134-45.

2. Minshall RD, Malik AB. Transport across the endothelium: regulation of endothelial permeability. Handb Exp Pharmacol. 2006(176 Pt 1):107-44.

3. Vanhoutte PM, Shimokawa H, Tang EH, Feletou M. Endothelial dysfunction and vascular disease. Acta Physiol (Oxf). 2009;196(2):193-222.

4. Riasu W. Mechanisms of angiogenesis. Nature. 1997;386(6626):671-4.

5. Cines DB, Pollak ES, Buck CA, Loscalzo J, Zimmerman GA, McEver RP, Pober JS, Wick TM, Konkle BA, Schwartz BS, Barnathan ES, McCrae KR, Hug BA, Schmidt AM, Stern DM. Endothelial cells in physiology and in the pathophysiology of vascular disorders. Blood. 1998;91(10):3527-61.

6. Fishman AP. Endothelium: a distributed organ of diverse capabilities. Ann N Y Acad Sci. 1982(401):1-8.

7. Dejana E. Endothelial cell-cell junctions: happy together. Nat Rev Mol Cell Biol. 2004;5(4):261-70.

8. Lampugnani MG, Dejana E. Adherens junctions in endothelial cells regulate vessel maintenance and angiogenesis. Thromb Res. 2007;120 Suppl 2:S1-6.

9. Gallagher PJ. Histology for pathologists. 2nd ed2005.

10. Gerhardt H, Betsholtz C. Endothelial-pericyte interactions in angiogenesis. Cell Tissue Res. 2003;314(1):15-23.

11. Sato Y, Rifkin DB. Inhibition of endothelial cell movement by pericytes and smooth muscle cells: activation of a latent transforming growth factor-beta 1-like molecule by plasmin during co-culture. J Cell Biol. 1989;109(1):309-15.

12. Orlidge A, D'Amore PA. Inhibition of capillary endothelial cell growth by pericytes and smooth muscle cells. J Cell Biol. 1987;105(3):1455-62.

13. Gaengel K, Genové G, Armulik A, Betsholtz C. Endothelial-mural cell signaling in vascular development and angiogenesis. Arterioscler Thromb Vasc Biol. 2009;29(5):630-8.

14. Garlanda C, Dejana E. Heterogeneity of endothelial cells. Arterioscler Thromb Vasc Biol. 1997;17(7):1193-202.

15. Dejana E. Endothelial adherens junctions: implications in the control of vascular permeability and angiogenesis. J Clin Invest. 1996;98(9):1949-53.

16. Ofori-Acquah SF, King J, Voelkel N, Schaphorst KL, Stevens T. Heterogeneity of barrier function in the lung reflects diversity in endothelial cell junctions. Microvasc Res. 2008;75(3):391-402.

17. Ghitescu L, Robert M. Diversity in unity: the biochemical composition of the endothelial cell surface varies between the vascular beds. Microsc Res Tech. 2002;57(5):381-9.

18. Tse D, Stan RV. Morphological heterogeneity of endothelium. Semin Thromb Hemost. 2010;36(3):236-45.

19. Aird WC. Phenotypic heterogeneity of the endothelium: I. Structure, function, and mechanisms. Circ Res. 2007;100(2):158-73.

20. dela Paz NG, D'Amore PA. Arterial versus venous endothelial cells. Cell Tissue Res. 2009;335(1):5-16.

21. Chi JT, Chang HY, Haraldsen G, Jahnsen FL, Troyanskaya OG, Chang DS, Wang Z, Rockson SG, van de Rijn M, Botstein D, Brown PO. Endothelial cell diversity revealed by global expression profiling. Proc Natl Acad Sci U S A. 2003;100(19):10623-8.

22. Zhu DZ, Cheng CF, Pauli BU. Mediation of lung metastasis of murine melanomas by a lung-specific endothelial cell adhesion molecule. Proc Natl Acad Sci U S A. 1991;88(21):9568-72.

23. Seaman S, Stevens J, Yang MY, Logsdon D, Graff-Cherry C, St Croix B. Genes that distinguish physiological and pathological angiogenesis. Cancer Cell. 2007;11(6):539-54.

24. Gonlugur U, Efeoglu T. Vascular adhesion and transendothelial migration of eosinophil leukocytes. Cell Tissue Res. 2004;318(3):473-82.

25. Carmeliet P. Angiogenesis in life, disease and medicine. Nature. 2005 15 Dec 2005;438(7070):932-6.

26. Carmeliet P. Angiogenesis in health and disease. Nat Med. 2003;9(6):653-60.

27. Semenza GL. Vasculogenesis, angiogenesis, and arteriogenesis: mechanisms of blood vessel formation and remodeling. J Cell Biol. 2007;102(4):840-7.

28. Mignatti P, Rifkin DB. Plasminogen activators and matrix metalloproteinases in angiogenesis. Enzyme protein. 1996;49(1-3):117-37.

29. Moses MA. The regulation of neovascularization by matrix metalloproteinases and their inhibitiors. Stem Cells. 1997;15(3):180-9.

30. Lamalice L, Le Boeuf F, Huot J. Endothelial cell migration during angiogenesis. Circ Res. 2007;100(6):782-94.

31. Conway EM, Collen D, Carmeliet P. Molecular mechanisms of blood vessel growth. Cardiovasc Res. 2001;49(3):507-21.

32. Papetti M, Herman IM. Mechanisms of normal and tumor-derived angiogenesis. Am J Physiol Cell Physiol. 2002;282(5):C497-C970.

33. Kalluri R. Basement membranes: structure, assembly and role in tumour angiogenesis. Nat Rev Cancer. 2003;3(6):422-33.

34. Roy H, Bhardwaj S, Ylä-Herttuala S. Biology of vascular endothelial growth factors. FEBS Lett. 2006;580(12):2879-87.

35. Shweiki D, Itin A, Soffer D, Keshet E. Vascular endothelial growth factor induced by hypoxia may mediate hypoxia-initiated angiogenesis. Nature. 1992;359(6398):843-5.

36. Otrock ZK, Makarem JA, Shamseddine AI. Vascular endothelial growth factor family of ligands and receptors: review. Blood Cells Mol Dis. 2007;38(3):258-68.

37. Staton CA, Kumar I, Reed MW, Brown NJ. Neuropilins in physiological and pathological angiogenesis. J Pathol. 2007;212(3):237-48.

38. Gerhardt H. VEGF and endothelial guidance in angiogenic sprouting. Organogenesis. 2008;4(4):241-6.

39. Lohela M, Bry M, Tammela T, Alitalo K. VEGFs and receptors involved in angiogenesis versus lymphangiogenesis. Curr Opin Cell Biol. 2009;21(2):154-65.

40. Distler JH, Hirth A, Kurowska-Stolarska M, Gay RE, Gay S, Distler O. Angiogenic and angiostatic factors in the molecular control of angiogenesis. Q J Nucl Med. 2003;47(3):149-61.

41. Breier G, Risau W. The role of vascular endothelial growth factor in blood vessel formation. Trends Cell Biol. 1996;6(12):454-6.

42. Carmeliet P, Ferreira V, Breier G, Pollefeyt S, Kieckens L, Gertsenstein M, Fahrig M, Vandenhoeck A, Harpal K, Eberhardt C, Declercq C, Pawling J, Moons L, Collen D, Risau W, Nagy A. Abnormal blood vessel development and lethality in embryos lacking a single VEGF allele. Nature. 1996;380(6573):435-9.

43. Barkefors I, Le Jan S, Jakobsson L, Hejll E, Carlson G, Johansson H, Jarvius J, Park JW, Li Jeon N, Kreuger J. Endothelial cell migration in stable gradients of vascular endothelial growth factor A and fibroblast growth factor 2: effects on chemotaxis and chemokinesis. J Biol Chem. 2008;283(20):13905-12.

44. Schott RJ, Morrow LA. Growth factors and angiogenesis. Cardiovasc Res. 1993;27(7):1155-61.

45. Otrock ZK, Mahfouz RA, Makarem JA, Shamseddine AI. Understanding the biology of angiogenesis: review of the most important molecular mechanisms. Blood Cells Mol Dis. 2007;39(2):212-20.

46. Neufeld G, Kessler O. Pro-angiogenic cytokines and their role in tumor angiogenesis. Cancer Metastasis Rev. 2006;25(3):373-85.

47. Beck L Jr, D'Amore PA. Vascular development: cellular and molecular regulation. FASEB J. 1997;11(5):365-73.

48. Karamysheva AF. Mechanisms of angiogenesis. Biochemistry (Mosc). 2008;73(7):751-62.

49. Hellström M, Kalén M, Lindahl P, Abramsson A, Betsholtz C. Role of PDGF-B and PDGFR-beta in recruitment of vascular smooth muscle cells and pericytes during embryonic blood vessel formation in the mouse. Development. 1999;126(14):3047-55.

50. Silva R, D'Amico G, Hodivala-Dilke KM, Reynolds LE. Integrins: the keys to unlocking angiogenesis. Arterioscler Thromb Vasc Biol. 2008;28(10):1703-13.

51. Rüegg C, Dormond O, Mariotti A. Endothelial cell integrins and COX-2: mediators and therapeutic targets of tumor angiogenesis. Biochim Biophys Acta. 2004;1654(1):51-67.

52. Ribatti D. Endogenous inhibitors of angiogenesis: a historical review. Leuk Res. 2009;33(5):638-44.

53. Boosani CS, Nalabothula N, Sheibani N, Sudhakar A. Inhibitory effects of arresten on bFGF-induced proliferation, migration, and matrix metalloproteinase-2 activation in mouse retinal endothelial cells. Curr Eye Res. 2010;35(1):45-55.

54. Mundel TM, Kalluri R. Type IV collagen-derived angiogenesis inhibitors. Microvasc Res. 2007;74(2-3):85-9.

55. Sudhakar A, Boosani CS. Inhibition of tumor angiogenesis by tumstatin: insights into signaling mechanisms and implications in cancer regression. Pharm Res. 2008;25(12):2731-9.

56. Kamphaus GD, Colorado PC, Panka DJ, Hopfer H, Ramchandran R, Torre A, Maeshima Y, Mier JW, Sukhatme VP, Kalluri R. Canstatin, a novel matrix-derived inhibitor of angiogenesis and tumor growth. J Biol Chem. 2000;275(2):1209-15.

57. O'Reilly MS, Boehm T, Shing Y, Fukai N, Vasios G, Lane WS, Flynn E, Birkhead JR, Olsen BR, Folkman J. Endostatin: an endogenous inhibitor of angiogenesis and tumor growth. Cell. 1997;88(2):277-85.

58. Noh YH, Matsuda K, Hong YK, Kunstfeld R, Riccardi L, Koch M, Oura H, Dadras SS, Streit M, Detmar M. An N-terminal 80 kDa recombinant fragment of human thrombospondin-2 inhibits vascular endothelial growth factor induced endothelial cell migration in vitro and tumor growth and angiogenesis in vivo. J Invest Dermatol. 2003;121(6):1536-43.

59. Minuzzo S, Moserle L, Indraccolo S, Amadori A. Angiogenesis meets immunology: cytokine gene therapy of cancer. Mol Aspects Med. 2007;28(1):59-86.

60. Nyberg P, Xie L, Kalluri R. Endogenous inhibitors of angiogenesis. Cancer Res. 2005;65(10):3967-79.

61. Krajewska E, Lewis CE, Chen YY, Welford A, Tazzyman S, Staton CA. A novel fragment derived from the beta chain of human fibrinogen, beta43-63, is a potent inhibitor of activated endothelial cells in vitro and in vivo. Br J Cancer. 2010;102(3):594-601.

62. Staton CA, Stribbling SM, García-Echeverría C, Bury JP, Tazzyman S, Lewis CE, Brown NJ. Identification of key residues involved in mediating the in vivo anti-tumor/anti-endothelial activity of Alphastatin. J Thromb Haemost. 2007;5(4):846-54.

63. Brown NJ, Staton CA, Rodgers GR, Corke KP, Underwood JC, Lewis CE. Fibrinogen E fragment selectively disrupts the vasculature and inhibits the growth of tumours in a syngeneic murine model. Br J Cancer. 2002;86(11):1813-6.

64. Bootle-Wilbraham CA, Tazzyman S, Marshall JM, Lewis CE. Fibrinogen E-fragment inhibits the migration and tubule formation of human dermal microvascular endothelial cells in vitro. Cancer Res. 2000;60(17):4719-24.

65. Reynolds LP, Killilea SD, Redmer DA. Angiogenesis in the female reproductive system. FASEB J. 1992;6(3):886-92.

66. Abulafia O, Sherer DM. Angiogenesis of the ovary. Am J Obstet Gynecol. 2000;182(1 Pt 1):240-6.

67. Krikun G, Schatz F, Lockwood CJ. Endometrial angiogenesis: from physiology to pathology. Ann N Y Acad Sci. 2004;1034:27-35.

68. Bauer SM, Bauer RJ, Velazquez OC. Angiogenesis, vasculogenesis, and induction of healing in chronic wounds. Vasc Endovascular Surg. 2005;39(4):293-306.

69. Folkman J, Shing Y. Angiogenesis. J Biol Chem. 1992;267(16):10931-4.

70. Folkman J, Klagsbrun M. Angiogenic factors. Science. 1987;235(4787):442-7.

71. Folkman J. Tumor angiogenesis: therapeutic implications. N Eng J Med. 1971;285(21):1182-6.

72. Folkman J. Anti-angiogenesis: new concept for therapy of solid tumors. Ann Surg. 1972;175(3):409-16.

73. Liekins S. Angiogenesis: regulators and clinical applications. Clinical Pharmacology. 2001;61(3):253-70.

74. Pepper MS. Manipulating angiogenesis: from basic science to the bedside. Arterioscler Thromb Vasc Biol. 1997;17(4):605-19.

75. Larcher F, Murillas R, Bolontrade M, Conti CJ, Jorcano JL. VEGF/VPF overexpression in skin of transgenic mice induces angiogenesis, vascular hyperpermeability and accelerated tumor development. Oncogene. 1998;17(3):303-11.

76. Dvorak HF. Angiogenesis: update 2005. J Thromb Haemost. 2005;3(8):1835-42.

77. Chung AS, Lee J, Ferrara N. Targeting the tumour vasculature: insights from physiological angiogenesis. Nat Rev Cancer. 2010;10(7):505-14.

78. Dudek A, Gupta K, Ramakrishnan S, Mukhopadhyay D. Tumor angiogenesis. J Oncol. 2010:[Epub ahead of print].

79. Nussenbaum F, Herman IM. Tumor angiogenesis: insights and innovations. J Oncol. 2010:[Epub ahead of print].

80. Virmani R, Kolodgie FD, Burke AP, Finn AV, Gold HK, Tulenko TN, Wrenn SP, Narula J. Atherosclerotic plaque progression and vulnerability to rupture: angiogenesis as a source of intraplaque hemorrhage. Arterioscler Thromb Vasc Biol. 2005;25(10):2054-61.

81. Pandya NM, Dhalla NS, Santani DD. Angiogenesis--a new target for future therapy. Vascul Pharmacol. 2006;44(5):265-74.

82. Crawford TN, Alfaro DV 3rd, Kerrison JB, Jablon EP. Diabetic retinopathy and angiogenesis. Curr Diabetes Rev. 2009;5(1):8-13.

83. Heidenreich R, Röcken M, Ghoreschi K. Angiogenesis drives psoriasis pathogenesis. Int J Exp Pathol. 2009;90(3):232-48.

84. Paleolog EM. Angiogenesis in rheumatoid arthritis. Arthritis Res. 2002;4 Suppl 3:S81-90.

85. Reynolds LP, Grazul-Bilska AT, Redmer DA. Angiogenesis in the female reproductive organs: pathological implications. Int J Exp Pathol. 2002;83(4):151-63.

86. Bhadada SV, Goyal BR, Patel MM. Angiogenic targets for potential disorders. Fundam Clin Pharmacol. 2010;25(1):29-47.

87. Kazazi-Hyseni F, Beijnen JH, Schellens JH. Bevacizumab. Oncologist. 2010;15(8):819-25.

88. Gupta K, Zhang J. Angiogenesis: a curse or cure? Postgrad Med J. 2005;81(954):236-42.

89. Ellis LM, Hicklin DJ. VEGF-targeted therapy: mechanisms of anti-tumour activity. Nat Rev Cancer. 2008;8(8):579-91.

90. Abdelrahim M, Konduri S, Basha R, Philip PA, Baker CH. Angiogenesis: an update and potential drug approaches (review). Int J Oncol. 2010;36(1):5-18.

91. Taraboletti G, Giavazzi R. Modelling approaches for angiogenesis. Eur J Cancer. 2004;40(6):881-9.

92. Mavria G, Vercoulen Y, Yeo M, Paterson H, Karasarides M, Marais R, Bird D, Marshall CJ. ERK-MAPK signaling opposes Rho-kinase to promote endothelial cell survival and sprouting during angiogenesis. Cancer Cell. 2006;9(1):33-44.

93. Staton CA, Stribbling SM, Tazzyman S, Hughes R, Brown NJ, Lewis CE. Current methods for assaying angiogenesis in vitro and in vivo. Int J Exp Pathol. 2004;85(5):233-48.

94. Staton CA, Reed MW, Brown NJ. A critical analysis of current in vitro and in vivo angiogenesis assays. Int J Exp Pathol. 2009;90(3):195-221.

95. Staton CA, Lewis C, Bicknell R. Angiogenesis Assays. A critical appraisal of current techniques. West Sussex: John Wiley and Sons Ltd; 2006.

96. Chan J, Bayliss PE, Wood JM, Roberts TM. Dissection of angiogenic signaling in zebrafish using a chemical genetic approach. Cancer Cell. 2002;1(3):257-67.

97. Ellertsdóttir E, Lenard A, Blum Y, Krudewig A, Herwig L, Affolter M, Belting HG. Vascular morphogenesis in the zebrafish embryo. Dev Biol. 2010;341(1):56-65.

98. Rosen JN, Sweeney MF, Mably JD. Microinjection of zebrafish embryos to analyze gene function. J Vis Exp. 2009(25).

99. Wakatsuki T, Wysolmerski RB, Elson EL. Mechanics of cell spreading: role of myosin II. J Cell Sci. 2003;116(Pt 8):1617-25.

100. Le Clainche C, Carlier MF. Regulation of actin assembly associated with protrusion and adhesion in cell migration. Physiol Rev. 2008;88(2):489-513.

101. Ridley AJ, Schwartz MA, Burridge K, Firtel RA, Ginsberg MH, Borisy G, Parsons JT, Horwitz AR. Cell migration: integrating signals from front to back. Science. 2003;302(5651):1704-9.

102. Mellor H. Cell motility: Golgi signalling shapes up to ship out. Curr Biol. 2004;14(11):R434-5.

103. Kupfer A, Louvard D, Singer SJ. Polarization of the Golgi apparatus and the microtubule-organizing center in cultured fibroblasts at the edge of an experimental wound. Proc Natl Acad Sci U S A. 1982;79(8):2603-7.

104. Nabi IR. The polarization of the motile cell. J Cell Sci. 1999;112(Pt 12):1803-11.

105. Disanza A, Steffen A, Hertzog M, Frittoli E, Rottner K, Scita G. Actin polymerization machinery: the finish line of signaling networks, the starting point of cellular movement. Cell Mol Life Sci. 2005;62(9):955-70.

106. Small JV, Stradal T, Vignal E, Rottner K. The lamellipodium: where motility begins. Trends Cell Biol. 2002;12(3):112-20.

107. Horwitz AR, Parsons JT. Cell migration--movin' on. Science. 1999;286(5442):1102-3.

108. Zamir E, Geiger B. Molecular complexity and dynamics of cell-matrix adhesions. J Cell Sci. 2001;114(20):3583-90.

109. Dubash AD, Menold MM, Samson T, Boulter E, García-Mata R, Doughman R, Burridge K. Chapter 1. Focal adhesions: new angles on an old structure. Int Rev Cell Mol Biol. 2009;277:1-65.

110. Legate KR, Wickström SA, Fässler R. Genetic and cell biological analysis of integrin outside-in signaling. Genes Dev. 2009;23(4):397-418.

111. Berrier AL, Yamada KM. Cell-matrix adhesion. J Cell Physiol. 2007;213(3):565-73.

112. Nobes CD, Hall A. Rho, rac, and cdc42 GTPases regulate the assembly of multimolecular focal complexes associated with actin stress fibers, lamellipodia, and filopodia. Cell. 1995;81(1):53-62.

113. Wolfenson H, Henis YI, Geiger B, Bershadsky AD. The heel and toe of the cell's foot: a multifaceted approach for understanding the structure and dynamics of focal adhesions. Cell Motil Cytoskeleton. 2009;66(11):1017-29.

114. Hotulainen P, Lappalainen P. Stress fibers are generated by two distinct actin assembly mechanisms in motile cells. J Cell Biol. 2006;173(3):383-94.

115. Endlich N, Otey CA, Kriz W, Endlich K. Movement of stress fibers away from focal adhesions identifies focal adhesions as sites of stress fiber assembly in stationary cells. Cell Motil Cytoskeleton. 2007;64(12):966-76.

116. Parsons JT, Horwitz AR, Schwartz MA. Cell adhesion: integrating cytoskeletal dynamics and cellular tension. Nat Rev Mol Cell Biol. 2010;11(9):633-43.

117. Deakin NO, Turner CE. Paxillin comes of age. J Cell Sci. 2008;121(Pt 15):2435-44.

118. Critchley DR. Biochemical and structural properties of the integrin-associated cytoskeletal protein talin. Annu Rev Biophys. 2009;38:235-54.

119. Goult BT, Gingras AR, Bate N, Roberts GC, Critchley DR, Barsukov IL. NMR assignment of the C-terminal actin-binding domain of talin. Biomol NMR Assign. 2008;2(1):17-9.

120. Goldmann WH. Correlation between the interaction of the vinculin tail domain with lipid membranes, its phosphorylation and cell mechanical behaviour. Cell Bio Int. 2010;34(4):339-42.

121. Humphries JD, Wang P, Streuli C, Geiger B, Humphries MJ, Ballestrem C. Vinculin controls focal adhesion formation by direct interactions with talin and actin. J Cell Biol. 2007;179(5):1043-57.

122. Turner CE, Glenney JR Jr, Burridge K. Paxillin: a new vinculin-binding protein present in focal adhesions. J Cell Biol. 1990;111(3):1059-68.

123. Scheswohl DM, Harrell JR, Rajfur Z, Gao G, Campbell SL, Schaller MD. Multiple paxillin binding sites regulate FAK function. J Mol Signal. 2008;3:1.

124. Tomar A, Schlaepfer DD. Focal adhesion kinase: switching between GAPs and GEFs in the regulation of cell motility. Curr Opin Cell Biol. 2009;21(5):676-83.

125. Brown MC, Cary LA, Jamieson JS, Cooper JA, Turner CE. Src and FAK kinases cooperate to phosphorylate paxillin kinase linker, stimulate its focal adhesion localization, and regulate cell spreading and protrusiveness. Mol Biol Cell. 2005;16(9):4316-28.

126. Bellis SL, Miller JT, Turner CE. Characterization of tyrosine phosphorylation of paxillin in vitro by focal adhesion kinase. J Biol Chem. 1995;270(29):17437-41.

127. Vicente-Manzanares M, Ma X, Adelstein RS, Horwitz AR. Non-muscle myosin II takes centre stage in cell adhesion and migration. Nat Rev Mol Cell Biol. 2009;10(11):778-90.

128. Kirfel G, Rigort A, Borm B, Herzog V. Cell migration: mechanisms of rear detachment and the formation of migration tracks. Eur J Cell Biol. 2004;83(11-12):717-24.

129. Kreis TE, Birchmeier W. Stress fiber sarcomeres of fibroblasts are contractile. Cell. 1980;22(2 Pt 2):555-61.

130. Burridge K. Are stress fibres contractile? Nature. 1981;294(5843):691-2.

131. Pellegrin S, Mellor H. Actin stress fibres. J Cell Sci. 2007;120(Pt 20):3491-9.

132. Sugi H. Molecular mechanism of ATP-dependent actin-myosin interaction in muscle contraction. Jpn J Physiol. 1993;43(4):435-54.

133. Raftopoulou M, Hall A. Cell migration: Rho GTPases lead the way. Dev Biol. 2004;265(1):23-32.

134. Amano M, Ito M, Kimura K, Fukata Y, Chihara K, Nakano T, Matsuura Y, Kaibuchi K. Phosphorylation and activation of myosin by Rho associated kinase (Rho-kinase). J Biol Chem. 1996;271(34):20246-9.

135. Kawabata S, Usukura J, Morone N, Ito M, Iwamatsu A, Kaibuchi K, Amano M. Interaction of Rho-kinase with myosin II at stress fibres. Genes Cells. 2004;9(7):653-60.

136. Jaffe AB, Hall A. Rho GTPases: biochemistry and biology. Annu Rev Cell Dev Biol. 2005;21:247-69.

137. Etienne-Manneville S, Hall A. Rho GTPases in cell biology. Nature. 2002;420(6916):629-35.

138. Ridley AJ. Rho family proteins: coordinating cell responses. Trends in Cell Biology. 2001;11(12):471-7.

139. Fryer BH, Field J. Rho, Rac, Pak and angiogenesis: old roles and newly identified responsibilities in endothelial cells. Cancer Letters. 2005;229(1):13-23.

140. Bryan BA, D'Amore PA. What tangled webs they weave: Rho-GTPase control of angiogenesis. Cell Mol Life Sci. 2007;64(16):2053-65.

141. Wennerberg K, Rossman KL, Der CJ. The Ras superfamily at a glance. J Cell Sci. 2005;118(Pt 5):843-6.

142. Wennerberg K, Der CJ. Rho-family GTPases: it's not only Rac and Rho (and I like it). J Cell Sci. 2004;117(Pt 8):1301-12.

143. Bustelo XR, Sauzeau V, Berenjeno IM. GTP-binding proteins of the Rho/Rac family: regulation, effectors and functions in vivo. Bioessays. 2007;29(4):356-70.

144. Vetter IR, Wittinghofer A. The guanine nucleotide-binding switch in three dimensions. Science. 2001;294(5545):1299-304.

145. Vega FM, Ridley AJ. Rho GTPases in cancer cell biology. FEBS Lett. 2008;582(14):2093-101.

146. Paduch M, Jeleń F, Otlewski J. Structure of small G proteins and their regulators. Acta Biochim Pol. 2001;48(4):829-50.

147. Takai Y, Sasaki T, Matozaki T. Small GTP-binding proteins. Physiol Rev. 2001;81(1):153-208.

148. Bishop AL, Hall A. Rho GTPases and their effector proteins. Biochem J. 2000;348(Pt 2):241-55.

149. Schmidt A, Hall A. Guanine nucleotide exchange factors for Rho GTPases: turning on the switch. Genes Dev. 2002;16(13):1587-609.

150. Van Aelst L, D'Souza-Schorey C. Rho GTPases and signalling networks. Genes Dev. 1997;11(18):2295-322.

151. Olofsson B. Rho Guanine Dissociation Inhibitors Pivotal Molecules in Cellular Signalling. Cell Signal. 1999;11(8):545-54.

152. Schiller MR. Coupling receptor tyrosine kinases to Rho GTPases--GEFs what's the link. Cell Signal. 2006;18(11):1834-43.

153. Kjoller L, Hall A. Signaling to Rho GTPases. Exp Cell Res. 1999;253(1):166-79.

154. Ridley AJ. Rho: theme and variations. Curr Biol. 1996;6(10):1256-64.

155. Matozaki T, Nakanishi H, Takai Y. Small G-protein networks: their crosstalk and signal cascades. Cell Signal. 2000;12(8):515-24.

156. Cau J, Hall A. Cdc42 controls the polarity of the actin and microtubule cytoskeletons through two distinct signal transduction pathways. J Cell Sci. 2005;118(Pt 12):2579-87.

157. Ladwein M, Rottner K. On the Rho'd: the regulation of membrane protrusions by Rho-GTPases. FEBS Lett. 2008;582(14):2066-74.

158. Ridley AJ. Rho GTPases and actin dynamics in membrane protrusions and vesicle trafficking. Trends Cell Biol. 2006;16(10):522-9.

159. Amano M, Chihara K, Kimura K, Fukata Y, Nakamura N, Matsuura Y, Kaibuchi K. Formation of Actin Stress Fibers and Focal Adhesions Enhanced by Rho-Kinase. Science. 1997;275(5304):1308-11.

160. Katoh K, Kano Y, Ookawara S. Rho-kinase dependent organization of stress fibers and focal adhesions in cultured fibroblasts. Genes Cells. 2007;12(5):623-38.

161. Ridley AJ, Hall A. The small GTP-binding protein rho regulates the assembly of focal adhesions and actin stress fibers in response to growth factors. Cell. 1992;70(3):389-99.

162. Chrzanowska-Wodnicka M, Burridge K. Rho-stimulated contractility drives the formation of stress fibers and focal adhesions. J Cell Biol. 1996;133(6):1403-15.

163. Hall A. Rho GTPases and the control of cell behaviour. . Biochem Soc Trans. 2005;33(Pt 5):891-5.

164. Lee TY, Gotlieb AI. Mircrofilaments and microtubules maintain endothelial integrity. Microsc Res Tech. 2003;60(1):115-27.

165. Nobes CD, Hall A. Rho GTPases control polarity, protrusion, and adhesion during cell movement. J Cell Biol. 1999;144(6):1235-44.

166. van Nieuw Amerongen GP, Koolwijk P, Versteilen A, van Hinsbergh VW. Involvement of RhoA/Rho kinase signaling in VEGF-induced endothelial cell migration and angiogenesis in vitro. Arterioscler Thromb Vasc Biol. 2003;23(2):211-7.

167. Merajver SD, Usmani SZ. Multifaceted role of Rho proteins in angiogenesis. J Mammary Gland Biol Neoplasia. 2005;10(4):291-8.

168. Rousseau S, Houle F, Huot J. Integrating the VEGF Signals Leading to Actin-Based Motility in Vascular Endothelial Cells. Trends Cardiovasc Med. 2000;10(8):321-7.

169. Bayless KJ, Davis GE. The Cdc42 and Rac1 GTPases are required for capillary lumen formation in three-dimensional extracellular matrices. J Cell Sci. 2002;115(Pt 6):1123-36.

170. Connolly JO, Simpson N, Hewlett L, Hall A. Rac regulates endothelial morphogenesis and capillary assembly. Mol Biol Cell. 2002;13(7):2474-85.

171. Tan W, Palmby TR, Gavard J, Amornphimoltham P, Zheng Y, Gutkind JS. An essential role for Rac1 in endothelial cell function and vascular development. FASEB J. 2008;22(6):1829-38.

172. Zhao L, Xu G, Zhou J, Xing H, Wang S, Wu M, Lu YP, Ma D. The effect of RhoA on human umbilical vein endothelial cell migration and angiogenesis in vitro. Oncol Rep. 2006;15(5):1147-52.

173. Hoang MV, Whelan MC, Senger DR. Rho activity critically and selectively regulates endothelial cell organization during angiogenesis. Proc Natl Acad Sci U S A. 2004;101(7):1874-9.

174. Kroll J, Epting D, Kern K, Dietz CT, Feng Y, Hammes HP, Wieland T, Augustin HG. Inhibition of Rho-dependent kinases ROCK I/II activates VEGF-driven retinal neovascularization and sprouting angiogenesis. Am J Physiol Heart Circ Physiol. 2009;296(3):H893-9.

175. Beckers CM, van Hinsbergh VW, van Nieuw Amerongen GP. Driving Rho GTPase activity in endothelial cells regulates barrier integrity. Thromb Haemost. 2010;103(1):40-55.

176. Spindler V, Schlegel N, Waschke J. Role of GTPases in control of microvascular permeability. Cardiovasc Res. 2010;87(2):243-53.

177. Wojciak-Stothard B, Tsang LY, Paleolog E, Hall SM, Haworth SG. Rac1 and RhoA as regulators of endothelial phenotype and barrier function in hypoxia-induced neonatal pulmonary hypertension. Am J Physiol Lung Cell Mol Physiol. 2006;290(6):L1173-82.

178. Essler M, Amano M, Kruse HJ, Kaibuchi K, Weber PC, Aepfelbacher M. Thrombin inactivates myosin light chain phosphatase via Rho and its target Rho kinase in human endothelial cells. J Biol Chem. 1998;273(34):21867-74.

179. Fiedler LR. Rac1 regulates cardiovascular development and postnatal function of endothelium. Cell Adh Migr. 2009;3(2):143-5.

180. Waschke J, Baumgartner W, Adamson RH, Zeng M, Aktories K, Barth H, Wilde C, Curry FE, Drenckhahn D. Requirement of Rac activity for maintenance of capillary endothelial barrier properties. Am J Physiol Heart Circ Physiol. 2004;286(1):H394-401.

181. Broman MT, Mehta D, Malik AB. Cdc42 regulates the restoration of endothelial adherens junctions and permeability. Trends Cardiovasc Med. 2007;17(5):151-6.

182. Kouklis P, Konstantoulaki M, Vogel S, Broman M, Malik AB. Cdc42 regulates the restoration of endothelial barrier function. Circ Res. 2004;94(2):159-66.

183. Ramchandran R, Mehta D, Vogel SM, Mirza MK, Kouklis P, Malik AB. Critical role of Cdc42 in mediating endothelial barrier protection in vivo. Am J Physiol Lung Cell Mol Physiol. 2008;295(2):L363-9.

184. Luna A, Matas OB, Martínez-Menárguez JA, Mato E, Durán JM, Ballesta J, Way M, Egea G. Regulation of protein transport from the Golgi complex to the endoplasmic reticulum by CDC42 and N-WASP. Mol Biol Cell. 2002;13(3):866-79.

185. Nakamura T, Hayashi T, Nasu-Nishimura Y, Sakaue F, Morishita Y, Okabe T, Ohwada S, Matsuura K, Akiyama T. PX-RICS mediates ER-to-Golgi transport of the N-cadherin/beta-catenin complex. Genes Dev. 2008;22(9):1244-56.

186. Sander EE, ten Klooster JP, van Delft S, van der Kammen RA,. Rac downregulates Rho activity: reciprocal balance between both GTPases determines cellular morphology and migratory behavior. J Cell Biol. 1999;147(5):1009-22.

187. Wildenberg GA, Dohn MR, Carnahan RH, Davis MA, Lobdell NA, Settleman J, Reynolds AB. P120-catenin and P190RhoGAP regulate cell-cell adhesion by coordinating antagonism between Rac and Rho. Cell. 2006;127(5):1027-39.

188. Rolfe BE, Worth NF, World CJ, Campbell JH, Campbell GR. Rho and vascular disease. Atherosclerosis. 2005;183(1):1-16.

189. Budzyn K, Marley PD, Sobey CG. Targeting Rho and Rho-kinase in the treatment of cardiovascular disease. Trends Pharmacol Sci. 2006;27(2):97-104.

190. Gómez del Pulgar T, Benitah SA, Valerón PF, Espina C, Lacal JC. Rho GTPase expression in tumourigenesis: evidence for a significant link. Bioessays. 2005;27(6):602-13.

191. Gouw LG, Reading NS, Jenson SD, Lim MS, Elenitoba-Johnson KS. Expression of the Rho family GTPase gene RHOF in lymphocyte subsets and malignant lymphomas. Br J Haematol. 2005;129(4):531-3.

192. Fritz G, Just I, Kaina B. Rho GTPases are over-expressed in human tumors. Int J Cancer. 1999;81(5):682-7.

193. Ridley AJ. Rho proteins and cancer. Breast Cancer Res Treat. 2004;84(1):13-9.

194. Lozano E, Betson M, Braga VM. Tumor progression: small GTPases and loss of cell–cell adhesion. Bioessays. 2003;25(5):452-63.

195. Ellenbroek SI, Collard JG. Rho GTPases: functions and association with cancer. Clin Exp Metastsis. 2007;24(8):657-72.

196. Novatchkova M, Eisenhaber F. Can molecular mechanisms of biological processes be extracted from expression profiles? Case study: endothelial contribution to tumor-induced angiogenesis. Bioessays. 2001;23(12):1159-75.

197. Vignal E, De Toledo M, Comunale F, Ladopoulou A, Gauthier-Rouvière C, Blangy A, Fort P. Characterization of TCL, a new GTPase of the rho family related to TC10 and Cdc42. J Bio Chem. 2000;275(46):36457-64.

198. Abe T, Kato M, Miki H, Takenawa T, Endo T. Small GTPase Tc10 and its homologue RhoT induce N-WASP-mediated long process formation and neurite outgrowth. J Cell Sci. 2003;1;116(Pt 1):155-68.

199. Neudauer CL, Joberty G, Tatsis N, Macara IG. Distinct cellular effects and interactions of the Rho-family GTPase TC10. Curr Biol. 1998;8(21):1151-60.

200. Chiang SH, Hou JC, Hwang J, Pessin JE, Saltiel AR. Cloning and functional characterization of related TC10 isoforms, a subfamily of Rho proteins involved in insulin-stimulated glucose transport. J Biol Chem. 2002;12;277(15):13067-73.

201. Nishizuka M, Arimoto E, Tsuchiya T, Nishihara T, Imagawa M. Crucial role of TCL/TC10beta L, a subfamily of Rho GTPase, in adipocyte differentiation. J Biol Chem. 2003;278(17):15279-84.

202. Kawaji A, Nishizuka M, Osada S, Imagawa M. TC10-like/TC10betaLong regulates adipogenesis by controlling mitotic clonal expansion. Biol Pharm Bull. 2010;33(3):404-9.

203. De Toledo M, Senic-Matuglia F, Salamero J, Uze G, Comunale F, Fort P, Blangy A. The GTP/GDP cycling of rho GTPase TCL is an essential regulator of the early endocytic pathway. Mol Biol Cell. 2003;14(12):4846-56.

204. Aspenström P, Fransson A, Saras J. Rho GTPases have diverse effects on the organization of the actin filament system. Biochem J. 2004;377(Pt 2):327-37.

205. Billottet C, Rottiers P, Tatin F, Varon C, Reuzeau E, Maître JL, Saltel F, Moreau V, Génot E. Regulatory signals for endothelial podosome formation. Eur J Cell Biol. 2008;87(8-9):543-54.

206. Herbert JM, Stekel D, Sanderson S, Heath VL, Bicknell R. A novel method of differential gene expression analysis using multiple cDNA libraries applied to the identification of tumour endothelial genes. BMC Genomics. 2008;9:153.

207. Ades EW, Candal FJ, Swerlick RA, George VG, Summers S, Bosse DC, Lawley TJ. HMEC-1: establishment of an immortalized human microvascular endothelial cell line. J Invest Dermatol. 1992;99(6):683-90.

208. Williams RL, Courtneidge SA, Wagner EF. Embryonic lethalities and endothelial tumors in chimeric mice expressing polyoma virus middle oncogene. Cell. 1988;52(1):121-31.

209. Williams RL, Risau W, Zerwes HG, Drexler H, Aguzzi A, Wagner EF. Endothelioma cells expressing the polyoma middle T oncogene induce hemangliomas by host cell recruitment. Cell. 1989;57(6):1053-63.

210. Maciag T, Cerundolo J, Ilsley S, Kelley PR, Forand R. An endothelial cell growth factor from bovine hypothalamus: identification and partial characterization. Proc Natl Acad Sci U S A. 1979;76(11):5674-8.

211. Kapiotis S, Sengoelge G, Sperr WR, Baghestanian M, Quehenberger P, Bevec D, Li SR, Menzel EJ, Mühl A, Zapolska D, Virgolini I, Valent P, Speiser W. Ibuprofen inhibits pyrogen-dependent expression of VCAM-1 and ICAM-1 on human endothelial cells. Life Sci. 1996;58(23):2167-81.

212. Reynolds A, Leake D, Boese Q, Scaringe S, Marshall WS, Khvorova A. Rational siRNA design for RNA interference. Nature Biotechnol. 2004;22(3):326-30.

213. Nakatsu MN, Davis J, Hughes CC. Optimized fibrin gel bead assay for the study of angiogenesis. J Vis Exp. 2007(3):186.

214. Boyden S. The chemotactic effect of mixtures of antibody and antigen on polymorphonuclear leucocytes. J Exp Med. 1962;115:453-66.

215. Zicha D, Dunn GA, Brown AF. A new direct-viewing chemotaxis chamber. J Cell Sci. 1991;99(Pt 4):769-75.

216. Robaye B, Mosselmans R, Fiers W, Dumont JE, Galand P. Tumor necrosis factor induces apoptosis (programmed cell death) in normal endothelial cells in vitro. Am J Pathol. 1991;138(2):447-53.

217. Polunovsky VA, Wendt CH, Ingbar DH, Peterson MS, Bitterman PB. Induction of endothelial cell apoptosis by TNF alpha: modulation by inhibitors of protein synthesis. Exp Cell Res. 1994;214(2):584-94.

218. Petrache I, Verin AD, Crow MT, Birukova A, Liu F, Garcia JG. Differential effect of MLC kinase in TNF-alpha-induced endothelial cell apoptosis and barrier dysfunction. Am J Physiol Lung Cell Mol Physiol. 2001;280(6):L1168-78.

219. Bell E, Ivarsson B, Merrill C. Production of a tissue-like structure by contraction of collagen lattices by human fibroblasts of different proliferative potential in vitro. Proc Natl Acad Sci U S A. 1979;76(3):1274-8.

220. Vernon RB, Sage EH. Contraction of fibrillar type I collagen by endothelial cells: a study in vitro. J Cell Biochem. 1996;60(2):185-97.

221. Abraham S, Yeo M, Montero-Balaguer M, Paterson H, Dejana E, Marshall CJ, Mavria G. VE-Cadherin-mediated cell-cell interaction suppresses sprouting via signaling to MLC2 phosphorylation. Curr Biol. 2009;19(8):668-74.

222. Gering M, Patient R. Hedgehog signalling is required for adult blood stem cell formation in zebrafish embryos. Dev Cell. 2005;8(3):389-400.

223. Piette D, Hendrickx M, Willems E, Kemp CR, Leyns L. An optimized procedure for whole-mount in situ hybridization on mouse embryos and embroid bodies. Nat Protoc. 2008;3(7):1194-201.

224. Isogai S, Lawson ND, Torrealday S, Horiguchi M, Weinstein BM. Angiogenic network formation in the developing vertebrate trunk. Development. 2003;130(21):5281-90.

225. Heath VL, Bickenll R. Anticancer strategies involving the vasculature. Nat Rev Clin Oncol. 2009;6(7):395-404.

226. Adams RH, Alitalo K. Molecular regulation of angiogenesis and lymphangiogenesis. Nat Rev Mol Cell Biol. 2007;8(6):464-78.

227. Xia H, Mao Q, Paulson HL, Davidson BL. siRNA-mediated gene silencing in vitro and in vivo. Nat Biotehnol. 2002;20(10):1006-10.

228. Sledz CA, Holko M, de Veer MJ, Silverman RH, Williams BR. Activation of the interferon system by short-interferring RNAs. Nat Cell Biol. 2003;5:834-9.

229. Anderson E, Boese Q, Khvorova A, Karpilow J. Identifying siRNA-induces off-targets by microarray analysis. Methods Mol Biol. 2008;442:45-63.

230. Clemens MJ. Translational control in virus-infected cells: models for cellular stress responses. Semin Cell Dev Biol. 2005 Feb 2005;16(1):13-20.

231. Espert L, Rey C, Gonzalez L, Degols G, Chelbi-Alix MK, Mechti N, Gongora C. The exonuclease ISG20 is directly induced by synthetic dsRNA via NF-kappaB and IRF1 activation. Oncogene. 2004;23(26):4636-40.

232. Bagasra O, Prilliman KR. RNA interference: the molecular immune system. J Mol Histol. 2004;35(6):545-53.

233. Kubota Y, Kleinman HK, Martin GR, Lawley TJ. Role of laminin and basement membrane in the morphological differentiation of human endothelial cells into capillary-like structures. J Cell Biol. 1988;107(4):1589-98.

234. Lawley TJ, Kubota Y. Induction to morphologic differentiation of endothelial cells in culture. J Invest Dermatol. 1989;93(2 Suppl):59S-61S.

235. Auerbach R, Lewis R, Shinners B, Kubai L, Akhtar N. Angiogenesis assays: a critical overview. Clin Chem. 2003;49(1):32-40.

236. Bikfalvi A, Cramer EM, Tenza D, Tobelem G. Phenotypic modulations of human umbilical vein endothelial cells and human dermal fibroblasts using two angiogenic assays. Biol Cell. 1991;72(3):275-8.

237. Bayless KJ, Salazar R, Davis GE. RGD-dependent vacuolation and lumen formation observed during endothelial cell morphogenesis in three-dimensional fibrin matrices involves the alpha(v)beta(3) and alpha(5)beta(1) integrins. Am J Pathol. 2000;156(5):1673-83.

238. Yarrow JC, Perlman ZE, Westwood NJ, Mitchison TJ. A high-throughput cell migration assay using scratch wound healing, a comparison of image based readout methods. BMC Biotechnol. 2004;4:21.

239. Boamah EK, White DE, Talbott KE, Arva NC, Berman D, Tomasz M, Bargonetti J. Mitomycin-DNA adducts induce p53 dependant and p53 independant cell death pathways. ACS Chem Biol. 2007;2(6):399-407.

240. Collins K, Jacks T, Pavletich NP. The cell cycle and cancer. Proc Natl Acad Sci U S A. 1997;94(7):2776-8.

241. Welsh CF. Rho GTPases as key transducers of proliferative signals in G1 cell cycle regulation. Breast Cancer Res Treat. 2004;84(1):33-42.

242. Van Engeland M, Nieland LJ, Ramaekers FC, Schutte B, Reutelingsperger CP. Annexin V-affinity assay: a review on an apoptosis detection system based on phosphatidylserine exposure. Cytometry. 1998;31(1):1-9.

243. Darzynkiewicz Z, Bruno S, Del Bino G, Gorczyca W, Hotz MA, Lassota P, Traganos F. Features of apoptotic cells measured by flow cytometry. Cytometry. 1992;13(8):795-808.

244. Segura I, Serrano A, De Buitrago GG, González MA, Abad JL, Clavería C, Gómez L, Bernad A, Martínez-A C, Riese HH. Inhibition of programmed cell death impairs in vitro vascular-like structure formation and reduces in vivo angiogenesis. FASEB J. 2002;16(8):833-41.

245. Chen CS, Mrksich M, Huang S, Whitesides GM, Ingber DE. Geometric control of cell life and death. Science. 1997;279(5317):1425-8.

246. Krueger EW, Orth JD, Cao H, McNiven MA. A dynamin-cortactin-Arp2/3 complex mediates actin reorganization in growth factor-stimulated cells. Mol Biol Cell. 2003;14(3):1085-96.

247. Buccione R, Orth JD, McNiven MA. Foot and mouth: podosomes, invadopodia and circular dorsal ruffles. Nat Rev Mol Cell Biol. 2004;5(8):647-57.

248. Linder S, Aepfelbacher M. Podosomes: adhesion hot-spots of invasive cells. Trends Cell Biol. 2003;13(7):376-85.

249. Linder S, Kopp P. Podosomes at a glance. J Cell Sci. 2005;118(Pt 10):2079-82.

250. Whither RNAi? Nat Cell Biol. [Editorial]. 2003;5(6):489-90.

251. Lauffenburger DA, Horwitz AF. Cell migration: a physically integrated molecular process. Cell. 1996;84(3):359-69.

252. Svitkina TM, Verkhovsky AB, McQuade KM, Borisy GG. Analysis of the actin-myosin II system in fish epidermal keratocytes: mechanism of cell body translocation. J Cell Biol. 1997;139(2):397-415.

253. Crowley E, Horwitz AF. Tyrosine phosphorylation and cytoskeletal tension regulate the release of fibroblast adhesions. J Cell Biol. 1995;131(2):525-37.

254. Riento K, Ridley AJ. ROCKs: multifunctional kinases in cell behaviour. Nat Rev Mol Cell Biol. 2003;4(6):446-56.

255. Michael KE, Dumbauld DW, Burns KL, Hanks SK, García AJ. Focal adhesion kinase modulates cell adhesion strengthening via integrin activation. Mol Biol Cell. 2009;20(9):2508-19.

256. Siekmann AF, Lawson ND. Notch signalling and the regulation of angiogenesis. Cell Adh Migr. 2007;1(2):104-9.

257. Cunningham CC. Actin polymerization and intracellular solvent flow in cell surface blebbing. J Cell Biol. 1995;129(6):1589-99.

258. Charras GT, Coughlin M, Mitchison TJ, Mahadevan L. Life and times of a cellular bleb. Biophys J. 2008;94(5):1836-53.

259. Charras GT, Hu CK, Coughlin M, Mitchison TJ. Reassembly of contractile actin cortex in cell blebs. J Cell Biol. 2006;175(3):477-90.

260. Charras GT. A short history of blebbing. J Microsc. 2008;231(3):466-78.

261. Straight AF, Cheung A, Limouze J, Chen I, Westwood NJ, Sellers JR, Mitchison TJ. Dissecting temporal and spatial control of cytokinesis with a myosin II Inhibitor. Science. 2003;299(5613):1743-7.

262. Kovács M, Tóth J, Hetényi C, Málnási-Csizmadia A, Sellers JR. Mechanism of blebbistatin inhibition of myosin II. J Biol Chem. 2004;279(34):35557-63.

263. Leung T, Chen XQ, Manser E, Lim L. The p160 RhoA-binding kinase ROK alpha is a member of a kinase family and is involved in the reorganization of the cytoskeleton. Mol Biol Cell. 1996;16(10):5313-27.

264. Nakamura N, Rabouille C, Watson R, Nilsson T, Hui N, Slusarewicz P, Kreis TE, Warren G. Characterization of a cis-Golgi matrix protein, GM130. J Cell Biol. 1995;131(6 Pt 2):1715-26.

265. Gavard J. Breaking the VE-cadherin bonds. FEBS Lett. 2009;583(1):1-6.

266. Uehata M, Ishizaki T, Satoh H, Ono T, Kawahara T, Morishita T, Tamakawa H, Yamagami K, Inui J, Maekawa M, Narumiya S. Calcium sensitization of smooth muscle mediated by a Rho-associated protein kinase in hypertension. Nature. 1997;389(6654):990-4.

267. Ikenoya M, Hidaka H, Hosoya T, Suzuki M, Yamamoto N, Sasaki Y. Inhibition of rho-kinase-induced myristoylated alanine-rich C kinase substrate (MARCKS) phosphorylation in human neuronal cells by H-1152, a novel and specific Rho-kinase inhibitor. J Neurochem. 2002;81(1):9-16.

268. Davies SP, Reddy H, Caivano M, Cohen P. Specificity and mechanism of action of some commonly used protein kinase inhibitors. Biochem J. 2000;1;351(Pt 1):95-105.

269. Dumbauld DW, Shin H, Gallant ND, Michael KE, Radhakrishna H, García AJ. Contractility modulates cell adhesion strengthening through focal adhesion kinase and assembly of vinculin-containing focal adhesions. J Cell Physiol. 2010;223(3):746-56.

270. Naumanen P, Lappalainen P, Hotulainen P. Mechanisms of actin stress fibre assembly. J Microsc. 2008;231(3):446-54.

271. Bazzoni G, Dejana E. Endothelial cell to cell junctions: molecular organisation and role in vascular homeostasis. Physiol Rev. 2004;84(3):869-901.

272. Ren XD, Kiosses WB, Sieg DJ, Otey CA, Schlaepfer DD, Schwartz MA. Focal adhesion kinase suppresses Rho activity to promote focal adhesion turnover. J Cell Sci. 2000;113(Pt 20):3673-8.

273. Charras G, Paluch E. Blebs lead the way: how to migrate without lamellipodia. Nat Rev Mol Cell Biol. 2008;9(9):730-6.

274. Sahai E, Marshall CJ. Differing modes of tumour cell invasion have distinct requirements for Rho/ROCK signalling and extracellular proteolysis. Nat Cell Biol. 2003;5(8):711-9.

275. Tinevez JY, Schulze U, Salbreux G, Roensch J, Joanny JF, Paluch E. Role of cortical tension in bleb growth. Proc Natl Acad Sci U S A. 2009;106(44):18581-6.

276. Blaser H, Reichman-Fried M, Castanon I, Dumstrei K, Marlow FL, Kawakami K, Solnica-Krezel L, Heisenberg CP, Raz E. Migration of zebrafish primordial germ cells: a role for myosin contraction and cytoplasmic flow. Dev Cell. 2006;11(5):613-27.

277. Fackler OT, Grosse R. Cell motility through plasma membrane blebbing. J Cell Biol. 2008;181(6):879-84.

278. Paluch E, Sykes C, Prost J, Bornens M. Dynamic modes of the cortical actomyosin gel during cell locomotion and division. Trends Cell Biol. 2006;16(1):5-10.

279. Vicente-Manzanares M, Zareno J, Whitmore L, Choi CK, Horwitz AF. Regulation of protrusion, adhesion dynamics, and polarity by myosins IIA and IIB in migrating cells. J Cell Biol. 2007;176(5):573-80.

280. Kimmel CB, Ballard WW, Kimmel SR, Ullmann B, Schilling TF. Stages of embryonic development of the zebrafish. Dev Dyn. 1995;203(3):253-310.

281. Tang R, Dodd A, Lai D, McNabb WC, Love DR. Validation of zebrafish (Danio rerio) reference genes for quantitative real-time RT-PCR normalization. Acta Biochim Biophys Sin (Shanghai). 2007;39(5):384-90.

282. Schier AF. The Maternal-Zygotic Transition: Death and Birth of RNAs. Science. 2007;316(5823):406-7.

283. Xiong JW. Molecular and Developmental Biology of the Hemangioblast. Dev Dyn. 2008;237(5):1218-31.

284. Isogai S, Horiguchi M, Weinstein BM. The vascular anatomy of the developing zebrafish: an atlas of embryonic and early larval development. Dev Biol. 2001;230(2):278-301.

285. Thompson MA, Ransom DG, Pratt SJ, MacLennan H, Kieran MW, Detrich HW 3rd, Vail B, Huber TL, Paw B, Brownlie AJ, Oates AC, Fritz A, Gates MA, Amores A, Bahary N, Talbot WS, Her H, Beier DR, Postlethwait JH, Zon LI. The cloche and spadetail genes differentially affect hematopoiesis and vasculogenesis. Dev Biol. 1998;197(2):248-69.

286. Thisse B, Thisse C. Fast Release Clones: A High Throughput Expression Analysis. ZFIN Direct Data Submission (http://zfinorg). 2004.

287. Ekker SC. Morphants: a new systemic vertebrate functional genomics approach. Yeast. 2000;17(4):302-6.

288. Schmajuk G, Sierakowska H, Kole R. Antisense oligonucleotides with different backbones. Modification of splicing pathways and efficacy of uptake. J Biol Chem. 1999;274(31):21783-9.

289. Summerton J, Weller D. Morpholino antisense oligomers: design, preparation, and properties. Antisense Nucleic Acid Drug Dev. 1997;7(3):187-95.

290. Corey DR, Abrams JM. Morpholino antisense oligonucleotides: tools for investigating vertebrate development. Genome Biol. 2001(5):1015.

291. Heasman J. Morpholino oligos: making sense of antisense? Dev Biol. 2002;243(2):209-14.

292. Lawson ND, Weinstein BM. In vivo imaging of embryonic vascular development using transgenic zebrafish. Dev Biol. 2002;248(2):307-18.

293. Weinberg ES, Allende ML, Kelly CS, Abdelhamid A, Murakami T, Andermann P, Doerre OG, Grunwald DJ, Riggleman B. Developmental regulation of zebrafish MyoD in wild-type, no tail and spadetail embryos. Developmental. 1996;122(1):271-80.

294. Shaw KM, Castranova DA, Pham VN, Kamei M, Kidd KR, Lo BD, Torres-Vasquez J, Ruby A, Weinstein BM. Fused-somites-like mutants exhibit defects in trunk vessel patterning. Dev Dyn. 2006;235(7):1753-60.

295. Torres-Vázquez J, Gitler AD, Fraser SD, Berk JD, Van N Pham, Fishman MC, Childs S, Epstein JA, Weinstein BM. Semaphorin-plxin signalling guides patterning of the developing vasculature. Dev Cell. 2004;7(1):117-23.

296. Ilić D, Furuta Y, Kanazawa S, Takeda N, Sobue K, Nakatsuji N, Nomura S, Fujimoto J, Okada M, Yamamoto T. Reduced cell motility and enhanced focal adhesion contact formation in cells from FAK-deficient mice. Nature. 1995;377(6549):539-44.

297. Henry CA, Crawford BD, Yan YL, Postlethwait J, Cooper MS, Hille MB. Roles for zebrafish focal adhesion kinase in notochord and somite morphogenesis. Dev Biol. 2001;240(2):474-87.

298. Crawford BD, Henry CA, Clason TA, Becker AL, Hille MB. Activity and distribution of paxillin, focal adhesion kinase, and cadherin indicate cooperative roles during zebrafish morphogenesis. Mol Biol Cell. 2003;14(8):3065-81.

299. Eisen JS, Smith JC. Controlling morpholino experiments: don't stop making antisense. Development. 2008;135(10):1735-43.

300. Thorsen DH, Hale ME. Development of zebrafish (Danio rerio) pectoral fin musculature. J Morphol. 2005;266(2):241-55.

301. Salas-Vidal E, Meijer AH, Cheng X, Spaink HP. Genomic annotation and expression analysis of the zebrafish Rho small GTPase family during development and bacterial infection. Genomics. 2005;86(1):25-37.

302. Wittkopp PJ. Genomic sources of regulatory variation in cis and in trans. Cell Mol Life Sci. 2005;62(16):1779-83.

303. Stone JR, Wray GA. Rapid evolution of cis-regulatory sequences via local point mutations. Mol Biol Evol. 2001;19(9):1764-70.

304. Ludwig MZ. Functional evolution of noncoding DNA. Curr Opin Genet Dev. 2002;12(6):634-9.

305. Walls JR, Coultas L, Rossant J, Henkelman RM. Three-dimensional analysis of vascular development in the mouse embryo. PLoS One. 2008;3(8):e2853.

306. Sadler JE. Biochemistry and genetics of von Willebrand factor. Annu Rev Biochem. 1998;67:395-424.

307. Lampugnani MG, Resnati M, Raiteri M, Pigott R, Pisacane A, Houen G, Ruco LP, Dejana E. A novel endothelial-specific membrane protein is a marker of cell-cell contacts. J Cell Biol. 1992;118(6):1511-22.

308. Gorzelniak K, Janke J, Engeli S, Sharma AM. Validation of endogenous controls for gene expression studies in human adipocytes and preadipocytes. Horm Metab Res. 2001;33(10):625-7.

309. Meldgaard M, Fenger C, Lambertsen KL, Pedersen MD, Ladeby R, Finsen B. Validation of two reference genes for mRNA level studies of murine disease models in neurobiology. J Neurosci Methods. 2006;156(1-2):101-10.

310. Bohnsack JF, Brown EJ. The role of the spleen in resistance to infection. Ann Rev Med. 1986;37:49-59.

311. Cai AQ, Landman KA, Hughes BD, Witt CM. T cell development in the thymus: from periodic seeding to constant output. J Theor Biol. 2007;249(2):384-94.

312. Kruisbeek AM. Regulation of T cell development by the thymic microenvironment. Semin Immunol. 1999;11(1):1-2.

313. Anderson G, Jenkinson EJ. Lymphostromal interactions in thymic development and function. Nature Rev Immunol. 2001;1(1):31-40.

314. Charbonneau H, Tonks NK. 1002 protein phosphatases? Annu Rev Cell Biol. 1992;8:463-93.

315. Thomas ML. The Leukocyte common antigen family. Annu Rev Immunol. 1989;7:339-69.

316. Jenkinson W, Jenkinson E, Anderson G. Preparation of 2-dGuo-treated thymus organ cultures. J Vis Exp. 2008(18).

317. Holthöfer H, Virtanen I, Kariniemi AL, Hormia M, Linder E, Miettinen A. Ulex europaeus I lectin as a marker for vascular endothelium in human tissues. Lab Invest. 1982;47(1):60-6.

318. West JB. Blood flow to the lung and gas exchange. Anesthesiology. 1974;41(2):124-38.

319. Gil J. The normal lung circulation. State of the art. Chest. 1988;93(3):80S-2S.

320. Griffith AV, Fallahi M, Nakase H, Gosink M, Young B, Petrie HT. Spatial mapping of thymic stromal microenvironments reveals unique features influencing T lymphoid differentiation. Immunity. 2009;31(6):999-1009.

321. Sprent J, Kishimoto H. The thymus and central tolerance. Philos Trans R Soc Lond B Biol Sci. 2001;29(1409):609-16.

322. Smits K, Iannucci V, Stove V, Van Hauwe P, Naessens E, Meuwissen PJ, Ariën KK, Bentahir M, Plum J, Verhasselt B. Rho GTPase Cdc42 is essential for human T-cell development. Haematologica. 2010;95(3):367-75.

323. Wojciak-Stothard B, Ridley AJ. Rho GTPases and the regulation of endothelial permeability. Vascul Pharmacol. 2002;39(4-5):187-99.

324. Van Nieuw Amerongen GP, Beckers CM, Achekar ID, Zeeman S, Musters RJ, van Hinsbergh VW. Involvement of Rho kinase in endothelial barrier maintenance. Arterioscler Thromb Vasc Biol. 2007;27(11):2332-9.

325. Kudo S, Fukuda M. Tissue-specific transcriptional regulation of human leukosialin (CD43) gene is achieved by DNA methylation. J Biol Chem. 1995;270(22):13298-302.

326. Jones PA. The DNA methylation paradox. Trends Genet. 1999;15(1):34-7.

327. Hamik A, Wang B, Jain MK. Transcriptional regulators of angiogenesis. Arterioscler Thromb Vasc Biol. 2006;26(9):1936-47.

328. Hollenhorst PC, Jones DA, Graves BJ. Expression profiles frame the promoter specificity dilemma of the ETS family of transcription factors. Nucleic Acids Res. 2004;32(18):5693-702.

329. Sato Y. Role of ETS family transcription factors in vascular development and angiogenesis. Cell Struct Funct. 2001;26(1):19-24.

330. Randi AM, Sperone A, Dryden NH, Birdsey GM. Regulation of angiogenesis by ETS transcription factors. Biochem Soc Trans. 2009;37(6):1248-53.

331. Hashiya N, Jo N, Aoki M, Matsumoto K, Nakamura T, Sato Y, Ogata N, Ogihara T, Kaneda Y, Morishita R. In vivo evidence of angiogenesis induced by transcription factor Ets-1: Ets-1 is located upstream of angiogenesis cascade. Circulation. 2004;109(24):3035-41.

332. Birdsey GM, Dryden NH, Amsellem V, Gebhardt F, Sahnan K, Haskard DO, Dejana E, Mason JC, Randi AM. Transcription factor Erg regulates angiogenesis and endothelial apoptosis through VE-cadherin. Blood. 2008;111(7):3498-506.

333. Ayadi A, Zheng H, Sobieszczuk P, Buchwalter G, Moerman P, Alitalo K, Wasylyk B. Net-targeted mutant mice develop a vascular phenotype and up-regulate egr-1. EMBO. 2001;20(18):5139-52.

334. Kutcher ME, Kolyada AY, Surks HK, Herman IM. Pericyte Rho GTPase mediates both pericyte contractile phenotype and capillary endothelial growth state. Am J Pathol. 2007;171(2):693-701.

335. Li Z, Aizenman CD, Cline HT. Regulation of rho GTPases by crosstalk and neuronal activity in vivo. Neuron. 2002;33(5):741-50.

336. Minobe S, Sakakibara A, Ohdachi T, Kanda R, Kimura M, Nakatani S, Tadokoro R, Ochiai W, Nishizawa Y, Mizoguchi A, Kawauchi T, Miyata T. Rac is involved in the interkinetic nuclear migration of cortical progenitor cells. Neurosci Res. 2009;63(4):294-301.

337. Kaur S, Leszczynska K, Abraham S, Scarcia M, Hiltbrunner S, Marshall CJ, Mavria G, Bicknell R, Heath VL. RhoJ/TCL Regulates Endothelial Motility and Tube Formation and Modulates Actomyosin Contractility and Focal Adhesion Numbers. Arterioscler Thromb Vasc Biol. 2011;31(3):657-64.

338. Romer LH, Birukov KG, Garcia JG. Focal adhesions: paradigm for a signaling nexus. Circ Res. 2006;98(5):606-16.

339. Nayal A, Webb DJ, Brown CM, Schaefer EM, Vicente-Manzanares M, Horwitz AR. Paxillin phosphorylation at Ser273 localizes a GIT1-PIX-PAK complex and regulates adhesion and protrusion dynamics. J Cell Biol. 2006;173(4):587-9.

340. van Nieuw Amerongen GP, Natarajan K, Yin G, Hoefen RJ, Osawa M, Haendeler J, Ridley AJ, Fujiwara K, van Hinsbergh VW, Berk BC. GIT1 mediates thrombin signaling in endothelial cells: role in turnover of RhoA-type focal adhesions. Circ Res. 2004;94(8):1041-9.

341. Frank SR, Hansen SH. The PIX-GIT complex: a G protein signaling cassette in control of cell shape. Semin Cell Dev Biol. 2008;19(3):234-44.

342. Bishop ET, Bell GT, Bloor S, Broom IJ, Hendry NF, Wheatley DN. An in vitro model of angiogenesis: basic features. Angiogenesis. 1999;3(4):335-44.

343. Donovan D, Brown NJ, Bishop ET, Lewis CE. Comparison of three in vitro human 'angiogenesis' assays with capillaries formed in vivo. Angiogenesis. 2001;4(2):113-21.

344. Adams RH, Eichmann A. Axon guidance molecules in vascular patterning. Cold Spring Harb Perspect Biol. 2010;2(5):a001875.

345. Webb DJ, Parsons JT, Horwitz AF. Adhesion assembly, disassembly and turnover in migrating cells -- over and over and over again. Nat Cell Biol. 2002;4(4):E97-100.

346. Matafora V, Paris S, Dariozzi S, de Curtis I. Molecular mechanisms regulating the subcellular localization of p95-APP1 between the endosomal recycling compartment and sites of actin organization at the cell surface. J Cell Sci. 2001;114(Pt 24):4509-20.

347. Rosenberger G, Kutsche K. AlphaPIX and betaPIX and their role in focal adhesion formation. Eur J Cell Biol. 2006;85(3-4):265-74.

348. Di Cesare A, Paris S, Albertinazzi C, Dariozzi S, Andersen J, Mann M, Longhi R, de Curtis I. P95-APP1 links membrane transport to Rac-mediated reorganization of actin. Nat Cell Biol. 2000;2(8):521-30.

349. Cascone I, Giraudo E, Caccavari F, Napione L, Bertotti E, Collard JG, Serini G, Bussolino F. Temporal and spatial modulation of Rho GTPases during in vitro formation of capillary vascular network. Adherens junctions and myosin light chain as targets of Rac1 and RhoA. J Biol Chem. 2003;278(50):50702-13.

350. Davies PF, Robotewskyj A, Griem ML. Quantitative studies of endothelial cell adhesion. Directional remodeling of focal adhesion sites in response to flow forces. J Clin Invest. 1994;93(5):2031-8.

351. Girard PR, Nerem RM. Shear stress modulates endothelial cell morphology and F-actin organization through the regulation of focal adhesion-associated proteins. J Cell Physiol. 1995;163(1):179-93.